(2) LEVEL II

TARADCOM R and D LABORATORY

TECHNICAL REPORT

NO. 12397

TRACK DYNAMICS PROGRAM

FINAL REPORT

OCTOBER, 1978

U. S. ARMY
TANK-AUTOMOTIVE RESEARCH AND DEVELOPMENT COMMAND

Contract No. DAAE07-76-C-0163
CLIN 0002, Task No. 77-1

by H. C. Meacham, Jr., J. C. Seaton, J. P. Wilcox, and E. R. Doyle

BATTELLE
Columbus Division
Advanced Systems Laboratory
505 King Avenue
Columbus, Ohio 43201

U.S. ARMY TANK-AUTOMOTIVE RESEARCH AND DEVELOPMENT COMMAND
Warren, Michigan 48090

NOTICES

1. The findings in this report are not to be construed as an official Department of Army position unless so designated by other authorized documents.

2. The citation of commercial products in this report does not constitute an official endorsement or approval of such products.

(2)

(6) TRACK DYNAMICS PROGRAM

CLIN 0002 Task No. 71-1

(19) TAKHDCOM

(9) Final Report No. (19) TR-12397

by

(10) Howard C. Meacham, Jr., James C. Swain, John P. Wilcox and George R. Doyle

(15) Prepared Under Contract DAAE07-76-C-0165

for

U. S. ARMY
TANK-AUTOMOTIVE RESEARCH AND DEVELOPMENT COMMAND
Warren, Michigan 48090

by

BATTELLE
COLUMBUS LABORATORIES
505 King Avenue
Columbus, Ohio 43201

(11) October 1978

(12) 207 p.

ABSTRACT

A comprehensive study of track/track dynamics was undertaken, utilizing analytical, laboratory test, and field test techniques to develop a better understanding of track dynamics and performance. Analytical techniques were developed to predict track vibration modes, chordal action effects, dynamic tension and path, energy dissipation, tension going over obstacles, tension distribution, pin/bushing stresses and deflections, temperature buildup, and end connector tightening effectiveness. Double-pin track for heavy tanks was analyzed with these techniques, and designs for improved track suitable for the XM-1 tank were developed. A laboratory bushing research machine was designed, and a track-mounted telemetry system was built.

FOREWORD

The continuing trend to greater mobility and maneuverability required in today's ground combat environment leads to increasing problems for the designers and users of tracked vehicles. Higher speeds and high maneuverability create much higher dynamic forces on the track system, which is already taxed in its capabilities. For example, problems already exist due to excessive weight, excessive noise and vibration, overheating of rubber track elements and road wheels, chunking of the pads, pin and bushing failures, breaking or throwing of a track, and so forth. Therefore, today's tracks are expensive items not only in terms of initial costs and replacement costs, but in terms of men, resources and capabilities lost because of failures in the field.

To develop improved track, it was realized that the basic area of track dynamics should be examined in detail. This led to the formulation of the Track Dynamics Program, which was proposed as a broad and innovative technical approach to the problem of track, and was envisioned as the first phase (1-1/2 years) of a total program covering three to four years and including two or three phases.

The objectives of the Track Dynamics Program included the development of analytical, laboratory, and field-usable tools to assess the dynamic performance of existing track and to guide the design of new and improved track. The program was conducted as a CLIN C002 task under the Concept Formulation function provided by Battelle's Columbus Division for TARADCOM under Contract DAAE07-76-C-0165. The program was authorized on November 15, 1976, and extended to September 30, 1978. With the completion of this program, it became obvious that another phase of similar scope would indeed be valuable, enabling the analysis to be extended to other aspects of track dynamics.

ACKNOWLEDGMENT

The work reported herein was performed for the Tank-Automotive Concepts Laboratory of the U. S. Army Tank-Automotive Research and Development Command (TARADCOM), Warren, Michigan. Dr. Jack Parks, Director of the TACL, monitored the project. The encouragement and support of General O. C. Decker, Jr., Commanding General of TARADCOM, Dr. Parks, and Mr. Frederick L. Bagby, head of the Concepts Formulation Group, are greatly appreciated, and their help and guidance in carrying out the Track Dynamics Program are gratefully acknowledged.

TABLE OF CONTENTS

TABLE OF CONTENTS (Continued)

TABLE OF CONTENTS (Continued)

TABLE OF CONTENTS (Continued)

TABLE OF CONTENTS (Continued)

LIST OF FIGURES

LIST OF FIGURES (Continued)

LIST OF FIGURES (Continued)

LIST OF FIGURES (Continued)

LIST OF TABLES

LIST OF TABLES (Continued)

FINAL SUMMARY REPORT

TRACK DYNAMICS PROGRAM
CLIN 0002 TASK NO. 77-1

from the

BATTELLE
ADVANCED SYSTEMS LABORATORY
(Contract DAAE07-76-C-0165)

to the

U. S. ARMY
TANK-AUTOMOTIVE RESEARCH AND DEVELOPMENT COMMAND
Warren, Michigan

October, 1978

INTRODUCTION

The Track Dynamics Program (TDP) was a research program whose objectives included the development of analytical, laboratory, and field-usable tools to assess the dynamic performance of track so that new and improved track concepts could be designed and demonstrated. The TDP was conducted as a CLIN 0002 task under the Concept Formulation function provided by Battelle's Columbus Division for TARADCOM under Contract DAAE07-76-C-0165. The program was authorized on November 15, 1976, and extended to September 30, 1978.

OBJECTIVES

The objectives of the TDP were developed during the first part of the program, as follows:

- To develop a better understanding of vehicle track dynamics and track design
- To develop tools and methodology for the design of track, including analytical, laboratory, and field techniques
- To apply the design tools and methodology to improve current track types, evolve new track concepts, and construct partial sections of new track.

The scope of work was defined as follows:

- Determine past efforts and state of the art of track dynamics and design
- Conduct field test program to obtain realistic service conditions
- Conduct laboratory tests to ensure duplication of field conditions
- Mathematically simulate vehicle track dynamics
- Analyze the test data effects on the track system
- Apply results to development of improved hardware .

After the first part of the TDP, during which an assessment of the state of the art and present track problems was made, it was concluded that the following order of priority should be followed in the analysis of track dynamics:

- Linked track for heavy armored vehicles
- Linked track for lighter vehicles
- Other track types, such as band track.

Therefore, while many of the techniques developed were general and could be applied to any tracked vehicle, in the majority of cases, specific solutions were obtained for the M-60 tank using T-97 (integral pad) or T-142 (replaceable pad) track, which was also being considered in slightly modified form for the Army's newest heavy tank, the XM-1. This approach was considered to be the most valuable to the Army, and allowed some results of the program to be considered by the designers of the XM-1 track.

The three stated objectives were met, particularly the development of a better understanding of track dynamics and the development of analytical techniques to evaluate track design. In the future, there needs to be additional application of these analytical tools to all types of track, thereby expanding the application from the few types of double pin linked track for heavy armored vehicles which were chosen as first priority for use in developing and applying analytical techniques during this program.

SUMMARY AND CONCLUSIONS

The first three months of the TDP was an orientation period during which many people in the track community were contacted, and an extensive literature search and review was made.

Following this, a summary of track problems was prepared. One of the most urgent problems appeared to be road pad thermal blowout at high speed on the Chrysler XM-1 modified T-97 design. A second XM-1 problem involves satisfying the user requirements for an aggressive steel grouser without giving up the weight advantage of an integral pad design. On the T-142 track, the primary problems appear to be pin breakage and road pad chunking. Track guidance and resistance to throwing was felt to be an area where improvement might be made on all track designs. On single pin tracks the prime areas of continuing concern to the designer are bushing life and shoe structural fatigue. However, no evidence of particular distress on current designs was found.

Based on these findings, a comprehensive analytical program was undertaken, with complementary laboratory and field tests to support the analytical work and a hardware conceptual design task to incorporate all the results. Table 1 is a summary of the more important analyses conducted during the Track Dynamics Program, and a summary of the important findings is given below, listed according to the main headings used in the body of the report.

Track Natural Frequencies. Track natural frequencies and mode shapes for T-142 track on an M-60 tank were calculated by two methods--using tensioned string equations and using TRACKVIBE, a finite element computer code. The first 20 natural frequencies ranged from 0.94 Hz to 15.80 Hz using TRACKVIBE: these frequencies were approximately 15 percent higher than those given by the string equations (which do not take into account the bending stiffness). The multitude of track natural frequencies shows that there is a high probability of a forcing function (in particular, track shoe passage frequency) coinciding with a natural frequency at any speed, a condition conductive to high vibration amplitudes unless the track is well damped.

TABLE 1. TRACK DYNAMICS PROGRAM ANALYSES

	Analysis	Type	Main Output	Condition
(1)	BUSHSTRESS	Computer	Rubber bushing stresses	Track assembled; no tension (2D)
(2)	PINSTRESS II	Hand	Pin stresses and deflections, bushing deflections	Static condition--uniform or nonuniform tension across track width (3D)
(3)	TRACKOB II	Computer	Localized track path and tension	Uniform obstacle across track width (2D)
(4)	TRACKOB III	Computer	Localized track path and tension	Nonuniform obstacle across track width (3D)
(5)	TRACKVIBE	Computer	Vibration frequencies and amplitudes	Track sections free vibration
(6)	CHORDACT	Computer	Localized tensions and deflections	Track moving over sprocket or front idler
(7)	TRACKCENT	Hand	Overall track path and tension	Track moving (centrifugal force effects)
(8)	TRACKDYNE	Computer	Localized tension, path, energy loss, force	Track moving over front idler and road wheel (2D)
(9)	WEDGEND	Hand	End connector bolt torque versus bushing torque	Tightening wedge-type end connector
(10)	SHOETEMP II	Computer	Track shoe temperature distribution	Vehicle moving on smooth, hard surface (2D)
(11)	SHOETEMP III	Computer	Track shoe temperature distribution	Vehicle moving on smooth, hard surface (3D)

Chordal Action. The variation in velocity as the track passes over a sprocket or roller (front idler or road wheel) is called chordal action. Assuming a constant sprocket speed and tank speed, these velocity variations cyclically stretch and release the track, causing periodic variations in track tension. These tension variations were calculated for the M-60 tank with T-142 track by three methods--hand calculations, a small computer program called CHORDACT, and the larger TRACKDYNE computer program. The peak-to-peak tension excursions at the sprocket were found to be surprisingly low--on the order of 3000 pounds, which is an order of magnitude below other forces in the track. Therefore, it was concluded that the forces due to chordal action are not a source of distress to the track, although the cyclic forces transmitted into the hull may well be a serious source of noise and vibration.

Track Dynamic Tension and Path. The track dynamic tension and path were analyzed first by hand calculation (TRACKCENT) and then by use of the TRACKDYNE program developed for this purpose. The TRACKDYNE program is a real-time, two-dimensional computer simulation of double-pin track running over the front idler and down the span to the front road wheel. Data output includes time histories throughout a pitch-passage cycle of track tension as seen by each individual link, shoe-to-idler force normal and tangential to the wheel surface as seen by each shoe, and idler-to-hull force in horizontal and vertical components. Positions and velocities of individual parts as a function of time are also available. An energy balance is made by determining the energy dissipated in all the dampers during one cycle, the energy put into the system mechanically, and the energy stored mechanically in the system.

Runs were made at speeds between 20 and 70 mph, and with apparent tension between 1500 lb and 15,000 lb with geometry corresponding to the T-142 track on the M60 tank. Typical findings were as follows:

- Track tension excursions due to chordal action and other cyclic dynamic effects on the idler and at the road wheel entrance are typically on the order of 1000 to 2000 lb peak-to-peak, and do not become more severe at increased speed as expected.
- Idler-to-hull force excursions are typically on the order of 3000 lb peak-to-peak. They are highly nonsinusoidal, with an important content of higher-order harmonics evident.
- Impact when the shoes contact the idler and road wheel is generally not severe.

- The energy dissipated in this portion of the track circuit is small at normal operating speeds, but it can become substantial at higher speeds, reaching 121 hp at 70 mph and 15,000 lb tension.
- Relative to a continuous band with distributed stiffness and rotary inertia, the linked track with lumped parameters behaves as though it is stiffer and is less affected by its rotary inertia than was anticipated. The standing wave mode of operation predicted by TRACKCENT at high speed was verified. However, the transition to this mode was at a speed about 25 percent higher than expected.
- A mechanism was revealed whereby tractive force is developed between the idler and the track due to the kinematics of track roll-on and roll-off. Consequently, track tension on the idler was as much as 2000 lb more than anticipated, and sliding of the rubber surfaces could result.
- At higher speeds, a greater percentage of the total energy dissipated in the track went into the bushing.

Pin and Bushing Loads and Deflections. A technique (PINSTRESS II) was developed for calculating by hand the loads and deflections in some detail within the track. As an illustration of the output of this program, pin stresses and bushing effectiveness (ratio of minimum load to maximum load carried by two bushings on the same pin) were calculated for 5 types of track as follows:

	Pin Bending Stress, psi	Effectiveness of Center of Bushing
T-97 Track, 43,000-lb Load	112,000	0.36
T-14[illegible] Aluminum Shoe Track, 43,000-lb load	116,000	0.49
XM-1 Track Similar to T-97, 48,600-lb load	96,000	0.50
XM-1 Aluminum Shoe Track, 48,600-lb load	98,000	0.71
First Version of Enlarged Tubular Pin XM-1 Concept 48,600-lb load	74,000	0.82

These stresses are those which occur away from the spocket where tension is uniformly distributed across the width of the track. Pin stresses in the vicinity of the sprocket are known to be around 200,000 psi.

Reduced pin stresses and increases in bushing effectiveness occur mainly as the result of increased stiffness of pins and binocular tubes. While the XM-1 designs are better than the M-60 analogous designs, these values can be improved further, as evidenced by the results for the first version of the advanced hardware concept developed during this project (discussed later).

Calculations were also made for the case where--rather than being loaded uniformly across its width--the tensile forces are concentrated at the edges of the track, as is the case where the track is contacted by the sprocket and all the tractive effort is carried by the end connectors. A similar condition can exist anywhere along the track if a center guide is loose. Conversely, tensile load will be concentrated in a centerguide if an end connector is loose. For example, calculations showed that the load distribution between end connectors and center guide varied from 50-50 (end connectors and center guide tight) to 34-66 (end connectors and center guide loose), with the 66 percent carried by the center guide. Actual load distribution will vary statistically between these extremes, depending on the distribution of loose center guides and end connectors throughout the track.

Effects of Obstacle Negotiation. A two-dimensional model (TRACKOB II) was formulated to predict track tension when the track was deflected uniformly across its width by an obstacle, and a three-dimensional model (TRACKOB III) for the case where the obstacle was under only one edge of the track. The two-dimensional results were validated by comparing them with tensions measured in tests which were made on an M-60 tank in the TARADCOM laboratories at Warren, Michigan. The results showed that the tension increases by 20,000 pounds when traversing a 9-inch high block, with the greatest tension increase occurring when the block is halfway between two road wheels near the center of the tank. Of several track and vehicle parameters varied, increases in track longitudinal stiffness and coefficient of friction between road pad and ground were found to have the greatest effect on the tension. These increases in tension are significant because they are well above the nominal track preload of 12,000 pounds. In practice, the preload appears to be well below this, meaning the localized tension increase due to obstacles may be two or three times the normal tension.

For the same height obstacle loading the track at one edge only, the overall track tension increases less, as would be expected, but the end connector over the obstacle takes much more load, while the other end connector looses load (even going from tension to compression for obstacles on the order of 8 inches high).

Thermal Analysis. A two-dimensional thermal model (SHOETEMP II) and a three-dimensional model (SHOETEMP III) of the T-142 track shoe assembly were developed, using the computer code TRUMP. Transient thermal conditions were predicted, and the model was validated against temperatures measured in the track shoes during M-60 field tests at TARADCOM in January and February of 1978. Parameter studies were then made on the T-142 type tracks used on the M-60 and the XM-1 tanks. In both cases, the highest temperatures were obtained in the center of the volume of rubber on the road wheel path side of the track, with the center of the road pad building up to lower temperatures. These results should perhaps be evaluated from a qualitative than a quantitative standpoint, due to the lack of accurate input data on thermal heat generation and conduction properties of the rubber. At a constant running speed of 30 mph, the predicted temperature in the road wheel path on the M-60 reached 300 F after an hour, and stabilized at approximately 380 only after three hours of running. Comparable temperatures in the road pad were 230 and 280 F, respectively. Predicted temperatures in the XM-1 track were lower, but this is still a potential problem area, particularly when 50 mph speeds are used. Parameter studies indicated that while changes in the thermal properties of the rubber (and to a lesser extent, the metal components) affect temperatures somewhat, the single most effective way to reduce temperature buildup is to reduce the volume of rubber which is compressed, thereby reducing the heat generation directly. This translates to a reduction in depth of rubber in the road wheel path and pad. Additional studies in this area are needed, using these newly developed computer models.

Track Bushing Research. A finite element computer program (BUSHSTRESS) was developed and used to analyze strains in the bushings resulting from their

initial assembly into the binocular tubes. It was found that high strains exist in the "corner" where pin and bushing meet, and it was theorized that failures occurring in this area (and thought to be due to abrasion of the unbounded bushing sliding on the pin) may actually be caused or at least aggravated by the high assembly stresses. A limited series of laboratory insertion tests verified that damage can occur during insertion, and indicated the importance of using the proper lubricant during the assembly process. A review of past work indicated that earlier research had led to the same conclusion, and had even led to a new bushing cross-section designed to provide much more uniform strain, thereby alleviating the high stress concentration factor. Apparently this design was never tested, but in view of its apparent validity, work in this area should continue.

Considerable effort was also spent in developing requirements for a laboratory machine to facilitate bushing research. The requirements led to a machine having considerably more flexibility than the present TARCOM QPL test machine, and a detailed machine design effort was conducted. The design which was developed has separate servocontrolled hydraulic actuators to apply radial loads/deflections and torsional loads/deflections, enabling actual loading conditions to be simulated quite accurately. More detailed information on the bushing laboratory research machine is included in Appendix B. Due to priorities established in the last phases of the Track Dynamics program, the machine was not built.

Advanced Track Concept Development. Early in the program it was decided to focus a modest portion of the effort on attempts to conceive and develop new track concepts. At the outset both revolutionary (long-term) and evolutionary (short-term) ideas were considered. However, the revolutionary concepts were not carried forward and the attention was primarily given to evolutionary ideas. The prime target for the conceptual efforts was linked track for heavy armored vehicles, as opposed to linked track for lighter vehicles or unusual track such as the band track.

As the program progressed, an advanced track concept was developed which evolved around the use of larger, stiffer tubular pins, bushings and binocular tubes, and the use of a fabricated brazed steel shoe assembly. An integral pad version of this concept was then designed, and compared to present double-pin T-97 track, this design appeared to have lower weight, improved resistance to track throwing, lower stresses in the pins and bushing, less heat buildup, less looseness of end connectors, comparable first-cost,

and--as a result--improved life-cycle costs. Disadvantages included the fact that it did not include an agressive grouser and, in order to take full advantage of the enlarged pin/tube design, the pitch chosen was slightly greater than present track. Further analysis of the unique end connector design showed that stresses were excessive, and this led to a detailed analytical and laboratory study of the basic wedge-type end connector which resulted in a greatly improved version of the standard wedge-type connector. As time went on, it became apparent that the Army would require a replaceable pad, aggressive grouser type track for the XM-1. Therefore, near the end of the program, a new set of design constraints was evolved, based on the philosophy of moving toward an evoluationary rather than revolutionary approach in order to maximize the chances of a short-term hardware tryout. The constraints were:

- Both the shoe and end connector must use the same pitch as the current XM-1.
- The track must be interchangeable with the Leopard without drive sprocket changes or suspension changes.
- The shoe must have a replaceable pad.
- When the pad is removed the shoe must present at least a short aggressive grouser to the ground.
- The track should be designed to minimize the changes required on the M-60 to allow its later utilization thereon.
- Wedge-type end connectors will be used with the wedge action turned over to improve tightening and improve maintainability.
- Simple, straightforward pad attachment schemes will be used with emphasis on protection against thread corrosion.

The design effort in response to these constraints centered on a cast steel approach and a steel forging and tube approach. The latter approach was chosen as the most likely to merit additional development and consideration for the XM-1. A design was then carried forward in which the shoe structure consisted of a brazed assembly which employed one steel forging and three steel tubes. However, due to weight problems, the approach was modified to utilize a welded assembly of several forgings instead of a single forging. A set of 5 drawings which illustrate this final design concept are included in this report. Features of this final design concept include:

- o It is directly interchangeable with the XM-1 both as track sets or as individual pitches.
- o It contains a replaceable pad with ground contact area equal to the current XM-1, modified T-142, replaceable pad version.
- o It utilizes wedges with turned over action for greater effectiveness.
- o It contains a hardened steel forged 1/2-inch integral grouser.
- o It includes a scheme for preventing corrosion of the threads on the simple pad-attaching stud.
- o It contains a tubular pin of 1-5/8 inch outside diameter, which is 10 percent stiffer (in bending) than the current XM-1 pin.
- o It has a large center tube in the road wheel path area which reduces the rubber hysteretic heating in that zone.
- o It has a stiffer and stronger center guide with greater wear contact area with the roadwheels.

It is recommended that several individual pitches of this track be built and installed in an existing XM-1 track for testing. It can be thought of as a replaceable pad track with a competent steel grouser which is competitive in weight and potentially cheaper than the current XM-1 modified T-142, replaceable pad, aluminum forging version.

More complete recommendations on all aspects of the Track Dynamics Program are contained in the section entitled "Recommendations for Future Work", which starts on page 206.

TECHNICAL DISCUSSION

This section of the report covers the main technical activity and results of the entire Track Dynamics Program.

Orientation to Track Problems

The task order covering this program specifically required that an effective liaison be established with Army, industry, and academic personnel to determine past efforts and state of the art of track dynamics and design. This was to assure that this program was fully integrated with past and present Army effort on track and was nonduplicative. Therefore, a literature search and an extensive series of visits with members of the track community were carried out during the first three months of the program.

Visits to the Track Community

It was considered essential that this effort include the TARADCOM research groups, Army program offices, the primary vehicle builders, the track suppliers, and Army testing and/or using groups. During the first 60 days of the program, fifteen different organizations were visited, 40 people were contacted, and 33 man-days of consultation resulted. During the next weeks, 5 more organizations were visited, and 40 more people contacted, some by phone.

Table 2 shows the organizations contacted during this initial phase of the program, and Appendix A lists the people contacted.

Literature Search

An important contribution to establishing the present state of the art was the review of previously published information on track and track dynamics that had been developed by the technical community. This review, along with interviews with knowledgeable personnel, outlined the problem areas and previous attempted solutions. It also provided a better overall appreciation of the difficulties already encountered by past researchers.

TABLE 2. ORIENTATION PHASE CONTACTS

ARMY
TARADCOM
XM-1 Program Office
M-60 Program Office
M-113 Program Office
MICV Program Office
Aberdeen Proving Grounds
AMMRC
DARCOM
MERADCOM
Waterways Experiment Station
Ft. Hood
Ft. Knox
INDUSTRY
ALCOA
Chrysler XM-1
Chrysler M-60
Detroit Diesel Allison
FMC
Firestone
Goodyear
Standard Products
Bolt, Beranek and Newman
ACADEMIA
San Jose State
University of Michigan
Wayne State

The first step was to conduct a computerized literature search. Key words were defined to identify titles and abstracts of reports compiled by DOD, NTIS, NASA, Engineer Index, and Dissertation Abstracts. Based on the content of the abstracts, reports were ordered from the appropriate agencies. Upon receiving the ordered reports, other articles were identified in reference lists at the end of each report, and also ordered.

Although the computerized literature search did produce the largest single source of information, interviews with, and telephone calls to, personnel at several Army commands, industrial plants, and universities provided many of the more pertinent reports. In most cases, it was the individuals of the track community who called attention to work that had been done. Their cooperation, not only in citing the literature but also in providing interesting dialogue, enhanced the knowledge accumulated substantially.

As a result of the literature search, a number of reports, books, and other pieces of documentation relevant to the Track Dynamics Project were accumulated. A listing of these is attached as Appendix B. Throughout the course of the project, quest for the literature continued as an ongoing effort, with new information being dissiminated to key individuals whenever it was obtained.

Problems with Track

Throughout the initial orientation to problems with track, inquiry was particularly directed toward the area of high-speed (30-50 mph) dynamic problems. These were defined as those being resonance or inertially dominated, as opposed to other phenomena occurring merely because the tank is a moving, or dynamic, system (such as road pad blowout due to thermal effects at high speeds on pavement). Little concern over the high-speed dynamic problems was found. Some concern was expressed over resonance problems and excessive noise and vibration at intermediate (15-30 mph) operating speeds. In addition, two instances were cited of tests in which rubber bushed track allowed a higher vehicle top speed than did lubricated pin track. This suggested the possibility of important power-consuming dynamic phenomena in the lubricated pin track.

There was also substantial concern expressed about noise on certain tracked vehicles--particularly noise to which the driver/crew are exposed. Noise problems involve the complex interactions of track forcing functions with suspension and vehicle elements and structures. Substantial noise problems can

occur without large energy losses or damaging wear or material fatigue necessarily being involved. While noise studies, per se, were not considered to fall within the scope of the Track Dynamics Program, the results of the dynamic analysis and dynamic field tests were monitored for results that were pertinent to the noise/vibration problem.

The most salient problem identified was road pad thermal blowout on the XM-1 modified T-97 track at high speed. This problem appeared to be basically unsolved at the time.

The second most salient problem area was the T-142 track with its pin breakage and road pad chunking. Progress appeared to have been made on the chunking, but more needed to be done. Some people expressed the view that the chunking was more of a cosmetic problem than a real problem, and that chunking really does not influence useful wear life significantly. The pin problem evolved from the fact that the T-142 test and operating conditions were more severe than originally anticipated. The general concensus appeared to be that it was a mistake to retain the T-97 pin diameter for the T-142 track.

On the single pin track designs, two areas were of most concern--bushing life and shoe structural fatigue. Both of these appeared to be under good engineering control, and no unusual current problems were identified. A road pad thermal problem at high speed has existed on a single pin track used on the Dutch AIFV vehicle. The basic approach to handling this problem appeared to be to decrease road pad pressure by a slight increase in track width.

The basic contention that single pin track is only appropriate for smaller Army vehicles was expressed by most people contacted except the principal builders of single pin track, who believed that single pin designs could be appropriate for M-60 size vehicles. The limitation in applying single pin designs to larger vehicles had been bushing load capacity.

Figure 1 shows a general conclusion of current track problems which were identified during the initial review of the technology. Several items which appear were "product improvement" in nature rather than high-speed dynamic problems, per se. This reflected generally the opinions of that portion of the track community who dealt with the day-to-day problems of current tracks.

PROBLEM	SINGLE PIN	DOUBLE PIN		
		XM-1	T-142	T-97
ROAD PAD THERMAL BLOWOUT AT HIGH SPEED		PROBABLE		
ROAD PAD WEAR		POSSIBLE		X
PIN BREAKAGE			X	?
TRACK GUIDANCE AND THROWING	X	PROBABLE	X	X
ROAD PAD CHUNKING		PROBABLE	X	?
BUSHING LIFE	X	POSSIBLE		
END CONNECTORS			X	X
SHOE STRUCTURAL FAILURES	X			
SPROCKET AND DRIVE SURFACE WEAR	X	PROBABLE	X	X
ROAD WHEEL PATH THERMAL PROBLEMS AT HIGH SPEED		POSSIBLE		

FIGURE 1. TRACK PROBLEM AREAS IDENTIFIED DURING INITIAL ORIENTATION PERIOD

The information on the track problem and the state of the art of track design obtained during the first part of the program was sufficient to enable the track dynamics program to be planned in more detail. A three-fold approach was taken, that is, laboratory and field tests were used in addition to the analytical studies which were made. The major areas of investigation can be grouped as follows:

- o Dynamic effects
- o Load/stress distribution
- o Effect of obstacles
- o Thermal effects
- o Bushing studies
- o Advanced concepts for herdware
- o Field tests/instrumentation .

Each of these research areas is discussed in detail in the following sections of this report.

Track Dynamics

At the beginning of the program, analyses of several dynamic effects were made, using hand calculations or relatively simple computer program. These studies included the calculation of the natural resonant frequencies of track, calculation of the effects of the kinematic response called chordal action, and calculation of the effects of centrifugal force and link dynamics. Near the end of the program, a comprehensive computer program called TRACKDYNE was written, which takesinto account any and all dynamic effects, including those mentioned above. The computer programs TRACKVIBE, CHORDACT, and TRACKDYNE are described below, together with the analysis of the track's dynamic path and tension.

Track Natural Frequencies

The primary purpose of the dynamic analysis was to obtain a more basic derstanding of the motions and the forces in the track. The most fundamental p in understanding the behavior of any dynamic system is to determine its n .ral modes of vibration--that is, if the system is perturbed, at what frequencies and with what shapes will it vibrate. This can be done by formulating the e genproblem for the system and solving it with a computer program. The eigenproblem for the pitch plane motion of one complete T-142 track on an M-60 tank was coded and solved; the program was called TRACKVIBE.

Eigenproblem. The solution of the eigenproblem for the track yields two basic outputs. First, the lowest natural frequencies of vibration (eigenvalues) are determined. In any solution, all the natural frequencies can be determined, but it is usually the lowest that are of the greatest practical interest because they define a fairly simple motion and require less energy to excite. The shape of the motion of the track associated with any one eigenvalue is called the eigenvector, or mode shape. The first few eigenvectors will usually indicate that a small section of the track is responding at that section's nacural frequency, while the rest of the track has small displacements. At higher natural frequencies, greater portions of the track respond, and the eigenvector becomes more complicated. As expected, greater energy input is necessary to maintain the higher modes of motion.

It is important to understand that an eigenvector is only an indication of possible motions, and that the magnitude of the motion is determined by the magnitude of the input excitation. In general, a linear system that is perturbed from rest will vibrate with a linear combination of all its mode shapes. However, it is possible to cause the system to vibrate such that only one mode is the dominant motion by exciting that section of track at the appropriate natural frequency. This can be done by an internal input to the system, such as the impact of sprocket teeth on the track, or externally by traversing a periodic terrain.

The mode shape of an eigenvector is described in terms of normalized displacements--that is, the maximum displacement is defined as a unit displacement, and all other displacements are proportionally less, depending on the mode shape.

Analytical Model of Track. Because the number of moving parts associated with just one track represents several hundred degrees of freedom, a structural finite element computer code, ADINA, was used to model the system. The finite element code provides a systematic method of developing a mathematical model for complicated systems by automatically setting up the equations of motion of the system using input information provided by the user. In this case the input information included such items as overall geometry, length of shoes, stiffness of bushings, and masses of road wheels. The total number of degrees of freedom in the track finite element model was 546. This included 80 shoes and 80 end connectors with three degrees of freedom each, the road wheels, the front idler, together with its connecting linkage to the front road wheel, the road arms, and the center of gravity of the hull.

The shoes were modeled as beams having a very high stiffness 46×10^6 lb/in. The end connectors were modeled as beams with torsional and longitudinal stiffness characteristics of the rubber bushings. The road arms were stiff along their longitudinal axis, but had torsional characteristics equivalent to the torsion bar suspension characteristics. Beams were also used to model the front idler/front road wheel linkage. Finally, very rigid, massless beams were used to connect the road arms, the sprocket, the three support idlers, and the front idler pendulum to the c. g. of the tank. Spring elements were used to model the road wheels, the front idler, the support idlers, and the sprocket. The complete model is shown in Figure 2, and a more detailed representation in Figure 3.

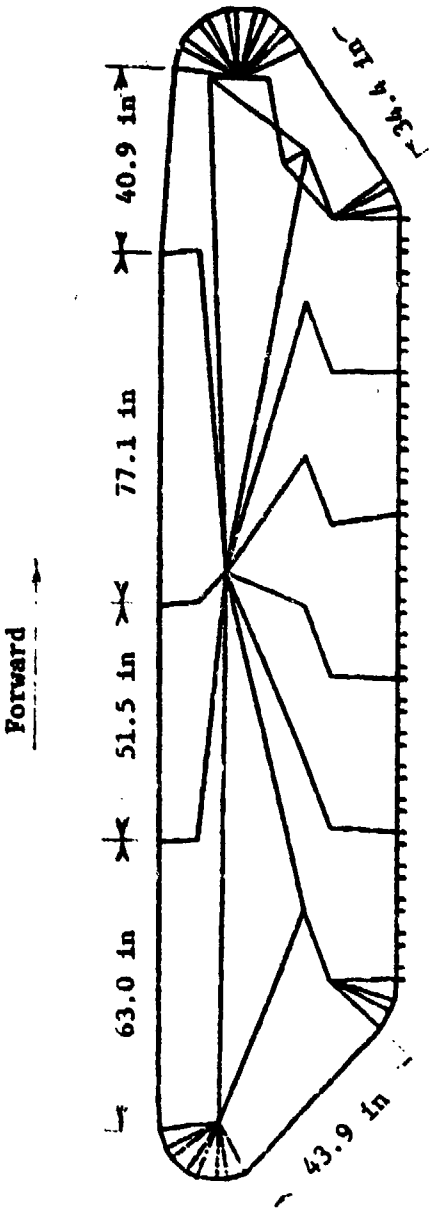

FIGURE 2. TWO-DIMENSIONAL FINITE ELEMENT MODEL OF T-142 TRACK ON M-60 TANK

Vibrating String Solution. The lengths of track which do not make contact with the ground can be approximately modeled as strings under tension supported at two points--for example, between support idlers. There is, however, one important difference involved in modeling the track as a tensioned string. In the classical solution of a vibrating tensioned string, it is assumed that the string has zero bending stiffness, whereas the track has a large bending stiffness due to the bushings. Nevertheless, as a general check on the finite element program, a comparison with frequencies based on vibrating string equations was considered worthwhile.

For a vibrating string of length, L, mass per unit length, ρ, and tension, T, the $r^{\underline{th}}$ harmonic, f_r, is given by

$$f_r = \frac{r}{2L} \sqrt{\frac{T}{\rho}}.$$

For the T-142 track, the value of ρ was approximately .0278 lb-sec^2/in^2. The nominal tension in the track was assumed to be 12,000 lb, so that the value of the radical was: $\sqrt{\frac{T}{\rho}}$ = 657 in./sec. The value of string natural frequencies for various lengths and harmonics is given in Table 3. The lengths used in Table 3 are the lengths of unsupported track shown in Figure 2.

TABLE 3. NATURAL FREQUENCIES, Hz, OF A VIBRATING STRING*

	Harmonic		
Length (in.)	1	2	3
77.1	4.261	8.522	12.783
63.0	5.214	10.428	15.642
51.5	6.379	12.758	19.137
43.9	7.483	14.966	22.449
40.9	8.032	16.064	24.096
34.4	9.549	19.099	28.647

(*) String tension = 12,000 lb

(*) String mass = .0278 lb-sec^2/in.^{2}.

Results. Following the calculation of frequencies based on vibrating string equations, the actual finite element model was exercised. The primary results of the eigenproblem solution are shown in Figure 3, in which the first 20 eigenvectors are plotted as dotted lines superimposed on the undeformed shape of the track (solid line). Only the track elements of the model are shown in those cases in which only the track is responding. When the road wheels respond, the complete finite element model is displayed in both the deformed and undeformed shape.

The first three eigenvectors are the longitudinal, pitch, and bounce modes, respectively, of the tank as a rigid body. The eigenvectors illustrated in Figure 3d, e, f, g, h, and k are analogous to the first modes of a tensioned string and can be compared to the first column of frequencies in Table 3 In general, all of the predicted natural frequencies for the first modes of the track section are about 15 percent higher than the tensioned string prediction. The reason for higher frequencies is that the track has a bending stiffness due to the bushings, whereas the classical tensioned string solution is assumed to have no bending stiffness. Mode h also shows the second mode of the 77.1-in. length track excited partially, whereas mode i shows that second mode shape as the primary excitation. Again, the predicted frequency for mode i (9.825 Hz) is 15 percent higher than the second mode of the tensioned string (8.522 Hz).

The tenth eigenvector in Figure 3j is actually a longitudinal mode of the track between the sprocket and front idler, although there are several transverse track modes being partially excited.

In Figure 3l, the twelfth track mode shape is the second mode between the rear support idler and sprocket, and has a natural frequency approximately 15 percent greater than the second mode of a 63-in. tensioned string.

The third mode of a 77.1-in. tensioned string and the second mode of a 51.5-in. tensioned string are approximately 12.8 Hz, as seen in Table 1. Both of these mode shapes are excited in the track at 14.79 Hz, Figure 3n, and 15.33 Hz, Figure 3r. There is also a partial response in Figures 3o, 3p, 3q, and 3s. Other mode shapes corresponding to a tensioned string are at frequencies higher than those calculated by the finite element code.

Forward →

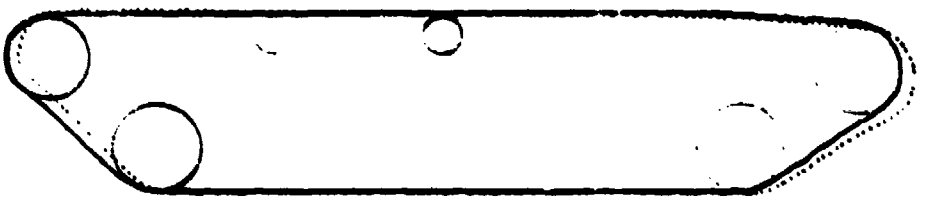

a. First Mode; f = .935 Hz

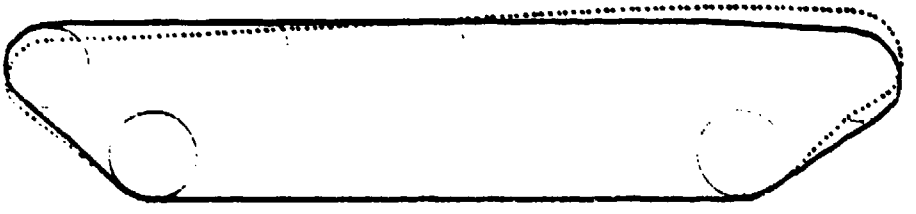

b. Second Mode, f = 1.858 Hz

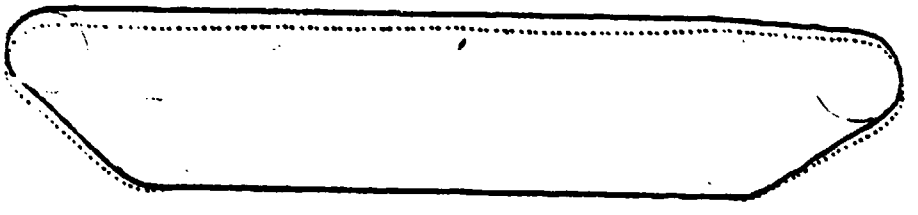

c. Third Mode, f = 2.321 Hz

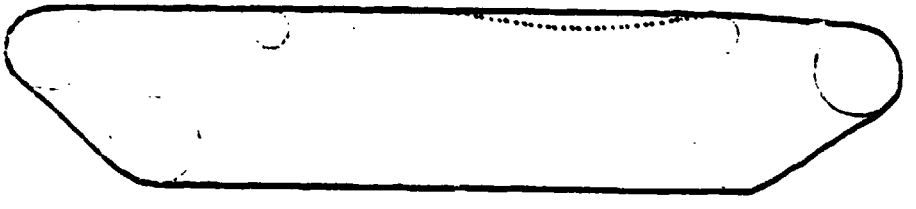

d. Fourth Mode, f = 4.873 Hz

FIGURE 3. MODE SHAPES OF T-142 TRACK

Forward

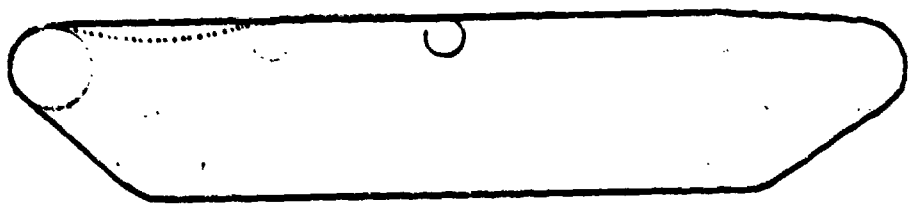

e. Fifth Mode, f = 6.015 Hz

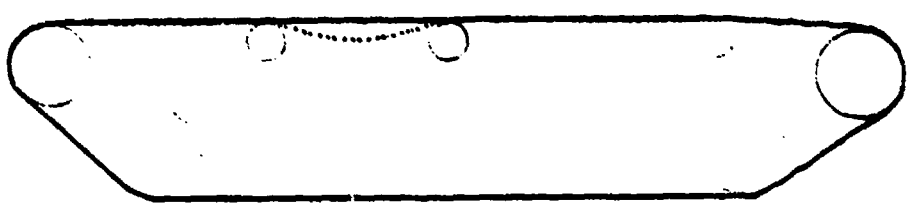

f. Sixth Mode, f = 7.393 Hz

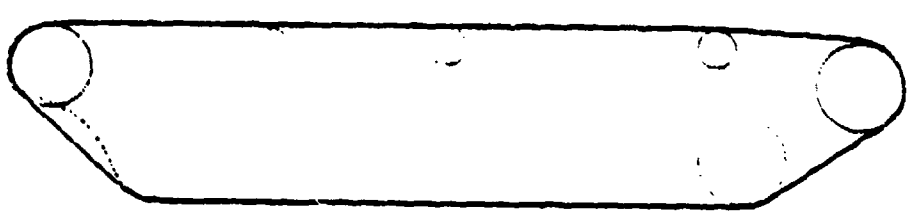

g. Seventh Mode, f = 8.806 Hz

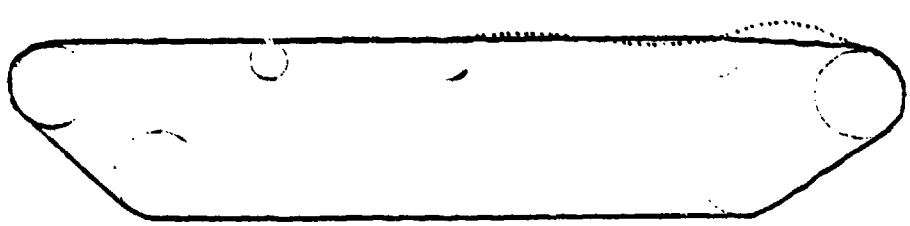

h. Eighth Mode, f = 9.320 Hz

FIGURE 3. (Continued) MODE SHAPES OF T-142 TRACK

Forward

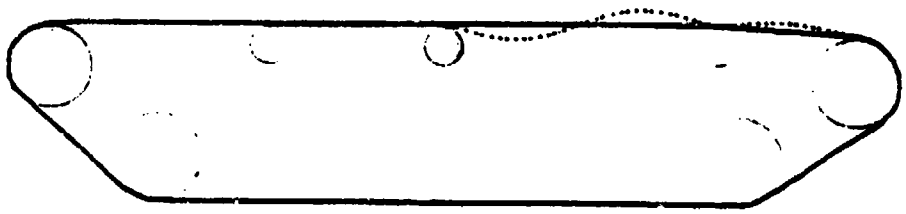

i. Ninth Mode, f = 9.825 Hz

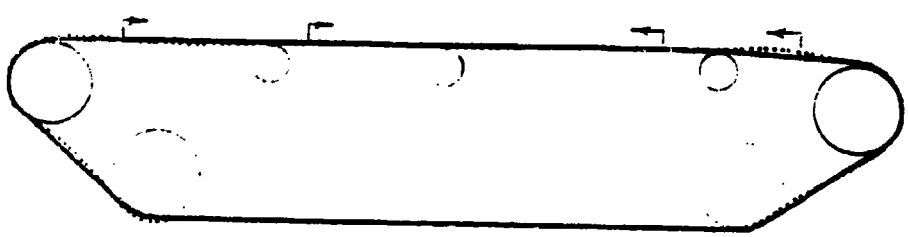

j. Tenth Mode, f = 10.05 Hz

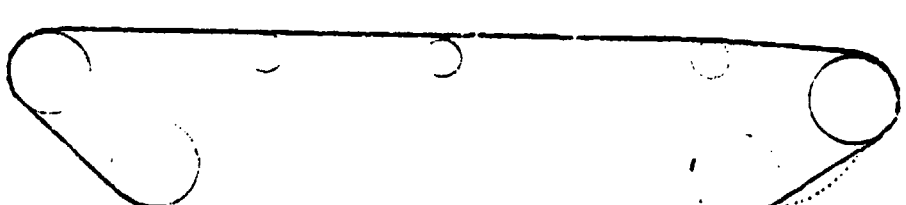

k. Eleventh Mode, f = 11.04 Hz

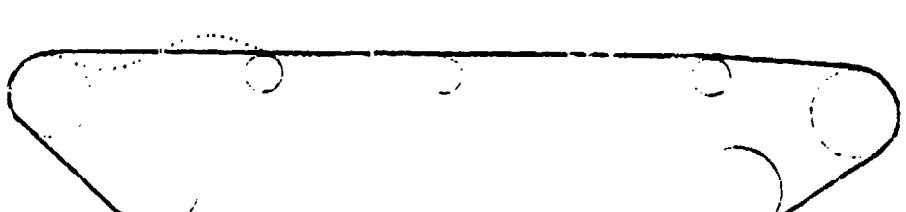

l. Twelfth Mode, f = 12.16 Hz

FIGURE 3. (Continued) MODE SHAPES OF T-142 TRACK

Forward →

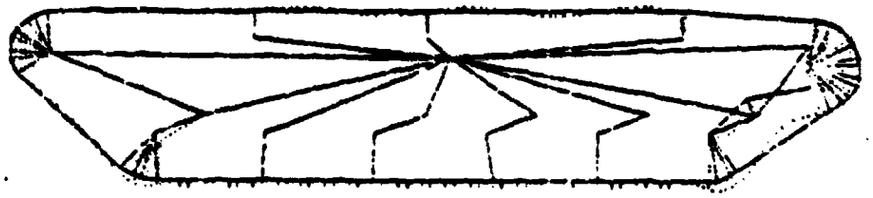

m. Thirteenth Mode, f = 14.73 Hz

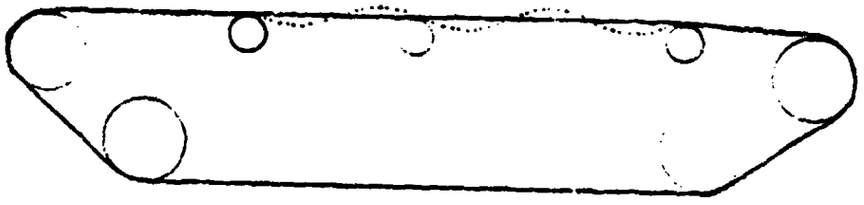

n. Fourteenth Mode, f = 14.79 Hz

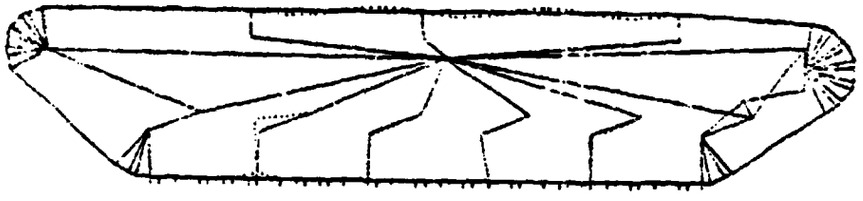

o. Fifteenth Mode, f = 14.82 Hz

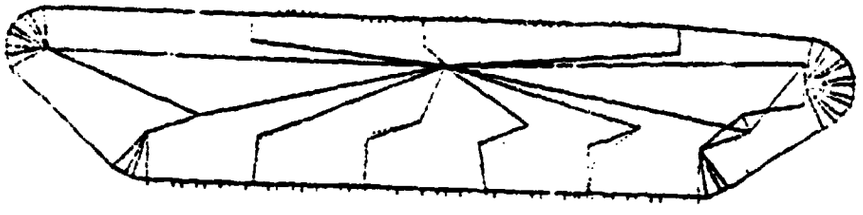

p. Sixteenth Mode, f = 14.90 Hz

FIGURE 3. (Continued) MODE SHAPES OF T-142 TRACK

Forward

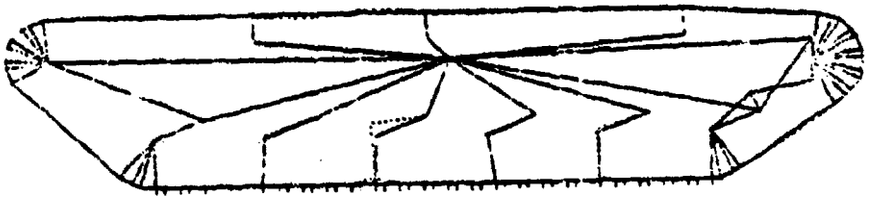

q. Seventeenth Mode, f = 15.00 Hz

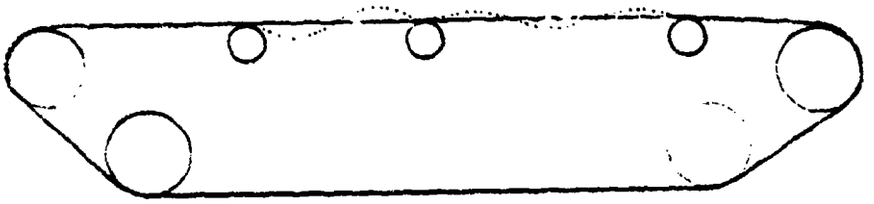

r. Eighteenth Mode, f = 15.33 Hz

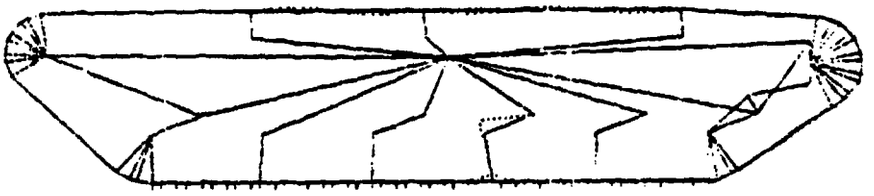

s. Nineteenth Mode, f = 15.46 Hz

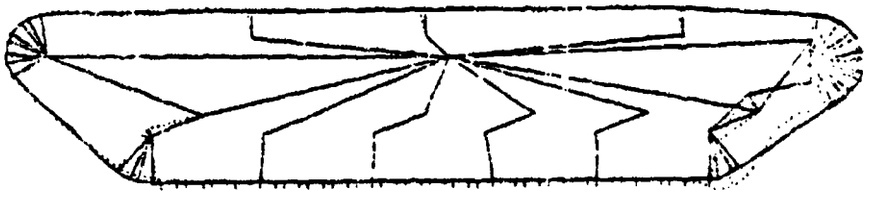

t. Twentieth Mode, f = 15.80 Hz

FIGURE 3. (Continued) MODE SHAPES FOR T-142 TRACK

The eigenvectors shown in Figures 3m, o, p, q, s, and t correspond primarily to road wheel hop natural frequencies at about 15 Hz. It is interesting to compare Figure 3m to 3t, in which both the front and rear road wheels are responding. In Figure 3m, the road wheel motion is in phase, whereas, in Figure 3t, the road wheels are out of phase. In both cases, the second mode of the track between the front idler and front road wheel is responding. Normally, this would not be expected until (1.15) x (19.099) = 21.96 Hz, but the interaction between the track and road wheel has reduced the responding frequency.

In summary, the results to date indicate the usefulness of finite element computer techniques for modeling complex dynamic systems. Note that in addition to predicting the frequencies at which the different lengths of track vibrate, the wheel hop and rigid body natural frequencies are also predicted. It can be observed that for the T-142 track, the track section natural frequencies are only 15 percent higher than can be determined by a tensioned string analysis. This percentage is, of course, dependent on the torsional stiffness of the bushings, and would be different for other track.

Chordal Action (CHORDACT)

As the track engages the sprocket, its effective moment arm varies a bit as the teeth move past the point of apparent tangency. Consequently, if the sprocket turns at constant angular velocity, the adjacent spans of track move sometimes faster and sometimes slower than their mean velocity, their speed varying cyclically as each link passes. Similar effects are seen at the road wheels and front idler. This variation of velocity has been widely recognized as a source of vibration in roller chain drives, and is known as chordal action.

If the tank also moves at constant velocity with respect to the ground, then the velocity variations must be absorbed by cyclically stretching and releasing the track in the span between the sprocket and the rear road wheel, and by shear deformation of the road pads. Periodic forces thus generated are transmitted to the hull through the sprocket shaft and the suspension, causing noise and vibration. In severe cases, the forces may also add significantly to the stressing of the track parts.

At highway speeds, sonic velocity in the track is no longer high enough to distribute the stretching throughout the available span of track in the available time. The excitation at the ends of the track spans generates force and deformation waves that travel along the track at sonic velocity. The amplitude of a sonic force wave is independent of the length of the track span or its initial tension. It is directly proportional to the velocity variation and to the square roots of the mass per unit length and the spring rate of the track. Sonic velocity in the T-142 track is only about 800 ft/sec, or a little more than 10 times the velocity of the track itself at 50 mph. Within the speed range of interest, therefore, increased speed results in stronger excitation of chordal effects.

The kinematics of the double-pin T-142 configuration on an 11-tooth sprocket can be worked out in detail if it is assumed that the span is straight, so that the track flexes about only one pin at a time. The maximum longitudinal displacement from mean position is ± .0062 inch, and the velocity variation is from -1.08% to +0.40%. If the .0062-inch displacement is distributed throughout the track strand from the sprocket to the rear road wheel, the resulting force is only 330 lb. At 50 mph, however, the sonic force wave resulting from a 1.08% velocity variation would peak at 2500 lb. This would be a compression wave at the sprocket entrance and a tension wave at the sprocket exit. The peak-to-peak tension variation would be 3450 lb. at both locations. These forces would not be high enough to cause distress to the track. Applied to the hull, however, they could be a significant source of noise.

By way of comparison, a single-pin track having the same 6.94-inch pitch would run on an 11-tooth sprocket with a longitudinal displacement from mean position of ± .018 inch and a maximum velocity variation of -2.68%. In practice, of course, the pitch of the single-pin track would probably be somewhat shorter than this.

The kinematics of the double-pin track as it rounds the rear road wheel were more difficult to define because the shoes are in rolling contact with the wheel, and their precise attitude at any time is not, in general, known. Two positions of symmetry do exist, however, if dynamic effects are ignored. These are when a shoe is centered half way between the entrance and exit points, and when an end connector is so centered. By assuming the middle of the centered link to lie tangent to the road wheel, it was possible to derive the positions of all of the links in contact with the wheel. It was calculated that there is .018 inch more track on the road wheel when the end connector is centered than when the shoe is centered. Thus, the longitudinal

displacement from mean position is at least 50% higher at the rear road wheel than at the sprocket. The sonic forces developed may well be higher, also. The front idler and the front road wheel may also be sources of higher sonic forces than the sprocket. Attention was focused on the rear wheel because the higher tension in the span from the sprocket down makes the system less forgiving there.

In the above analysis, it is assumed that the track flexes about only one pin at a time. In reality, bushing stiffness and link inertia cause the span to arch or assume a wave shape, so that several pins participate at once in the flexing of the track. This tends to smooth out chordal excitation. Furthermore, the whole system is softer because longitudinal displacement can be accomodated by pulling the span to a straighter profile instead of by stretching the track structure. Consequently, chordal forces approach the calculated magnitude only if apparent track tension is very high, and the anticipated increase of chordal force with speed may not be observed otherwise.

In order to determine whether resonance or superposition of waves traveling in opposite directions might generate high cyclical force in the highly-tensioned span between the sprocket and the rear road wheel, a simple two-dimensional finite-element computer simulation of this span (CHORDACT) was written. The model is shown in Figure 4. The span was assumed to be straight, with flexing about one pin at a time at each end, and no effects of track velocity were included. Consequently, the results are more to be trusted under low speed, high tractive effort conditions than when speed is high and engine power limits the tractive effort.

The finite-element model includes ten track pitches, the contacts with the sprocket, road wheel, and ground, and the motion of the road wheel on its suspension arm. It is excited at each end by imposing periodic motions having the amplitude, wave form, and phase relationship determined by the previously-described kinematic analysis. The frequency of excitation is varied to simulate different vehicle speeds. Figure 5 shows the wave form used for the excitation.

CHORDACT performs numerical integrations of the equations of motion of the various masses to determine the time histories of their positions, and from these positions it computes time histories of the various forces of interest. Figure 6 is typical of the program's output. The cyclical component of track tension at the sprocket entrance is plotted as a function of time, with the first .02 second of the run deleted because it was dominated by unreal-

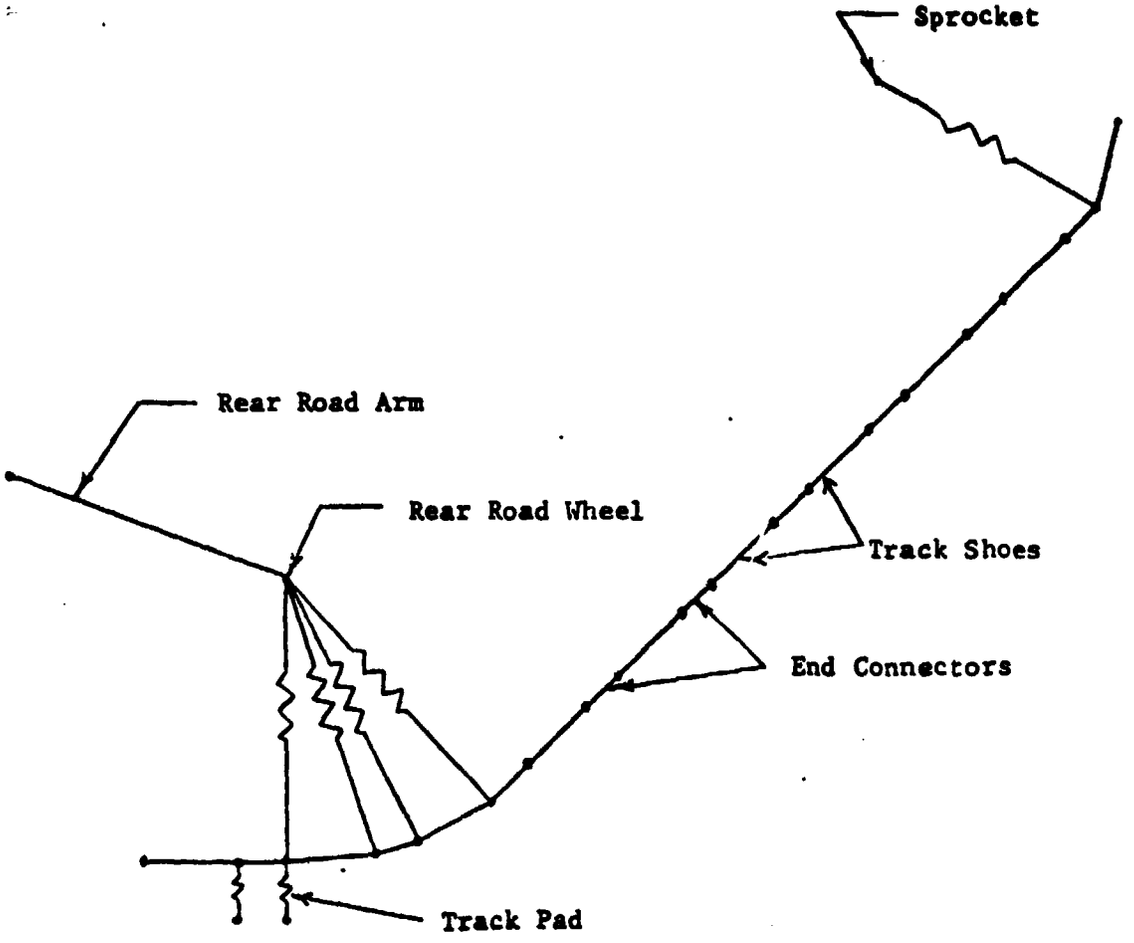

FIGURE 4. SKETCH OF T-142 TRACK SECTION MODELED TO PREDICT VARIATION IN TRACK TENSION DUE TO LONGITUDINAL CHORDAL ACTION AT SPROCKET ENTRANCE AND REAR ROAD WHEEL EXIT

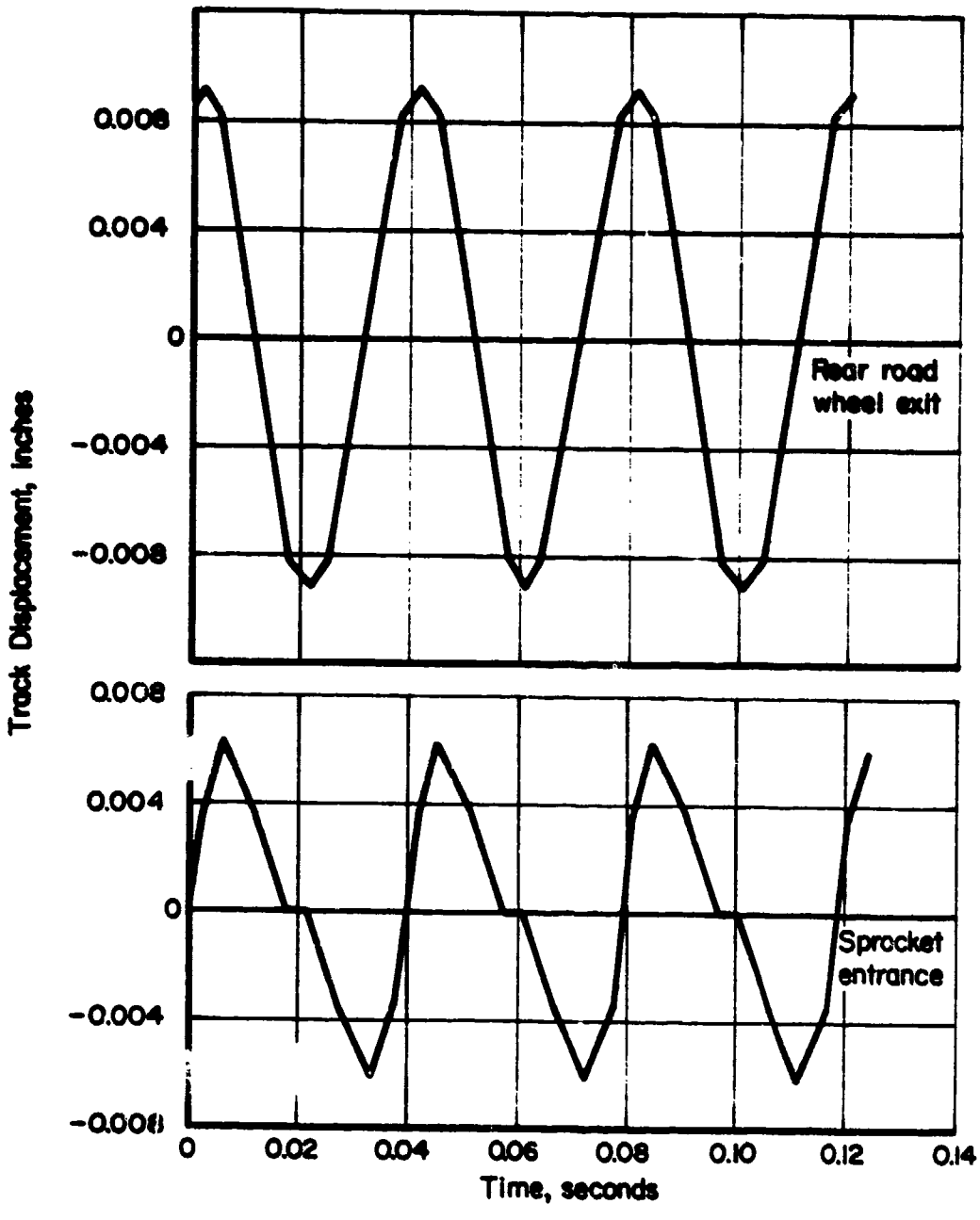

FIGURE 5. LONGITUDINAL DISPLACEMENT OF T-142 TRACK DUE TO CHORDAL ACTION AT 10 MPH

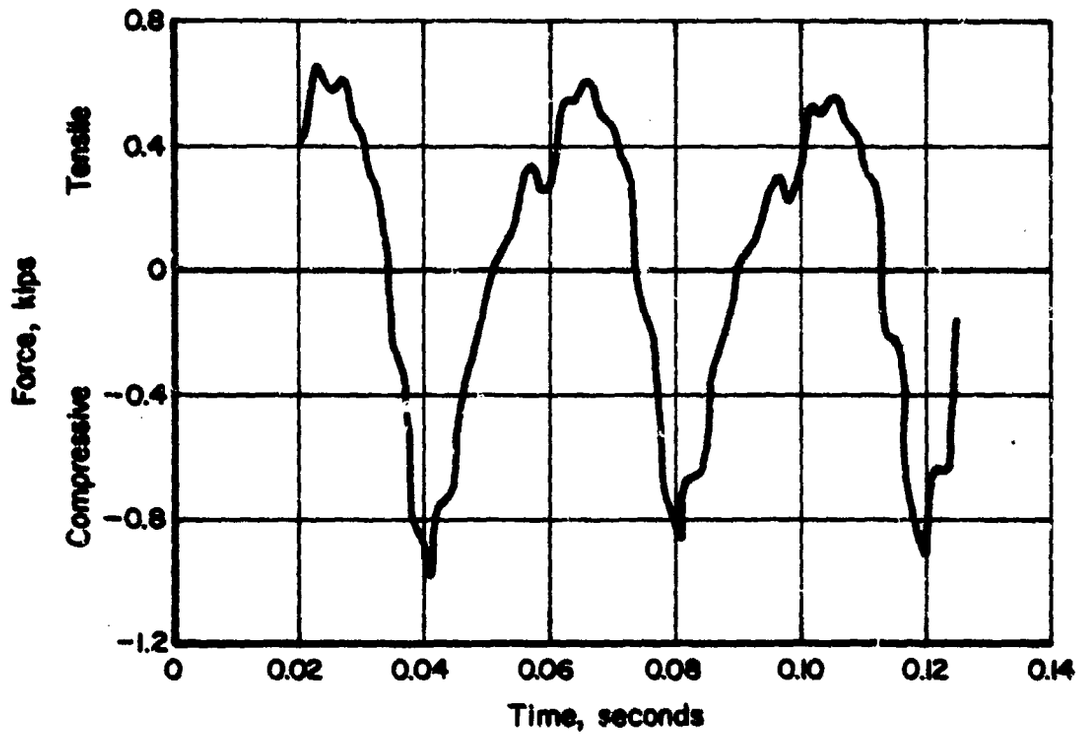

FIGURE 6. TIME VARIATION IN TRACK TENSION AT SPROCKET ENTRANCE DUE TO LONGITUDINAL CHORDAL ACTION AT SPROCKET ENTRANCE AND ROAD WHEEL EXIT AT A TANK SPEED OF 10 MPH (T-142 TRACK ON M-60 TANK)

istic transients. It can be seen that a steady-state periodic response is achieved very quickly. From this plot, the peak-to-peak tension variation can be determined for the particular operating conditions of the run.

The results of several CHORDACT runs at different speeds and with varying damping are shown in Figure 7. At 50 mph, a peak-to-peak tension variation of 3100 lb. is predicted, agreeing well with the 3450 lb. predicted by the simple sonic analysis described earlier. As the speed is decreased, sonic theory predicts that the tension variation should fall off rapidly, while CHORDACT detects resonances at 30 and 15 mph which cause the tension variation to remain high. In no case, however, does it exceed 3600 lb.

Comparing the results with those of TRACKVIB, the resonance at 30 mph (75 Hz) is thought to be the first longitudinal natural frequency of the track span. The resonance at 15 mph is near the 34 Hz wheel-hop frequency.

All of the CHORDACT runs were made with a 20,000 lb. mean tension. Critical clamping for a rubber-bushing pin was taken to be 140 in-lb. sec/rad in torsion and 380 lb. sec/in in the radial direction. The actual damping characteristics of the bushings are not known.

As described in the next section, the TRACKDYNE computer simulation of track running over the front idler includes the entire span from the idler to the front road wheel, and also a dummy span approaching the idler. It comprehends the cyclical tension generated in those spans from any phenomena operating at the idler or at the road wheel entrance. As shown in Figure 8, TRACKDYNE results verify that the cyclical tension depends importantly on apparent track tension, and that the magnitude is generally below that predicted by simplified analyses. Contrary to the results of simplified analyses, TRACKDYNE indicates that cyclical tension decreases as speed is increased from 35 to 70 mph, at least in the vicinity of the idler.

Resonance is to be expected when the chordal excitation frequency coincides with a natural frequency of the track as predicted by TRACKVIBE. At present, TRACKDYNE does not include enough of the track circuit to respond meaningfully in this regard. A run at 20 mph and 5000 lb apparent tension did, however, predict an unexpectedly large cyclical variation in the inlet tension of 2800 pounds, which was evidently the result of a resonance.

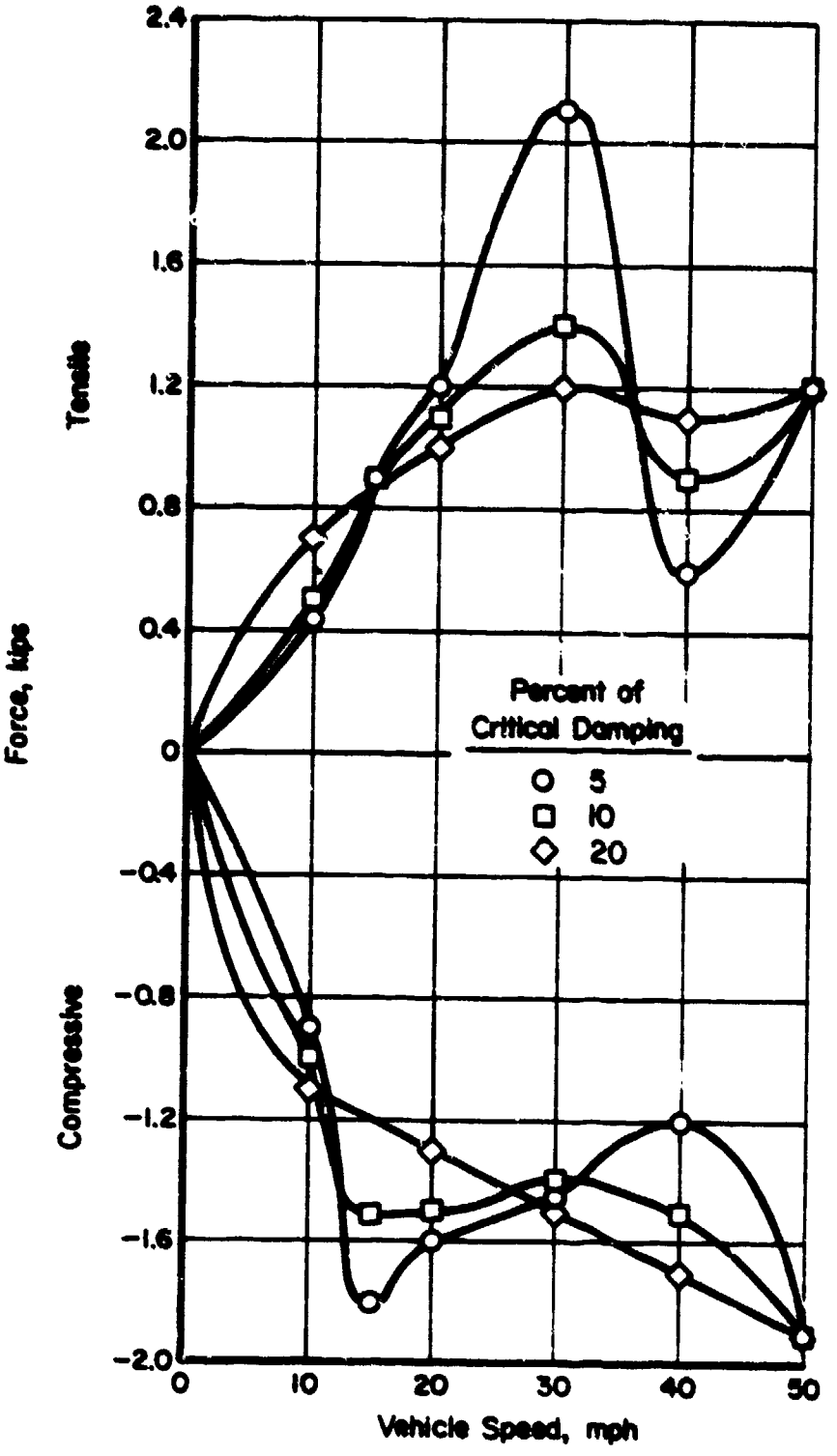

FIGURE 7. VARIATION IN TRACK TENSION AT SPROCKET ENTRANCE DUE TO LONGITUDINAL CHORDAL ACTION AT THE SPROCKET ENTRANCE AND REAR ROAD WHEEL EXIT (T-142 TRACK ON M-60 TANK)

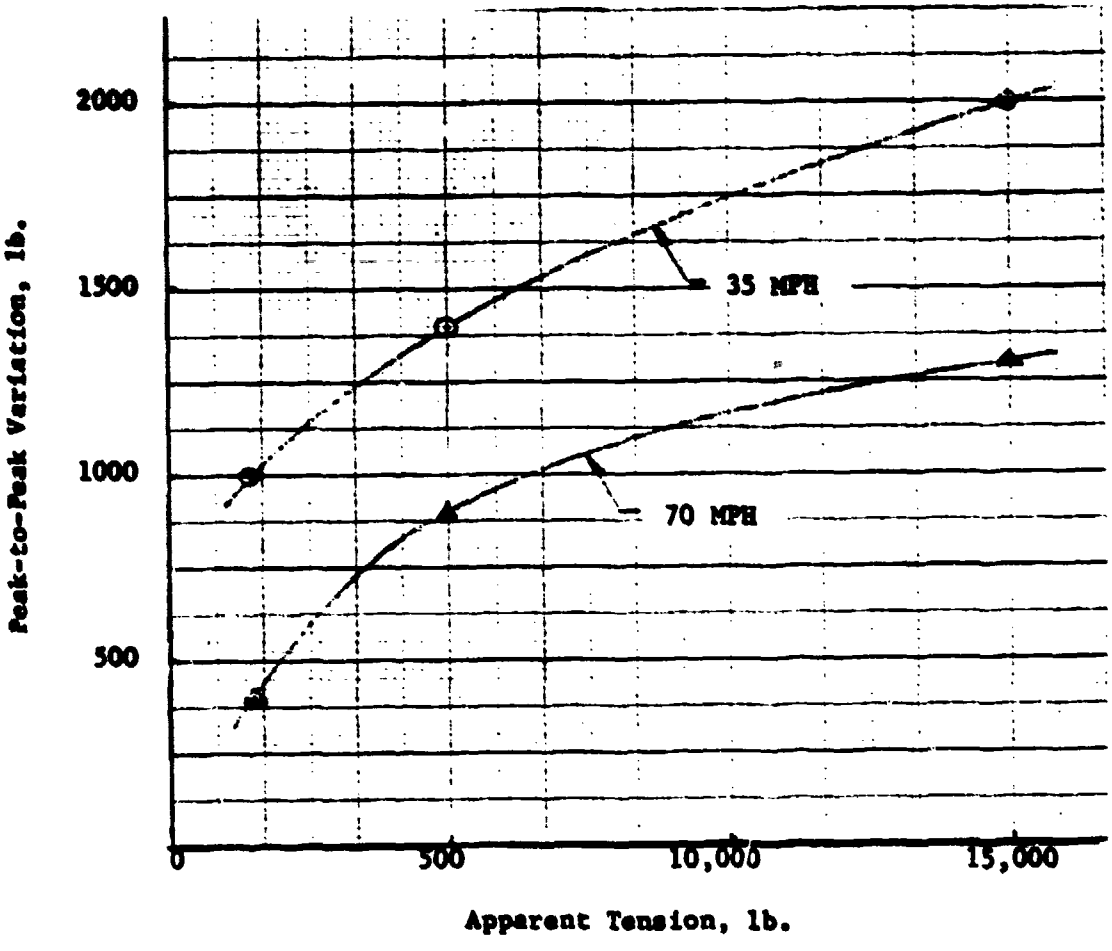

FIGURE 8. CYCLICAL TENSION IN TRACK ADJACENT IDLER AS GIVEN BY TRACKDYNE (T-142 TRACK)

In summary, tensile forces due to chordal action have not been identified as a source of distress to the track because the forces predicted are an order of magnitude below the design strength of the track. Cyclical forces transmitted to the hull could, however, be a source of annoying noise. The peak-to-peak tension excursion probably does not exceed 3000 pounds unless it is amplified by a resonant vibration. The magnitude of such vibrations could be predicted by an expanded version of the TRACKDYNE simulation that would include the entire track circuit.

Track Path and Dynamic Tension

If a track having no internal stiffness were stretched statically over a pair of sprockets (or a sprocket and a wheel), it would form a straight-line tangent to their surfaces, neglecting the effects of gravity. In a real track, the spring torque of the rubber bushings provides internal stiffness that causes the track to arch outward beyond the straight-line tangent. It then curves around the sprockets somewhat before becoming tangent to them, such that the arcs of contact are reduced. The amount of arching will be reduced if the track tension is increased by separating the sprockets. This tends to stretch the track path into a straighter line. Thus, the longitudinal spring rate of the track has components due to deformation of bushings and pins and another component due to straightening of the track path. Conversely, the track tension cannot be reduced to zero by any small decrease in the sprocket center distance. The track will respond by arching further to maintain its path length so that there is still some tension. In long horizontal runs, such as that from the drive sprocket to the front idler, gravity may cause the center of the arch to collapse, but the sections of track near the ends of the run will still maintain their arch shape.

If now the rubber-bushed track is considered to be operating at high speed, dynamic forces generated within the track influence its path in two important ways. First, a centrifugal tension is developed which, perhaps contrary to intuition, is almost independent of sprocket diameter and independent of angle of wrap. The centrifugal tension exists at all points along the length of the track and its magnitude is given by

$$T_c = m V^2$$

where m is the mass of the track per unit length, and V is its velocity relative to the sprocket centers. At 50 mph, a track having the mass of the T-142 will develop a centrifugal tension of 22,000 lb.

If the center of mass of the track were located on its pitch surface, the centrifugal tension would be equal everywhere in the track and completely independent of sprocket diameter. In fact, the center of mass of most tracks is farther out because of the weight of the road pads. Consequently, the center of mass travels at higher velocity on the sprockets than in the spans, and the TRACKDYNE results showed that centrifugal tension is a few hundred pounds higher there. The effect of centrifugal tension is to stretch the track by deformation of its bushings, pins, and other structural parts. The total path length is thus increased and the rubber-bushed track accommodates this by forming a more highly-arched path between the sprockets. The changes in track path and sprocket force are the same as those produced in the static case by decreasing the center distance. Thus, the preload forces carried through the hull are actually reduced if the center distance is fixed. The dynamic tension of a span is thus composed of two components--an apparent component that contributes to power transmission and forces transmitted to the hull, and a centrifugal component that is undetectable by force measurement external to the track except as its presence may be inferred by noting the result of a change in speed.

The second way in which dynamic forces influence the track path results from the rotary momentum of the track parts about their own centers of gravity as they exit from the sprockets. As the links tend to continue tumbling at sprocket angular velocity, they tend to carry the track in an arc paralleling the sprocket circumference, in a path that comes closer to the line between the sprocket centers than does the straight-line tangent. The dynamic effects of angular momentum thus influence the track path in the opposite direction from the arching produced by the rubber bushings. Roller chains, which have no springs associated with the pivots, behave in this way. As the chain moves farther from the sprocket, its tension eventually stops the rotation of the links and pulls them back toward the straight-line tangent path. Having reached that path, though, they now have outward velocity and continue past it. Oscillations continue about the straight-line path until they are damped by friction, forming standing waves. That is, the path form is sinusoidal and appears fixed in space to an observer who is stationary with respect to the sprocket centers. The phenomenon is familiar to anyone who has spun the free-hanging hand chain of a hoist and observed the path followed by the chain as it starts upward.

Solution for One Span. In order to quantify by hand calculations these various effects that simultaneously influence the track path, the track was modeled as a homogeneous band having the same stiffness, mass per unit length, and rotary inertia per unit length as the actual linked track. The band was considered to be running on a smooth drum having the pitch radius of the sprocket. The center distance was considered to be infinite, so that the band eventually became asymptotic to a straight line. Differential equations were formulated and a general solution was achieved.

The slope of the tangent to the track path at any distance, s, from the point of tangency is of the exponential form

$$\theta = \frac{1}{\beta r_p} e^{-\beta s}$$

where r_p = pitch radius of sprocket

$$\beta^2 = \frac{\text{total tension - centrifugal tension}}{\text{dynamic stiffness}}$$

The dynamic stiffness is defined as the difference between a bushing spring rate term and an angular momentum term:

$$\text{Dynamic stiffness} = \frac{\alpha}{n} - I_L N V^2$$

where α = torsion spring rate of bushings on one pin
n = number of pins per unit length
I_L = moment of inertia of one link
N = number of links per unit length
V = pitch line velocity.

This equation applies equally to the entrance and exit of the sprocket. It can be reduced to rectangular coordinates by taking the first few terms of the series expansions of the sine and cosine functions:

$$x = s - \frac{1}{4\beta^3 r_p^2}\left(1 - e^{-2\beta s}\right) - r_p \operatorname{SIN} \frac{1}{\beta r_p}$$

$$y = \frac{1}{\beta^2 r_p}\left[1 - e^{-\beta s} - \frac{1}{18\beta^2 r_p^2}\left(1 - e^{-3\beta s}\right)\right] + r_p \cos\frac{1}{\beta r_p}$$

The height of the arched profile is approximated by the offset of the asymptote from the tangent to the sprocket:

$$h = \frac{1}{\beta^2 r_p}\left[1 - \frac{1}{18\beta^3 r_p^2}\right] - r_p\left[1 - \cos\frac{1}{\beta r_p}\right].$$

The actual path length is longer than the straight-line tangent by

$$\Delta = \frac{1}{12\beta^3 r_p^2} .$$

The above solution applies to low and moderate speeds, where the dynamic tension is positive and the track follows an arched path. If the speed is sufficiently increased, it can be seen that the angular momentum term becomes larger than the bushing spring rate term. The dynamic tension then becomes negative and β becomes imaginary. The physical meaning of this is that the track has gone into a standing wave mode of operation. For a track with the characteristics of the T-142, this transition was predicted at 46 mph.

In the above analysis, the effective moment of inertia of one link, I_L, was taken to be the moment of inertia of the two shoes about their center of mass, plus the effect of a pin and half the mass of the associated connectors acting as point masses located at the pin centerlines. However, later experience with the TRACKDYNE computer simulation, which predicts the path of an actual linked track, indicated that the dynamic stiffness calculated this way was actually too low. Consequently, the transition speed may be 10 or 15 mph higher than indicated by the continuous band analysis.

Transition to the standing wave mode does not mean that the track tension suddenly becomes substantially higher or that rough operation will necessarily result. The transition speed is best understood, on the contrary, as the speed at which the tension required to make the track follow a straight-line-tangent path becomes zero. At this one speed, the track has no tendency to take up slack length by making arcs or waves, so that a disorganized fluctuation of the path shape would be expected. It is thought, however, that

there is substantially less ability to store and redeliver the rotary kinetic energy of the links as the standing wave mode is approached and entered. The potential power loss, if this is true, is several hundreds of horsepower, and one objective of the TRACKDYNE computer simulation was to further explore the mechanisms of power loss at high speed.

Solution for Track Circuit. The actual operating tension of the track under various conditions of speed, tractive effort, and initial preload may be found by simultaneous application of the solutions for each span to all of the sprocket or wheel entrance or exit points in the track unit. The strand on the ground is assumed to follow the straight-line tangent path. This leaves the exit from the rear road wheel and the entrance to the drive sprocket operating at high tension, and four other points operating at low tension. The solution proceeds as follows:

Assuming the initial tension to be acting statically everywhere in the track, the path length can be calculated knowing the number of pitches and the amount each will be stretched by the preload. β can be evaluated taking $V = 0$, and the difference between the path length and the straight-line tangent length can be calculated. The straight-line tangent length of the track circuit is then known.

If tractive effort and speed are now applied, about one-third of the track length, from an effective point of ground contact up to the drive sprocket, is highly tensioned so that it is stretched and straightened. The rest of the track contracts correspondingly, and its tension may increase or decrease depending on the relative values of speed and tractive effort. In general, the total path length will be longer.

Tight and slack side tensions are most easily found by iteration. If a tight side tension is assumed, the slack side tension is calculated knowing the tractive effort. The total length of the track path can be calculated, knowing the portion of track exposed to each tension. The difference between path length and straight-line tangent length can also be calculated for each strand, yielding a trial value for the total straight-line tangent length of the track circuit. This value should be the same as that calculated for the static preload case. If not, the tight side tension is appropriately changed and another trial is made.

Calculations have been made for the T-142 track, assuming a static preload of 12,000 lb. The results of the extreme cases were as follows:

	Tight Side Tension	Slack Side Tension
Slow Speed, 40,000 lb Tractive Effort	43,040 lb	3,050 lb
35 mph, 3500 lb Tractive Effort (about 750 hp)	15,670 lb	12,170 lb

The sprocket exit and entrance paths for 35 mph and 3500 lb tractive effort are plotted in Figure 9. It can be seen that the slack side leaves the sprocket 23.3 degrees before the point of apparent tangency and arches to a point 1.01 inches beyond the straight-line tangent. The tight side enters the sprocket 12.7 degrees beyond the point of apparent tangency and arches only 0.30 inch. The centrifugal tension in this case is 10,700 lb. Since centrifugal tension is almost as high as the slack side tension, arching there is pronounced.

Steady-State Dynamic Track Stimulation (TRACKDYNE)

During the last six months of the project, a computer programming task was undertaken to simulate in detail the actual running of a double-pin track around its circuit by computing, over a period of time, the simultaneous motions of the component parts as they interact with their neighbors in the track and with the wheels, sprocket, and ground. This effort was made because of continued uncertainty as to the motions of track parts as they enter and leave contact with the wheels and sprocket. It is necessary to know their motions to assess the energy lost in accelerating and decelerating the links, to evaluate with confidence the severity of impact and vibration, and to predict the results of design changes which affect the weight, spring rate, or damping of the parts.

To adequately answer these questions, the simulation must be detailed enough to accurately model the interaction of the track with its surroundings. When a track shoe contacts a wheel, for instance, the center of contact may be near the center of the flat of the shoe, or it may be near the edge of the flat, or the corner of the shoe may be indenting the wheel. The spring rate

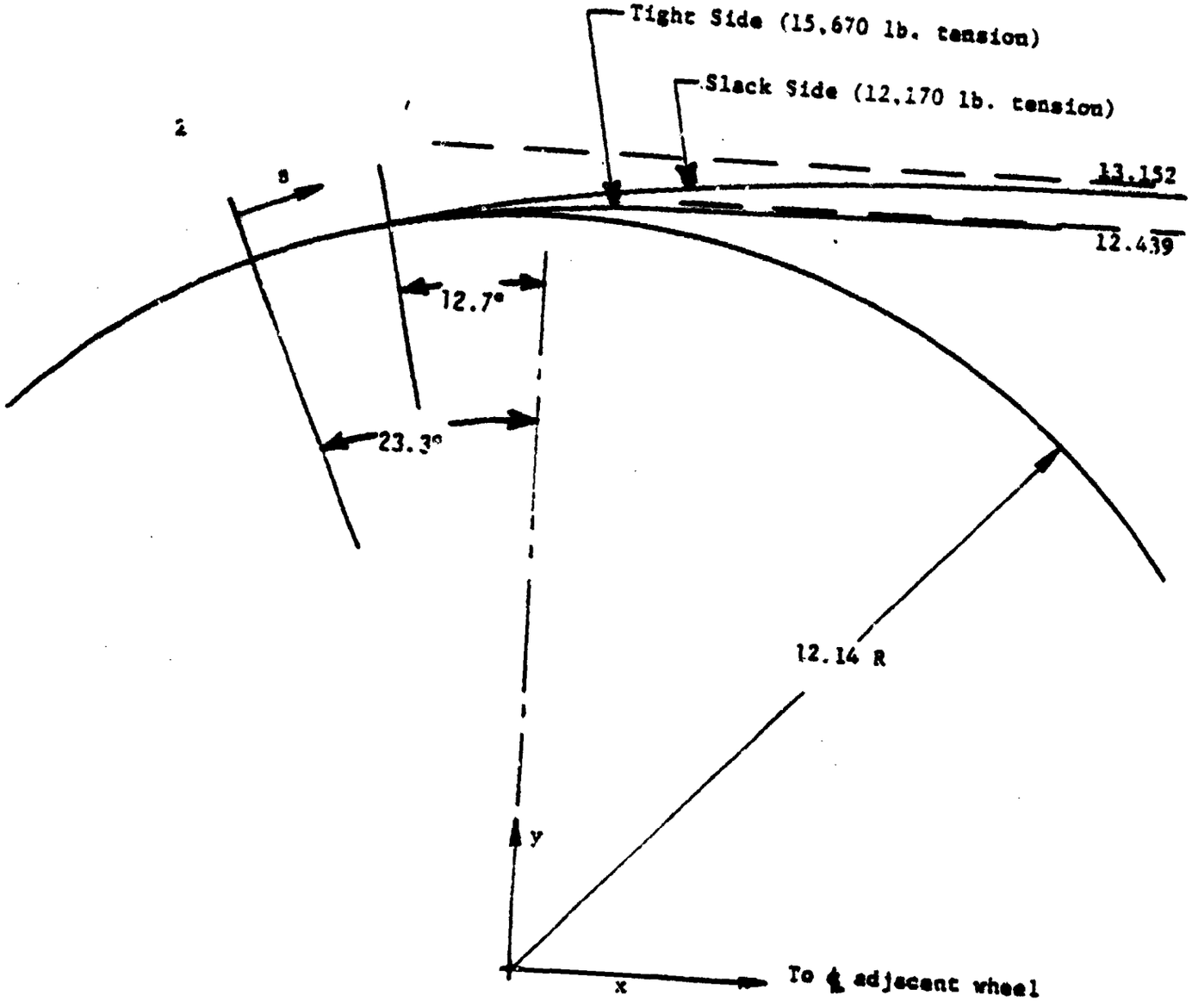

FIGURE 9. MEAN DYNAMIC PATH OF TRACK

T-142 track at 35 mph, 3500 lb/side tractive effort, 12,000 lb static preload.

and damping varies accordingly, and, in addition, the spring is nonlinear because the rounded surfaces bring more area into contact under heavier loads. The spring rates and damping in the tangential direction are different than those in the normal direction, and there is also sliding, depending on the normal force and the coefficient of friction. On the other hand, a three-dimensional model is not needed because the operating conditions of interest are steady-state ones that impose generally uniform conditions across the width of the track. The PINSTRESS analysis provides spring rates by which the radial sag of the track center on the sprocket can be included.

Since the task was challenging, a logical first step was to write a portion of the program dealing with track action over the front idler and down onto the front road wheel. This also appeared to be a portion of the task that could be completed soon enough to bring a useful return of information within the present report period. This IDLER portion of the TRACKDYNE program is now completely operational and it has been used to study the dynamic action of the T-142 Track both at conventional speeds and at higher speeds that have not yet been reached by actual tracked vehicles. As far as is known, this is the most advanced program that has been developed for studying the precise dynamics of rubber-bushed, linked track.

The TRACKDYNE program provides a detailed history throughout a pitch-passage cycle of the motions of the track parts and the forces affecting them. It also sums the energy dissipated in each damping element during a cycle and performs an energy balance for the entire system. The IDLER section provides a framework that can readily be expanded to include the entire track circuit.

Description of Model. The present TRACKDYNE model includes a span of track approaching the idler, the wrap-on, carry-around, and wrap-off areas of the idler, the full span to the front road wheel, and the wrap-on at the front road wheel. As many as thirty track links can be simulated at any given time, though only twenty-three are needed to reproduce the M-60 geometry. The circuit geometry is illustrated by Figures 10a and 10b, which are actual Calcomp plots of the track geometry under two different conditions. Figure 10a shows the track geometry when running at 35 mph with 1500 pounds apparent

tension, while Figure 10b represents the 70 mph, 1500 pound apparent tension condition. (These plots are discussed further on page 72.)

In the TRACKDYNE computer simulation, the track is allowed to remain on the road wheel until it is carried around out of the area of interest, where successive links are removed from the system as they arrive. At the same time, new links are successively introduced at Position 1 so that there are always 23 in the system and the available running time is unlimited. The dimensions and number of shoes in the system are easily changeable, and the idler may have a different diameter than the road wheel.

Each link of the double-pin track is modeled as two independent rigid masses, one representing the two shoes, and the other representing a combination of the two end connectors, the centerguide, and the two pins. Only motions in the plane of the track circuit are considered. The center of shoe mass may be offset from the line connecting the pin centers. The masses are connected by linear springs and viscous dampers representing the combined tensile deflections of the bushings, pins, and binocular tubes in two directions, and by torsional springs and viscous dampers representing the torsional characteristics of the bushings.

The idler and road wheel are modeled as rigid masses (except for their rubber surfaces) of appropriate moment of inertia turning on frictionless bearings. Since only part of the track circuit is being simulated, the centers of the wheels are fixed.

The shoe-to-wheel (or idler) contact is modeled as a combination of a linear spring and a spring whose force varies as the square of deflection. The system is predominantly square-rate because of the increase in contact area as the round wheel indents the flat of the shoe. A combination of viscous and dry friction dampers is used to reproduce the damping characteristics of the shoe, which were determined by tests at Battelle earlier in the program. Tangential deflections are modeled similarly, but with different spring rates and damping constants. Sliding is allowed when the ratio of tangential force to normal force exceeds a specified coefficient of friction. Lower spring rates and damping constants are used if the center of contact is off center on the flat of the shoe, or if the corner of the shoe is in contact with the surface of the wheel.

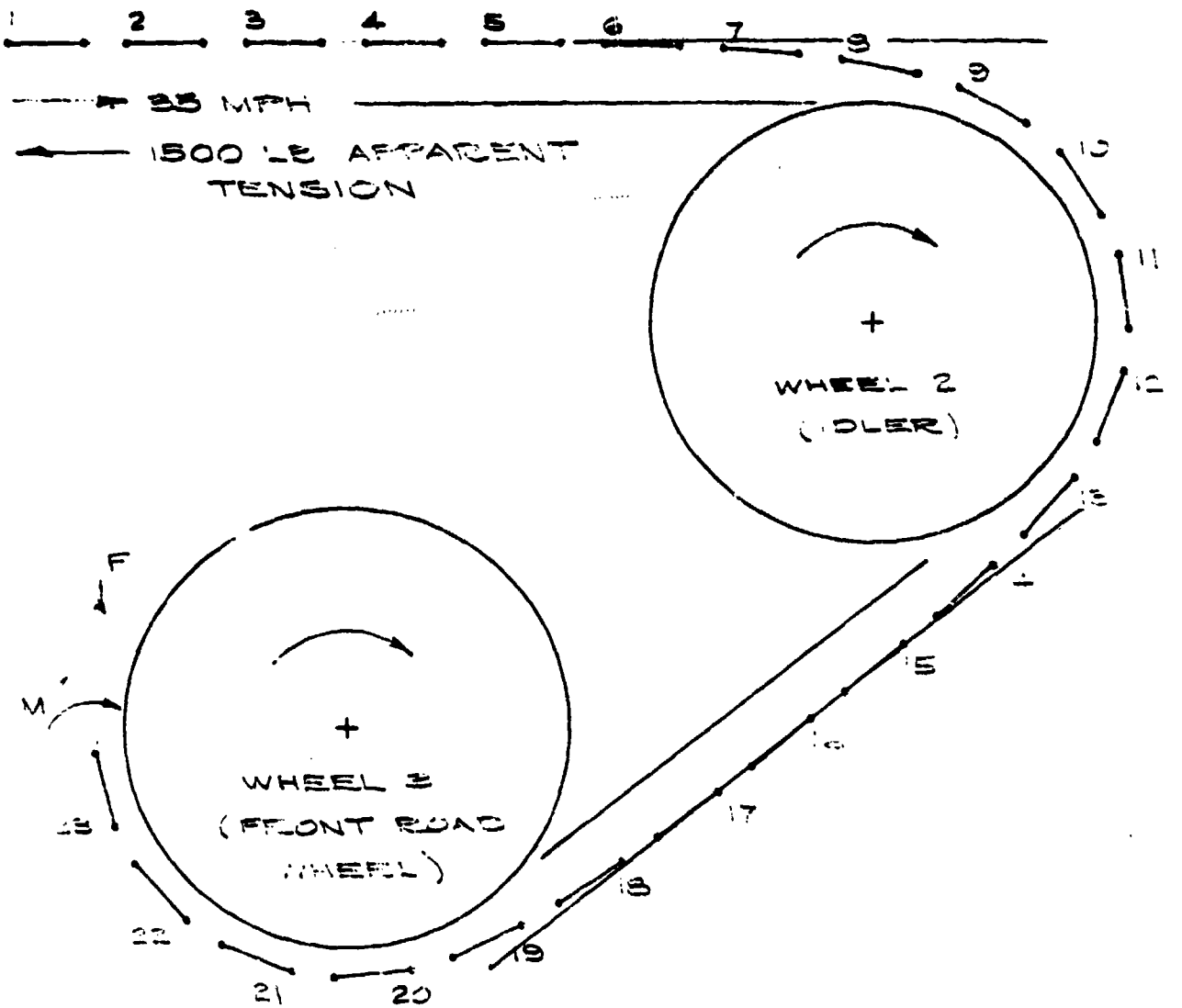

FIGURE 10a. TRACKDYNE PLOT SHOWING EFFECT OF SPEED ON TRACK PATH (35 MPH, 1500 LB APPARENT TENSION)

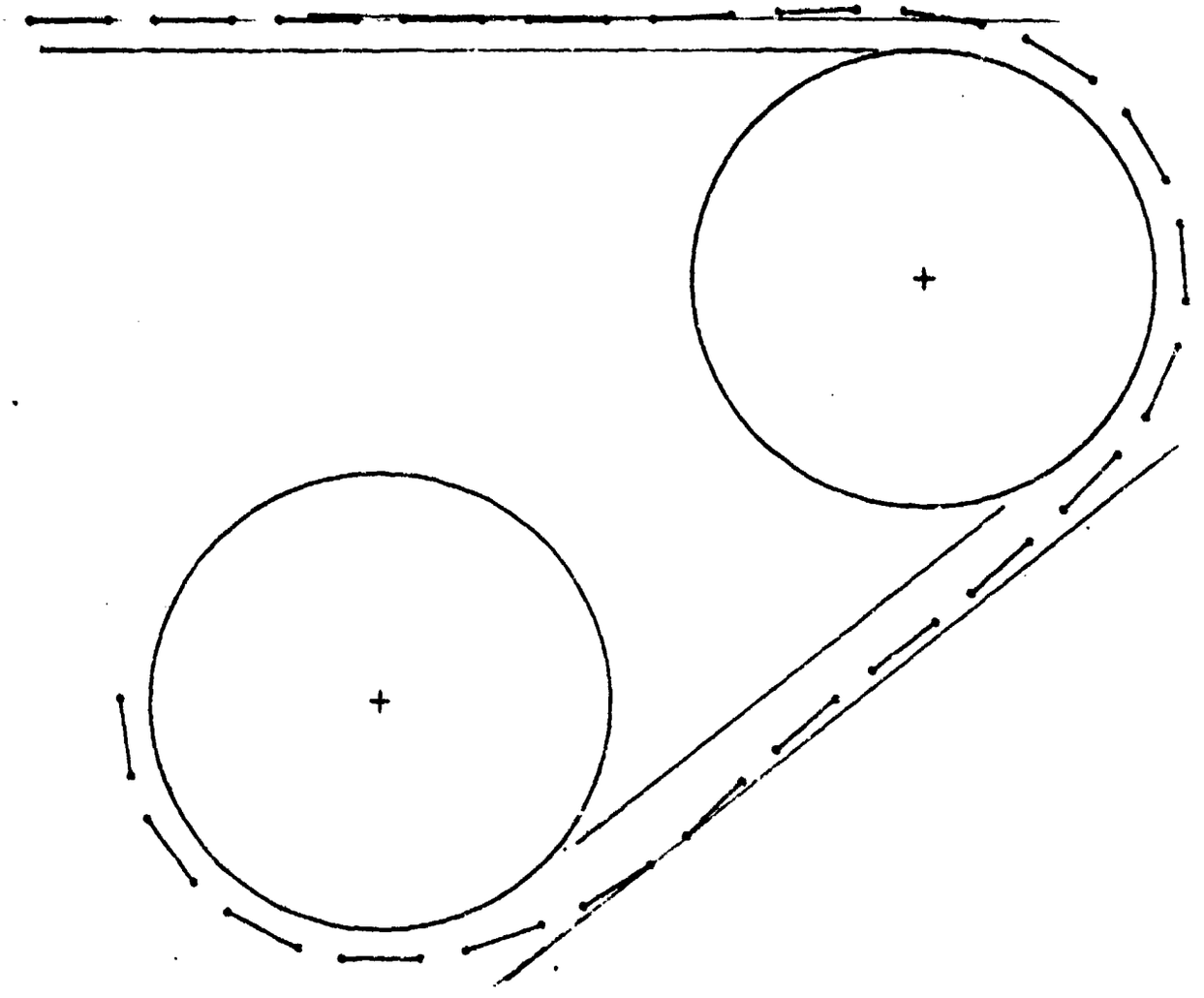

FIGURE 10b. TRACKDYNE PLOT SHOWING EFFECT OF SPEED ON TRACK PATH (70 MPH, 1500 LB APPARENT TENSION)

Dimensions, masses, spring rates, and damping constants defining the system are easily changed by repunching only a few cards.

Operation of Program. Initial positions, velocities, and accelerations of all the parts must be defined at time zero to give the simulation a point from which to start. Initial conditions may be read from cards that were punched with the final conditions of an earlier run, or they may be calculated by the program, given the speed and apparent tension at which it is desired to run.

To calculate the initial conditions, the program first approximates the track path using the exponential equations defining the shape of a continuous band of similar stiffness and rotary inertia. The dynamic tension is estimated at all points along the path as a function of path curvature and speed, and contact forces with the wheels are estimated. The individual links are then positioned with their pins on the path, spaced so that the "bushing" springs provide the desired local track tension and the wheel contact pads provide the desired contact force. Velocities are calculated for compatibility between adjacent links.

The incoming path shape (Links 1 through 8) is calculated as a span from a dummy wheel (not shown on Figure 10) having the same diameter as the idler and located horizontally to its left so that Link 1 is at mid-span.

Initial conditions having been established, the simulation begins. The time history of the movement of each part is determined by integrating its velocities and accelerations. The integration proceeds in finite steps of time. At each step, the forces acting on all parts are calculated as functions of their relative positions and velocities. The instantaneous accelerations of all parts are then calculated as functions of these forces and their masses, and the average accelerations over the coming time interval are estimated as functions of the instantaneous acceleration and the accelerations calculated at the previous two time steps. Average velocities are similarly estimated for the time interval, and from them new positions of the parts are calculated. At 35 mph, 1000 integration steps per pitch-passage cycle have been found appropriate.

Tension is controlled by pulling on the leading link (number 23) with a constant force and moment that are calculated by the initial condition routine to give the desired average apparent tension in the straight at link number 1. Speed is controlled by constraining link number 1 to move horizontally with constant velocity.

When the track has moved through one pitch distance, a new link is introduced at the trailing end and an extraneous one is removed at the leading end. The identifying numbers are indexed backward so that they remain approximately fixed in space.

Simulation is continued for a sufficiently long time to allow transients to decay and the steady-state operation to be observed. Detailed data is then recorded for the last cycle. Final conditions may be punched on cards, enabling the run to be continued for any number of additional cycles at any later date. Full data may also be recorded for selected cycles during the run, if desired.

The number of cycles required for adequate accuracy in the parameters of interest must be decided by the operator, based on past experience and study of the preliminary results of the particular run. A few selected items of data are printed at the end of each cycle so that the damping of transients may be observed. Since the running time required depends largely on the quality of the initial condition calculations, care has been taken to make that part of the program sophisticated.

Among the data recorded at the end of each cycle are the offsets, relative to a straight-line-tangent path from wheel to wheel, of the centers of gravity of links 6 and 15. If these offsets vary from cycle to cycle, vibrating-string type transverse vibrations of the track spans are indicated. Figure 11 shows the transverse motions of these two links during two fairly long runs at similar conditions. Link 15 is of greatest interest, since it is near the center of the idler-to-road-wheel span, which is completely comprehended by the model. In Run 22, the initial conditions evidently did not specify enough arcing of this span, and therefore a transverse vibration at about 3.5 Hz was excited at turn-on. In Run 25, the continuous-band model used by the initial condition routine was modified toward a stiffer band, which produces more arcing. The correction was

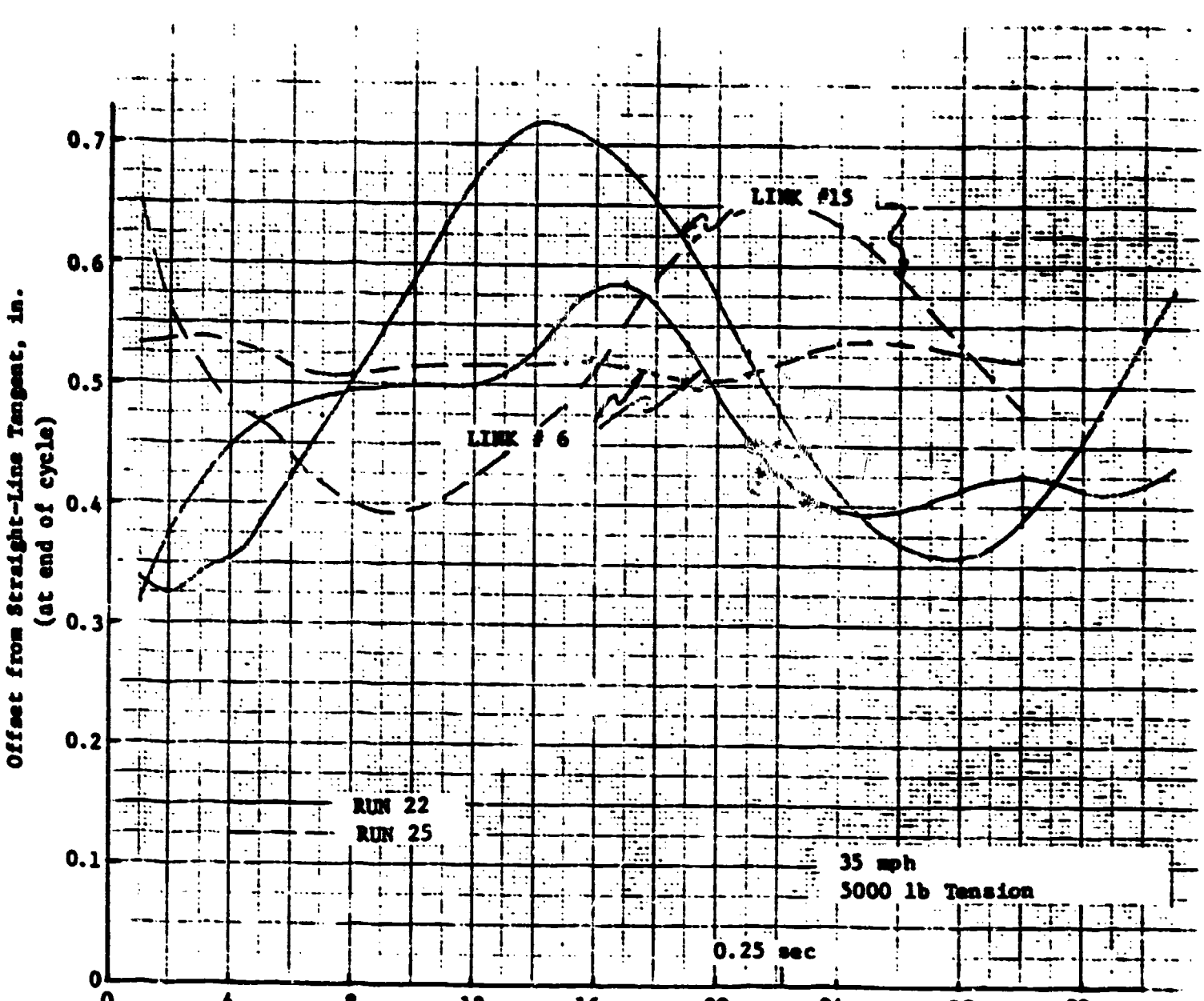

FIGURE 11. TRACKDYNE PROGRAM OUTPUT SHOWING TRANSVERSE VIBRATION TRACK IN SPANS

evidently too great, as a transverse vibration of opposite phase resulted. In subsequent runs, an intermediate correction to the initial condition has been made.

These transverse vibrations of entire spans are so poorly damped that it would be impractical to run long enough for them to die out. So long as their amplitude is moderate, however, it has been found that they do not significantly affect the cyclical (at pitch passage frequency) nature of the track tension, wheel contact forces, and hull forces that are the main output of the program.

Data Produced. During the last cycle, plus any other cycles where full data are requested, data are recorded at 100 evenly-spaced time stations throughout the pitch-passage cycle.

As presently programmed, data are printed for every other station, and include apparent tension at Link 1, offsets of shoes 6 and 15 from straight-line-tangent, rectangular position and velocity coordinates for all shoes, total tension in each link, normal and tangential components of shoe-to-wheel force for each shoe, compression and shear deflections of these contacts, and location of each center of contact relative to the shoe pad center. For the idler and road wheel, angular velocities are printed, plus horizontal and vertical components of the total force transmitted to the hull.

Other data such as accelerations or connector motions can be made available if the need arises.

Calcomp plots may be made of selected data from any cycle where full data is requested. The present program produces five plots.

Figure 10 was a Calcomp plot which is a graphic presentation of the positions of the shoes at the beginning of a cycle, from which the shape of the track path can be viewed. The large circles represent the outer diameters of the idler and the road wheel. Figures 12a, b, and c are similar plots showing the effect of bushing torsional stiffness.

Figures 13a, b, c, etc. are superimposed plots of total tension history for one cycle for selected links. Link 1 is at the inlet, and Link 19

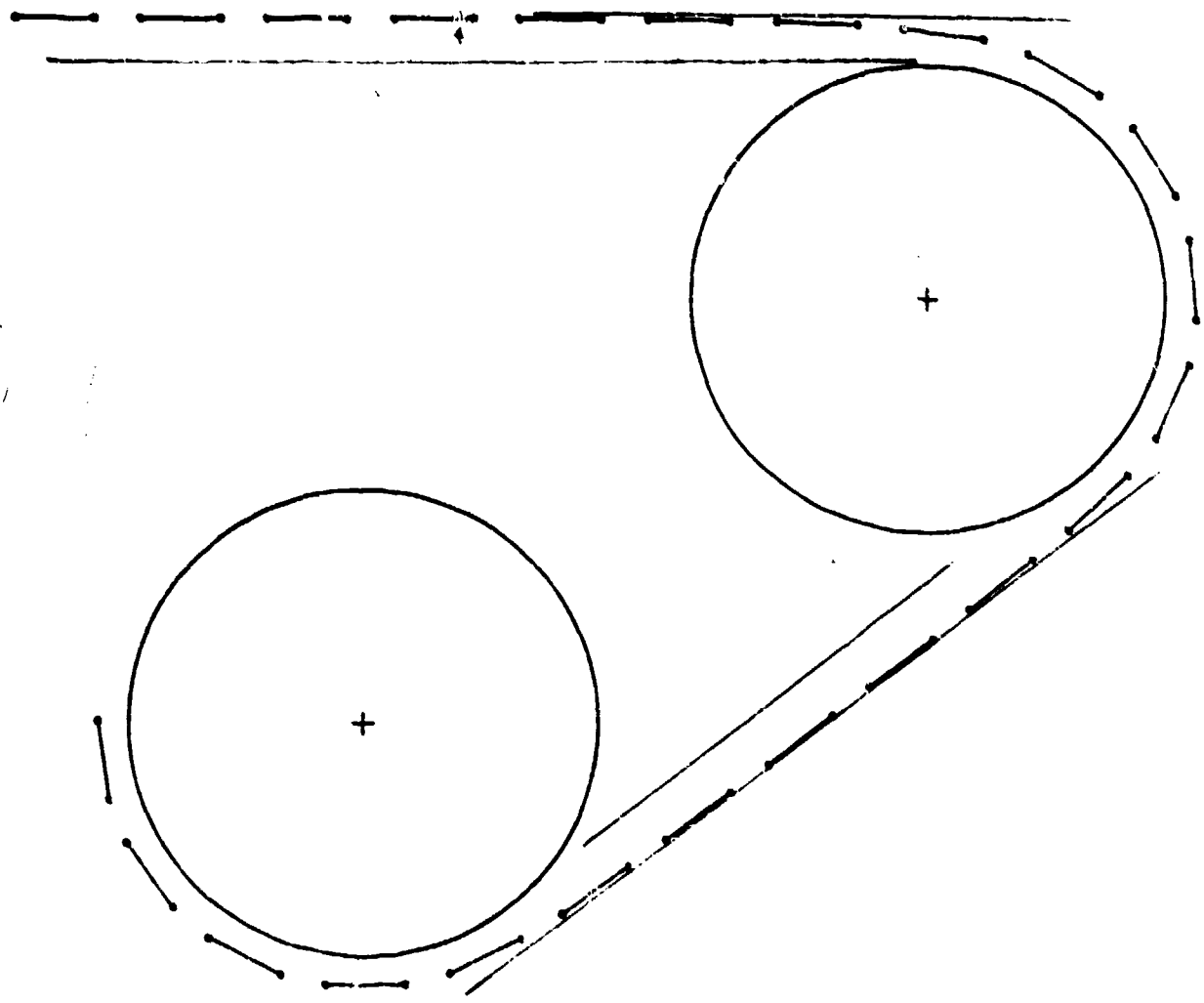

FIGURE 12a. TRACKDYNE PLOT SHOWING EFFECT OF BUSHING TORSIONAL STIFFNESS ON TRACK PATH
(50 MPH, 5000 LB APPARENT TENSION, TORSIONAL SPRING RATE NORMAL)
(See page 74 for further discussion.)

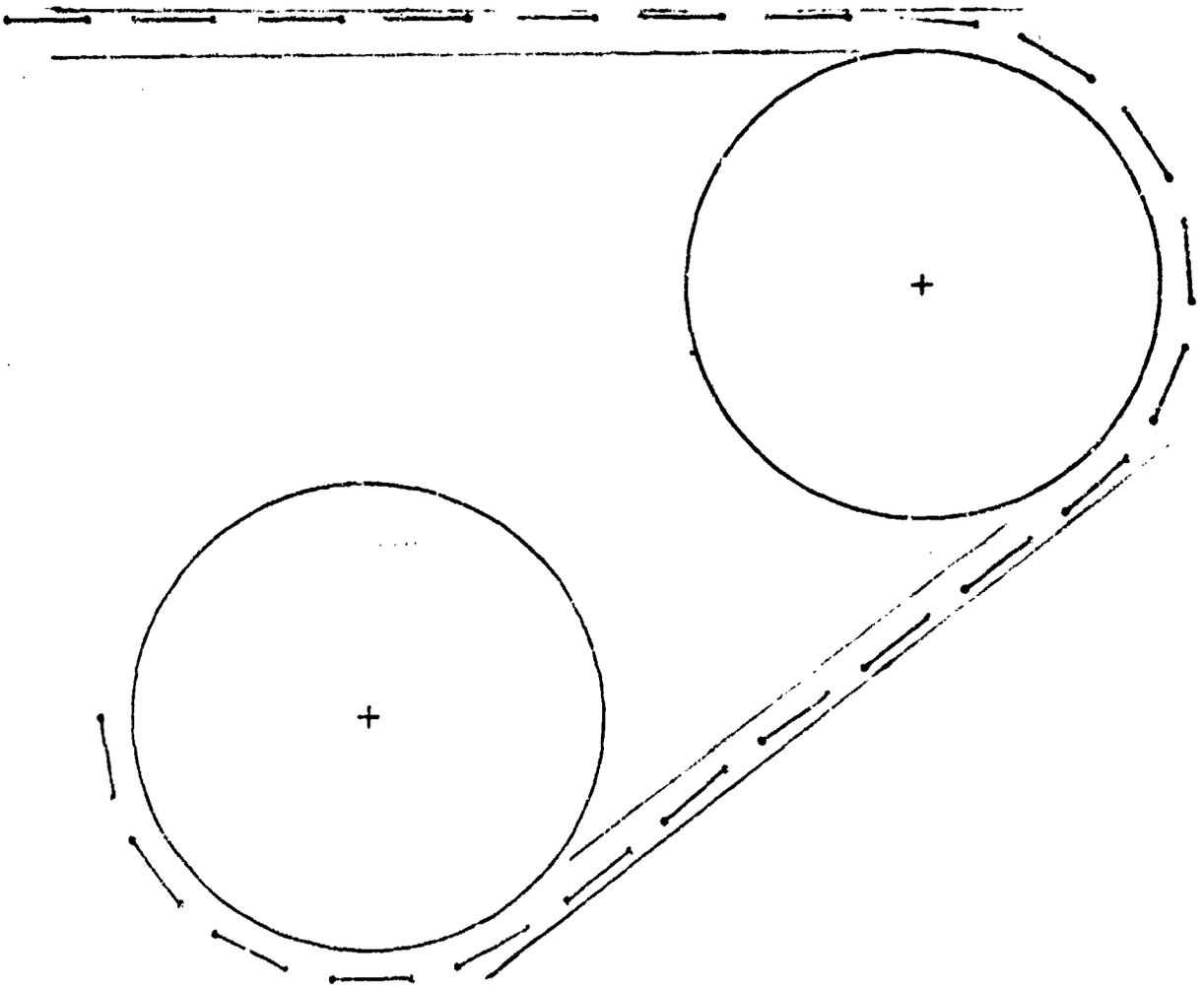

FIGURE 12b. TRACKDYNE PLOT SHOWING EFFECT OF BUSHING TORSIONAL STIFFNESS ON TRACK PATH (50 MPH, 5000 LB APPARENT TENSION, TORSIONAL SPRING RATE 1/4 NORMAL)
(See Page 74 for further discussion.)

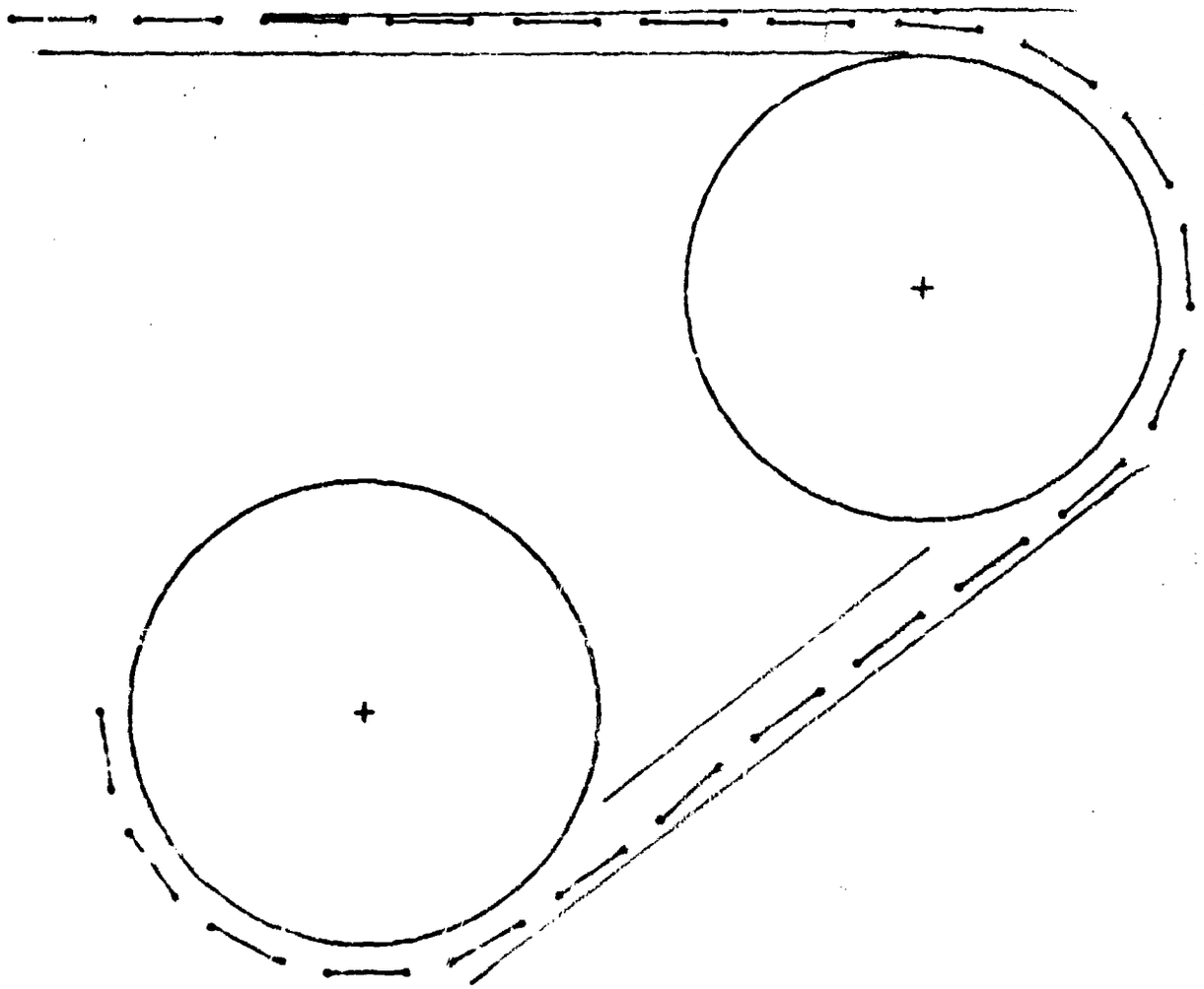

FIGURE 12c. TRACKDYNE PLOT SHOWING EFFECT OF BUSHING TORSIONAL STIFFNESS ON TRACK PATH (50 MPH, 5000 LB APPARENT TENSION, TORSIONAL SPRING RATE 1/16 NORMAL)

(See page 74 for further discussion.)

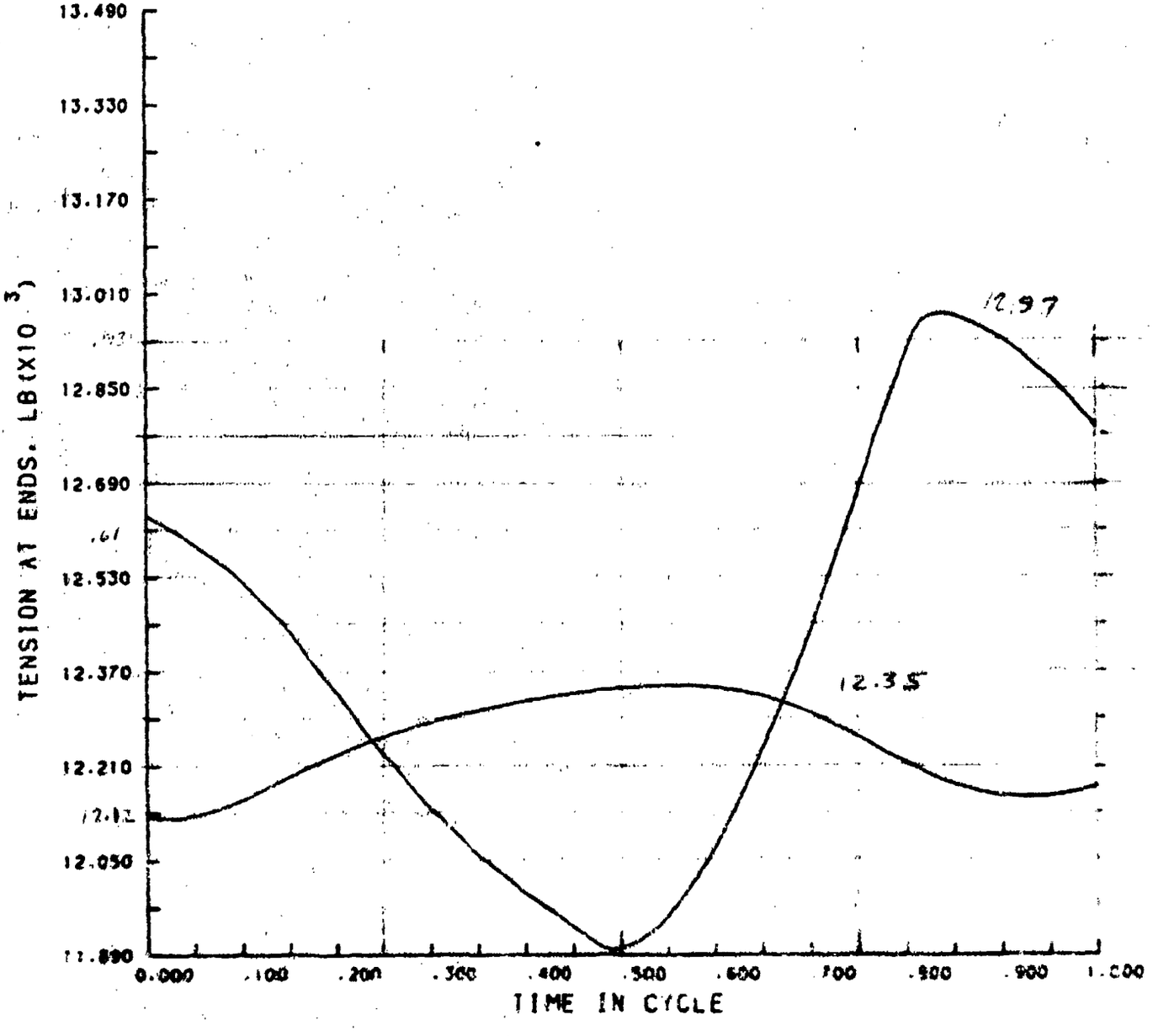

FIGURE 13a. TRACHDYNE PLOT OF TENSION HISTORY AT INLET AND NEAR FRONT ROAD WHEEL (35 MPH, 1500 LB APPARENT TENSION)

Smooth curve is at Connector 1
Larger excursion is at Connector 19

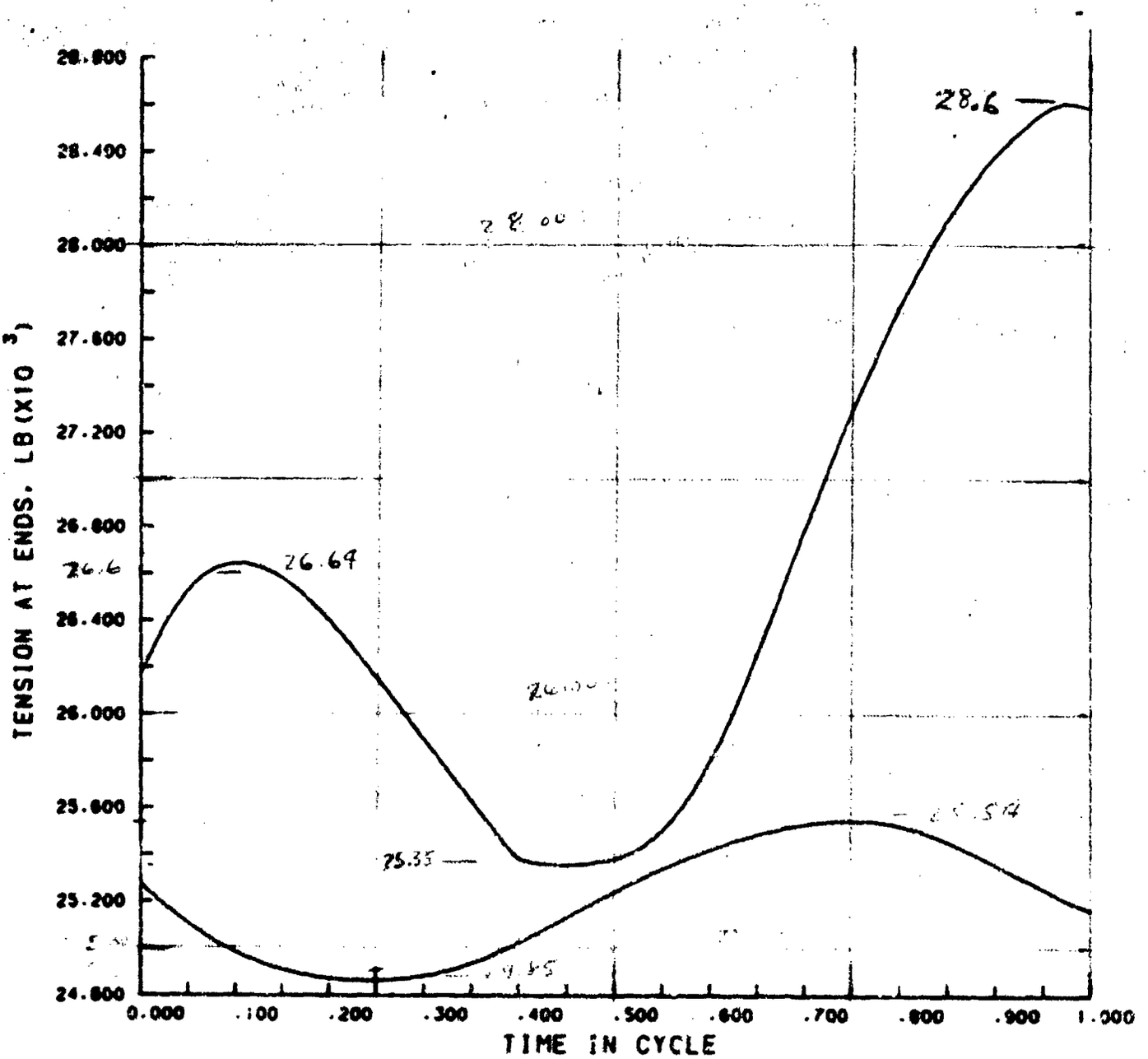

FIGURE 13b. TRACKDYNE PLOT OF TENSION HISTORY AT INLET AND NEAR FRONT ROAD WHEEL (35 MPH, 15,000 LB APPARENT TENSION)

Upper curve is at Connector 19
Lower curve is at Connector 1

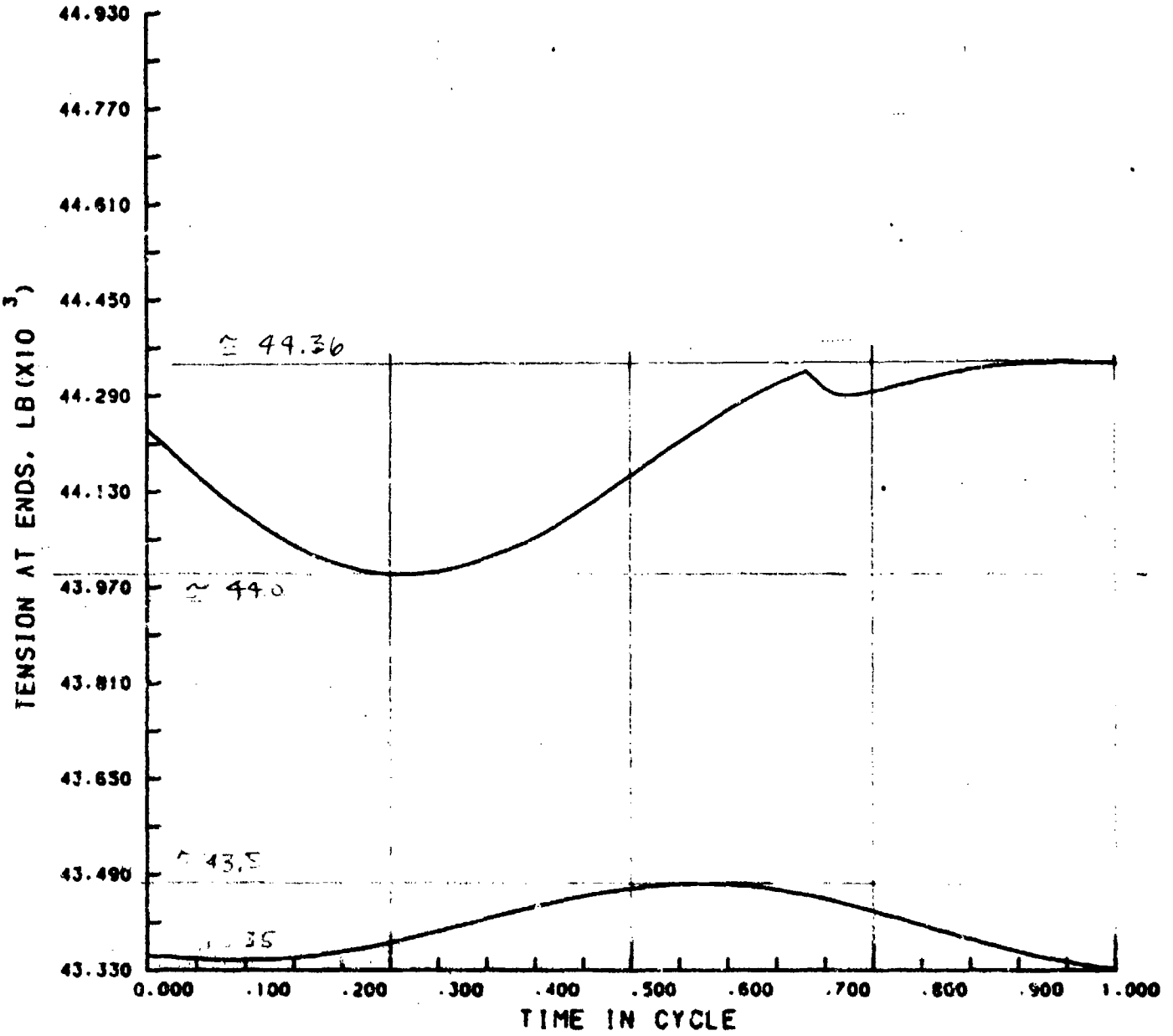

FIGURE 13c. TRACKDYNE PLOT OF TENSION HISTORY AT INLET AND NEAR FRONT ROAD WHEEL (70 MPH, 1500 LB APPARENT TENSION)

Upper curve is at Connector 19
Lower curve is at Connector 1

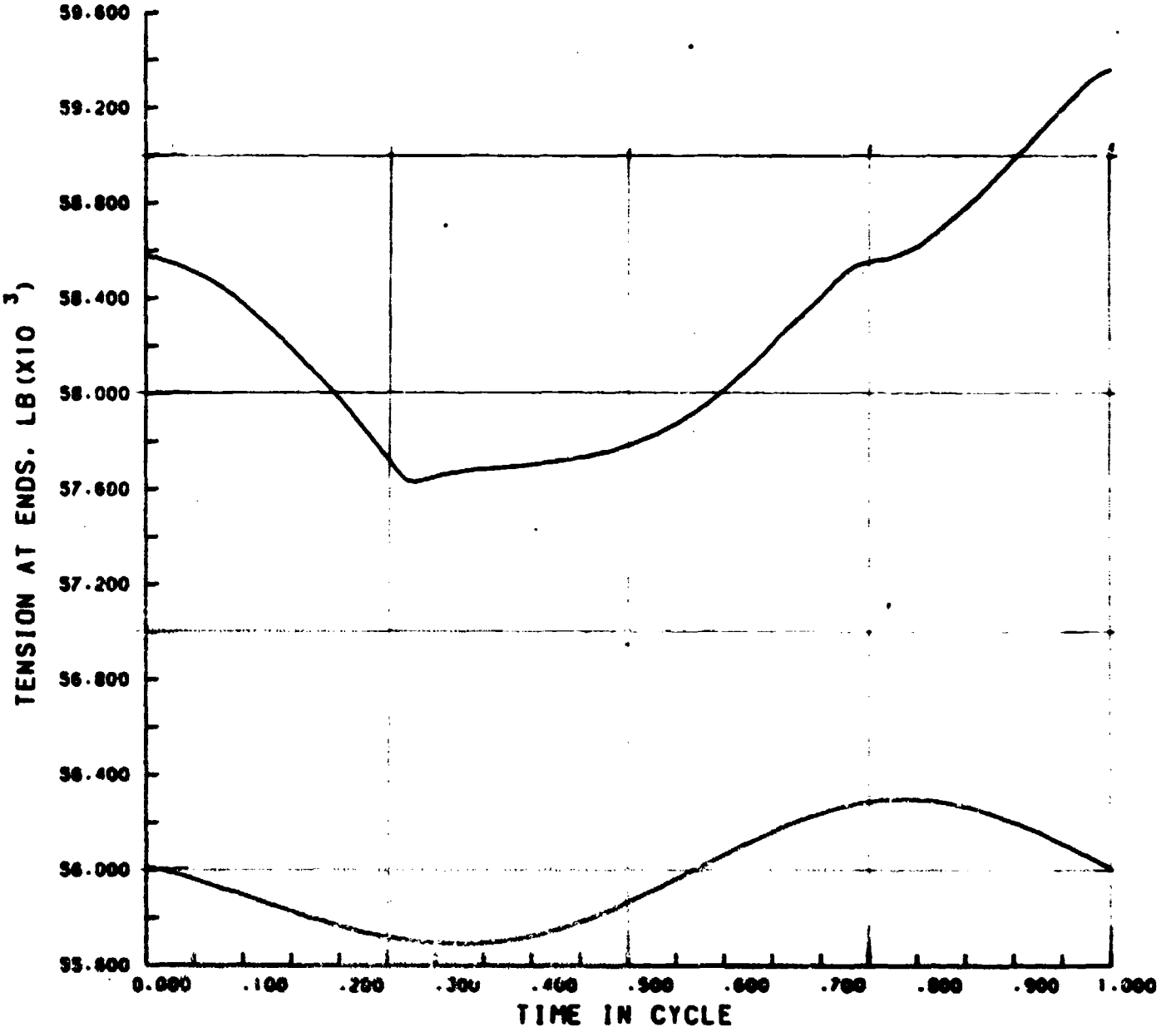

FIGURE 13d. TRACKDYNE PLOT OF TENSION HISTORY AT INLET AND NEAR FRONT ROAD WHEEL (70 MPH, 15,000 LB APPARENT TENSION

Upper curve is at Connector 19
Lower curve is at Connector 1

is near the entrance of the road wheel. If steady state has been achieved, these curves should be the same for whichever cycle is plotted. These curves do not return to their initial values at the end of the cycle because the point being observed has traveled down the track path by one pitch length during the cycle.

Figures 14 a, b, c, etc. show the track tension history in a connector as it rounds the idler. The time scale extends through seven cycles to include the total time during which adjacent shoes may contact the idler. Actually, these curves are produced by splicing together the tension histories of seven consecutive connectors during a single cycle. The quality of the splice points indicates the extent to which steady-state operation has been attained.

Figures 15 a, b, c, etc. show the idler contact force history of a shoe as it rounds the idler. Again, seven cycles are plotted by splicing together results for seven adjacent shoes. Components of force normal and tangential to the idler surface are shown. The normal force is always positive; the tangential force curve defines equal areas above and below the zero force line. A small amount of sliding is usually evident just before contact ends. The coefficient of friction between shoe and idler was taken to be 0.8.

Figures 16 a, b, c, etc. show the history through one cycle of the forces transmitted to the rest of the tank through the idler hub. These are periodic curves which return to their initial values. The components plotted are oriented to the incoming strand of track, so that they are actually 4 degrees away from vertical and horizontal for the M60 geometry. The rapid force variation due to initial contact with an incoming shoe is generally apparent in the vertical force curve. The highly nonsinusoidal nature of these curves suggests that noise would be excited in the hull over a wide frequency spectrum.

Energy Balance. At the end of the printout, the program itemizes energy dissipated in each bushing during the cycle via torsional and via radial deflection, and the energy dissipated in each shoe contact via normal damping, tangential damping, and sliding. By summing the energy inputs to, for instance, all 23 leading bushings during the one cycle, the heating seen by a single leading bushing while traversing the 23-pitch track path may be determined. Since no experimental data is available at present on the actual damping properties of the rubber bushings, the program

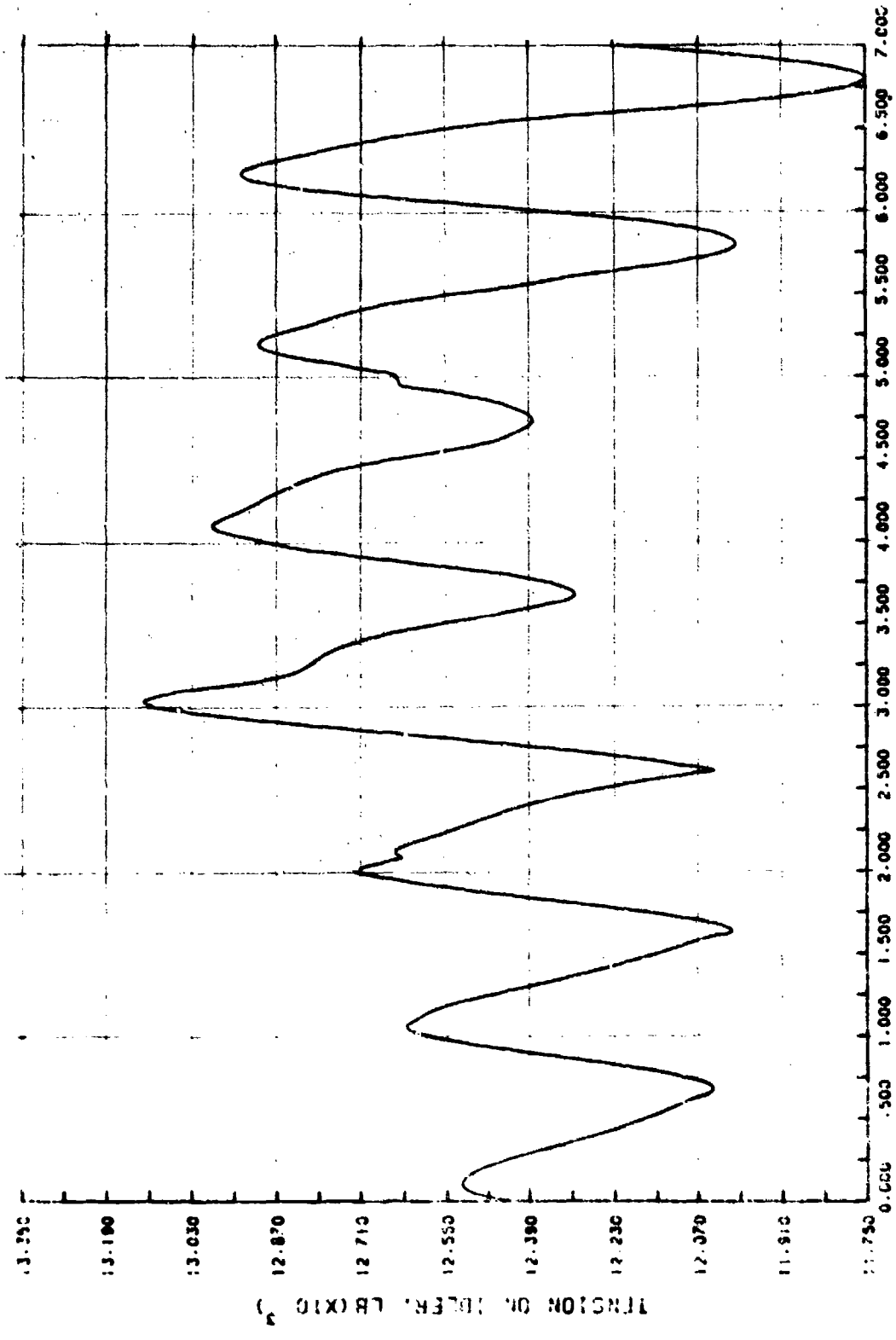

FIGURE 14a. TRACKDYNE PLOT OF TENSION HISTORY ON IDLER
(35 MPH, 1500 LB APPARENT TENSION)

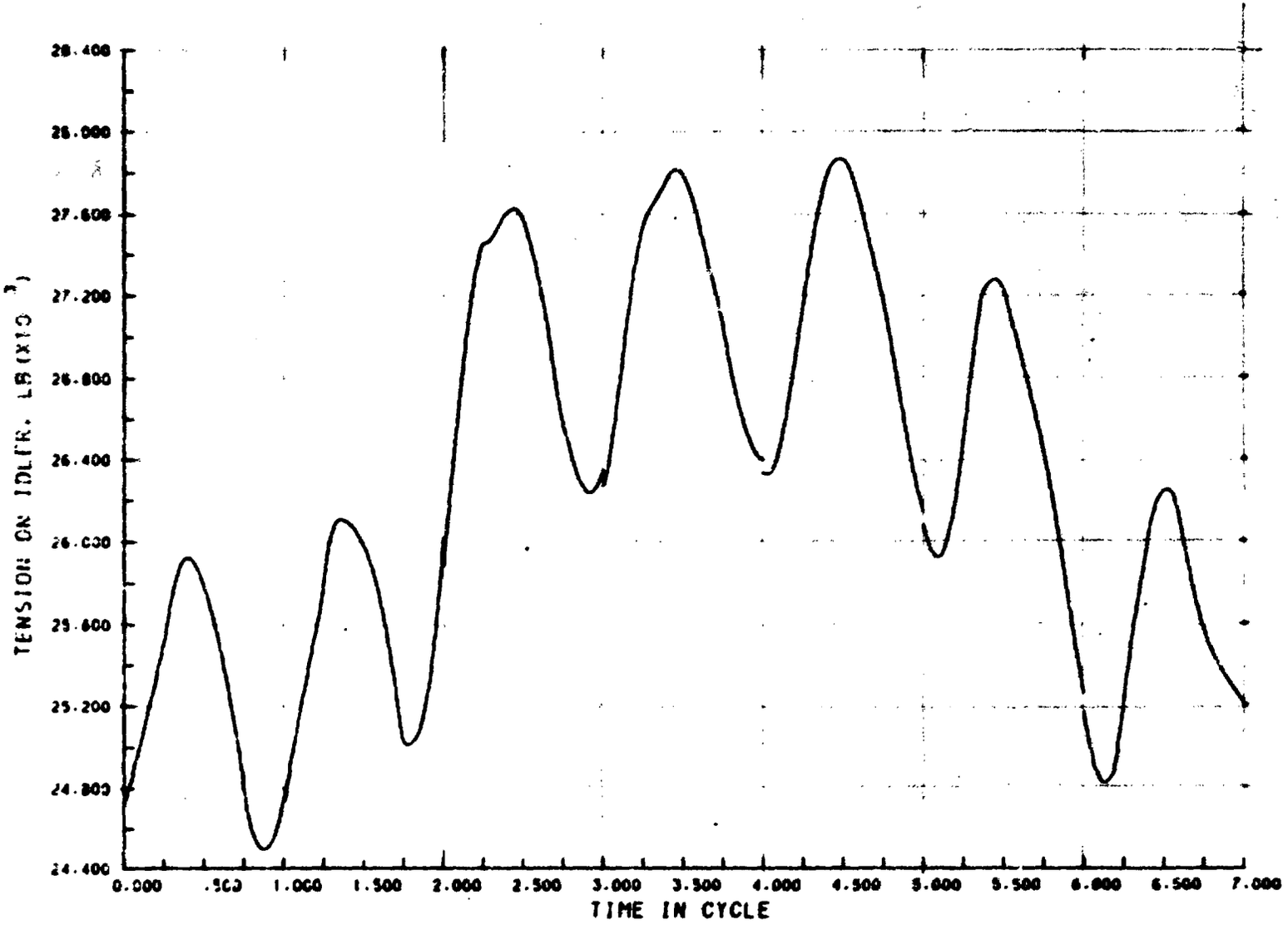

FIGURE 14b. TRACKDYNE PLOT OF TENSION HISTORY ON IDLER (35 MPH, 15,000 LB APPARENT TENSION)

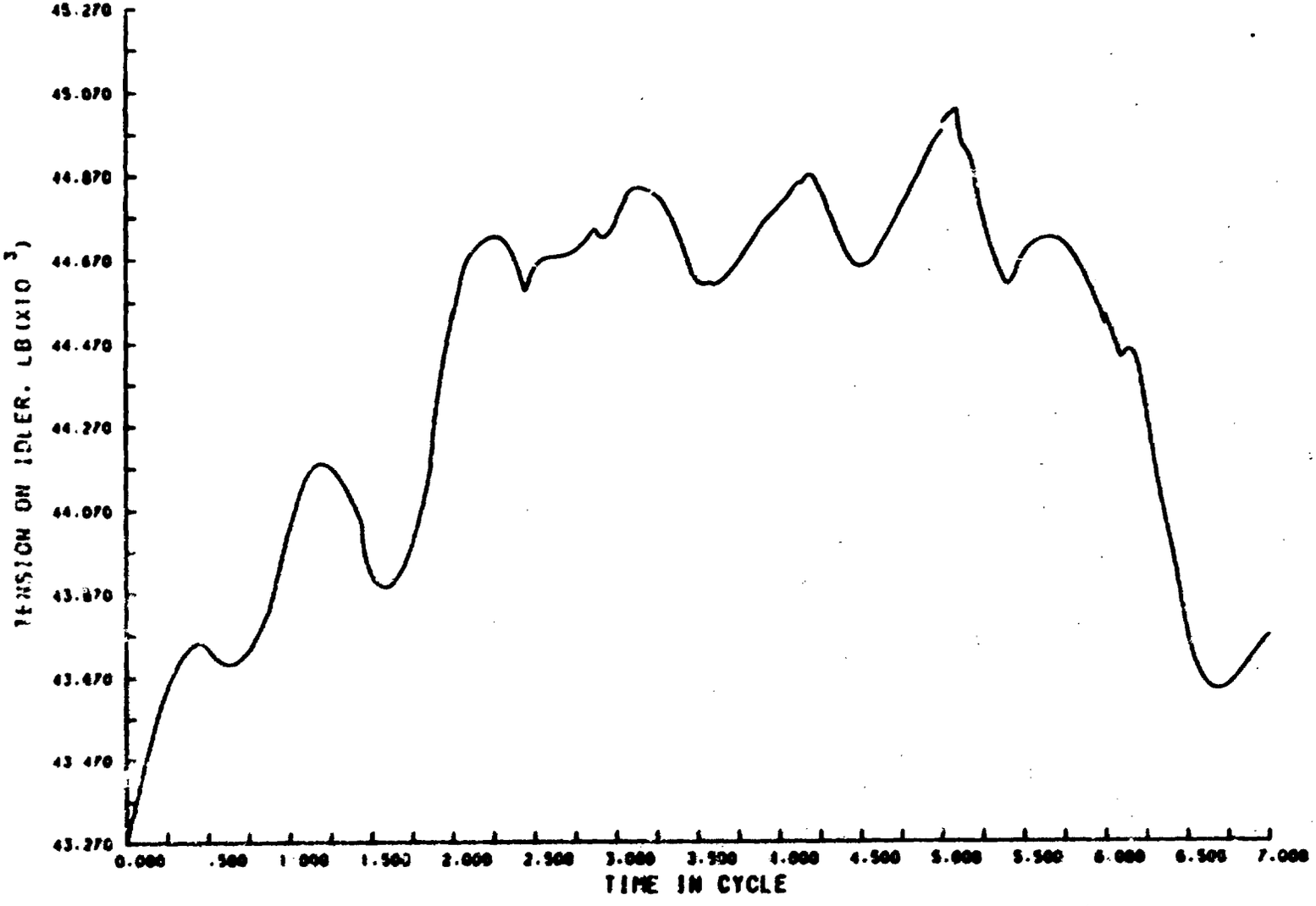

FIGURE 14c. TRACKDYNE PLOT OF TENSION HISTORY ON IDLER
(70 MPH, 1500 LB APPARENT TENSION)

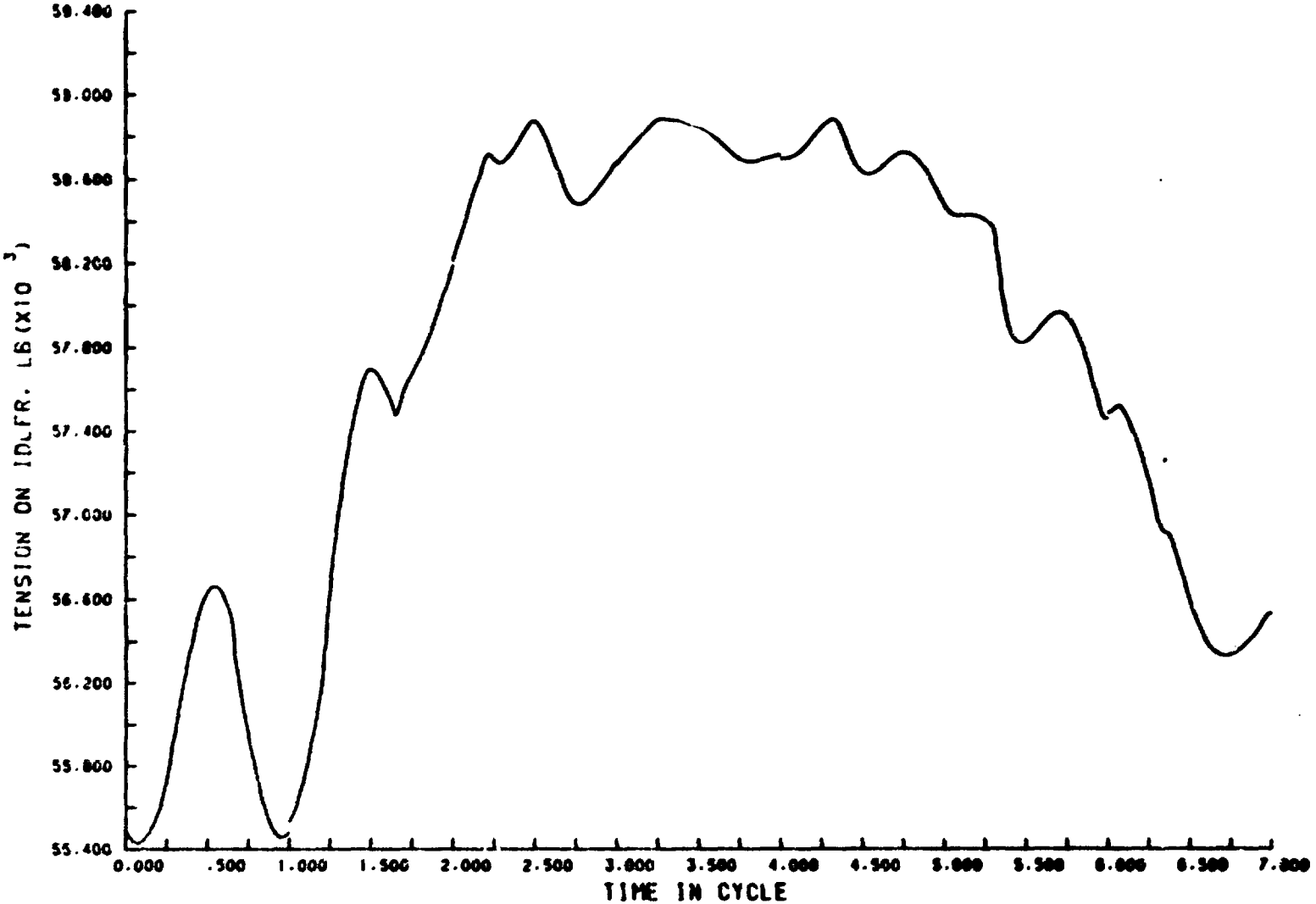

FIGURE 14d. TRACKDYNE PLOT OF TENSION HISTORY ON IDLER
(70 MPH, 15,000 LB APPARENT TENSION)

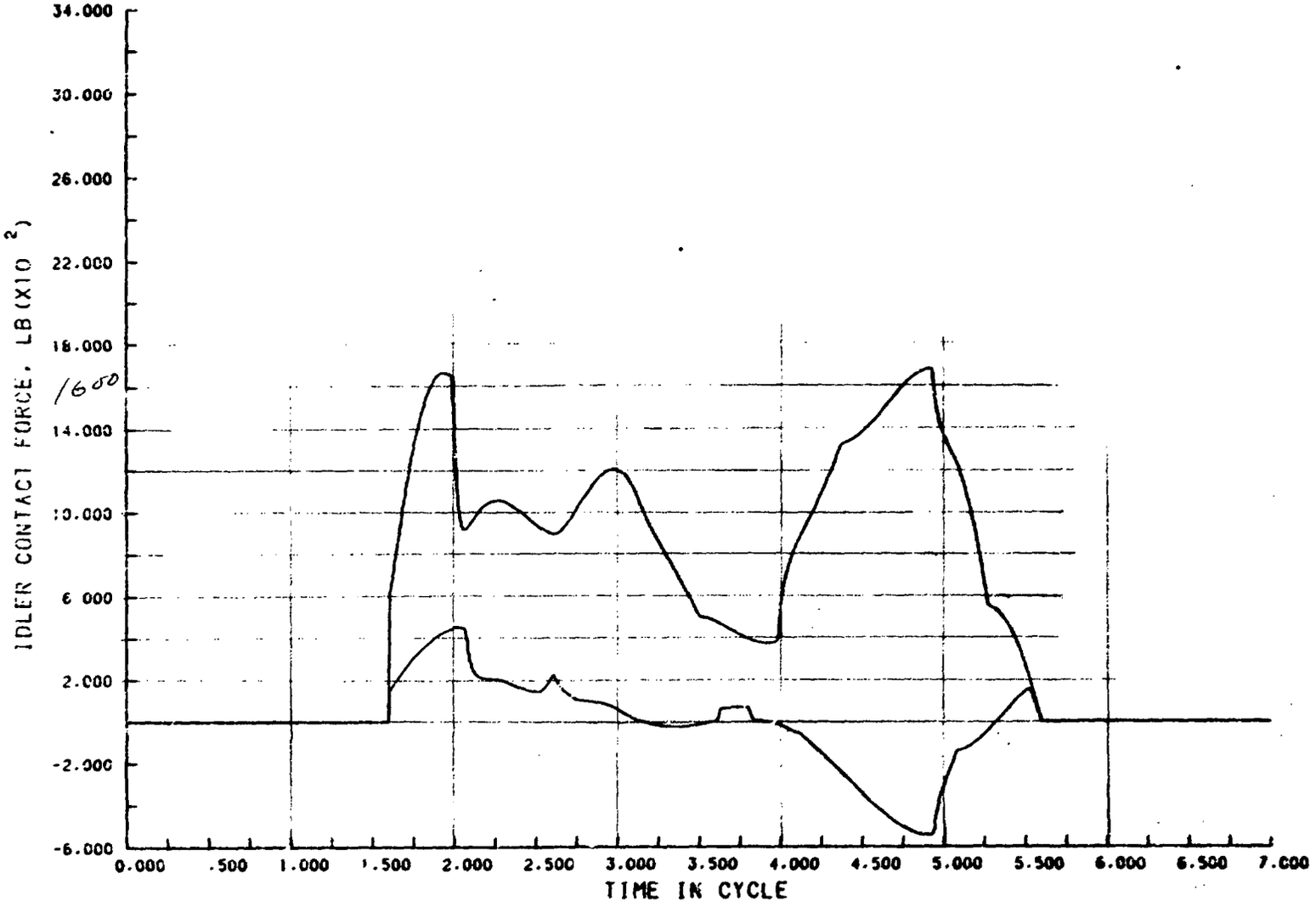

FIGURE 15a. TRACKDYNE PLOT OF SHOE-TO-IDLER FORCE HISTORY (35 MPH, 1500 LB APPARENT TENSION)

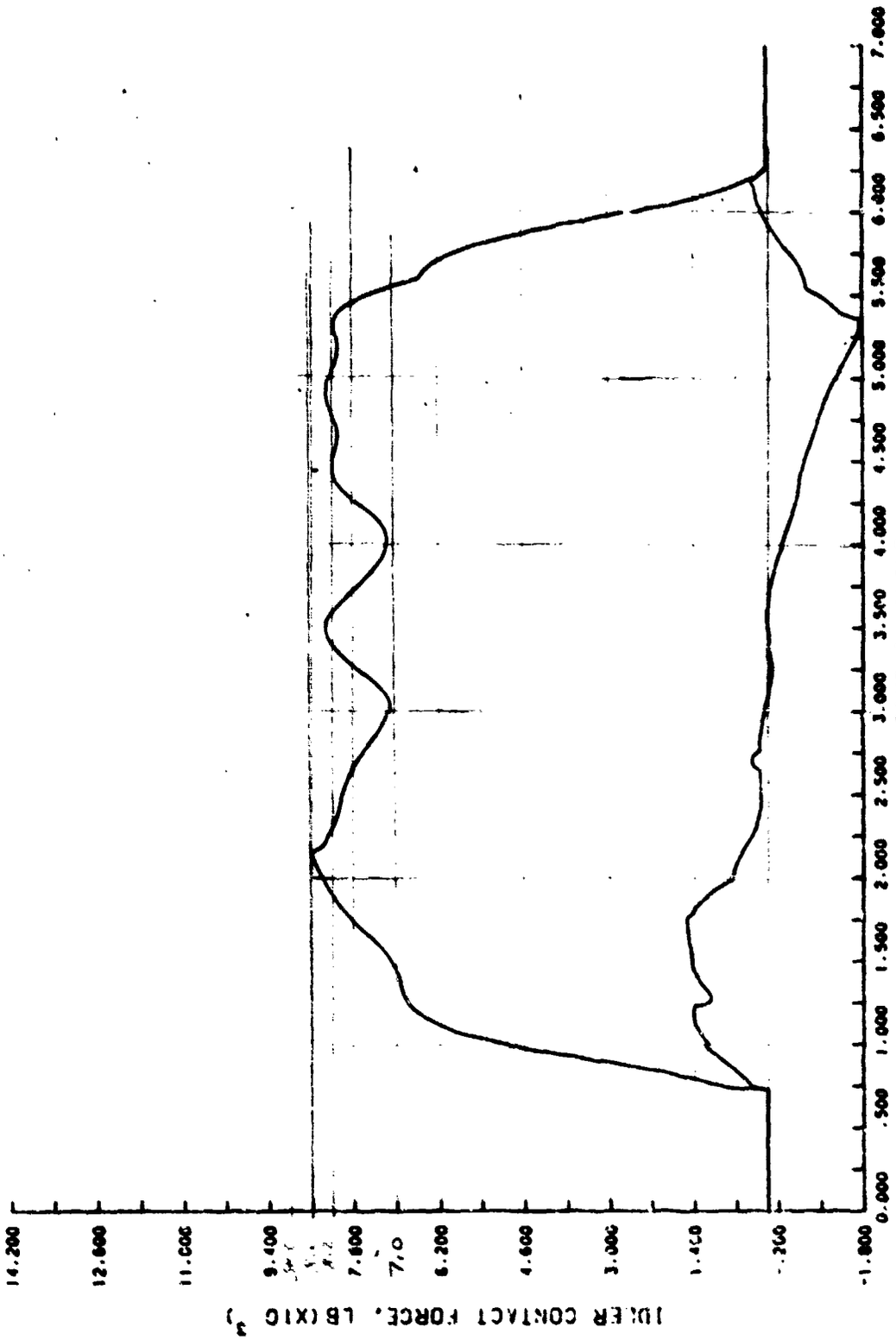

FIGURE 15b. TRACKDYNE PLOT OF SHOE-TO-IDLER FORCE HISTORY
(35 MPH, 15,000 LB APPARENT TENSION)

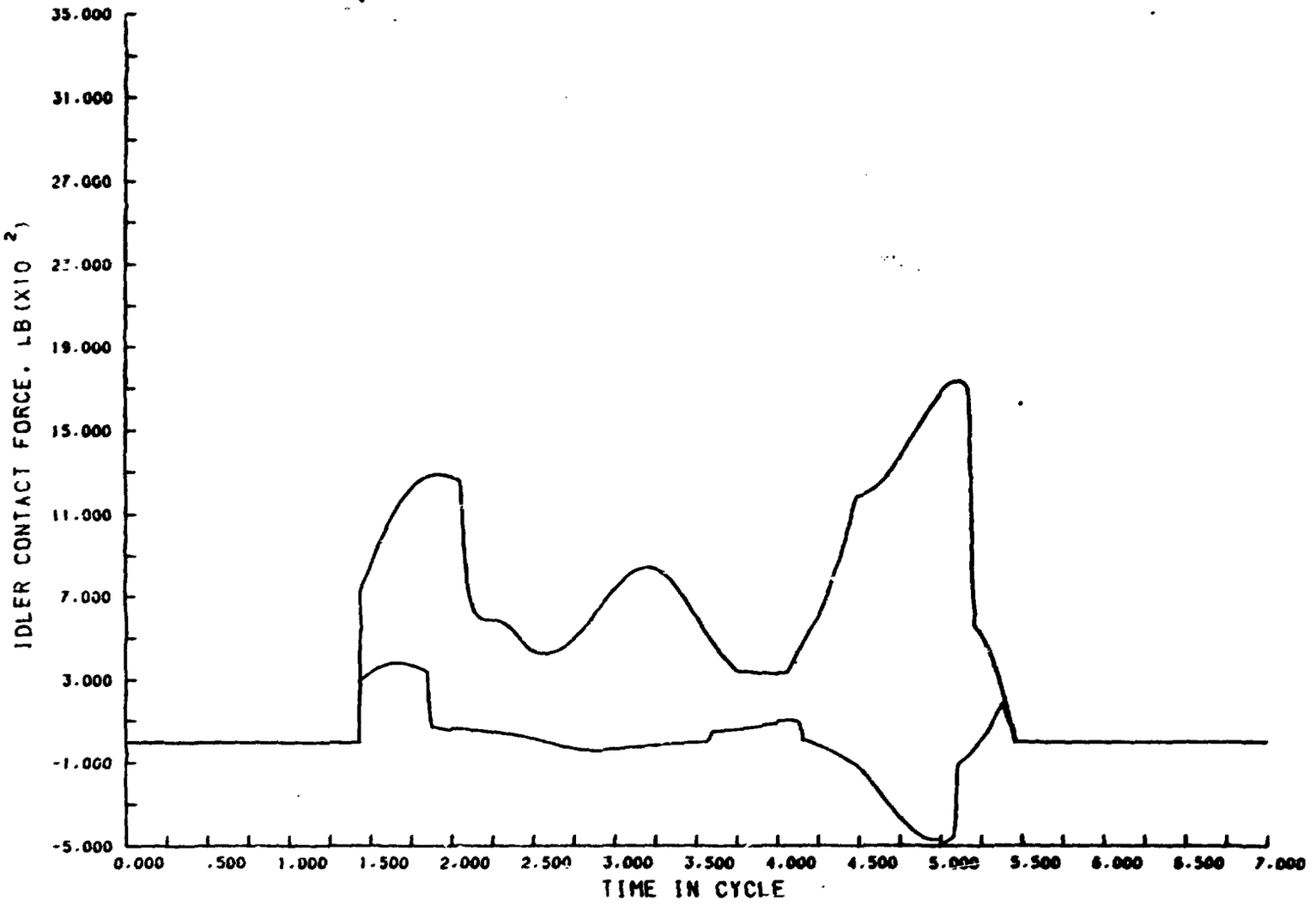

FIGURE 15c. TRACKDYNE PLOT OF SHOE-TO-IDLER FORCE HISTORY
(70 MPH, 1500 LB APPARENT TENSION)

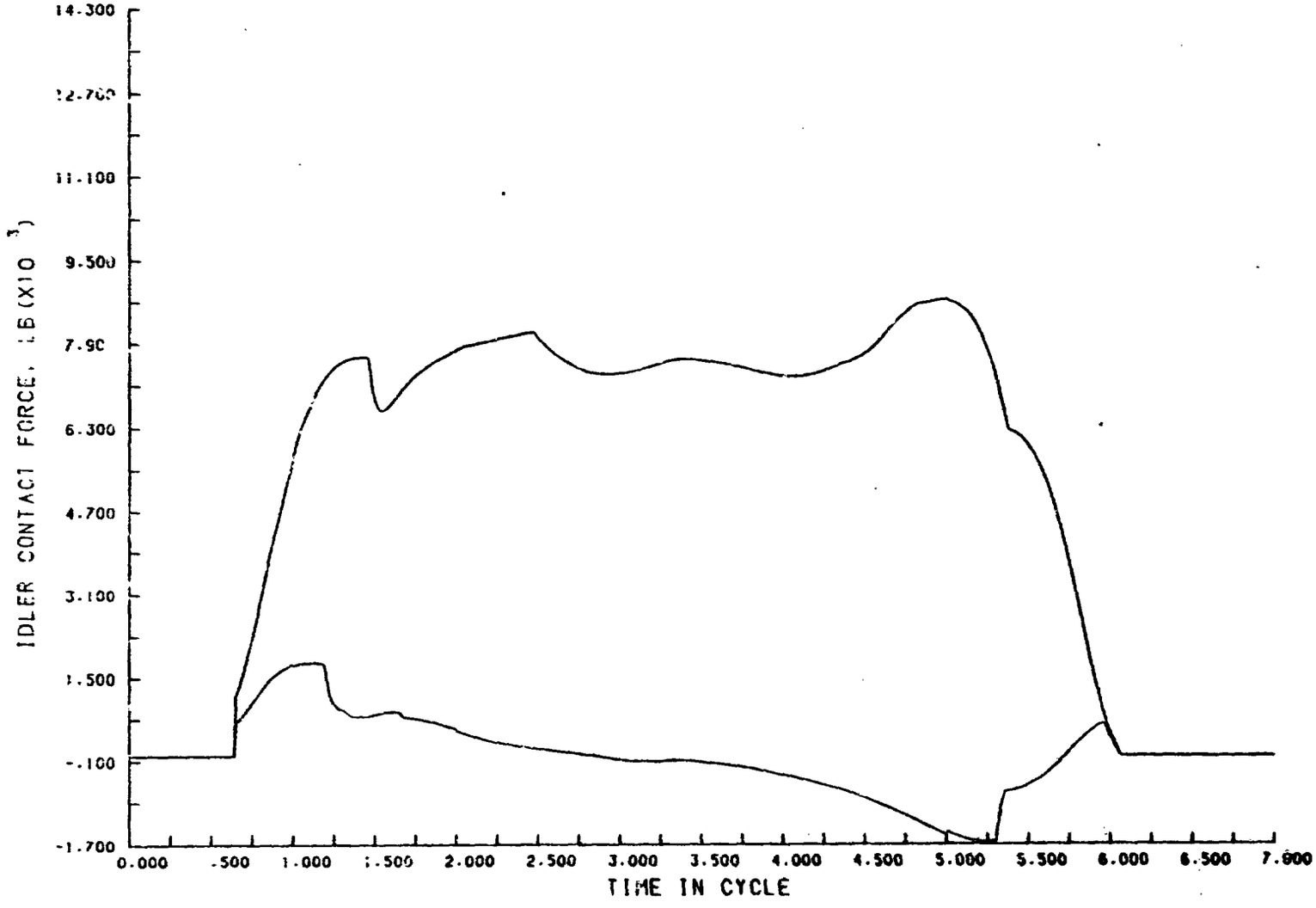

FIGURE 15d. TRACKDYNE PLOT OF SHOE-TO-IDLER FORCE HISTORY (70 MPH, 15,000 LB APPARENT TENSION)

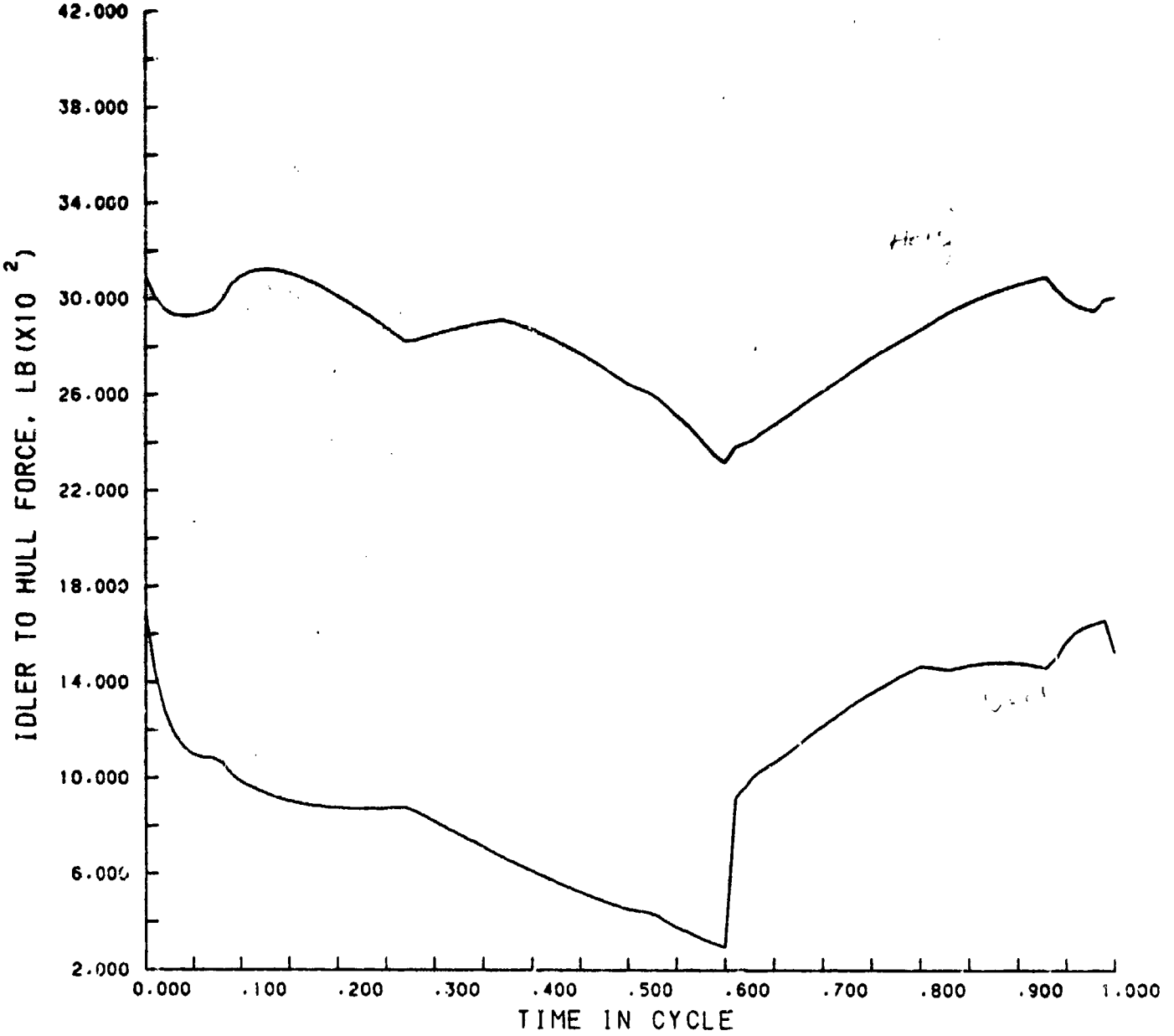

FIGURE 16a. TRACKDYNE PLOT OF IDLER-TO-HULL FORCE HISTORY (35 MPH, 1500 LB APPARENT TENSION)

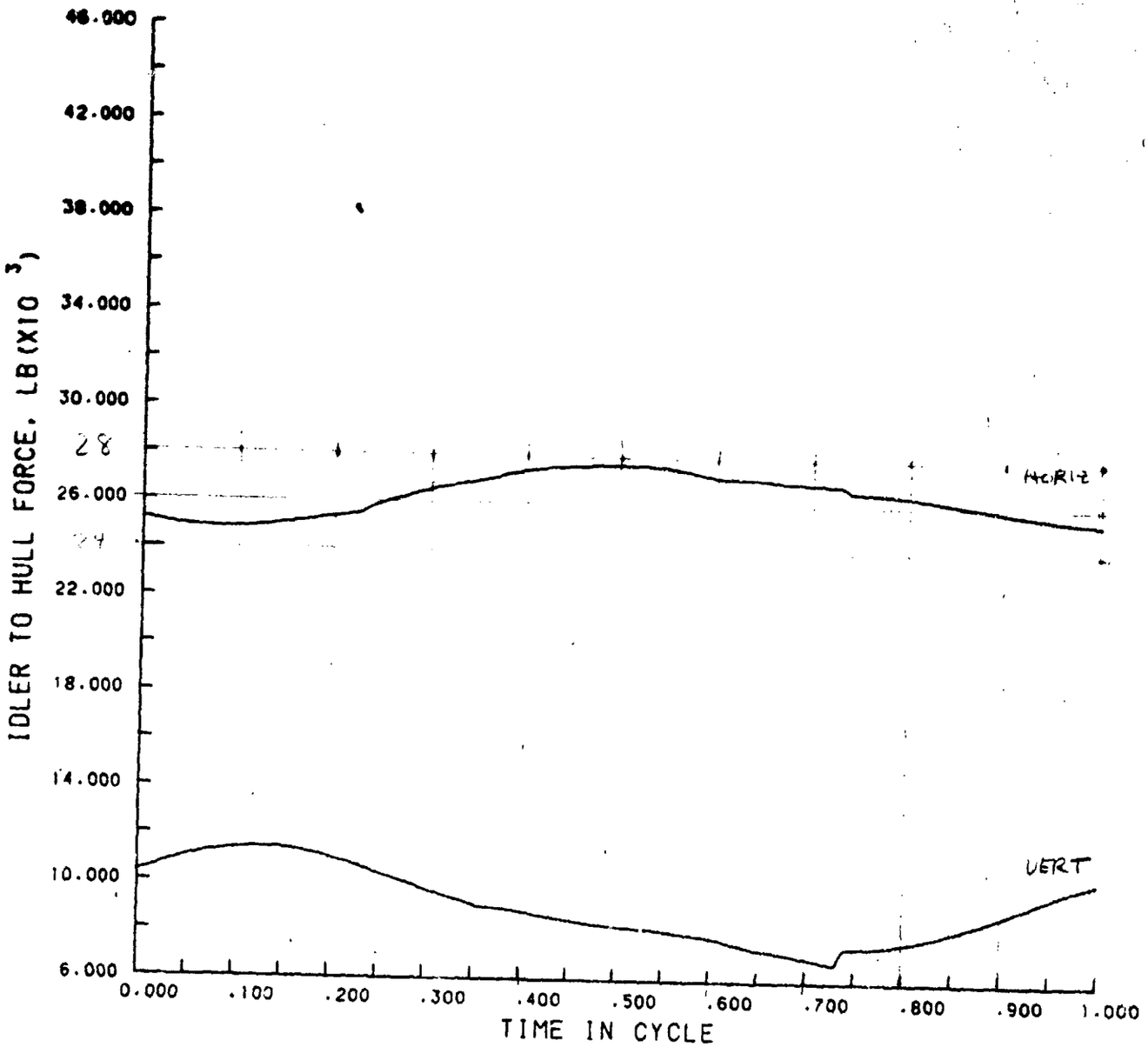

FIGURE 16b. TRACKDYNE PLOT OF IDLER-TO-HULL FORCE HISTORY (35 MPH, 15,000 LB APPARENT TENSION)

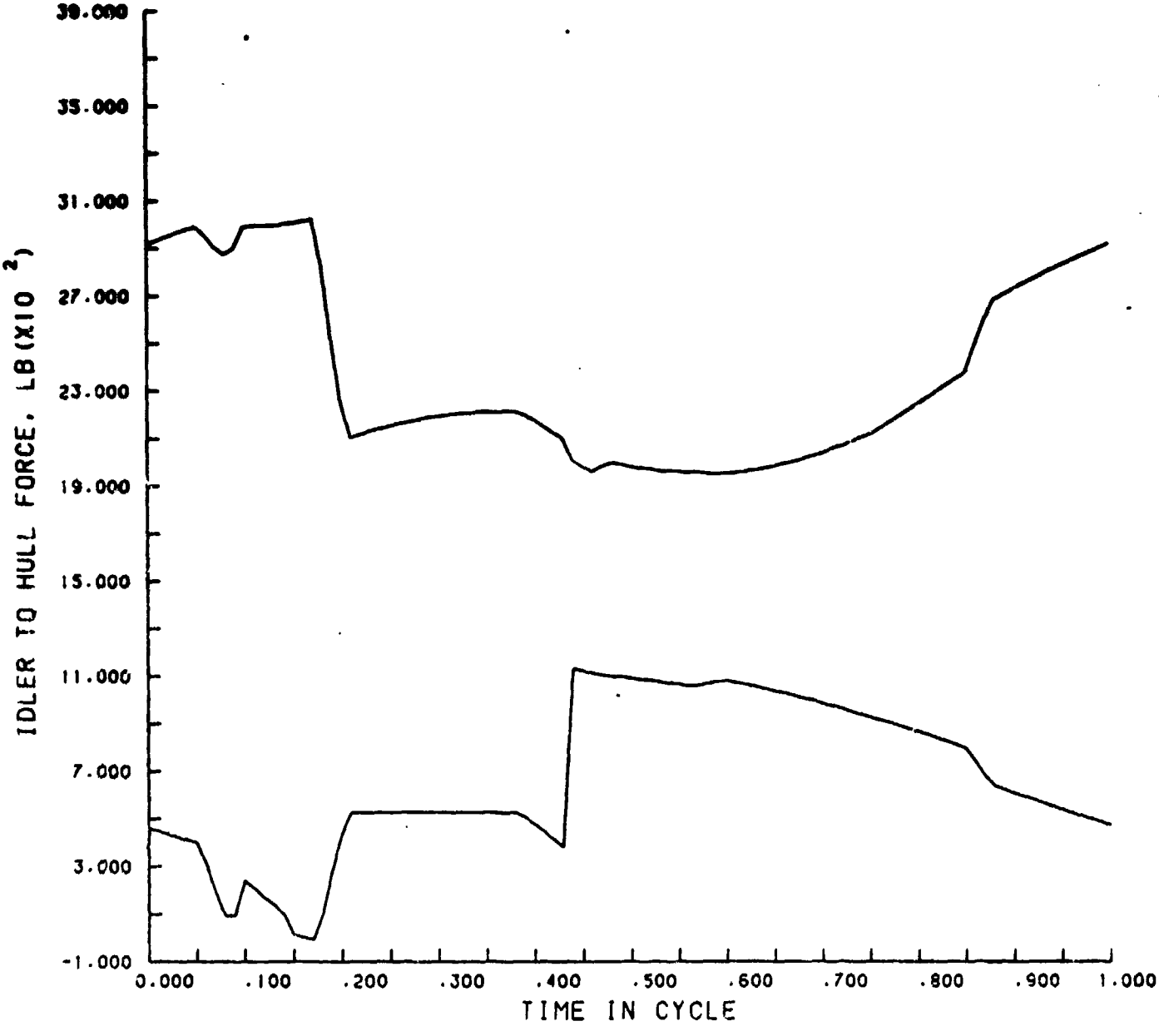

FIGURE 16c. TRACKDYNE PLOT OF IDLER-TO-HULL FORCE HISTORY
(70 MPH, 1500 LB APPARENT TENSION)

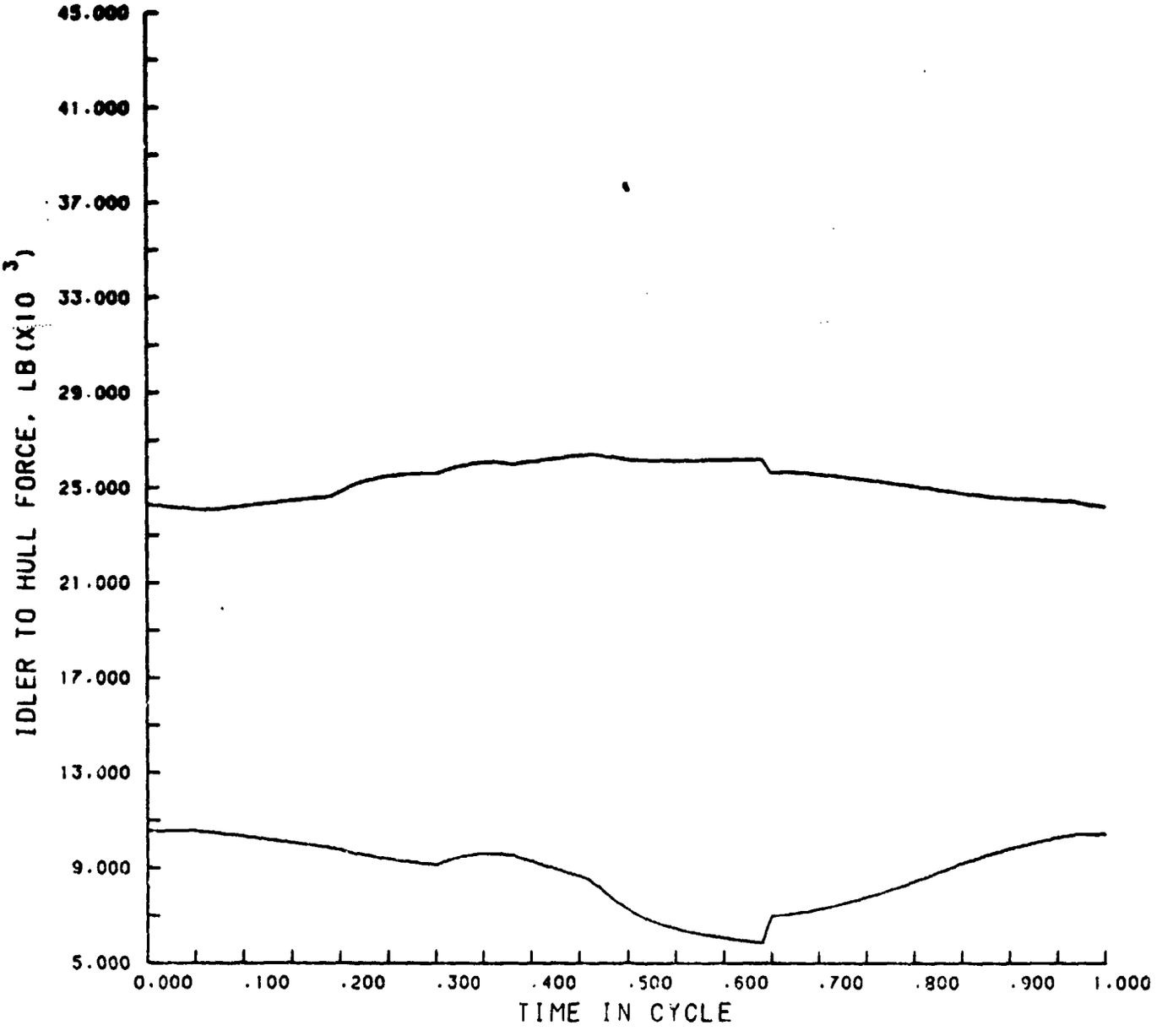

FIGURE 16d. TRACKDYNE PLOT OF IDLER-TO-HULL FORCE HISTORY
(70 MPH, 15,000 LB APPARENT TENSION)

is uncalibrated in this respect, and the numbers being generated are more of interest for the trends they disclose than for their absolute values. The damping properties of the shoe-to-wheel contacts are based on a limited amount of experimental work at Battelle that included only the rubber of the shoe.

To complete the energy balance, the total energy dissipated by damping is compared with the mechanical energy put into drive the system and the mechanical energy stored in the system during the cycle. Table 4 gives representative numbers from a run at 50 mph and 5000 lb apparent tension, illustrating the energy balance for the system. Additional documentation of the TRACKDYNE program is included as Appendix C.

Results. A number of runs were made with the T-142 geometry to determine the effects of speed and track tension. At 1500 lb apparent tension, runs were made at 35 and 70 mph; at 5000 lb apparent tension, runs were made at 20, 35, 50 and 70 mph; and at 15,000 lb apparent tension, runs were made at 35 and 70 mph. Thus, the lower speed runs can be correlated with field experience with the M-60 tank, while the higher speed runs are indicative of how the M-60 would run at speeds that have not yet been attainable in the field. Detailed results are presented in Figures 13 through 16 for four runs which bracket the range of speed and tension. In addition, the effects of reducing the torsional spring rate of the bushings and the associated damping have been examined at 50 mph, 5000 lb apparent tension. There has not been time to generate data on other configurations such as the XM-1 track.

The TRACKCENT predictions of centrifugal tension and path of a continuous band have been borne out in principal by TRACKDYNE, though the linked track does show some additional phenomena above the transition speed that were not anticipated. Track path is best seen when the apparent tension is low, as in Figures 10a and 10b, because the track span is stretched more nearly straight at higher tensions. Figure 10a (35 mph) shows the arched span from idler to road wheel that is characteristic of operation below the transition speed, where path shape is dominated by the torsional spring rate of the bushings. Figure 10b (70 mph) shows the standing wave path shape that is characteristic of operation above the transition speed, where rotary momentum of the links dominates. Figure 10b also shows an unanticipated tendency of the track to form local arches at the end of the spans. This is especially evident at the entrance of the idler, where the links were caused to approach along the straight-line-tangent path. These local arches apparently assist in transferring kinetic energy to and from the links without excessive impact.

TABLE 4. TYPICAL ENERGY BALANCE FOR ENTIRE (23-LINK) SYSTEM DURING ONE CYCLE AT 50 MPH, 5000 LB APPARENT TENSION

I. ENERGY DISSIPATION			
Trailing Bushings, radial damping	196 in lb.		
Trailing bushings, torsional damping	103		
Leading bushings, radial damping	192		
Leading bushings, torsional damping	94		
Total heating of bushings		586 in lb.	
Wheel contacts, normal damping	450		
Wheel contacts, tangential damping	131		
Wheel contacts, sliding	3		
Total heating of wheel contacts		584	
Total energy loss			1170 (22.2 hp)
II. ENERGY INPUT			
Work input to drive Link 23	192,648 in lb.		
Kinetic energy carried into system via Link 1	76,036		
Potential energy carried into system via bushings of Link 1	1,446		
Total energy in		270,130 in lb.	
Work delivered by Link 1 to drive rest of track	185,996		
Kinetic energy carried out of system via Link 23	81,374		
Potential energy carried out of system via bushings and wheel contact of Link 23	1,328		
Total energy out		268,698	
Net energy input			1431 (27.2 hp)
III. ENERGY STORED IN LINKS 1-22 AND WHEELS			
Kinetic energy at start of cycle	1,888,463 in lb.		
Kinetic energy at end of cycle	1,888,685		
Kinetic energy stored		222 in lb.	
Potential energy at start of cycle	29,784		
Potential energy at end of cycle	29,795		
Potential energy stored		11	
Energy gain of system			233 in lb.
IV. UNACCOUNTED ENERGY LOST			28 in lb.

Overall experience with TRACKDYNE indicates that TRACKCENT exaggerates somewhat the effective angular momentum of the links. Consequently, the transition speed for the T-142 track is now thought to be 10 to 15 mph higher than the 46 mph predicted by TRACKCENT.

Figures 12a, b, and c show that the effect on track path of reducing the bushing torsional spring rate is essentially as predicted by TRACKCENT. Figure 12a shows the track following an arched path at 50 mph and 5000 lb apparent tension, though the arch is not as pronounced as that of Figure 10a because the tension is higher and the speed is closer to the transition point. Figure 12b shows the effect of reducing the bushing torsional spring rate by a factor of four, everything else remaining unchanged. TRACKCENT predicts that this will reduce the transition speed by a factor of two, and, indeed, it can be seen that the track is now following a standing wave path. Though the angular momentum effects have not increased, they are now able to dominate because the stiffness of the track has been decreased. Figure 12c, where the bushing torsional spring rate was again reduced by a factor of four, shows that the standing wave amplitude has increased only slightly, indicating that it is now limited more by the 5000-lb tension than by track stiffness.

The horsepower dissipated in the 23-link system for the three runs described above was 23,25, and 33, respectively. Thus, more power was lost when operating above the transition speed, but the loss was not excessive. Another run was made with the bushing torsional spring rate reduced by a factor of four and the bushing torsional damping constant also reduced by a factor of four. The power dissipated in the bushings was reduced by only 20 percent and was still a bit larger than the dissipation in the wheel contacts. The dissipation in the wheel contacts increased so that the total power loss was still 23 hp. It was concluded that changing the torsional damping will affect the direct losses due to bending the track around the wheels and straightening it again, but will not much affect the losses due to impact and vibration which eventually show up in the dampers. The system simply increases its activity sufficiently to turn this energy into heat with whatever dampers it has.

The tension excursions due to chordal action were not much affected by the changes in bushing torsional spring rate and damping, though they did appear to be a little higher with the lower spring rate.

The tension curves of Figures 14b and 14d show that track tension is substantially higher on the idler than in the spans. The greater centrifugal tension on the wheels contributes to this effect, but by far the greater contribution comes from a mechanism related to the apparent tension. In Figures 15a, b, c, and d it can be seen that the tangential force between the shoes and the idler is, in all cases, positive near the idler entrance and negative near the idler exit. That is, the track tends to drive the idler near the entrance and the idler tends to drive the track near the exit, so that tension is locked into the track and compression into the idler surface. The net torque input to the idler should, of course, be zero, because the bearings are assumed frictionless and angular acceleration must average to zero over a cycle if steady-state operation has been achieved.

One can visualize how the pad of the shoe might tend to scrub forward on the idler surface as the shoe pivots into place about its leading pin. This would lock in a tangential force and an additional tension, as observed, and would tend to cause the idler to creep forward a bit relative to the track. Due to this creepage, the tangential force is relaxed and then becomes negative by the time the shoe reaches the exit area. As the shoe pivots out of contact with the idler, this time pivoting about its trailing pin, a similar kinematic action occurs, again in such a direction as to push the idler forward. This relieves the negative tangential force and generates a small positive tangential force, which is then relieved by sliding as the shoe comes out of contact with the idler. Some sliding is also evident at the entrance point in all of these curves.

Bouncing of the shoes or sliding at other times in the cycle has not been observed. Clearly, though, if the apparent tension were much below 1500 lb, the normal force curves of Figures 15a and c would fall to zero at a point about 60 percent of the way around the idler.

The chordal action amplitudes of Figure 8 were generally taken from tension plots near the idler entrance. The random appearance of the curves allows considerable lattitude for differing interpretations.

Figures 16 a, b, c, and d show the components of force transmitted to the hull by the idler. These are obtained by summing all of the forces applied to the idler by the individual track shoes. Since the suspension is

not modeled, the center of the idler is assumed fixed and the mass of the idler contributes no additional forces. The upper curves are the essentially horizontal component of force which is actually inclined upward to the rear by 4 degrees because the coordinate system is oriented to the incoming track span. The lower curves are the essentially vertical component of force which is actually directed downward and inclined to the rear by 4 degrees. The overall shape of these curves varies widely with operating condition and appears random because of the many contributing effects. The more important thing to observe is the harmonic content, which appears to be high, particularly in the vertical force curves. Vibrations within the hull could be excited over a wide range of frequencies.

The power required to drive the 23-link system at various speeds and tensions is summarized by Figure 17. Since each data point represents a run continued till stability is reached, the curves are necessarily drawn with meager data. The shape of the 5000-lb curve is adequately defined to show a much greater sensitivity to increased speed once the transition speed is passed. Since the simulated system is roughly one end of one track circuit, the loss for the total track on the vehicle would be approximately four times that shown plus the losses in shoes contacting the road. The data point at 70 mph and 15,000 lb apparent tension is academic, because there would never be enough power and preload to maintain such high tension at that speed. Nonetheless, a significant portion of the engine power would be absorbed at speeds above 50 mph.

In summary, TRACKDYNE represents perhaps the most powerful analytical tool developed to date for the study of the dynamics of linked track. Of particular interest is the ability to determine power losses in the track, and the fact that the power loss increases as the bushing stiffness decreases—a phenomenon somewhat contrary to intuition. The extreme case of reduced stiffness is, of course, the use of anti-friction bearings rather than rubber bushings, a solution one might otherwise have attempted to reduce power losses.

During the last month of the Track Dynamics Program, effort was directed toward the expansion of TRACKDYNE to include a complete track loop. The difficult problem here is the sprocket-track interaction. However, a technique was conceived to model this portion of the track circuit, taking advantage of certain equations developed in the PINSTRESS II program. Implementation of this technique will be one of the first priorities when and if the Track Dynamics Program resumes.

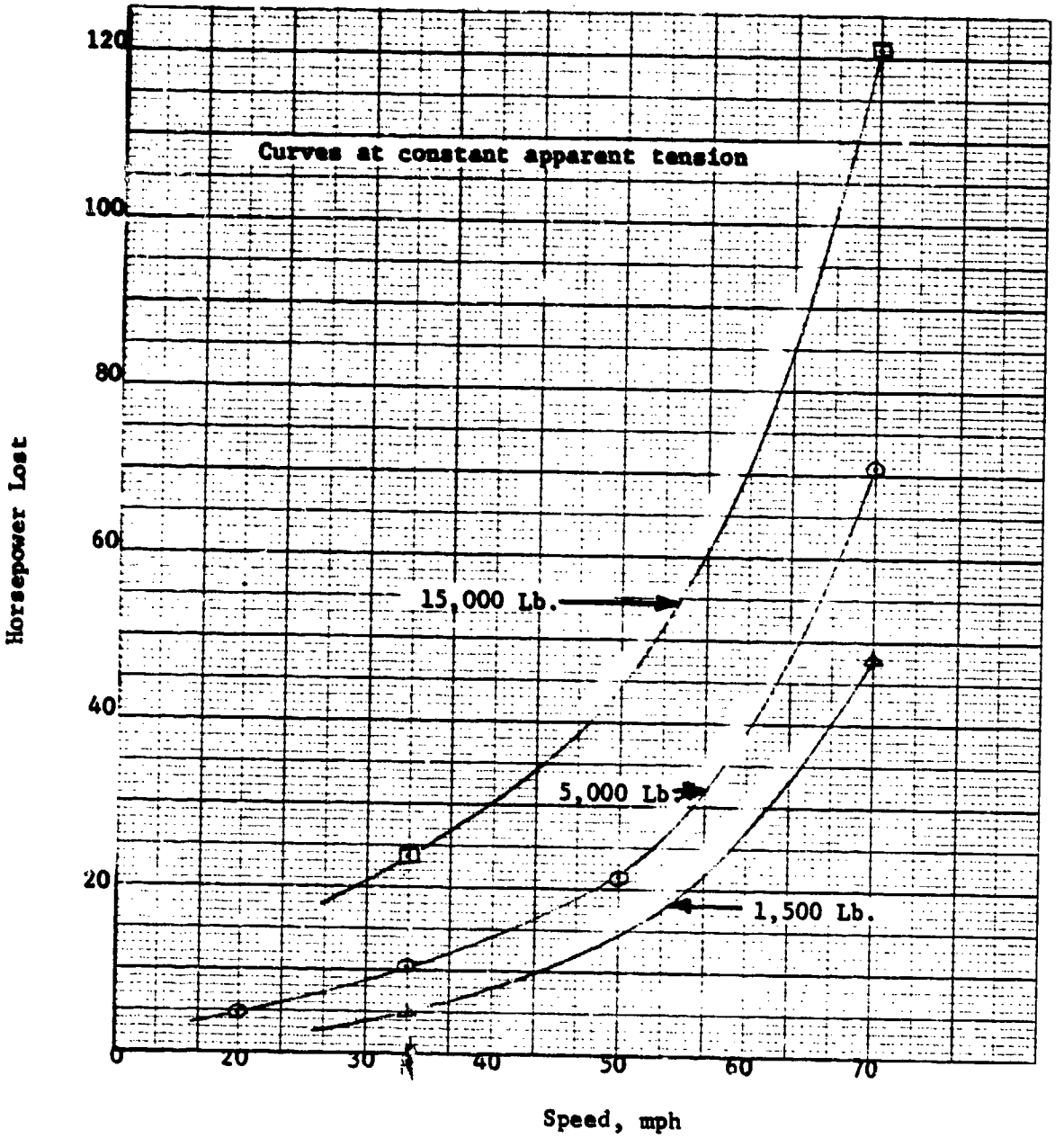

FIGURE 17. POWER REQUIRED TO DRIVE PORTION OF TRACK SIMULATED BY TRACKDYNE

Stress and Load Distribution in Pins and Bushings (PINSTRESS II)

In double-pin track, the pins and binocular tubes are unsupported over spans that are long in comparison to their diameters. They are loaded as beams by tractive forces carried through the rubber bushings. The distribution of this load is not readily apparent because the resulting beam deflections of the pin and tube tend to unload the rubber near the center of the span and to concentrate load near the ends of the span. Since reduction of bushing loads is a major objective of the double-pin track design, the effectiveness of the double-pin design depends, in part, on the ability of the pins and tubes to distribute load evenly along the length of the rubber bushing. An understanding of the load distribution is also desirable for an accurate calculation of pin and tube stresses.

A preliminary analysis using a simplified model indicated that load distribution on the bushings of the T-97 and T-142 tracks is poor. It also indicated that tube deflections are large enough to have an important influence on load distribution. Consequently, a more elaborate analysis (PINSTRESS II) was made based on a more detailed model of the pin and tube. This analysis was used to predict stresses and bushing loads for some of the simpler track loading situations where the positions of the end connectors and shoe bodies with respect to the centerguides were known or could be derived.

Later in the program, PINSTRESS II was revised to provide an input to the TRACKOB II computer simulation of a length of track subjected to localized loading. In effect, PINSTRESS II reduces the pin-bushing-tube assembly to a "black box" that applies forces and moments to the end connector and the shoe body in response to displacements and rotations of these parts with respect to the centerguide. TRACKOB II uses the characteristics of the "black boxes" to perform a simultaneous solution for the positions of the end connectors, centerguides, and shoe bodies of several track pitches. PINSTRESS II may then be used to calculate the stress in any selected pin as a function of its end connector and shoe body positions.

A similar modeling of the track structure in the vicinity of the sprocket contact would be of value, since the tooth forces applied to the end connectors evidently cause some of the highest stresses seen by the pins. An analysis by hand method became rather complicated and was not completed. A computer simulation similar to TRACKOB, using PINSTRESS as an input, would probably be more practical.

PINSTRESS II Analysis. As shown schematically as Figure 18, the model includes one half of one pin, with associated tube and rubber bushing. The

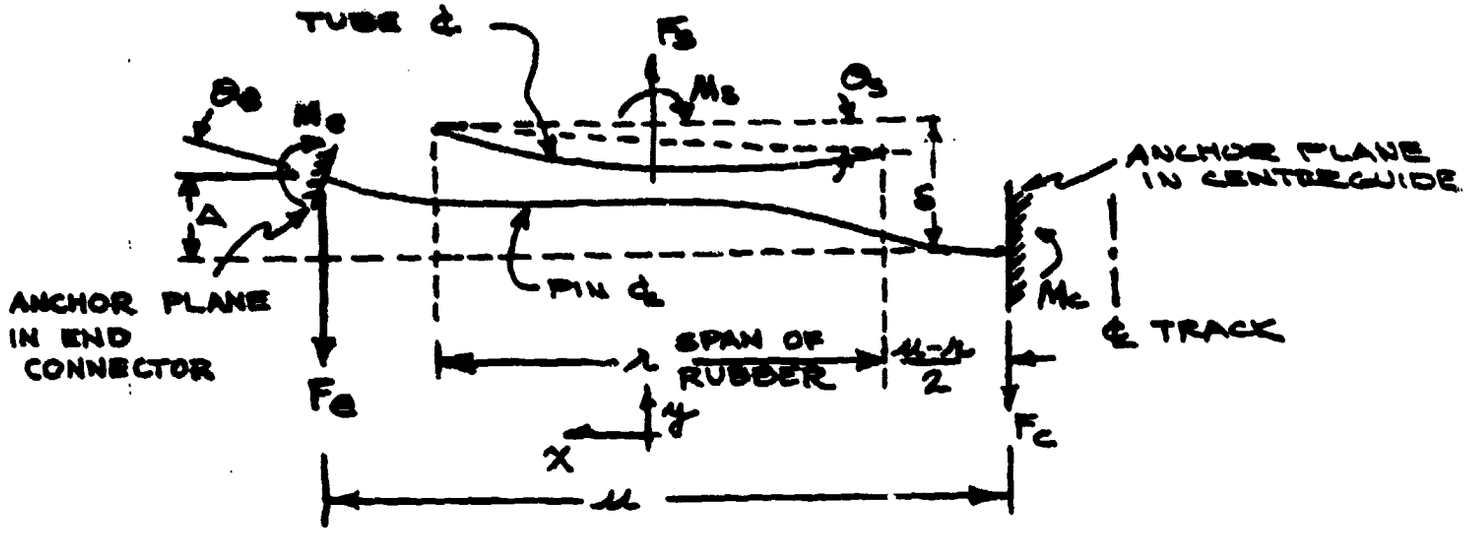

FIGURE 18. PINSTRESS II. MODEL OF PIN, BUSHING, AND TUBE.

pins are treated as three separate beams joined end-to-end, the center beam of length r being elastically supported by the rubber bushing, and the two shorter end beams being free of rubber. The ends of the pin are considered to be joined to the centerguide and end connector at effective anchor planes within these parts. Since the pin is neither completely immobilized from bending at the point where its clamped length begins, nor free to bend within the clamp, the location of the effective anchor planes requires judgement. Planes 0.5 inches within the end connector and the centerguide were used. Lack of rigidity in the clamping may be included, in a structural analysis of the track, as an additional torsion spring between the connectors and the anchor planes.

The tube is considered to have a parabolic deflection over the length r. The deflection at its center in response to transmitted track tension F_s is estimated as a function of its own stiffness and that of the binocular side plates. The deflection in response to end moment M_e and end force F_e are then calculated to provide an energy conservative system.

In T-142 track, the tube is further supported along its length by the shoe body through a thin layer of rubber, and in forged aluminum tracks there is a continuous supporting web. The maximum possible effect of this support has been found by considering the tube to be rigid.

The rubber bushing is considered to act as a linear spring providing force per unit length proportional to the offset between pin and tube centerlines. The spring rate is taken to be the same everywhere along the span r. Since direct data on the T-97 and T-142 bushings is not available, their spring rate was inferred from that of the assembled track, using the PINSTRESS II analysis. The value used was 56,000 lb/in^2.

The solution is outlined in Appendix D. The state of the system may be defined by the four forces F_s, M_s, F_e, and M_e, or by the four displacements δ, Θ_s, Δ, and Θ_e, or by any combination of four of these parameters. Euqations are given for finding the displacements in terms of the externally applied forces, and for finding the forces returned to the track structure in response to externally applied displacaments. For structural analysis, it is frequently convenient to define the system in terms of the track half tension F_s and three of the displacements.

The bending moment at any point along the pin and the radial load at any point along the bushing may be found whenever the state of the system is defined, by suitable manipulation. Though the analysis has considered primarily forces and displacements within the plane of the track, the equations may also be applied in the transverse plane. Since the stiffening effect of the binocular side plates will generally be less in this plane, the tube should be considered less rigid.

Results. If there are no nearby disturbances such as sprocket tooth forces or localized ground contact, and if the end connectors are completely rigid, a symmetrical state of track loading is obtained that is the simplest that may be considered. The track tension is divided one-fourth to each end connector and one-half to the centerguide. Then, by symmetry, Θ_s, Θ_e, and Δ are all zero, and the state of the PINSTRESS model can be defined by F_s alone. Comparison of various track designs under this symmetrical loading situation gives a meaningful indication of their relative merit, even though the stresses calculated will not be the highest seen by the track.

Table 5 compares the symmetrical-load pin stresses and bushing loads for five different track designs. The aluminum-shoe versions of the T-142 and XM-1 tracks are assumed to have no tube deflection. The "TACL Design" uses a 1.750 dia. pin with a 1.400 dia. hole through. The spans and loads are those of the XM-1, and the bushing O.D. is scaled up in proportion to the pin diameter.

TABLE 5. PIN STRESSES AND BUSHING LOADS IN SYMMETRICALLY-LOADED TRACK

	Pin Bending Stress, psi	Bushing Load Concentration Factor	Effectiveness of Center of Bushing
T-97 track, 43,000 lb load	112,000	1.64	.36
T-142 aluminum Shoe track, 43,000 lb load	116,000	1.42	.49
XM-1 track similar to T-97, 48,600 lb load	96,000	1.34	.59
XM-1 Aluminum Shoe track, 48,600 lb load	98,000	1.20	.71
TACL Design	74,000	1.12	.82

Computation of track tension is discussed in the section on Path Dynamics. The 43,000 lb. tension assumed for the T-97 track corresponds to a tractive effort of 40,000 lb. A higher tension was assumed for the XM-1 track because of the greater weight of the vehicle and the stiffer track. The bushing load concentration factor is defined as the load per unit length at the end of the bushing divided by the average load per unit length over the length of the bushing. The effectiveness of the center of the bushing is defined as the load per unit length at the center, divided by the load per unit length at the end.

In the XM-1 tracks, the pins and tubes are stiffer than those of the T-97 and T-142, while the spring rate of the rubber bushings remains about the same. This, taken together with the shorter beam spans, brings about a marked improvement in the load distribution on the rubber. Bending stresses are also reduced, though not as much as one might suppose from the larger pins and shorter spans. This is because the shifting of the rubber load toward the center of the span tends to increase the pin stress.

The computations for the aluminum shoe designs show that load distribution on the rubber can be significantly improved by immobilizing tube bending, at the penalty of a relatively small increase in pin stress. The conventional T-142 track, with its partially supported tube, would have stresses and loads somewhere between the values shown.

Tube deflections in the T-97 style designs are more important than would be supposed by comparison of the moments of inertia of tubes and pins, because the binocular side plates are not rigid enough to provide much support against rotation of the tube ends, while the pin ends are supported by the end connectors.

The clamping ability of the end connectors may be inferred from experimental data by consideration of a slightly more complex deformation pattern. If the end of the pin is restrained against rotation by a spring such that Θ_e is proportional to M_e, and if again there are no local disturbances, then the two pins in a given end connector have equal and opposite deflections, as do the two pins in a given shoe. Therefore, by symmetry, Δ and Θ_s are still zero, and the state of the system may be defined by F_s plus the rate of the end constraint spring.

If the end constraint spring has infinite stiffness, the symmetrical state previously considered results, and the tension carried by the end connector is $F_e = .5\ F_s$. More realistically, the end connector will deform in bending even though the clamps may be rigid. The spring rate of the end connector was estimated from its physical dimensions and when this rate was used in the PINSTRESS II equations, the result was $F_e = .490\ F_s$. That is, a portion of the tension was shifted from the end connector to the centerguide, but the amount shifted was very small. If, on the other hand, the clamps are completely loose, the end constraint spring has zero rate and PINSTRESS II yields $F_e = .341\ F_s$.

Experimental indications are that in real track, F_e is substantially less than $.5\ F_s$ and often closer to $.4\ F_s$. Comparison with the above theoretical results suggests that there is significant lack of rigidity in the right-angle constraint between the pin and the end connector, and that bending of the connector body is negligible in comparison.

More complex deformation patterns generally require the simultaneous solution of several pins to determine the positions of shoes and end connectors. Solutions have been obtained for a couple of configurations where the track was laid out flat, so that all deformations were in one plane. One of these was a calibration configuration where a span of three shoe sets and four connector sets was tensioned with the connector sets at the ends of the span loose. The other was a hypothetical configuration of a span of track extending to infinity in both directions and subjected to in-plane tooth loads by evenly-spaced teeth acting on five sets of end connectors at the center of the span. Solutions have not been carried through for three-dimensional configurations where the track is wrapped around a sprocket. Here the pins have components of deflection both within and normal to the plane defined by the connector set and its two pins, and these deflections are coupled by the motions of the adjacent shoes.

Effects of Obstacle Negotiation (TRACKOB II)

One of the primary objectives of the Track Dynamics Program was to develop analytical techniques that can be used to study the track. Although the final goal was to use these techniques to design track components, it was first necessary to establish the conditions under which track tension will increase. From the beginning of the program, slow, steady-state negotiation of an obstacle was identified as a probable cause of a significant increase in track tension.

To test this hypothesis, a two-dimensional model was formulated to predict track tension when the track rests on an obstacle which supports the track through its cross section. The model does not consider other tension-varying phenomena such as traction, centrifugal force, or other inertia effects. However, the increase in tension caused by any other mechanism can be added to the pretension, and then the effect of traversing the obstacle can be quantified at that modified pretension.

After the model was developed, tests were conducted at TARADCOM, Warren, Michigan, to measure track tension when traversing well-defined obstacles. These tests validated the model and provided confidence in the analytical technique developed for this study.

After this validation of the model and implementation of a number of refinements, several of the track parameters were varied to determine the effect of varying various track parameters in terms of the effect on track tension.

Description of Model. Since this study was concerned with the overall effect on track tension when a tracked vehicle negotiated an obstacle, the model was restricted to two dimensions. Accordingly, the simulation applied to obstacles such as logs or large rocks which produced an equally distributed lifting across the complete width of the track. It was not, for example,

applicable to a displacement input to the track occurring under a single end connector. In this case (which was analyzed later), the total track tension will be significantly less than that resulting from the symmetric displacement of the track, and the one end connector near the obstacle would experience a greater load than its partner on the other side of the same shoe.

A single track on the M60 tank consists of approximately 80 shoes. From a two-dimensional viewpoint, each shoe consists of a block element, an end connector/centerguide element, and a bushing/pin/binocular tube element. These shoes interact with road wheels, idlers, and the sprocket as well as with the ground. Assuming that there are three degrees of freedom for each end of an element (vertical, longitudinal, and pitch) leads to approximately 1,000 degrees of freedom that must be comprehended by a two-dimensional model of a single track. Therefore, to reduce the complexity of the model, only 16 track shoes and 4 road wheels were modeled in detail. The track between the center four road wheels was chosen because any increase in track tension would be greatest when an obstacle was in the vicinity of the center road wheels. If an obstacle was near the front or rear road wheels, track tension would be less, especially at the rear road wheel where there is no compensating idler as in the front. The effect of the front and rear road wheels and the remainder of the track was included, as will be discussed later.

Reducing the model from 80 track shoes to 16 track shoes resulted in a two-dimensional model with 218 degrees of freedom. Since this many degrees of freedom was still considered unwieldly for normal analytical approaches, a finite-element technique was chosen to solve the problem.

In general, finite-element techniques are specifically useful for systems which contain a large number of degrees of freedom. The unique aspect of finite element methods is that it is not necessary to develop any equations; only the geometry, element properties, and loading conditions must be defined. The finite-element code, which can be simply defined as a transformation between the loading conditions on the system and the displacements and internal forces of the system, establishes the equations of motion. Because of its capabilities and flexibilities, a newly developed proprietary finite-element code called SAVFEM (Structural Analysis Via Finite-Element Methodology) was used after unsuccessful attempts to model this system using readily available computer codes.

Modeling the tank track negotiating an obstacle presented five somewhat unusual problems. First, it was necessary to consider each road pad as an element that could react in compression but be free to lift off in tension. Second, each road pad had to withstand a maximum shear force equal to its normal load times the coefficient of friction between the rubber road pad and the ground. When the longitudinal shear force was greater than this maximum shear force, the road pads were allowed to slide until the forces were equilibrated. Both of these nonlinear property phenomena were available as a single friction/lift-off element in SAVFEM.

The third unusual feature was that as the track was lifted up between two road wheels, it tended to wrap around the adjacent road wheels. Since this event was just the opposite of the road pads breaking contact with the ground, part of the road wheel was modeled as a lift-off element which was not initially in contact with the track. However, if the track did displace high enough vertically to cause it to wrap around a road wheel, the frictional option of the element was not incorporated, i.e., the track became elastically attached to the road wheel.

The fourth peculiarity was that it was necessary to introduce a pretension into the track. This could not be done by simply pulling on the ends of the track as it rested on the ground under the appropriate wheel loads, because the road pads and the road wheels would be subjected to a shear load. Therefore, to eliminate any initial shear forces in the system, the first loading condition assumed a weightless track with no wheel loads and no contact between the ground and road pads, or between the track and the tank hull through the road wheel suspension. With these conditions, an initial displacement was applied to both ends of the track to introduce the pretension.

The last difficulty in modeling the track was that the track shoes underwent large displacements relative to their dimensions. Usually a finite-element technique is applied to small-displacement problems where it can be assumed that the overall system stiffness is not a function of the system displacements (linearity). But because the track displacements were large, the system stiffness was not constant, and it was necessary to use a nonlinear technique. The particular approach used in this study was to vertically displace one small section of track a fraction of the obstacle height and calculate the displacements of the total system. On the basis of these displacements, the system stiffness was reformulated and equilibrium

displacements were again calculated. This procedure was continued until a preset error criterion on the equilibrated forces acting at each section of track was satisfied. Then the track was displaced to a greater fraction of the obstacle height, and an iteration on the system stiffness again brought the track elements into equilibrium. The track was successively displaced in ten increasingly larger increments to the maximum obstacle height. Each step resulted in a static track configuration and the internal forces in the track.

Finite Element Coding. In this analysis, three types of finite-elements and two loading conditions were used to define the system. To model the steel portion of two blocks per shoe, a linear elastic beam element was utilized. In general, a linear elastic beam can respond to tension, compression and bending loads. The second element in the model, also a linear elastic beam, represented two end connectors and a center guide in parallel. The design pitches of the block and end connector sections are 4.442 and 2.5 inches, respectively. For convenience, pitches were assumed to be 4.5 and 2.5 inches. Based on the practice of removing one or sometimes two complete shoes from the track due to permanent set in the bushings after a short break-in period, the value of 4.5 inches for the block length may be slightly short, but it was a suitable value for this analysis.

A third set of linear elastic beams was used to model the rigid structure of the tank hull to which the six road wheel suspension systems were attached. These beams were not modeled to simulate the actual flexibility of the hull, but only to serve as a rigid member to which half of the tank's sprung weight was applied as a load. Hence, their area and moment of inertia values were assigned arbitrarily, such that their effective translational and rotational stiffness were several orders of magnitude greater than those of the other elements in the system.

The second type of element used in the analysis was a spring element which could undergo only a translational displacement in a specified direction, but not a bending displacement. In addition, this element could simulate a shear force perpendicular to its axis, and if that shear force was greater than a coefficient of friction times the normal load, the element would slip until the forces were balanced. Lastly, the spring element had an active/nonactive option that could be used to simulate an element which could take compressive but not tensile loads.

The second type of element used in the analysis was a spring element which could undergo only a translational displacement in a specified direction, but not a bending displacement. In addition, this element could simulate a shear force perpendicular to its axis, and if that shear force was greater than a coefficient of friction times the normal load, the element would slip until the forces were balanced. Lastly, the spring element had an active/nonactive option that could be used to simulate an element which could take compressive but not tensile loads.

The spring element was used to its fullest capability when modeling the road pads. Each set of two road pads on one shoe was modeled as two springs - one connected to each end of the beam element modeling the block cross section. The longitudinal separation between the two springs representing the road pad was equal to 4.5 inches - the same as the beam length representing the block. Although the 4.5 inch separation was slightly greater than actual (a worn pad is typically closer to 4.0 inches in effective length), this dimension should have negligible effect on track tension.

Spring elements were also used to model the road wheels. It was assumed that each of the four road wheels modeled was located symmetrically over a track block. Although this assumption was not quite true, it was a convenience used to simplify the model and should have a minimum effect on the accuracy of the solution. In addition to the two spring elements which supported the wheel load, the two center road wheels were modeled with two additional spring elements each. These springs became active when the track tended to wrap around the road wheel due to a high vertical displacement of the track between two road wheels.

A third use for the spring elements was to simulate the vertical component of stiffness in the torsion bar suspension. These elements were initially assumed to be 13 inches in length before compression. When the sprung weight of the tank was applied, the torsion bar springs compressed 5 to 6 inches, leaving a jounce capability of 7 to 8 inches, before hard stops were encountered. The hard stops were also modeled as springs which did not become active until the total jounce displacement of the road wheel was taken up.

Although only 16 track shoes were modeled in the simulation, the stiffness effect of the remaining shoes was simulated by spring elements at each end of the track. The stiffness of these two spring elements was established by considering the total number of effective pins in the track. The nominal number of track pins was 160. The finite-element model included 32 pins, and 8 pins around the sprocket were "locked out". This left 120 pins which contributed to the flexibility of the unmodeled segments of track. Therefore, the stiffness of the unmodeled segments of track was determined by dividing the radial stiffness of one pin bushing/binocular tube assembly by 120. To keep the model symmetric, the fact that there are fewer track shoes between the fifth road wheel and the sprocket than between the second road wheel around the front idler to the sprocket was ignored. The net result was that twice the stiffness of the total unmodeled track was specified at both ends of the modeled track.

Lastly, spring elements were used to account for the stiffness of the torsion bar, road wheel, and road pads at the first and sixth road wheel location. The value of these stiffnesses was calculated as the above three springs in series.

In addition to beams and springs, a third element was utilized in the model--the general elastic element. The general elastic element reflects a stiffness relation between any number of degrees of freedom within the structural model. This element can be used to model components whose geometric properties are difficult to define, but whose elastic-stiffness relationship with respect to the structure is known either through experimental data or analytical techniques. Because the general elastic element is mathematically very simple, its use in the finite element code is cost effective.

The general elastic element was utilized to model the pin/bushing/binocular tube stiffness in all three degrees of freedom at the interface between the shoe block and end connector elements. It was also used at each end of the track to account for the vertical and horizontal degrees of freedom. The radial stiffness of the pin/bushing/binocular tube was assumed for both the longitudinal and vertical pin/bushing/binocular tube stiffness. The torsion stiffness of the pin/bushing/binocular tube with respect to the shoe blocks was used for the rotational stiffness. The final form of the two-dimensional model (TRACKOB II) is shown in Figures 19 and 20a, and the three-dimensional model (TRACKOB III) is shown in Figure 20b.

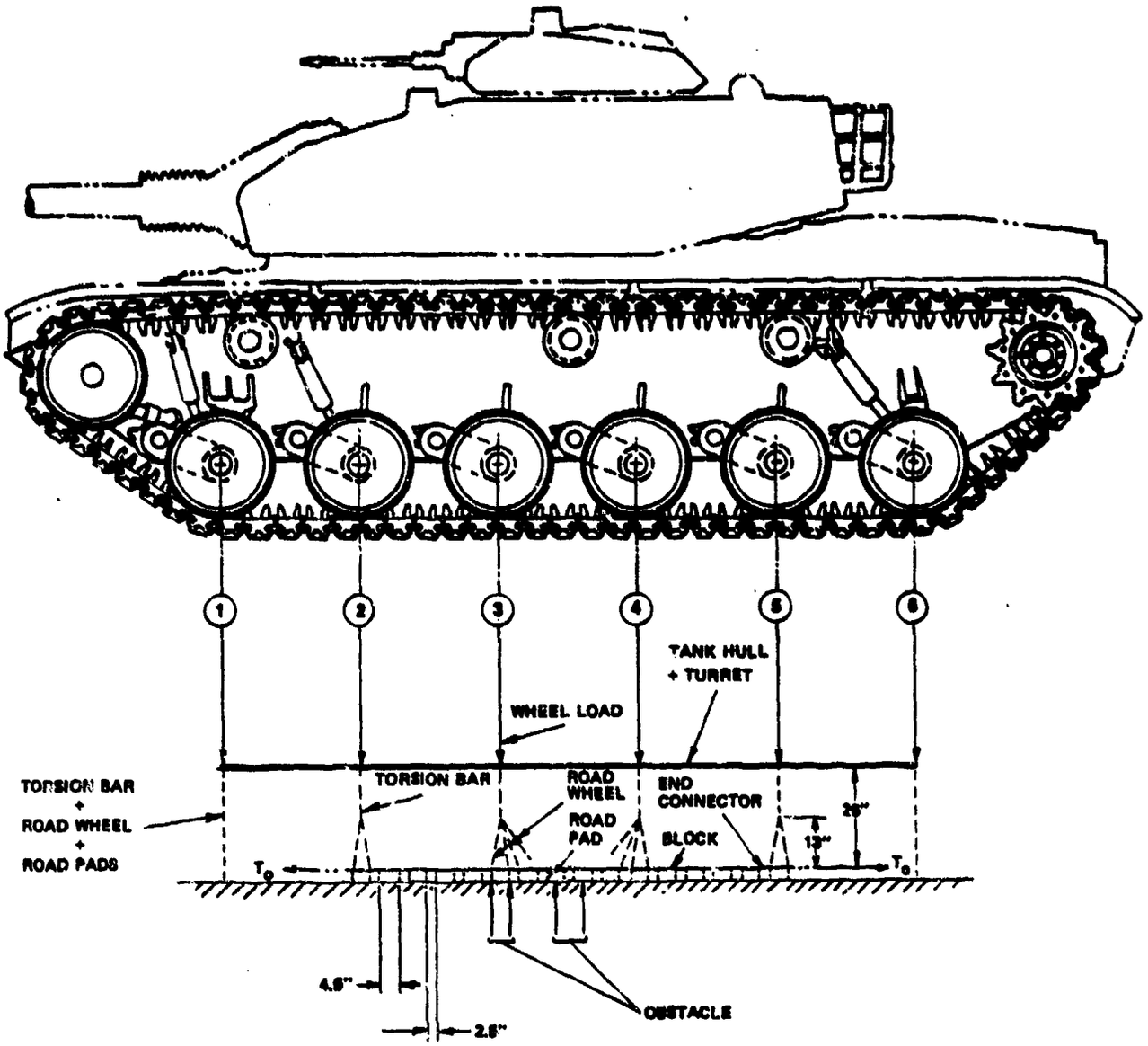

FIGURE 19. TRACKOB MODEL USED TO PREDICT TRACK LOADS AND DEFLECTIONS OVER OBSTACLES

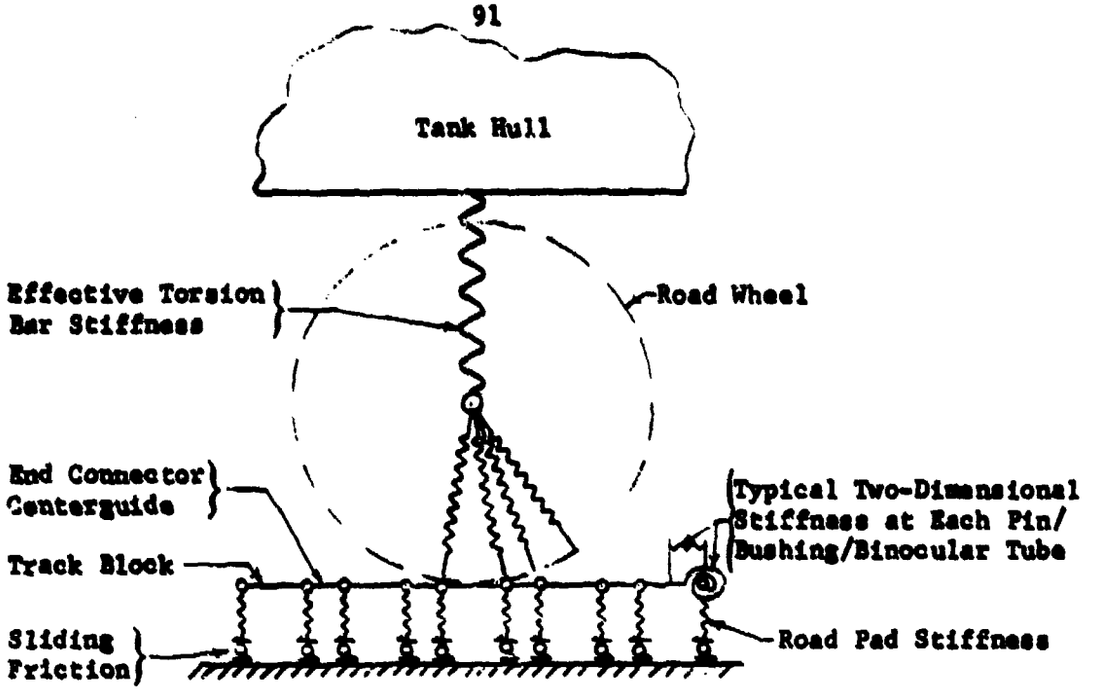

a. Two-Dimensional Finite-Element Model of Third Road Wheel and Track

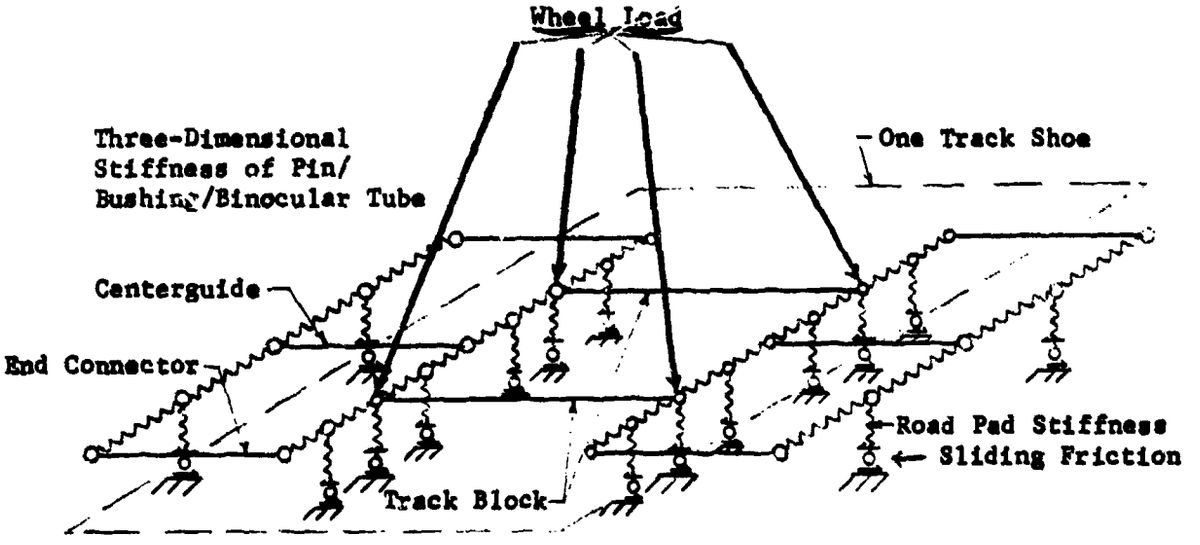

b. Three-Dimensional Finite-Element Model of Track Shoe (Under Third Road Wheel)

FIGURE 20. ENLARGED VIEW OF TRACKOB MODEL SHOWING DETAILED REPRESENTATION OF TRACK ELEMENTS

As stated above, two types of loading conditions were applied to the track at specific nodes, i.e., forces, and displacements. The forces included the wheel loads (one twelfth of the sprung weight of the tank) and the weights of the track shoes. Six equal wheel loads were applied directly above the road wheels to the beam elements representing the tank hull. The 75 pounds per track shoes was distributed over those elements representing the shoe block (47 pounds) and those representing the end connector/ centerguide (28 pounds).

The displacements imposed on the system were first, to establish a pretension in the track, and second, to simulate the track displaced vertically when resting on an obstacle. Knowing the stiffness of the modeled section of track (general elastic elements) and unmodeled sections of track (springs), equal and opposite longitudinal displacements at the two ends of the modeled sections of track were specified to establish a pretension in the track.

In the vertical direction, the displacement was assumed to occur symmetrically. When the obstacle was between two road wheels, its length was assumed to be 7", and the centers of two longitudinally adjacent shoe blocks were vertically displaced equally. When the obstacle was beneath one road wheel, both ends of the shoe block were vertically displaced equally. Two of these four displacements (in addition to the pretensioning displacements) were the only ones assigned for a given case. All other displacements were determined by satisfying static equilibrium conditions through iteration procedures in the finite-element code.

Physical Properties. Since the actual structural properties of a tank track would vary with age and mileage, it was not possible nor was it desirable to determine the exact values of the parameters necessary to conduct this study. However, the results were applicable to a generic group, i.e., a double-pin track on a 50-to 50-ton tank. Specifically, the track properties used in this study represented the T-142 track (replaceable pad), although the results could also be applied to the T-97 track (integral pad). The tank properties were those of the M60, but XM1 and M48 vehicles would exhibit similar results. In fact, the simulation of many tracked vehicles would yield comparable qualitative results.

The values of the parameters used in the track model are given in Table 6, and the parametric variations are listed in Table 7. The last four parameters in Table 2 were held constant, not because they did not have a range of values, but because their variation was considered to have a negligible effect on track tension.

Two of the parameters listed in Table 6 were not well defined. The first was stiffness of the suspension hard stop. On the M60 the hard stops for the four center road wheels are steel bosses welded to the tank hull. Their stiffness was not known. Since the road wheel displacement relative to the hull was always less than the available jounce for all simulation runs, its value was academic.

The second ill-defined parameter was the coefficient of friction between the rubber pad and the ground. Typically, the coefficient of friction between rubber and most hard dry surfaces exceeds unity, but that value was not applicable in this study for the following reason. In the analytical model the vehicle was assumed to be stationary in the longitudinal direction, and the obstacle was introduced by displacing the track in the vertical direction. If this event did occur, large shear forces would be developed in the rubber road pads, and a static coefficient of friction near unity would be a reasonable assumption for hard dry surfaces. But, when a tracked vehicle traverses an obstacle, the road pads which are initially off the ground will adjust their longitudinal position as the track is laid. On the other hand, the road pads in front of the obstacle are restrained by the weight of the vehicle and will experience some longitudinal shearing forces. The actual magnitude of the shearing forces on the road pads during this operation is difficult to determine, and was not addressed in this study. However, it is known that the road pads "walk" as the road wheels move over them and this adjusts their longitudinal position.

In this study shearing forces were considered by assuming that the road pads could generate a longitudinal force as great as the coefficient of friction times the normal load on the pad. A greater force caused the road pad to slip longitudinally until the shear force was reduced to the maximum frictional force. To accomplish this phenomenon, an arbitrarily low

TABLE 6. NOMINAL TRACK MODEL PARAMETERS

Tank sprung weight	8700 lb/road wheel
Road pad/ground friction coefficient	0.25
Track longitudinal stiffness[1]*	800,000 lb/in./pin
Suspension stiffness[2]	1600 lb/in./road wheel
Track rotational stiffness**	25,000 lb-in./rad/pin
Track pretension[2]	12,000 lb
Track weight	75 lb/shoe
Road pad vertical stiffness**	23,000 lb/in./pad
Road wheel rubber stiffness	15,000 lb/in./block
Suspension hard stop stiffness	1,000,000 lb/in./road wheel

** Experimentally determined by Battelle's Columbus Laboratories.

TABLE 7. VARIATIONS OF NOMINAL TRACK MODEL PARAMETERS

Tank sprung weight	7830; 9750 lb/road wheel
Road pad/ground friction coefficient	0.0; 0.50
Track longitudinal stiffness	600,000; 1,000,000 lb/in./pin
Suspension stiffness	1200; 2000 lb/in./road wheel
Track rotational stiffness	12,500; 37,500 lb-in./rad/pin
Track pretension	6000; 18,000; 24,000; 30,000; 36,000 lb

* Numbers in parentheses refer to references given at bottom of page.

(1) Gow, E. J., Jr., "Radial Pin Shift Investigation", Chrysler Defense Division/USATACOM, T142 Track Task Force Report, Task 2-7, September 25, 1974.

(2) Wolken, L. P., Input Data to Chrysler's Mathematical Model of M60 Tank.

value of 0.25 was chosen for the coefficient of friction. Variations in this value did produce significant changes in track tension as is discussed later.

There were several other properties which had to be specified for the track. In particular, the beam that modeled the shoe blocks and end connector/centerguide elements was assumed to be steel (elastic modulus = 29×10^6 psi, Poisson's ratio = 0.29). Representative cross-sectional areas and moments of inertia were calculated to provide realistic stiffness to the elements. However, because the steel sections of track possessed stiffnesses that were several orders of magnitude greater than those for the rubber sections, an accurate determination of their properties was unwarranted in this study.

Validation of Model. Since any mathematical model is only as good as its ability to simulate the system it is modeling, tests were conducted to establish the variation in track tension when the M60 traversed an obstacle.* The track tension was determined by mounting four strain gages on each of two pins at the end connectors and on either side of the centerguide. The strain gages were mounted to measure pin shear in such a manner that the sum of the four shear forces was the total track tension.

The two pins with strain gages were fitted into a T-142 track shoe. A two-shoe assembly was calibrated on a tensile testing machine and then installed in the T-142 track of an M60A1 tank.

The tests were carried out indoors on a concrete floor, and the obstacles were rectangular blocks of wood, which were longer than the width of the track. The track was initially tensioned to about 6,000 pounds (another pretension load of approximately 12,000 lbs., which is the nominal M60 track tension, was also used during the tests, and the M60A1 was driven over a 5" wooden block. The measured track tension (several inches from the obstacle) was recorded when the obstacle was under each road wheel and between each road wheel. The results are illustrated in Figure 21.

Several conclusions were immediately evident. First, the assumption that track tension would be greatest near the center road wheels was verified. Of particular interest was the decrease in track tension below the pretension value when the obstacle was under the sixth road

*Tests conducted by Battelle's Columbus Laboratories at TARADCOM, Warren, Michigan.

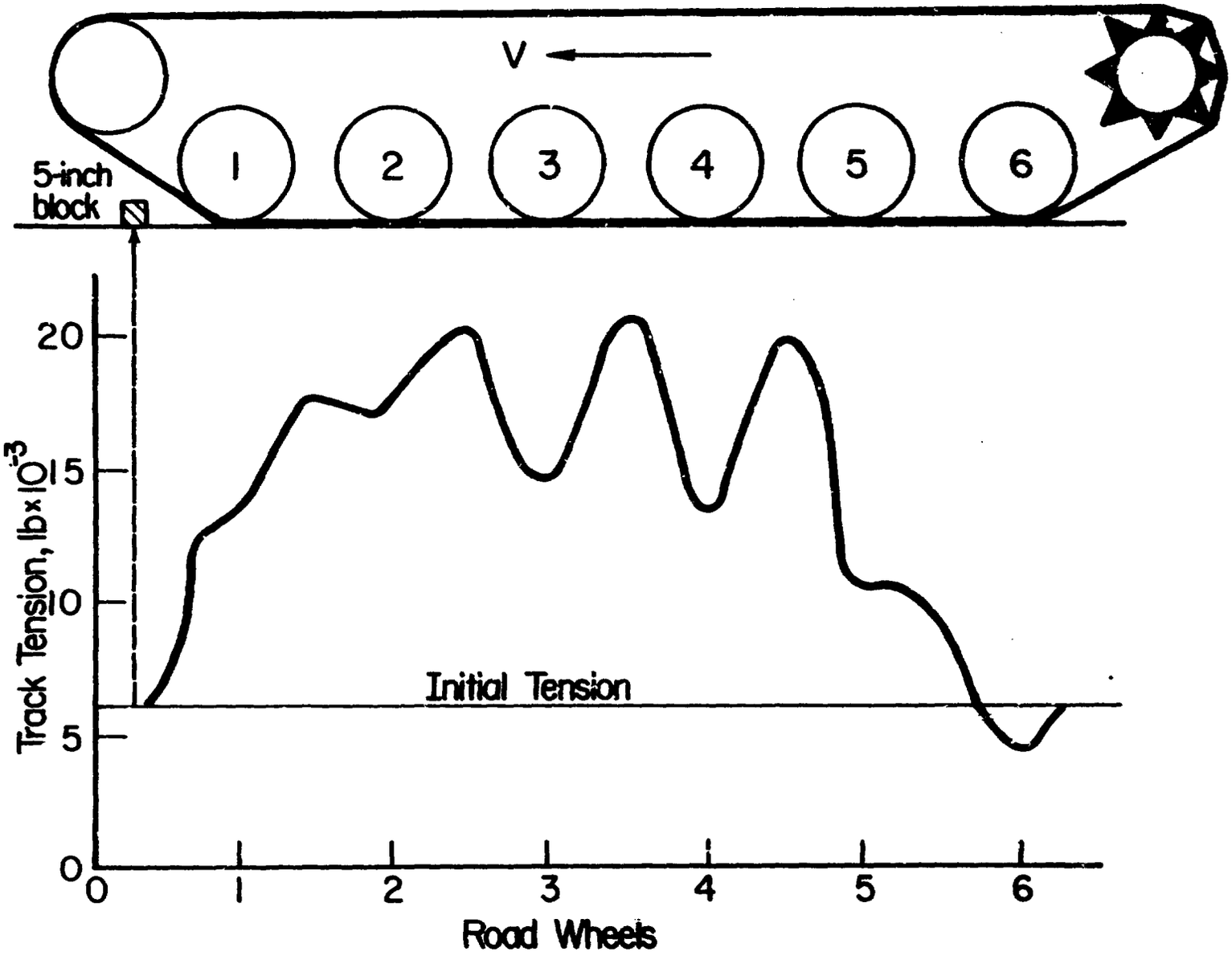

FIGURE 21. SPATIAL INFLUENCE OF 5-INCH OBSTACLE ON M60A1 TRACK TENSION
(Initial track tension ≈ 6,000 pounds; velocity ≈ 0.0 mph)

wheel. Also, it was apparent that there was a significantly higher track tension when the obstacle was between road wheels than when it was under a road wheel. These tests, along with the analytical model, identified the negotiation of obstacles as a major influence on track tension.

Other validations were also carried out. Using two pretension values and three obstacle heights, track tension was recorded when the obstacle was between road wheels 3 and 4, and under road wheel 3. For the same condition, the finite-element model was exercised to predict track tension as a function of obstacle height. A comparison of the measured and predicted track tension is displayed in Figure 22 for obstacle heights up to 10 inches. All the experimental data points plotted in Figure 22 were the results of a single test case, i.e., the values were not statistical averages. At this time, the statistical significance of the measured data is not known.

The three comparisons between theoretical and experimental results shown in Figure 22 have established the finite-element model as being accurate except perhaps for one phenomenon. In the two cases for the obstacle between road wheels 3 and 4, the theoretical prediction indicated a slightly less steep increase in the track tension after the third and fourth road wheels were lifted off the ground by the track (obstacle height about 4 inches). On the other hand, the experimental data suggested a nearly constant track tension above a 5-inch obstacle height. Although there was only one measured datum point above the 5-inch obstacle, similar results were obtained for initial track tensions of both 6,000 and 12,000 pounds.

Because of this significant discrepancy between theory and experiment, the original finite-element model was modified to include: road pad/ground friction, track wrap around the road wheels, the total sprung weight of the hull, and the first and sixth road wheels. All of these modifications had some effect on the shape of the predicted results, but none produced the large change in track tension slope shortly after the third and fourth road wheels were lifted. Therefore, if the phenomenon is realistic, as indicated by a small sample of test data, the mechanism is not understood at this time.

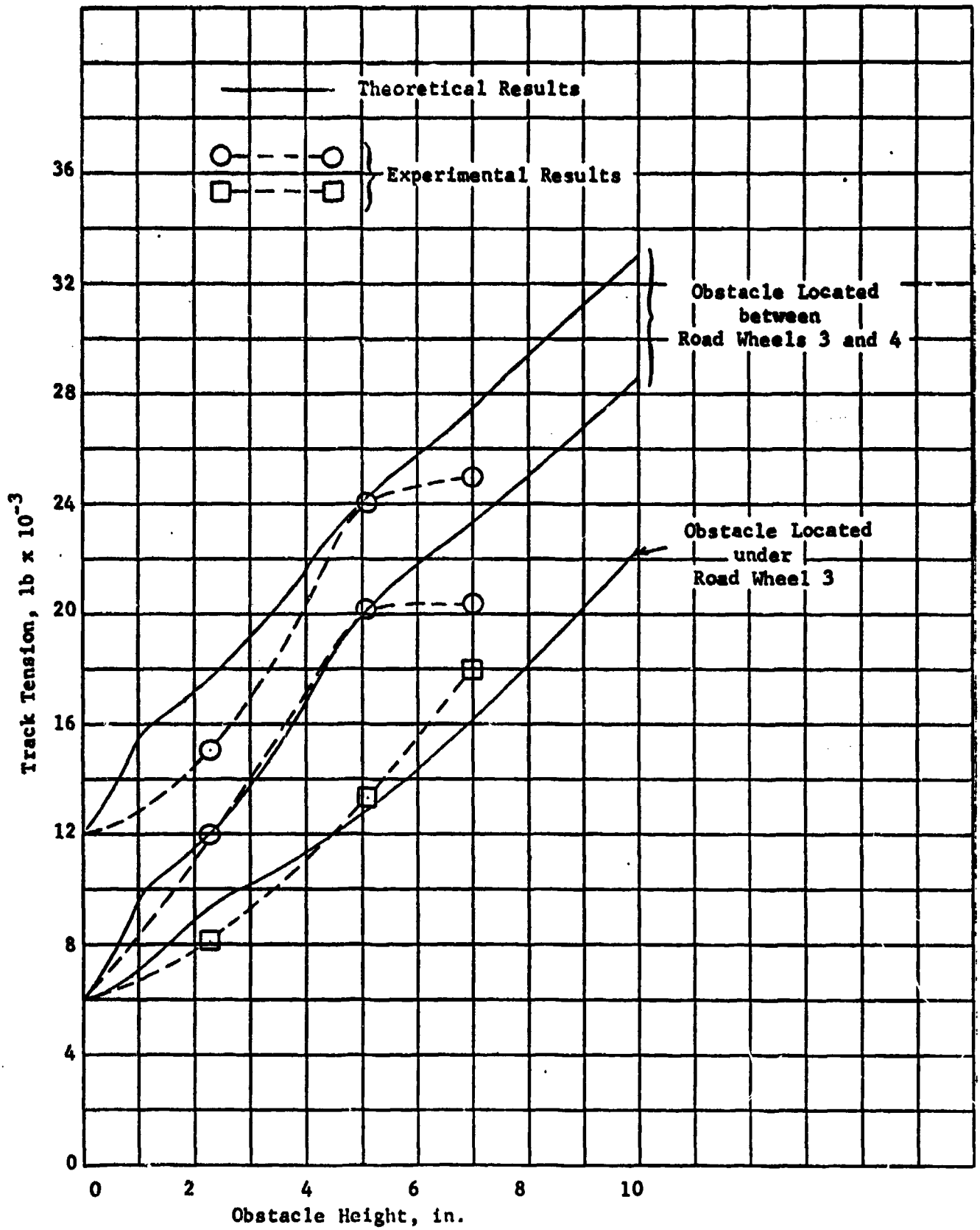

FIGURE 22 COMPARISON OF THEORETICAL AND EXPERIMENTAL RESULTS FOR M60 TRACK TENSION WHEN TRAVERSING AN OBSTACLE

Results of Parametric Study (Obstacle Between Road Wheels). The nominal track parameter values were given in Table 6. Of these parameters, six (see Table 7) were considered likely to have some effect on the track tension as the vehicle traversed an obstacle. Accordingly, the six parameters were varied over a realistic range to determine their effect on track tension. Because the track tension increase was greatest for the condition of the obstacle between the road wheels, that situation was simulated for all six parameter variations. Two of the parameters were found to have a small effect on track tension, and their variation was not considered when the obstacle was under a road wheel. In the following results, the values of all the track model parameters are those given in Table 6, except as noted on the figures.

Effect of Sprung Weight. The first parameter that was varied was the tank sprung weight. The M60 tank has a total weight of approximately 55 tons. Subtracting out the weight of the road wheels and the track in contact with the ground results in a sprung weight of about 8700 lb/road wheel. Variation in fuel, ammunition, and other equipment could conceivably alter the weight by as much as 5000 pounds. Therefore, a 10 percent change ($\pm$10,440 pounds) was considered the most extreme case possible. Figure 23 shows the predicted increase in track tension with obstacle height when the obstacle was between the third and fourth road wheels. Generally, the differences due to wheel load were small at all obstacle heights.

There were two noticeable changes in the slope of the curves for track tension when the obstacle was between road wheels. The first occurred at an obstacle height of about one inch, while the second occurred at an obstacle height of about four inches. Both of these changes represented a decrease in the stiffness of the system. A close examination of the finite-element results revealed that at obstacle heights of 1.1 inch or less, not all of the road pads were in maximum shear (coefficient of friction times normal load). At greater obstacle heights all of the road pads were under maximum shear force, and were slipping as the obstacle height increased.

At about the 4-inch obstacle height, the system underwent another significant change when the two road wheels adjacent to the obstacle were lifted off the ground by the track. As can be seen in Figure 23, the obstacle height at which this occurred did not depend on the road wheel load.

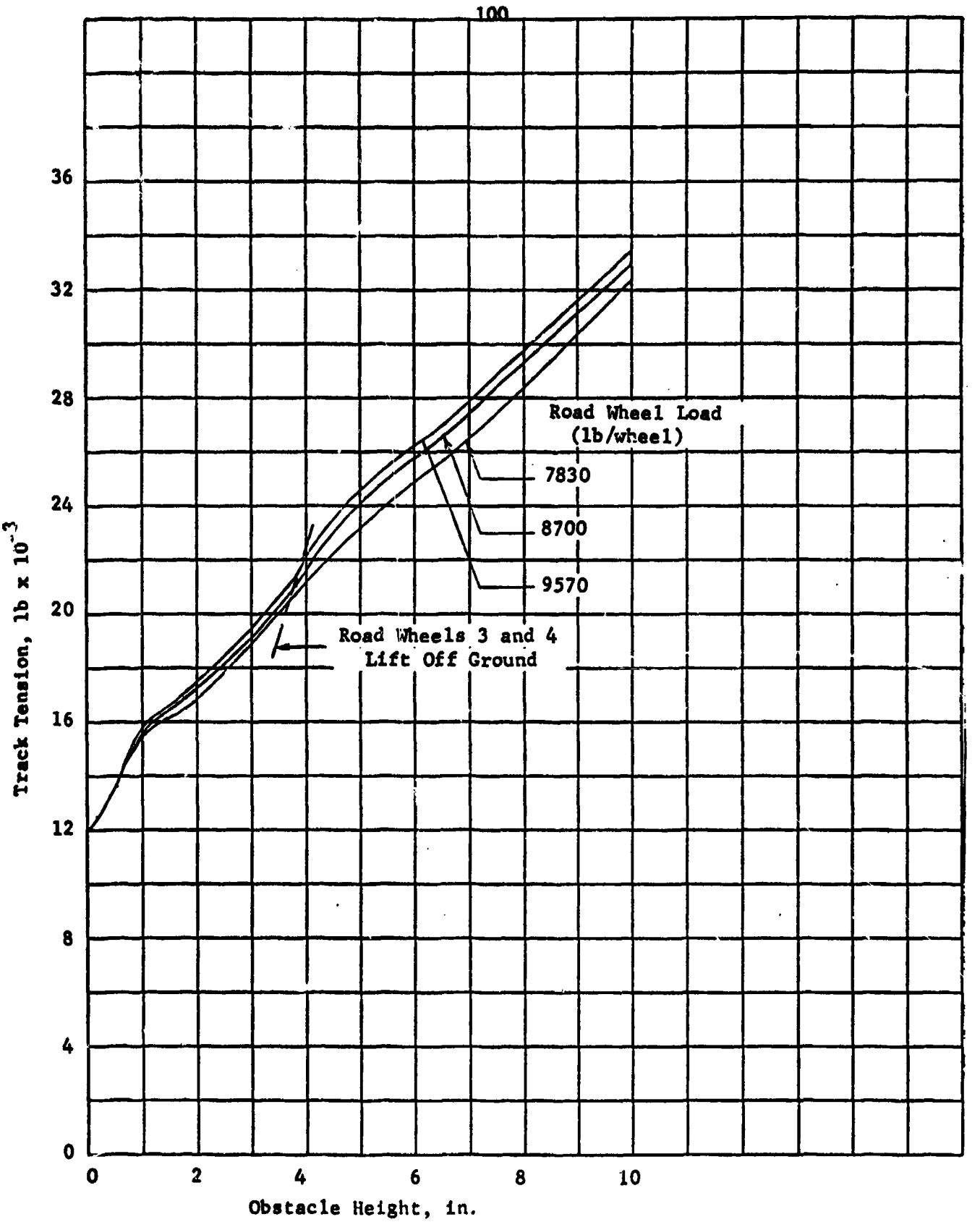

FIGURE 23. EFFECT OF ROAD WHEEL LOAD (TANK SPRUNG WEIGHT) ON M60 TRACK TENSION WHEN TRAVERSING AN OBSTACLE

The obstacle was located between Road Wheels 3 and 4.

Effect of Road Pad/Ground Friction. As explained previously, the actual magnitude of friction applicable to this simulation was difficult to ascertain because of the natural longitudinal adjustment that the track shoes make when the vehicle traverses an obstacle. Nevertheless, Figure 24 does indicate that the effective friction between the rubber road pads and the ground was significant for moderate-size obstacles. After the third and fourth road wheel had lifted, most of the road pads were no longer in contact with the ground. Above a 4-inch obstacle, friction was less effective and as can be seen by the results in Figure 24, the track tension became nearly identical for all friction values.

The shapes of the curves for the smaller obstacle heights were radically different. As already noted in Figure 23, the change in slope above the 1.1-inch obstacle height for a coefficient of friction equal to 0.25 was due to all the road pads slipping under a maximum shear force. With no friction, the road pads slip immediately, and the system exhibits a lower overall stiffness (slope of curve). When the friction coefficient was 0.5, the road pads under road wheels 3 and 4 did not slip until a 1.2-inch obstacle height was reached. All the road pads out to road wheels 2 and 5 were slipping at about 1.8 inches. Therefore, the change in slope of the 0.5 friction coefficient curve was more gradual than that for the 0.25 friction coefficient curve.

The second change in stiffness (slope of curve) at about a 4-inch obstacle height was similar for all three friction coefficients. As expected, a higher friction coefficient caused the road wheels adjacent to the obstacle to lift off sooner than they did for the lower friction coefficients. From physical considerations, if the road pad does not support a shear load, the extra length of track needed to accommodate the height of the obstacle can be obtained by stretching the track. However, if friction is high, the track cannot stretch as readily because it is being held by the shear forces in the pads. Nevertheless, although the friction coefficient had a significant effect on track tension for moderate obstacle heights, it had a small effect on wheel lift.

Effect of Track Longitudinal Stiffness. From a modeling viewpoint, the tank track is a sequence of springs in series. Because the bushing/pin/binocular tube stiffness was several orders of magnitude less than the stiffness of the

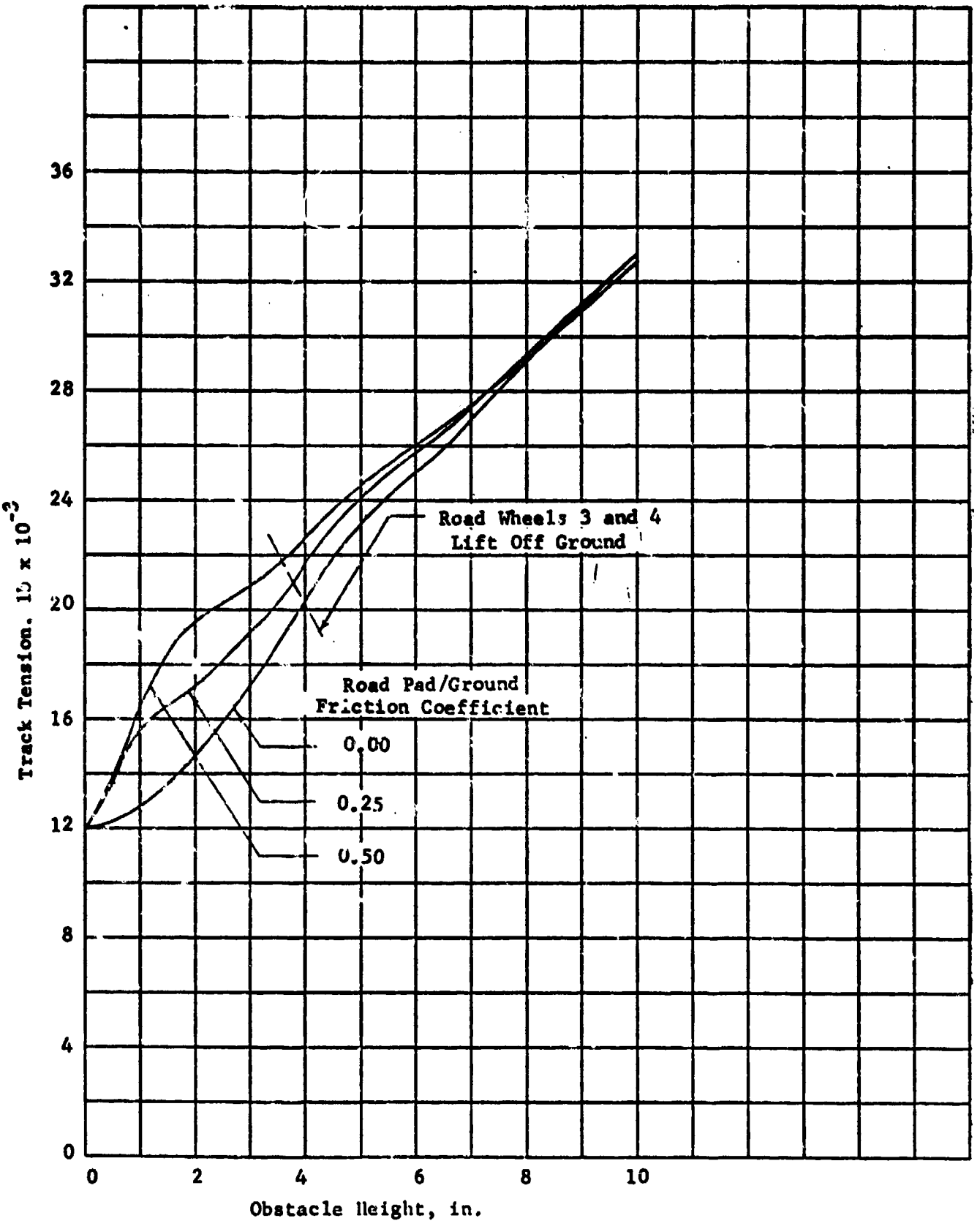

FIGURE 24. EFFECT OF ROAD PAD/GROUND FRICTION COEFFICIENT ON M60 TRACK TENSION WHEN TRAVERSING AN OBSTACLE

The obstacle was located between Road Wheels 3 and 4.

end connectors, centerguides, and blocks, only the bushing/pin/binocular tube stiffness was varied to change track longitudinal stiffness. The nominal value used for stiffness was determined experimentally. The 25 percent variation (shown in Figure 25) could be attributed to deterioration or heating of the rubber bushings which would lower the stiffness, or to cold-weather operations which would increase the stiffness. This parameter had a significant effect which increased with increasing obstacle height. The tendency for wheel lift was to maintain ground contact longer with a more flexible track because the track stretched more to envelop the obstacle.

Effect of Torsion Bar Suspension Stiffness. Although the torsion bar suspension stiffness has a major role in the dynamics of the tank, it proved to have only a small effect on track tension when traversing an obstacle, and then only after the road wheels lifted. The trend of decreasing track tension with decreasing suspension stiffness was expected because for the same obstacle height, the stiffer suspension on road wheels 3 and 4 supported a greater percentage of the tank's sprung weight. The reduction in the slope of the curve after the road wheels lift off suggested that the experimental data in Figure 22 might be more closely approximated by a less-stiff torsion bar suspension. But the small reduction illustrated in Figure 26 also suggested that it was not physically realistic to decrease the stiffness sufficiently to have an appreciable effect.

Effect of Track Bending Stiffness. Like track longitudinal stiffness, the bending stiffness of the track is dependent on the flexibility of the bushings. But, as seen in Figure 27, track bending stiffness had only a small effect on track tension as compared with longitudinal stiffness (see Figure 25). However, the effect was in a worsening direction in the sense that as the rubber ages it will become more flexible (lower bending stiffness), and the track tension will increase. The small increase due to bending stiffness would, however, be more than compensated for by the reduction resulting from the decrease in longitudinal stiffness.

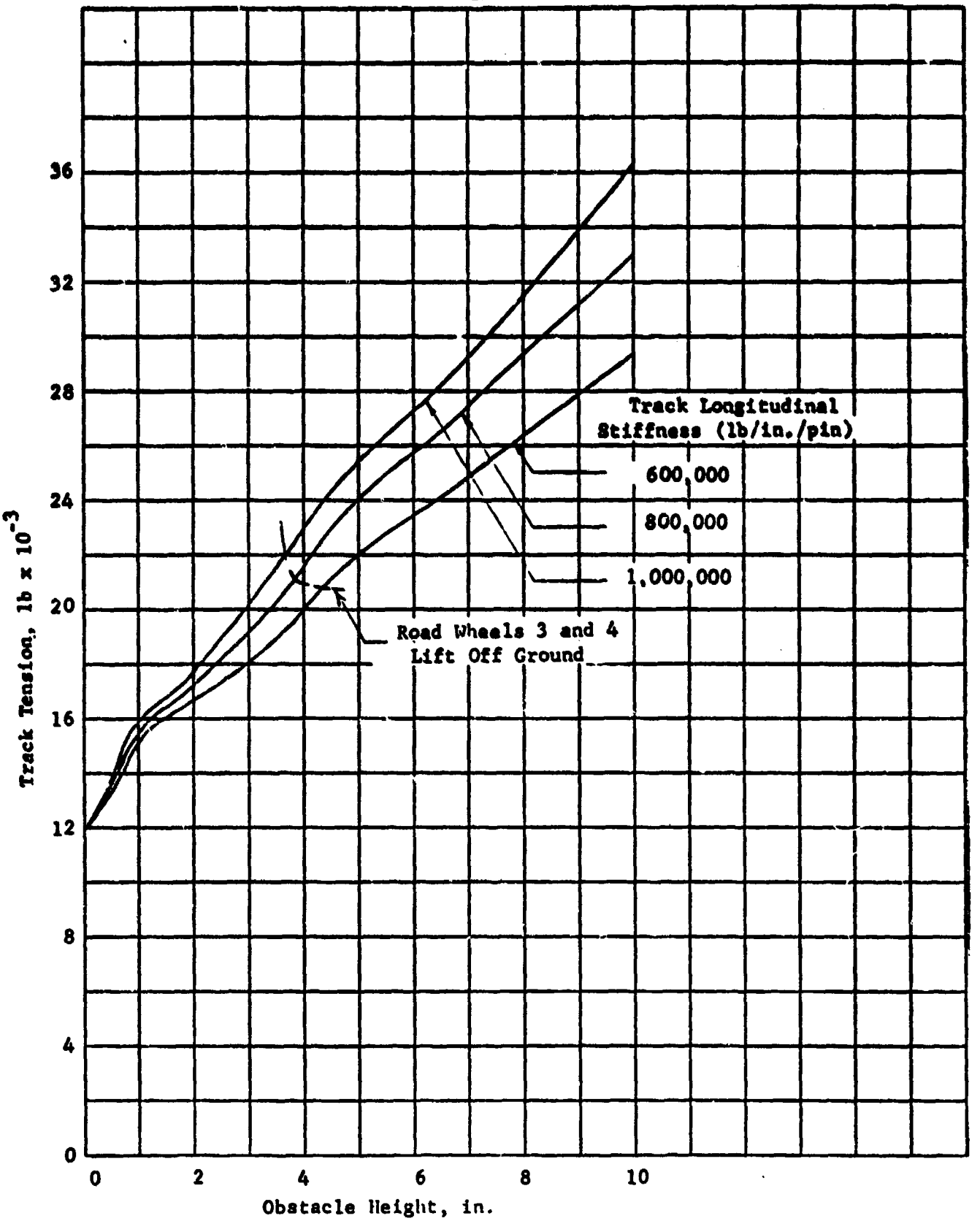

FIGURE 25. EFFECT OF TRACK LONGITUDINAL STIFFNESS ON M60 TRACK TENSION WHEN TRAVERSING AN OBSTACLE.

The obstacle was located between Road Wheels 3 and 4

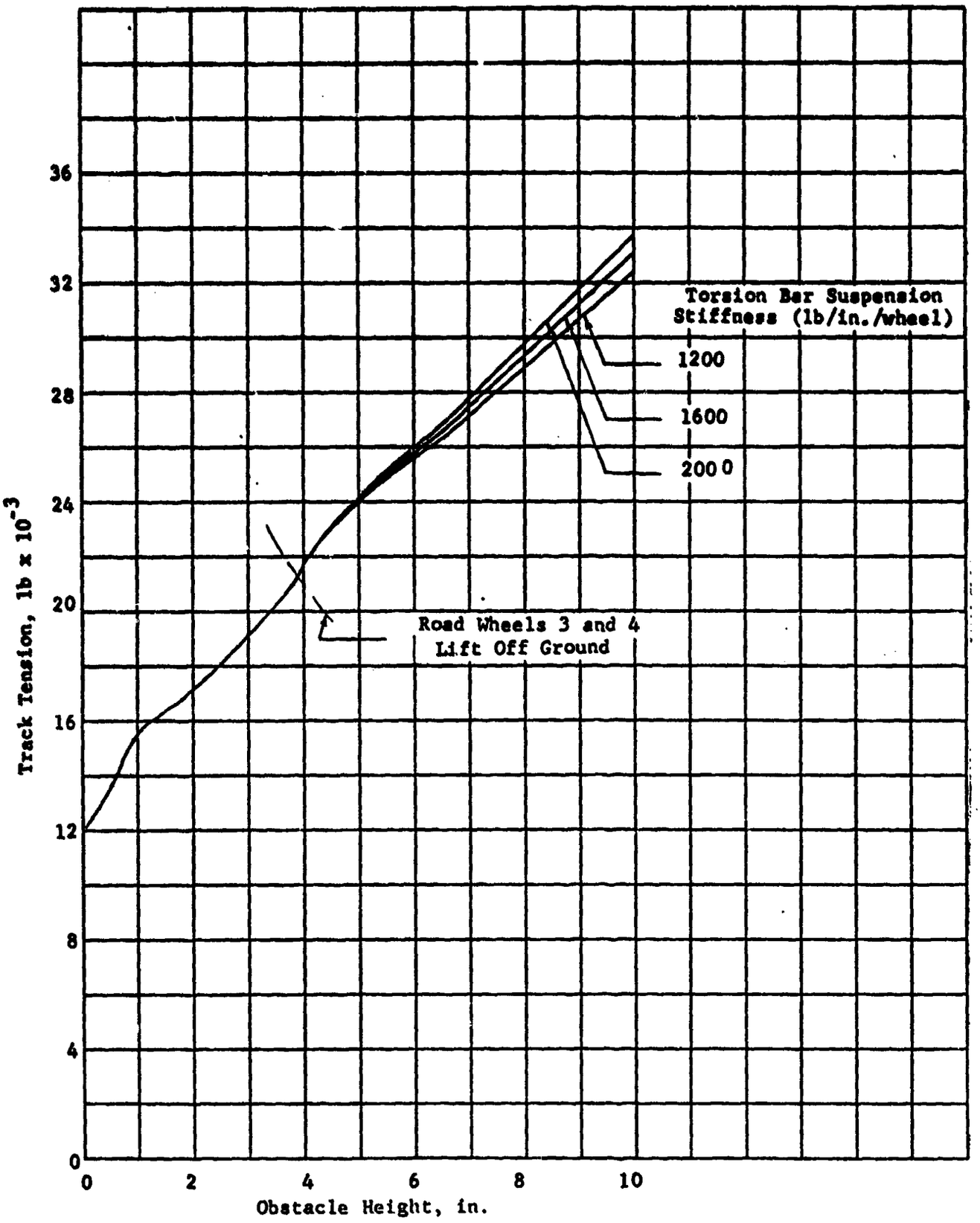

FIGURE 26 EFFECT OF TORSION BAR SUSPENSION STIFFNESS ON M60 TRACK TENSION WHEN TRAVERSING AN OBSTACLE

The obstacle was located between Road Wheels 3 and 4.

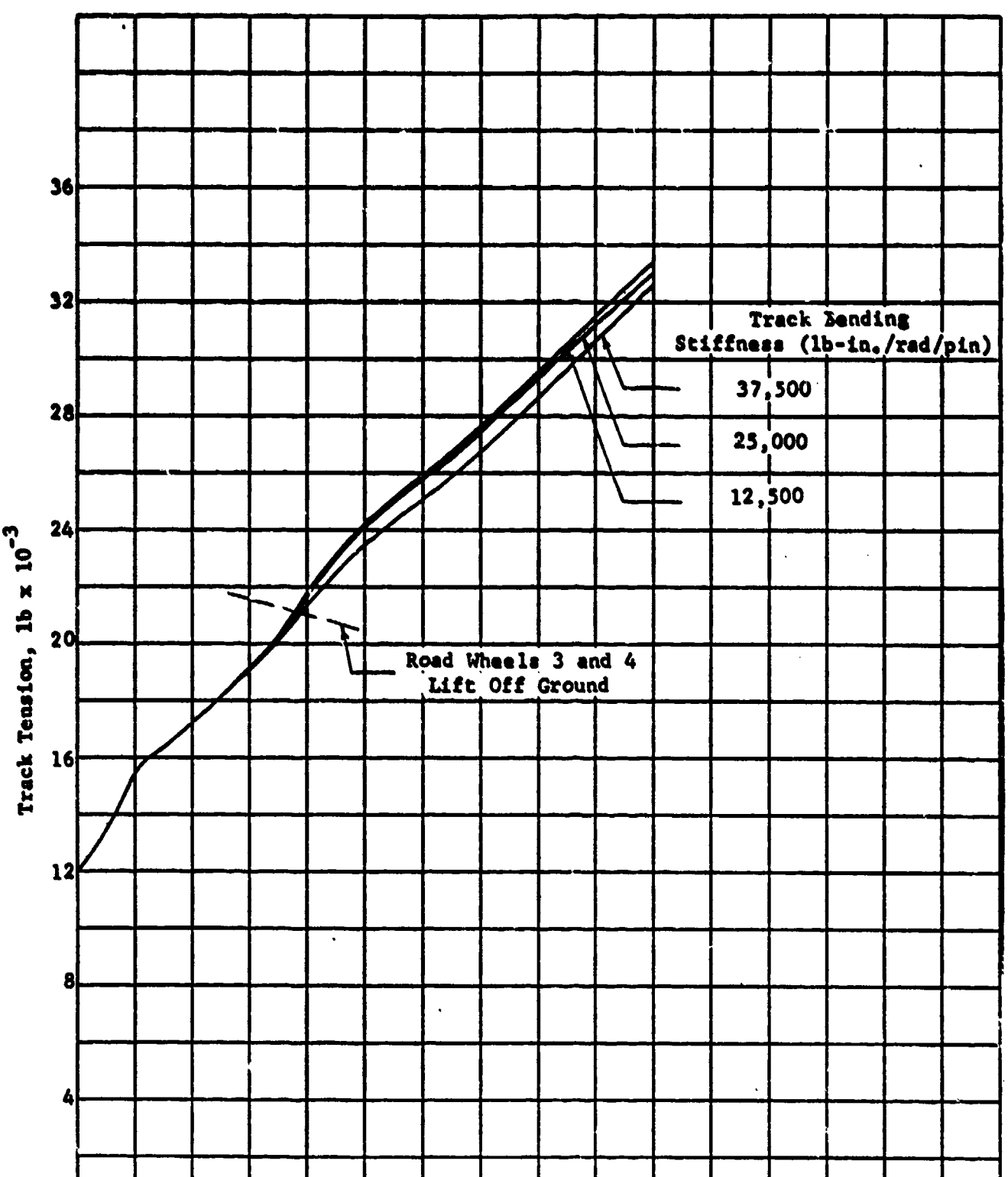

FIGURE 27. EFFECT OF TRACK BENDING STIFFNESS ON M60 TRACK TENSION WHEN TRAVERSING AN OBSTACLE

The obstacle was located between Road Wheels 3 and 4.

Effect of Track Pretension. Probably the parameter with the greatest variability in the track system is the pretension. Although the nominal operating track pretension is specified at 12,000 pounds[2], the actual value put in by the crew can be significantly higher. Also, if the tank is accelerating or under a heavy traction load, it is not unreasonable to expect the tension to be as high as 30,000 to 40,000 pounds on level ground. Given these high effective pretension loads in the track, obstacle negotiation can serve only to worsen the situation.

The pretension was varied by increments of 6,000 pounds (see Figure 28). One favorable result was that as the pretension increased, the obstacle height had a reduced effect both in percentage and magnitude of increased tension. For example, if the track pretension was nominal (12,000 pounds), a 5-inch high obstacle doubled the track tension to 24,000 pounds. But if the pretension was 24,000 pounds, a 5-inch high obstacle increased the tension by only 7,000 pounds.

Another expected prediction was the decrease in obstacle height necessary to lift road wheels 3 and 4 off the ground when the pretension was increased. In fact, for high obstacles and high pretension, road wheels 2 and 5 were lifted off the ground. Also, as the pretension increased, the change in slope of the stiffness curves occurring at wheel lift-off merged with the change in slope due to road pad slippage.

Results of Parametric Study (Obstacles Under a Road Wheel). When an obstacle was under a road wheel, rather than between two road wheels, the increase in track tension with obstacle height was only about half as great. The reason for the reduced increase in tension can be attributed to the greater length of track between the obstacle and the adjacent road wheels so that less of the load in the track is taken out in the longitudinal direction. With the greater length of track available, the adjacent road wheels did not lose contact with the ground until an obstacle height of about 7 inches was reached. Unlike the case when the obstacle was between road wheels, the stiffness of the track system did not noticeably change when the adjacent road wheels were lifted up.

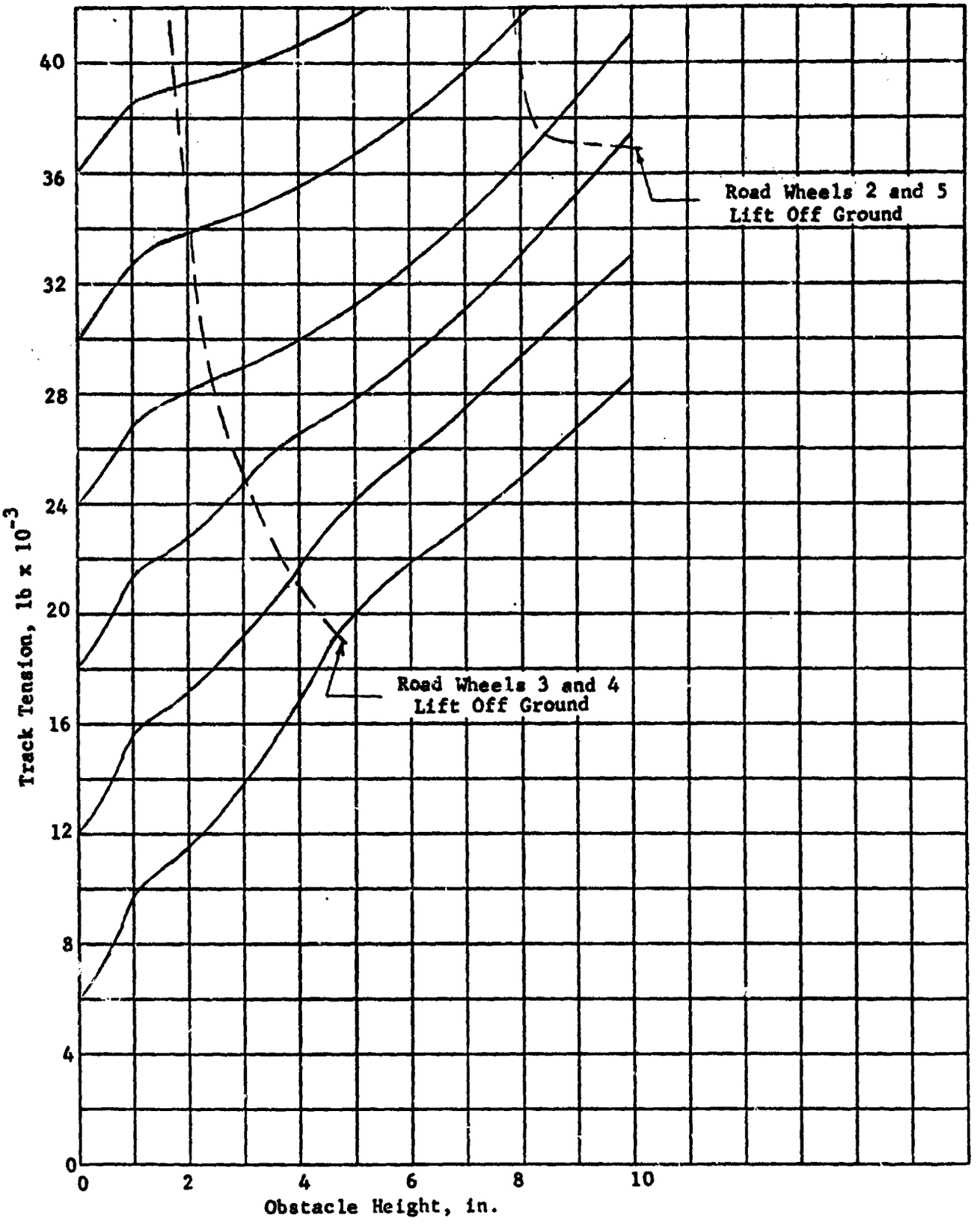

FIGURE 28. EFFECT OF TRACK INITIAL TENSION ON M60 TRACK TENSION WHEN TRAVERSING AN OBSTACLE

The obstacle was located between Road Wheels 3 and 4.

Effect of Sprung Weight. When the road wheel load was varied by ±10 percent, the change in track tension was small (Figure 29). A similar result was obtained when the obstacle was between road wheels (Figure 23).

Effect of Road Pad/Ground Friction. The noticeable increase in track tension for larger friction coefficients (Figure 30) resembled the trend for the obstacle between road wheels (Figure 24).

Effect of Track Longitudinal Stiffness. As was the case when the obstacle was between road wheels (Figure 25, the track longitudinal stiffness had a significant effect on track tension (Figure 31).

Effect of Track Pretension. Finally, track pretension had a similar effect on track tension when the obstacle was under a road wheel (Figure 32) as when it was between road wheels (Figure 28). Also, the obstacle height at which the two adjacent road wheels lifted up decreased with pretension, but not as rapidly as when the obstacle was between road wheels.

Three-Dimensional Computer Model of Track (TRACKOB III)

Following the success of the two-dimensional finite-element model in predicting track tension forces as the tank negotiates an obstacle, the SAVFEM computer code was used to develop a three-dimensional finite-element model of the T-142 track. The reason for developing a three-dimensional model was to provide the capability for predicting track tension and displacement distribution when the vertical displacements of the track are unsymmetric--for example, when only one edge of the track is in contact with an obstacle. It is this type of encounter which puts high stresses on one end connector and one end of the pin.

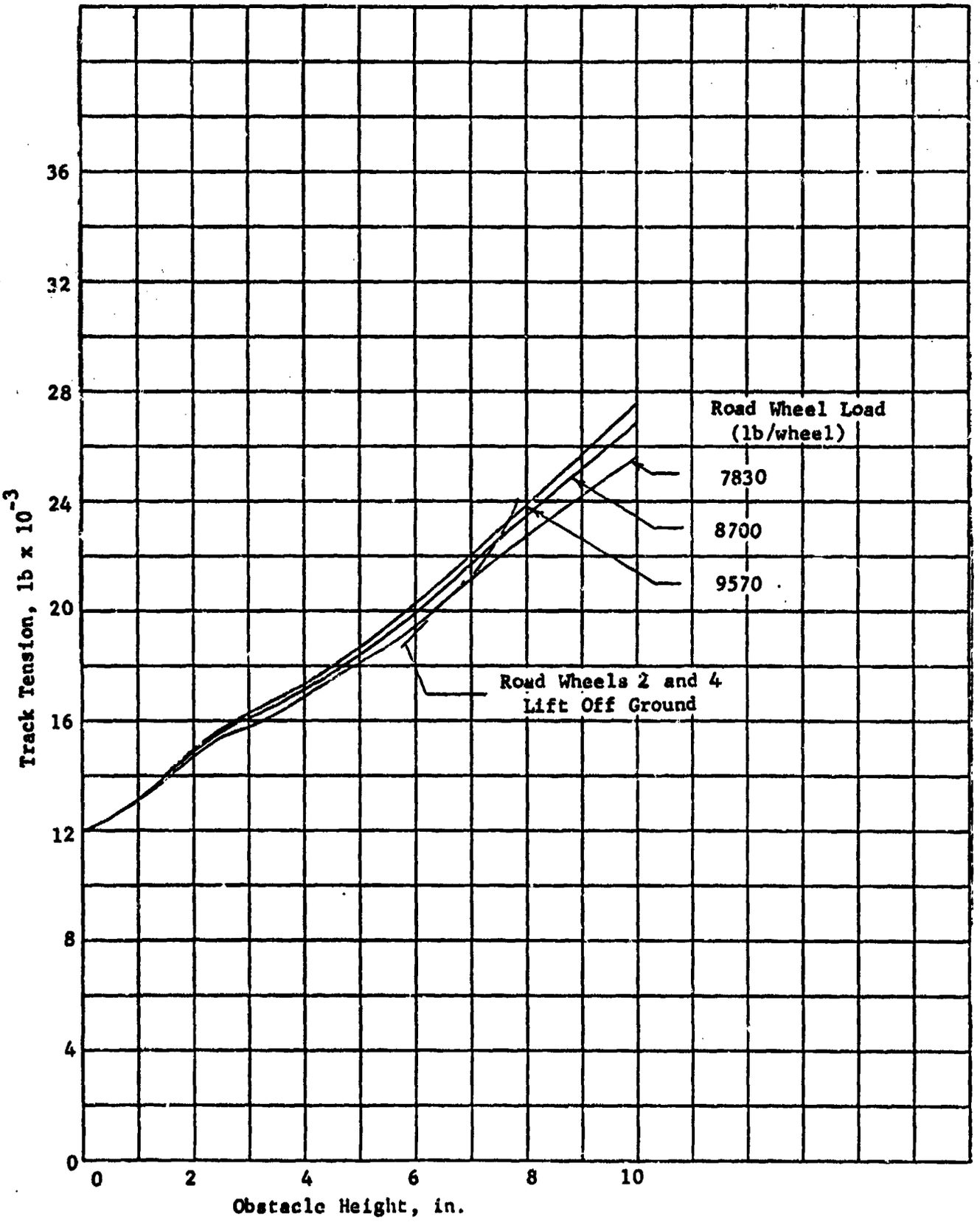

FIGURE 29. EFFECT OF ROAD WHEEL LOAD (TANK SPRUNG WEIGHT) ON M60 TRACK TENSION WHEN TRAVERSING AN OBSTACLE.

The obstacle was located under Road Wheel 3.

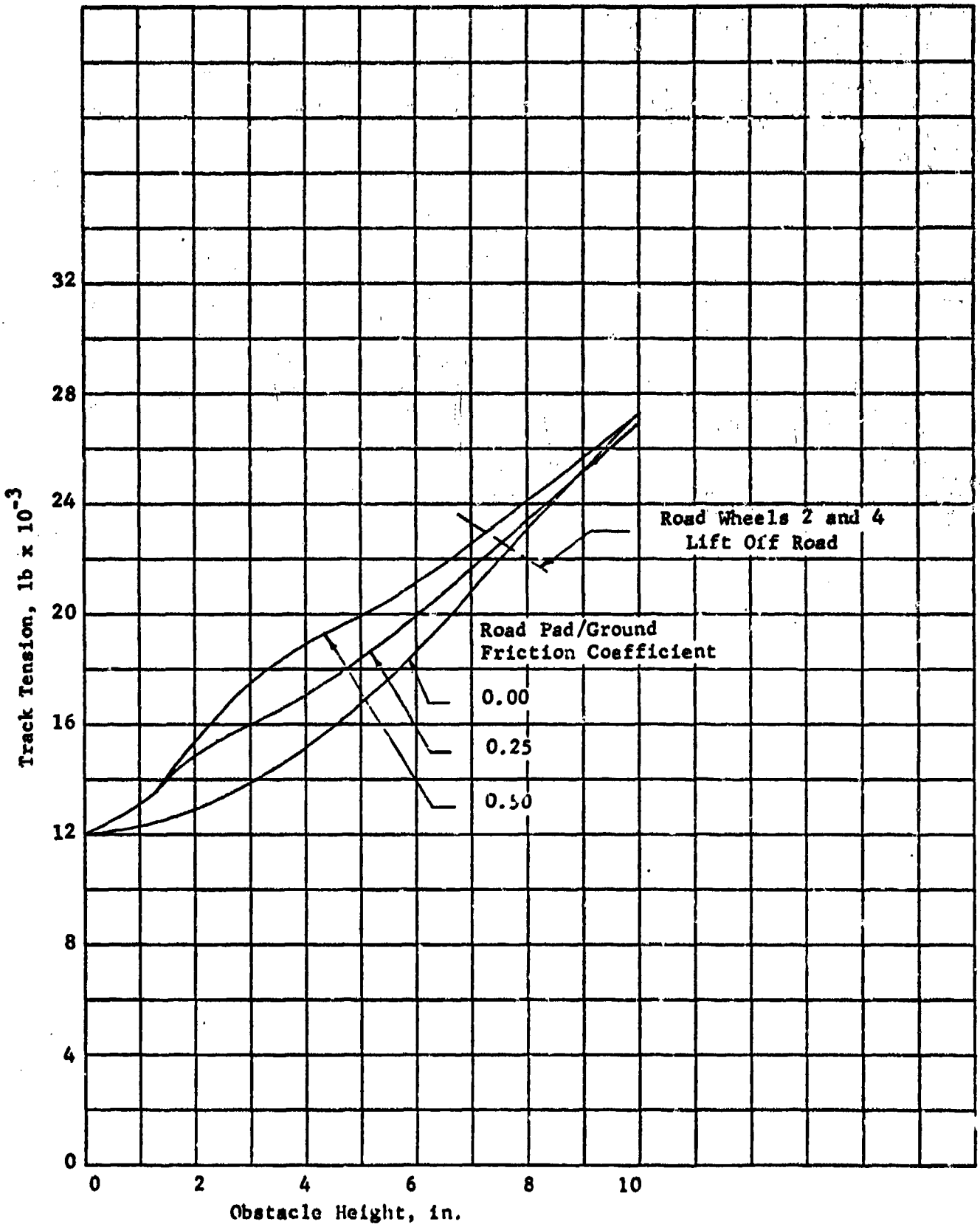

FIGURE 30. EFFECT OF ROAD PAD/GROUND FRICTION COEFFICIENT ON M60 TRACK TENSION WHEN TRAVERSING AN OBSTACLE

The obstacle was located under Road Wheel 3.

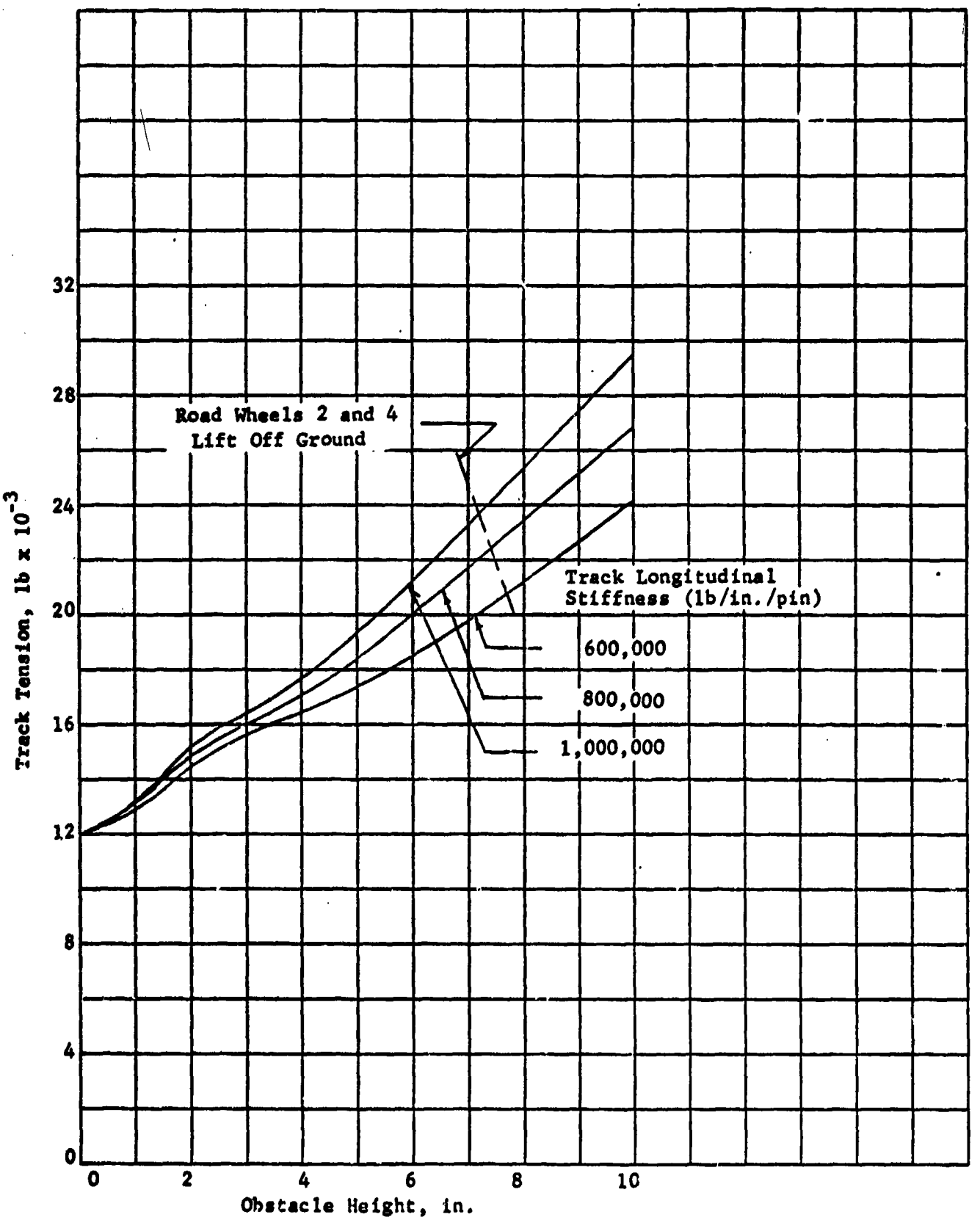

FIGURE 31. EFFECT OF TRACK LONGITUDINAL STIFFNESS ON M60 TRACK TENSION WHEN TRAVERSING AN OBSTACLE

The obstacle was located under Road Wheel 3.

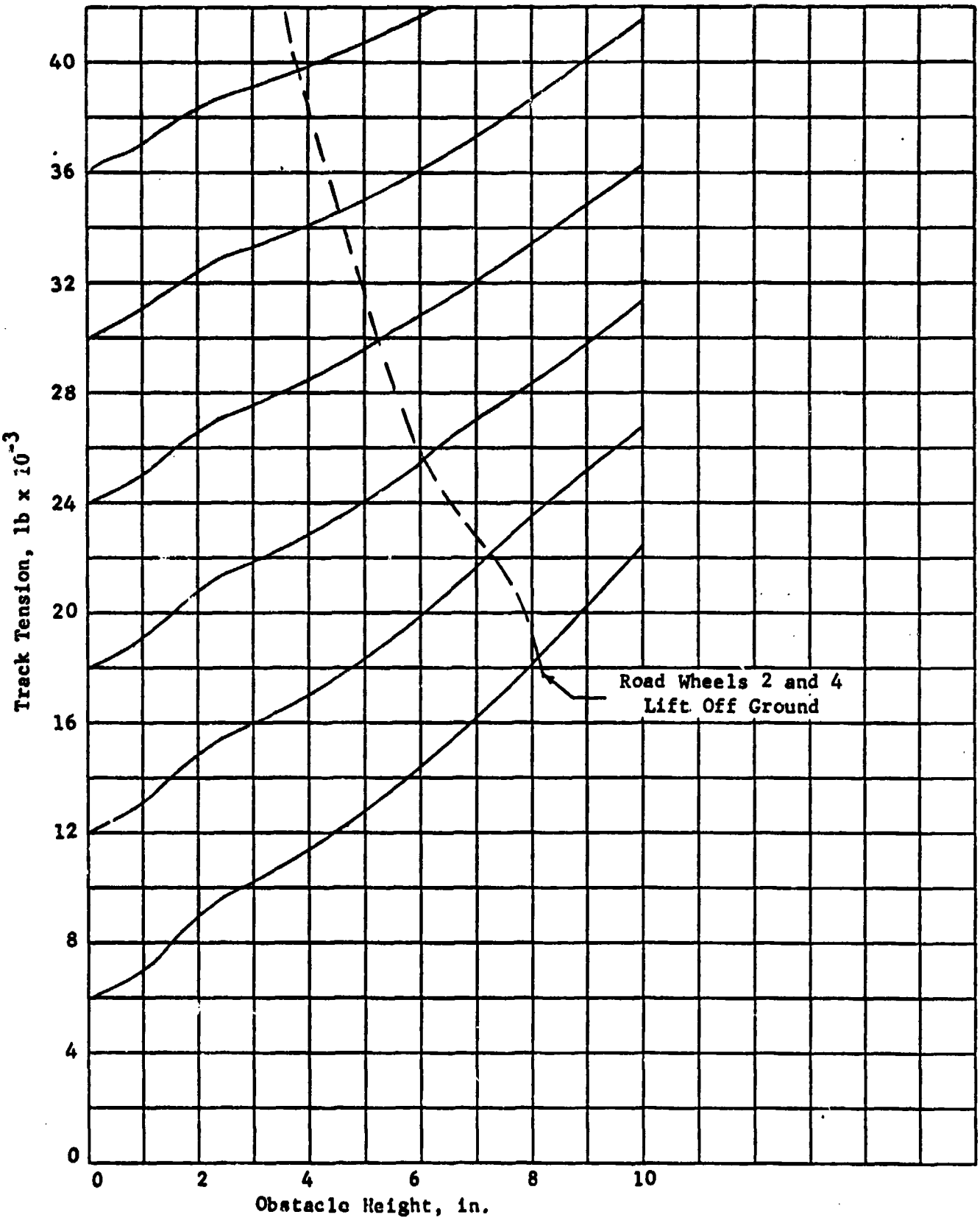

FIGURE 32. EFFECT OF TRACK INITIAL TENSION ON M60 TRACK TENSION WHEN TRAVERSING AN OBSTACLE

The obstacle was located under Road Wheel 3.

The three-dimensional track model was similar to the two-dimensional track model just described. Like the two-dimensional model, the three-dimensional model simulated 16 track shoes which were subjected to an initial specified track pretension. Due to the three-dimensional aspects of the model, it was possible to apply any percentage of the pretension to two end connectors and a centerguide--the total percentage being 100 percent. It was, therefore, possible to simulate unsymmetric tension distribution across the track.

Two test runs were made with the three-dimensional track model, one with a zero traction coefficient between the road pad and ground, and the other with a friction coefficient of 0.7. The obstacle was between the middle two road wheels, and the track was raised symmetrically in the longitudinal/vertical plane similar to the two-dimensional model. From Figure 33, the significance of road pad-to-ground sliding friction is apparent, especially at the lower block heights.

The results of two computer runs are shown in Figures 34 and 35, for the cases of (a) obstacle under outside end connector between Road Wheels 3 and 4, and (b) obstacle under outside end connector adjacent to Road Wheel 3. Also plotted on these figures are the results of the comparable two-dimensional case where the obstacle extends across the track width. The track parameters used in the three-dimensional analyses are those given in Table 6, except for the track longitudinal stiffness which was taken as 724,000 lb/in/pin instead of 800,000 lb/in/pin. A comparison between Figures 25 and 34 shows that the three- and two-dimensional models give the same results for total track tension when the obstacle was under the total track width between Road Wheels 3 and 4. A similar comparison can be made for the obstacle under the total track width under Road Wheel 3.

The results in Figures 34 and 35 show the extent to which the tension load is increased on the outside end connector and decreased on the inside end connector. The centerguide load also increases somewhat under the nonsymmetrical loading case. However, the increase in total track tension is less than for the symmetrical obstacle case, as might be expected. This loading condition was not used in the tests conducted on the M-60 tank at TARADCOM's laboratories in Warren, Michigan. Such a test would be of interest to fully validate the results predicted by TRACKOB III.

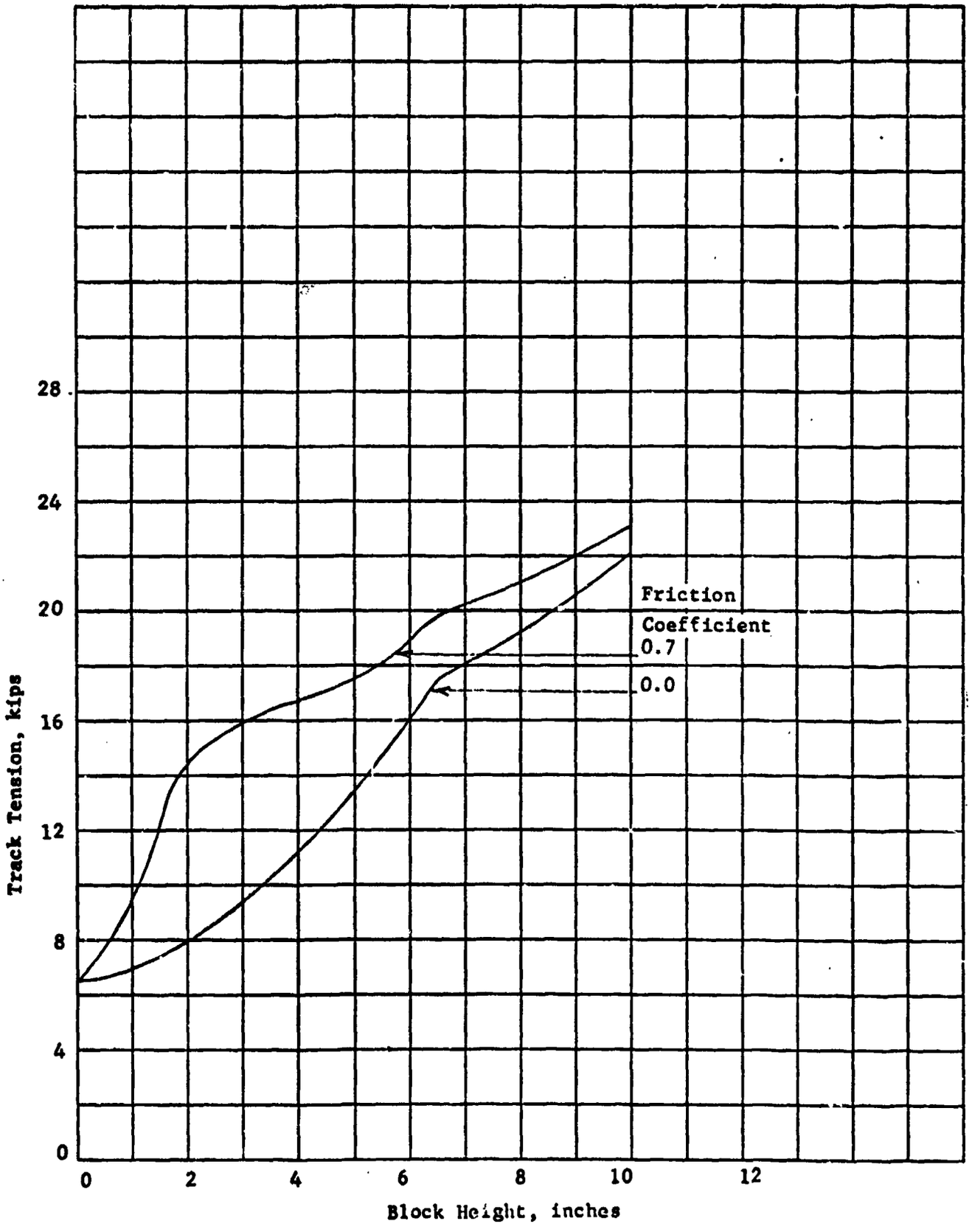

FIGURE 33. VARIATION IN TRACK TENSION AS M60A1 TANK NEGOTIATES VARIOUS OBSTACLE HEIGHTS-TENSION IS PREDICTED ADJACENT TO OBSTACLE BETWEEN THIRD AND FOURTH ROAD WHEELS

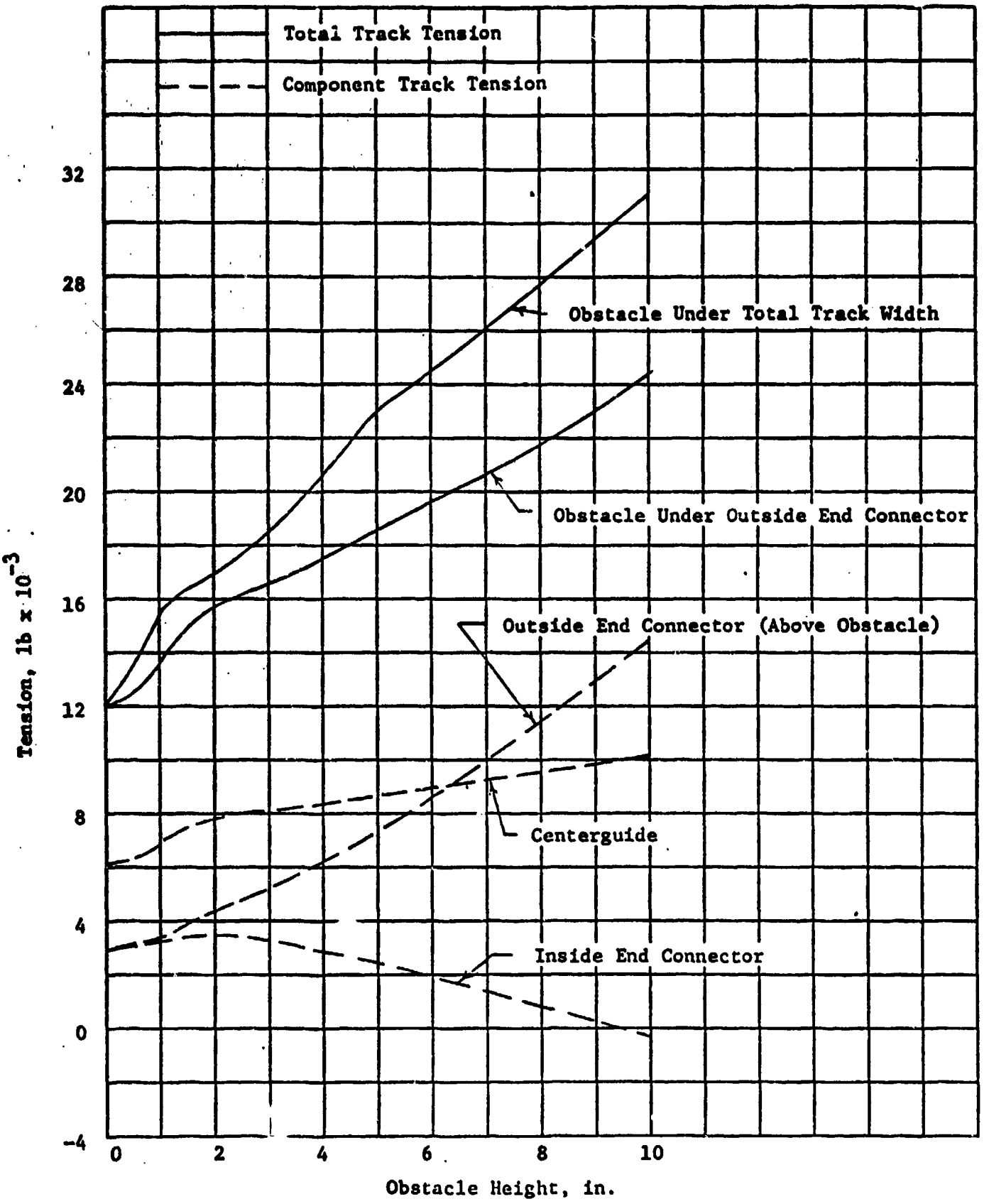

FIGURE 34. TRACK AND COMPONENT TENSION OF M60 TRACK WITH AN OBSTACLE UNDER THE OUTSIDE END CONNECTOR BETWEEN ROAD WHEELS 3 AND 4

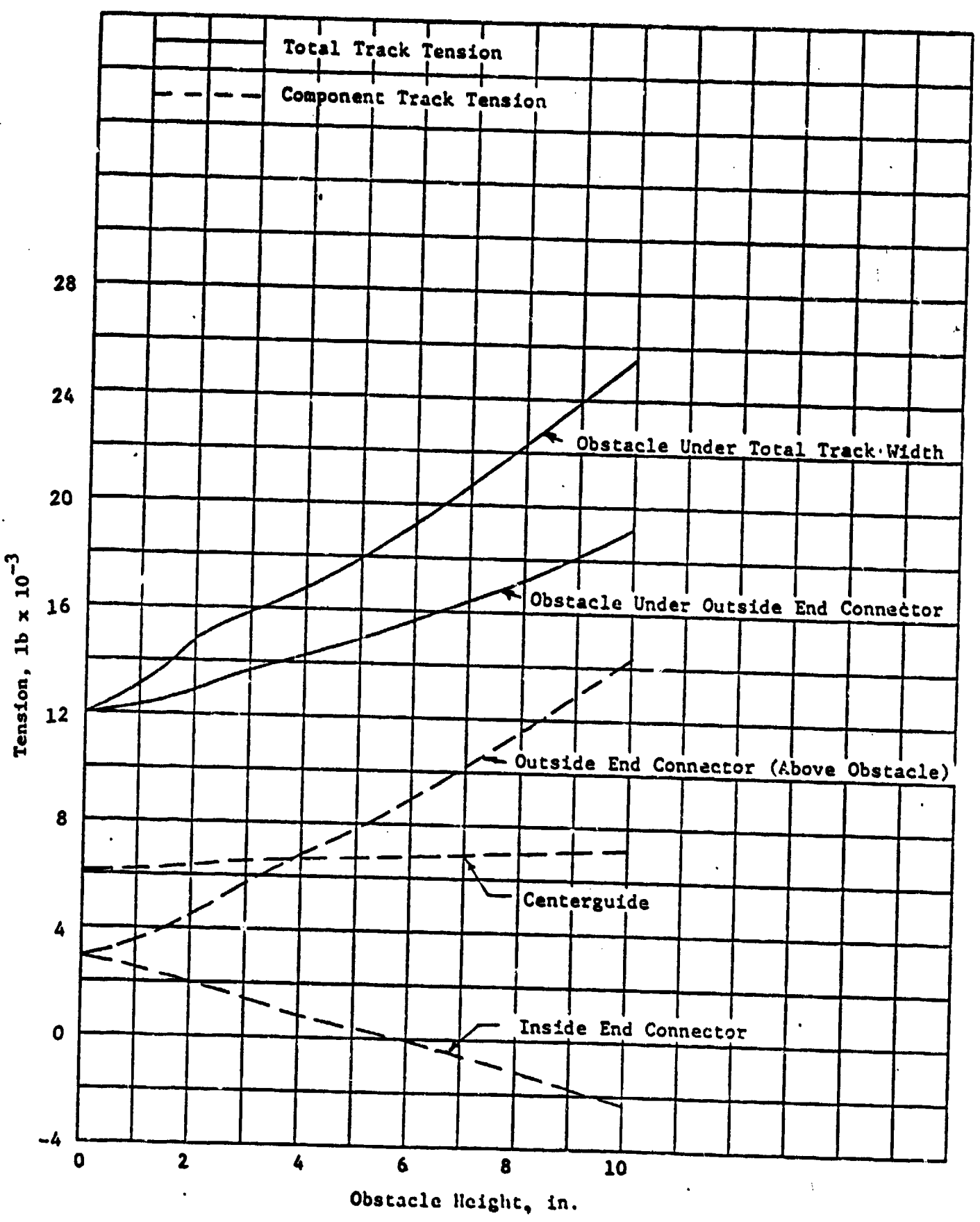

FIGURE 35. TRACK AND COMPONENT TENSION OF M60 TRACK WITH AN OBSTACLE UNDER THE OUTSIDE END CONNECTOR ADJACENT TO ROAD WHEEL 3

Track Thermal Analyses

Because of the complexity of the track shoe assembly, the use of a somewhat detailed model was considered necessary. A two-dimensional model was first developed, but this was expanded to a three-dimensional model in order to evaluate detail changes in the shoe assembly design.

Two-Dimensional Analysis of Shoe Temperatures (SHOETEMP II)

The first thermal model was a two-dimensional model formulated for T-142 track shoes for use with the TRUMP* computer program.

Model Formulation. For the first model, named SHOETEMP II, the cross-section of the track shoe was divided into thermally interconnected finite-volume regions, as shown in Figure 36. Temperatures were calculated at the center of each volume via a finite-differencing scheme which was incorporated within the TRUMP computer code. Since TRUMP was basically a transient computer program, the temperature profiles could be calculated at various simulated times up to a steady-state condition. The user had the option of selecting the time increments at which to print the intermediate results. This option allowed the analyst to closely match the output to any validation data that was available. Of course, if steady-state solutions were of the only importance, no intermediate outputs were specified.

The input data include (1) physical descriptions of each node or finite volume region, (2) thermal connections between nodes, (3) thermal connections between the nodes and the boundary conditions, (4) boundary conditions, (5) heat input, and (6) thermophysical properties of each material in the model. The internal thermal connection data (between nodes) may include the interface resistances due to contact between parts, such as the contact between the pad backing plate and the shoe body on T-142 tracks. The boundary conditions may be a function of time or temperature. The boundary connections can be convective, radiative and/or of a contact resistance nature. This variability in boundary connections permitted the accurate modeling of the heat transfer between the shoe and air, and the shoe and road surface.

---

* Edwards, A. L., TRUMP: A Computer Program for Transient and Steady-State Temperature Distributions in Multidimensional Systems, University of California/Livermore, September 1, 1972. Prepared for the U. S. Atomic Energy Commission under Contract No. W-7405-eng-48.

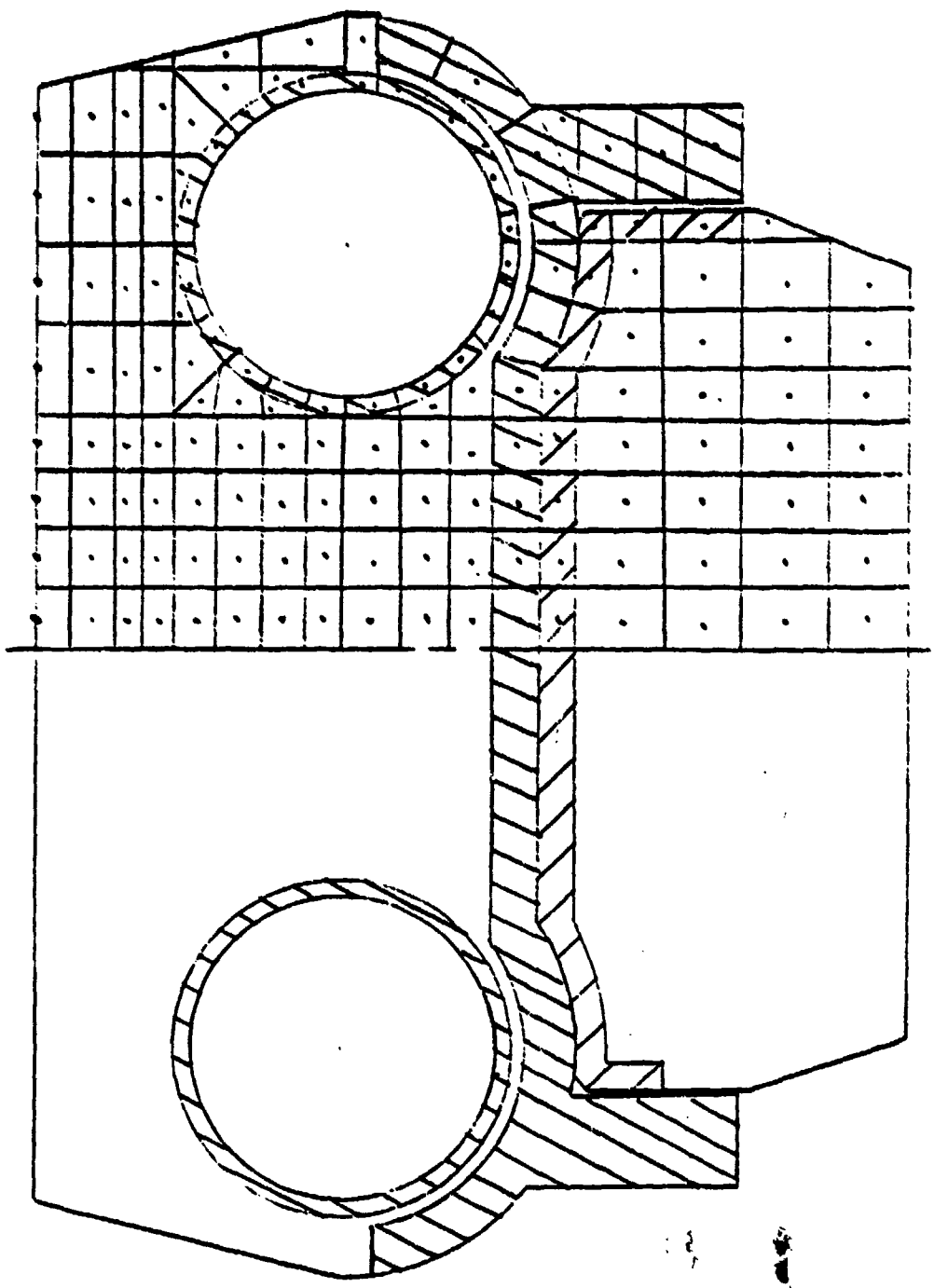

FIGURE 36. TWO-DIMENSIONAL MODEL OF A T-142 TRACK SHOE

The required thermophysical property data were then assembled. These data included density, thermal conductivity, and specific heat. Rubber properties were obtained from the Goodyear Tire and Rubber Company for their compound that is designated as SM8493. These data are shown in Table 8. Thermophysical properties of steel were obtained from the open literature and are shown in Table 11.

TABLE 8. THERMOPHYSICAL PROPERTIES OF SM 8493 RUBBER

Temperature, F	C_p, Btu/lb-F
Specific Heat, C_p	
116.6	.2545
134.6	.3226
152.6	.3327
170.6	.3484
188.6	.4308
206.6	.3808
224.6	.3574
242.6	.3676
260.6	.3609
278.6	.3646
296.6	.3703

Thermal Conductivity

K = 0.1089 Btu/hr-ft-F

Density

= 75 lb/ft^3

Source: The Goodyear Tire and Rubber Company, Akron, Ohio.

Contact resistances which occur at a steel/steel and a rubber/steel bond were located. The contact resistance between the rubber and the ground was not readily available, so it was approximated from data that relates to soft materials at high contact pressures.

Heat Input. The hysteretic heat input to the rubber components was experimentally determined in Battelle's fatigue laboratory for T-142 track components. These tests were conducted up to loading frequencies of 100 Hz and peak forces of 10,000 pounds. The results of these tests are shown in Figures 37 and 38 for the road wheel path and road pad, respectively. A linear regression technique was applied to the data to obtain a least squares curve fit. The equations which resulted from these analyses are indicated on the figures. Note that the experimental data indicated that the per-cycle hysteretic heat inputs to the road wheel path and road pad were not a function of the loading frequency, but depended on the peak force of each load application. The effect of load frequency (loadings per second) was to increase the total heat input per unit of time via an increase in the number of load applications. Peak loads would be affected by several variables, including track tension, acceleration, terrain roughness, etc.

A simple case for the T-142 track on an M-60 tank was first assumed--that each road wheel on each side supported an equal share of the tank weight. Since there are effectively 24 points on the tank track where the road wheels touch the track (12 sets of paired road wheels), the force on each pad is 1/24th of the tank weight. This force will be applied six times to each pad every time the track makes one complete revolution. The number of load applications to each road pad at any given speed (V, mph) is

$$\text{Number of Load Applications} = \frac{6 \text{ Impacts}}{\frac{560 \text{ Inches}}{17.6 \text{ V}}}$$

$$= .189 \text{ V impacts/second.}$$

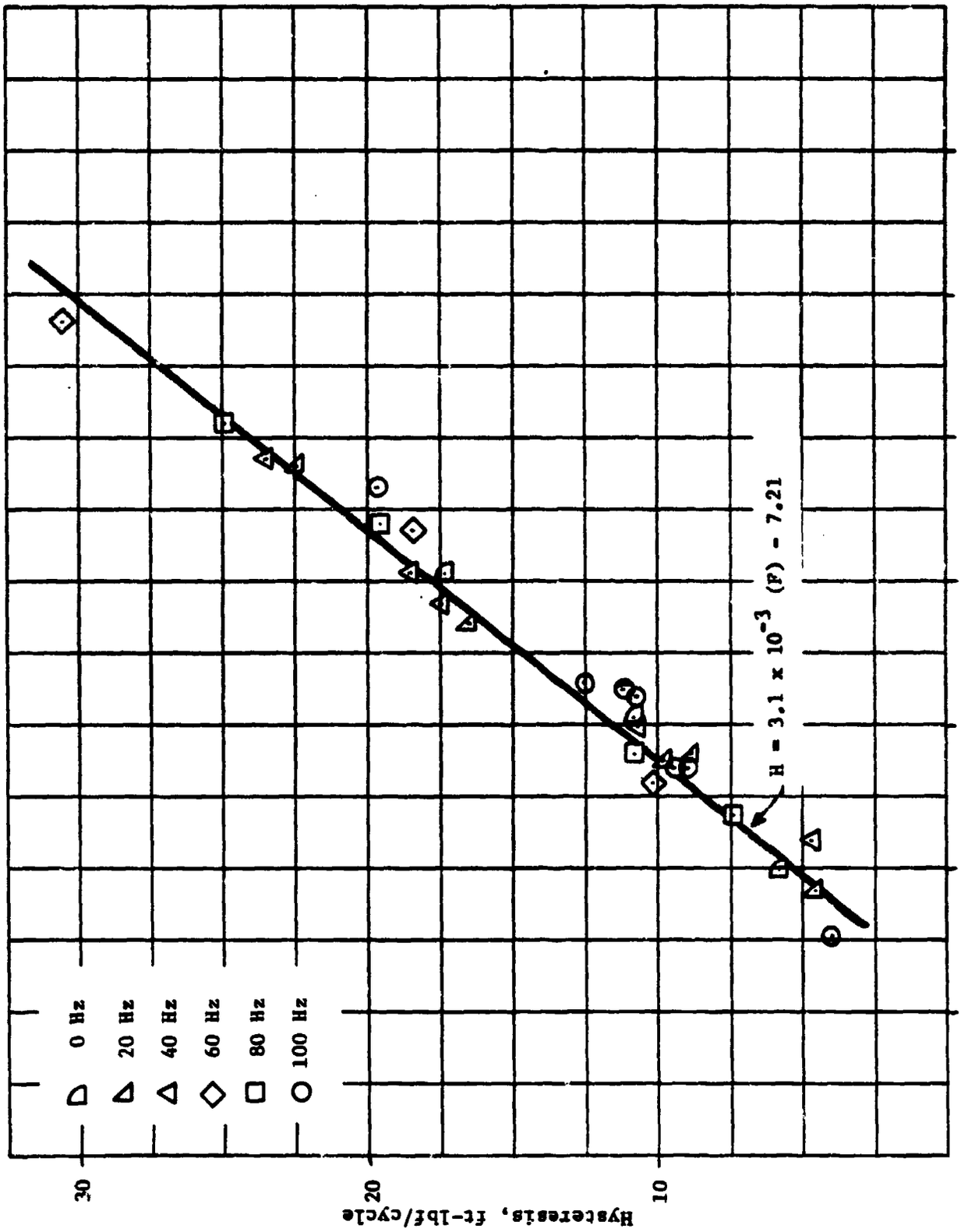

FIGURE 37. HYSTERESIS VERSUS PEAK FORCE FOR ROAD WHEEL PATH RUBBER ON T-142 TRACK SHOES

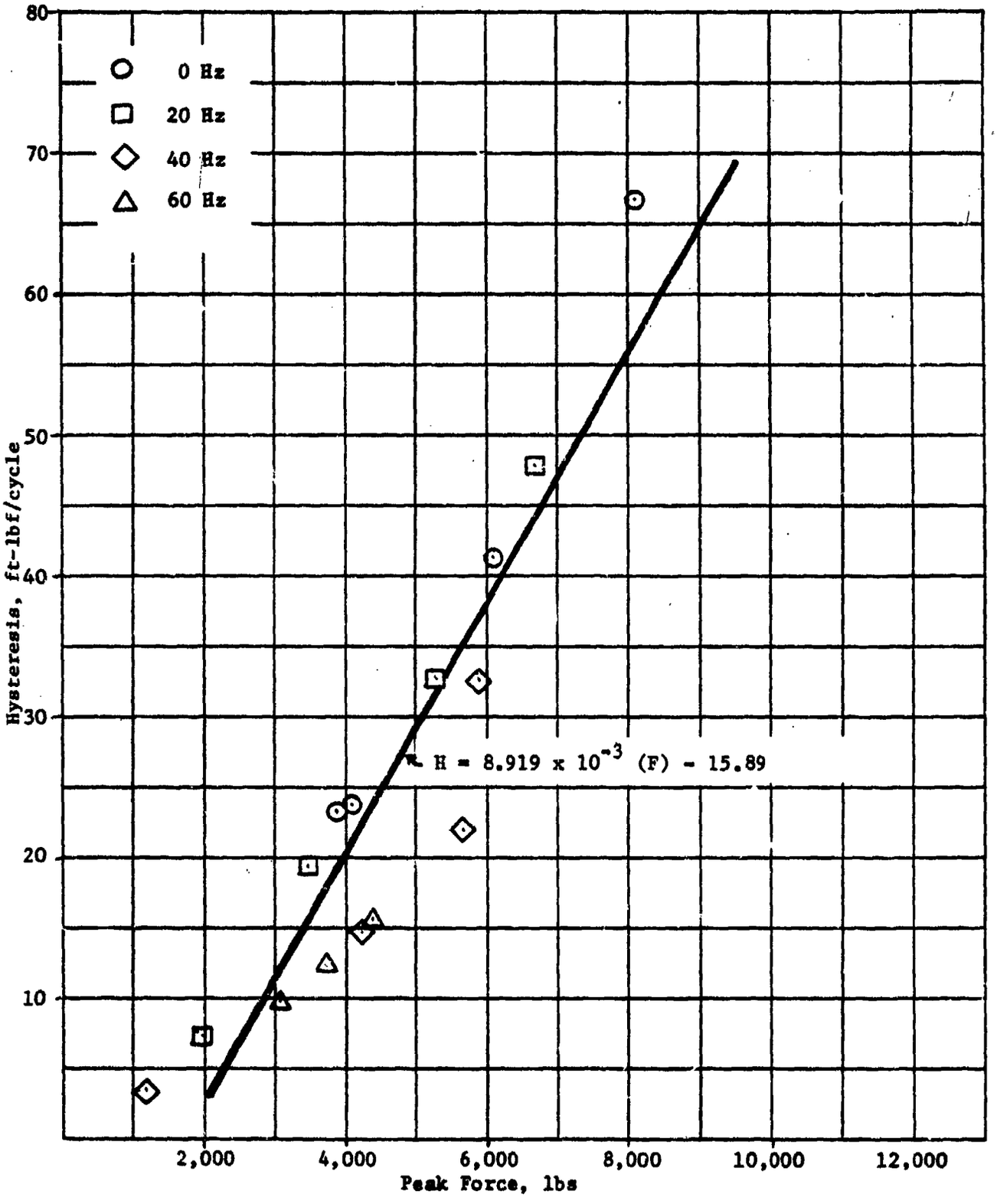

FIGURE 38. HYSTERESIS VERSUS PEAK FORCE FOR ROAD PAD RUBBER ON T-142 TRACK SHOES

Knowing the tank velocity and the hysteresis per impact or load cycle, an effective heating rate in Btu/hr could be calculated. These calculations were made using the data shown in Figures 37 and 38 for the road wheel path and road pad under the ideal conditions of each road wheel equally supporting the tank. The following equations resulted from these calculations, and were used to determine the heat input to the rubber components for any tank speed or weight.

Road Wheel Path

$$\text{Heat Input (Btu/hr)} = .189\ V\ (1.434 \times 10^{-2}\ \frac{W}{20} - 33.36) = Q_{path}$$

Road Pad

$$\text{Heat Input (Btu/hr)} = .189\ V\ (4.127 \times 10\text{-}2\ \frac{W}{20} - 73.53)$$

where

V = tank speed, mph
W = tank weight, lbs.

The heat input calculated with the above equations was distributed uniformly throughout the volume of rubber in the track shoe.

For the preliminary thermal analyses, a 30 mph case was used. Both transient and steady state results were obtained. The maximum rubber temperature occurred after nearly 4 hours of operation. As shown in Figure 39, the interesting observation is that the road-pad temperature is twice as high as the roadwheel-path temperature.

The two-dimensional model was then used to study the importance of other parameters. These parameters included (1) interface thermal resistance between the pad backing plate and the shoe body, (2) heat generation distribution in the roadwheel path, (3) rubber thermal conductivity, and (4) heat-transfer coefficient between the track shoe and the air. The results of these parametric analyses are discussed below.

Effects of Road Pad/Shoe Body Interface Thermal Resistance. The effects of thermal resistance variations in the road-pad backing plate to shoe

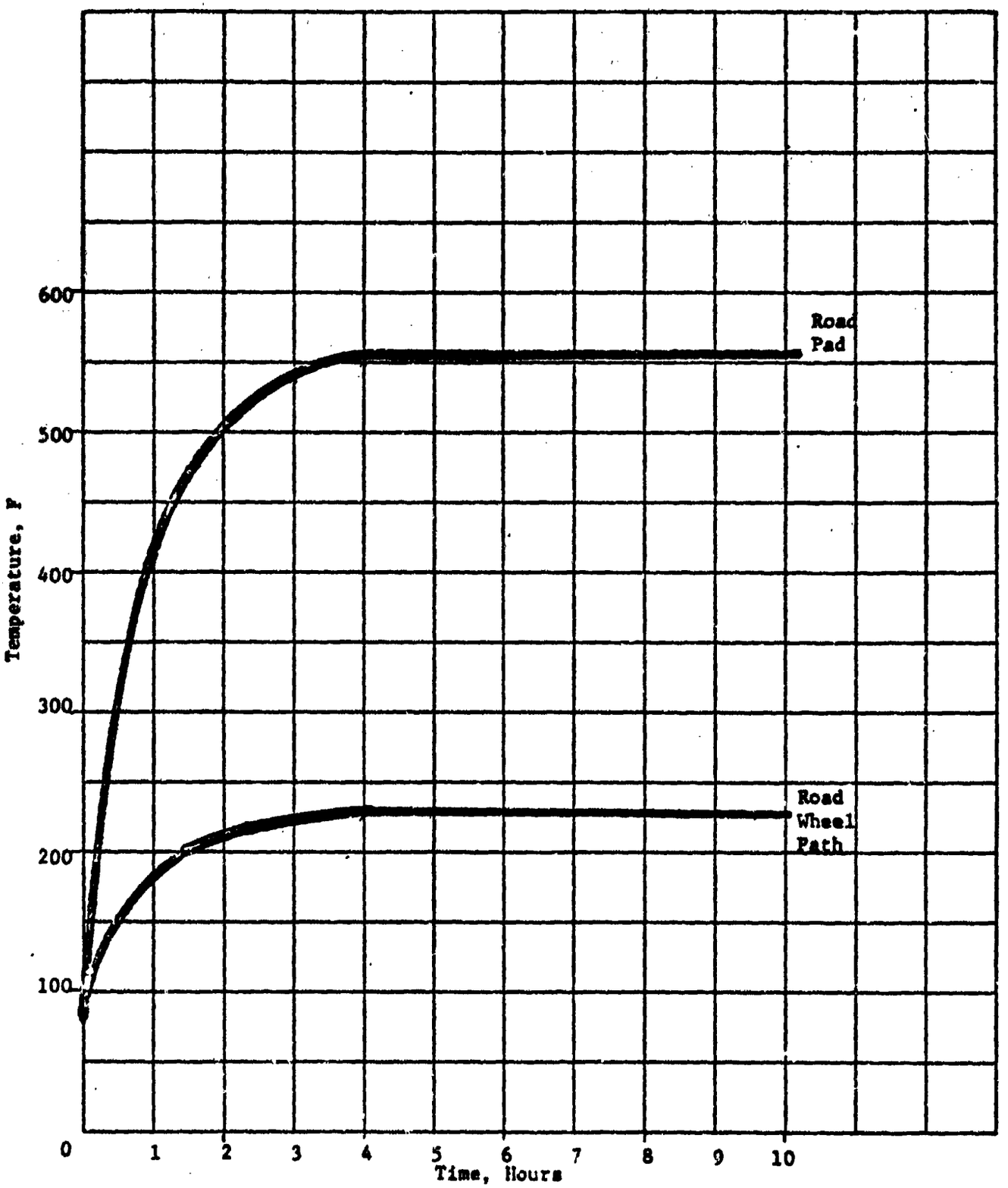

FIGURE 39. ROAD PAD AND ROAD WHEEL PATH TEMPERATURES AT 30 MPH

body interface were investigated by doing 20 mph transient simulations of up to 1 hour. The experimentally obtained heating values were used along with the following conditions:

- Hysteretic heating was uniformly distributed in the rubber
- Shoe-to-air heat transfer coefficient = 10 Btu/Hr-Ft^2-F = h_a
- Road pad-to-ground contact conductance = 150 Btu/Hr-Ft^2-F = h_r
- Rubber thermal conductivity = .109 Btu/Hr-Ft-F
- 50 F air temperature
- 60 F road temperature

Two runs were made wherein the interface resistance was varied from zero (perfect contact) to infinity (perfect insulation). The roadwheel-path temperatures and road-pad temperatures varied only a few degrees in these simulations indicating that this parameter has very little influence on the thermal behavior of the track shoes.

Effects of Heat Generation Distribution in the Roadwheel Path. The hysteretic heating data that were obtained previously in laboratory tests were modified somewhat to account for the effects of the roadwheel rolling over the roadwheel path. The laboratory tests were conducted by pressing a steel ram into the roadwheel path and obtaining a load/unload versus displacement loop. The ram had a 15 inch radius machined on it; therefore, it did not come into contact with the full width of the roadwheel path.

Since the roadwheel rolls across the roadwheel path and does compress all of the rubber in the path, it was felt that the measured heat input was too low. The measured heating was modified by multiplying the data by the ratio of the roadwheel path area to effective ram contact area. Thus, the measured data were increased by a factor of 1.84.

In addition to increasing the measured heating by 1.84, the distribution of the heat within the pad was modified to reflect the varied stiffness of the rubber throughout the roadwheel path. The result of this exercise was to generate more heat in the center portions of the rubber where the deflections are small. These modifications had a pronounced effect on the roadwheel-path temperature. Before the modification, the temperatures of the roadwheel path and road pad after one hour at 20 mph were 146 F and 267 F, respectively. After incorporating the modifications into the model, these temperatures were 198 F and 269 F, respectively. The simulation incorporating the refined heating distribution was run until steady state was reached. The resulting temperatures in the center of the road wheel path and road pad were 245 F and 319 F, respectively.

Effects of Variations in Rubber Thermal Conductivity. The effects of variations in rubber thermal conductivity were studied by varying the conductivity from 0.05 to 0.15 Btu/Hr-Ft-F. The thermal conductivity of rubber is highly influenced by the fillers in the compound. The value that was used is typical, but certainly not exact. Therefore, the effect of variations in this value are important to know. Parametric runs were made using the 2-D model and the revised heating distribution until steady state was reached. The results of these analyses are presented in Table 9. As expected, the effect of thermal conductivity was very pronounced. It is not unreasonable to expect the thermal conductivity to be in the range of 0.05 to 0.15 Btu/Hr-Ft-F. A variation over this range results in a temperature change by a factor of 2.

TABLE 9. EFFECT OF RUBBER THERMAL CONDUCTIVITY ON ROAD-PAD AND ROADWHEEL-PATH TEMPERATURES

(Temperatures are for 20 mph steady state)

Thermal Conductivity (Btu/Hr-Ft-F)	Road Pad (F)	Road Wheel Path (F)
0.05	587	419
0.109	319	245
0.15	256	204

Effects of Shoe-to-Air Heat Transfer Coefficients. The effects of variations in the heat transfer coefficient were studied (again using the 2-D model and the revised heating distribution) by allowing the value to range from 10 to 100 Btu/Hr-Ft^2-F. The heat transfer coefficient affects the road-wheel path temperature more strongly than it does the road-pad temperature. The results of these analyses are presented in Table 10.

TABLE 10. EFFECTS OF SHOE-TO-AIR HEAT TRANSFER COEFFICIENTS ON RUBBER TEMPERATURES

(Rubber thermal conductivity = 0.109 Btu/Hr-Ft-F)

Heat Transfer Coefficient ($Btu/Hr-Ft^2-F$)	Road Pad (F)	Roadwheel Path (F)
10	319	245
100	293	209

Three-Dimensional Thermal Model (SHOETEMP III)

Subsequent work on the thermal analysis task was directed toward development of a three-dimensional thermal model of the T-142 track shoe. This 3-D thermal model, as shown in Figure 40, was an expanded version of the two-dimensional model used previously.

In its final form, the three-dimensional model was composed of 350 finite volume regions or nodes which were thermally interconnected. These nodes were spread out over six sections along the axis of the pins, resulting in an average of 58 nodes per section where the temperature could be calculated. With this distribution, temperature gradients, and hence heat flows, could be calculated for the three directions.

This model was extremely flexible in its application of thermally modeling a T-142 track shoe because all of the key parameters could be varied. The two-dimensional thermal model used previously was not as accurate, since it assumed infinite width, thereby omitting end effects. Some of the more significant parameters that could be varied included:

- Heat loss from the end plates
- Heat loss to the road surface
- Heat loss to the air
- Axial heat conduction along the binocular tubes
- Complete spatial distribution of hysteretic heating within the rubber components
- Possibility of including the bushing heat
- Possibility of studying the heat dissipation effects of the pins.

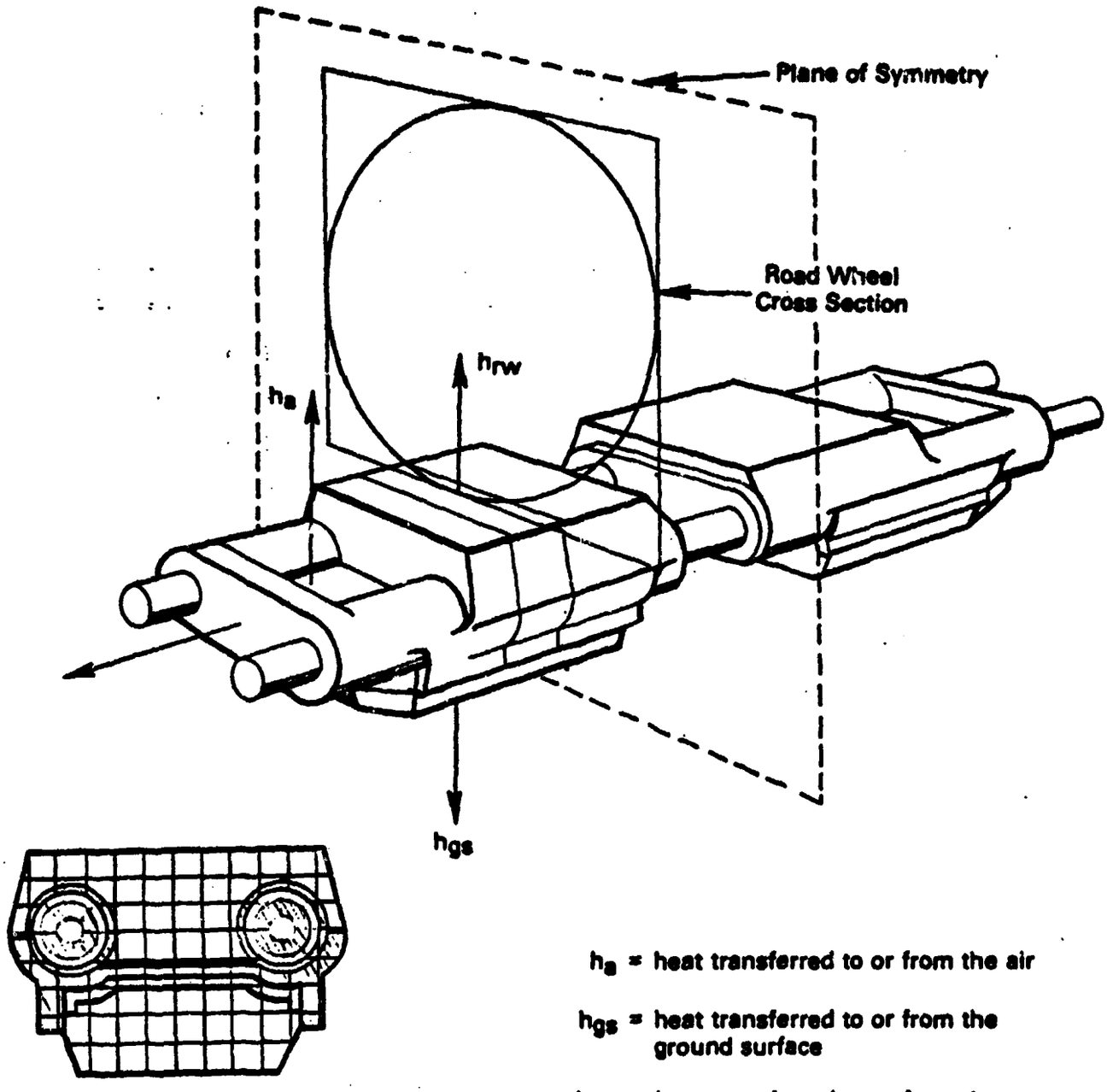

h_a = heat transferred to or from the air

h_{gs} = heat transferred to or from the ground surface

h_{rw} = heat transferred to or from the road wheel

FIGURE 40. THREE-DIMENSIONAL THERMAL MODEL OF TRACK SHOE

After the field tests were made at Warren in January of 1976, attempts were made to duplicate the field results with the model. In the SHOETEMP III model, a complete description of each of the 378 nodes representing the track shoe had to be supplied . This included not only thermal properties such as heat generation, specific heat, conductivity, etc.), but the 6 geometric descriptors which define the connection of each node to its surrounding material. This problem was compounded by the fact that in start-and-stop running such as the field test which was simulated, these conditions must be specified again after each start and stop.

Due to problems with simultaneous availability of tank, driver, and technician, it had been possible to make only one sustained test run. It was necessary to stop to read track temperatures so that the shape of the heating curve could be defined, and following a series of these readings, the sustained run was made--about 30 minutes of continuous running at roughly 25 mph. Since ambient temperatures were just above freezing, high temperature buildups in the track shoes were not obtained.

The validation of the SHOETEMP III model uncovered some problems in the data input, brought about by the simulation of the stop-and-go running, and also the variability of thermal properties of the two main materials--"rubber" and "steel". Both of these materials exhibit a wide range of thermal properties, depending on the specific rubber compound or steel alloy. In the absence of good data on these properties and the heat generated by the T-142 track, some variation of these properties had to be made to obtain good correlation with the field tests. Even after these properties were varied, it became obvious that there was one major discrepancy between the predicted and measured results, and this was the fact that the model consistently predicted lower temperatures in the road wheel path than were measured. In order to obtain good validation, it was necessary to raise the heat input in the road wheel path by a factor of 3 over that originally measured in the laboratory hysteresis tests. Input data for the first 8 runs of SHOETEMP III are shown in Table 11; note the increase of "Q_{path}" from 2258.7 (measured value) to 6776.0 (three times measured value).

TABLE 11. INPUT DATA USED IN SHOETEMP MODEL TO PREDICT T-142 TRACK TEMPERATURES*

Run No.	Date	K_{Steel}	K_{Rubber}	C_{P_R}	$C_{P_{ST}}$	h_r	h_a(V)	Q_{Path}
1	3/7/78	33	0.109	0.35	0.12	50	10 (0 mph)	0
							10 (20 mph)	2258.7
							10 (26 mph)	2936.3
2	3/9/78	25	0.109	0.35	0.12	50	10 (0 mph)	0
							10 (20 mph)	2258.7
							10 (26 mph)	2936.3
3	3/9/78	25	0.200	0.40	0.12	50	10 (0 mph)	0
							10 (20 mph)	4517.4
							10 (26 mph)	5872.6
4	3/14/78	25	0.200	0.40	0.12	50	10 (0 mph)	0
							10 (20 mph)	9034.8
							10 (26 mph)	11745.2
5	3/16/78	25	0.200	0.40	0.12	50	1 (0 mph)	0
							5 (20 mph)	6776.
							5 (26 mph)	8808.9
6	6/14/78	25	0.100	0.40	0.12	50	5 (0 mph)	0
							10 (20 mph)	6776.
							10 (26 mph)	8808.9
7**	6/15/78	25	0.200	0.40	0.12	50	10 (26 mph)	8808.9
8	7/14/78	25	0.200	0.40	0.12	50	10 (20 mph)	7964.2
							10 (26 mph)	10353.9

TABLE 12. PREDICTED AND MEASURED TEMPERATURES IN T-142 TRACK

Thermocouple Location	SHOETEMP Computer Run Number								Warren Field Test
	1	2	3	4	5	6	7	8	
13	62	62	95	148	150	110	120	119	140
11	115	114	152	250	196	215	180	215	220
10	100	104	128	188	153	169	150	170	148
5	75	77	87	98	100	78	100	94	121
6	160	164	138	146	143	156	128	148	132
7	209	209	170	173	163	195	148	175	—
8	85	85	90	90	73	85	70	76	—
12	120	125	138	180	146	142	170	163	—
9	140	148	145	167	136	124	179	192	135
1	140	148	145	167	137	135	189	173	130

* For units, see Page 120, 124, and 126.
** Run 7 was a 45-minute continuous heating run (≈25 mph).

Table 12 summarizes the predicted temperatures at the locations corresponding to the thermocouple locations in the instrumented shoe used in the field tests. The time-histories of predicted and measured temperatures for computer Run No. 6 are shown in Figures 41, 42, and 43. While the correlation is considered to be excellent, some differences remain--the main one being the lower predicted temperature in the steel at the center of the shoe, and the other being the faster cooling rate at the pin/bushing location.

After the computer program had been validated to the extent indicated by Run No. 6, a run simulating continuous running (no stops) for 180 minutes at 30 mph was made, using the same parameter values. The results are shown in Figure 44. Perhaps the most significant point indicated by this figure is the continuous rise of the temperature in the center of the road wheel path (Thermocouple #11) for the full three hours, at which time a steady state temperature of 380° has been reached. This is 340° above the assumed ambient temperature of 40°; on a hot summer day, with an ambient of 100°, maximum temperatures 60° higher could be expected. This would result in a temperature of 260° after only 30 minutes of continuous running.

Following these runs, the T-142 type track being considered for the X-M1 tank was simulated. However, because of the questionable hysteresis in the road wheel path rubber, the factor of 3 over the laboratory test data (used for the M-60 runs) was omitted. With this change, the "hot spot" switched from the road wheel path to the road pad. However, at 30 mph, the maximum temperature in the road pad (Location #7) of the XM-1 was 172°, compared to 276° for the M-60. At the 50 mph speed of the XM-1, the temperature again approaches the 280° mark.

Based on these results and the parameter studies made earlier, the single dominant parameter in the track thermal system is the hysteresis in the rubber, since the track does not dissipate heat effectively once it is generated. The SHORTEMP III model should be used to analyze designs in which the hysteresis is reduced by decreasing the thickness of the road pads and/or road wheel path rubber, decreasing the bearing pressure of pads and road wheel path, and using rubber of higher durometer.

A final point which might be made is that the pins and binocular tubes appear to do an effective job of dissipating heat generated in the bushings, so that bushing temperatures are lower than those in other locations.

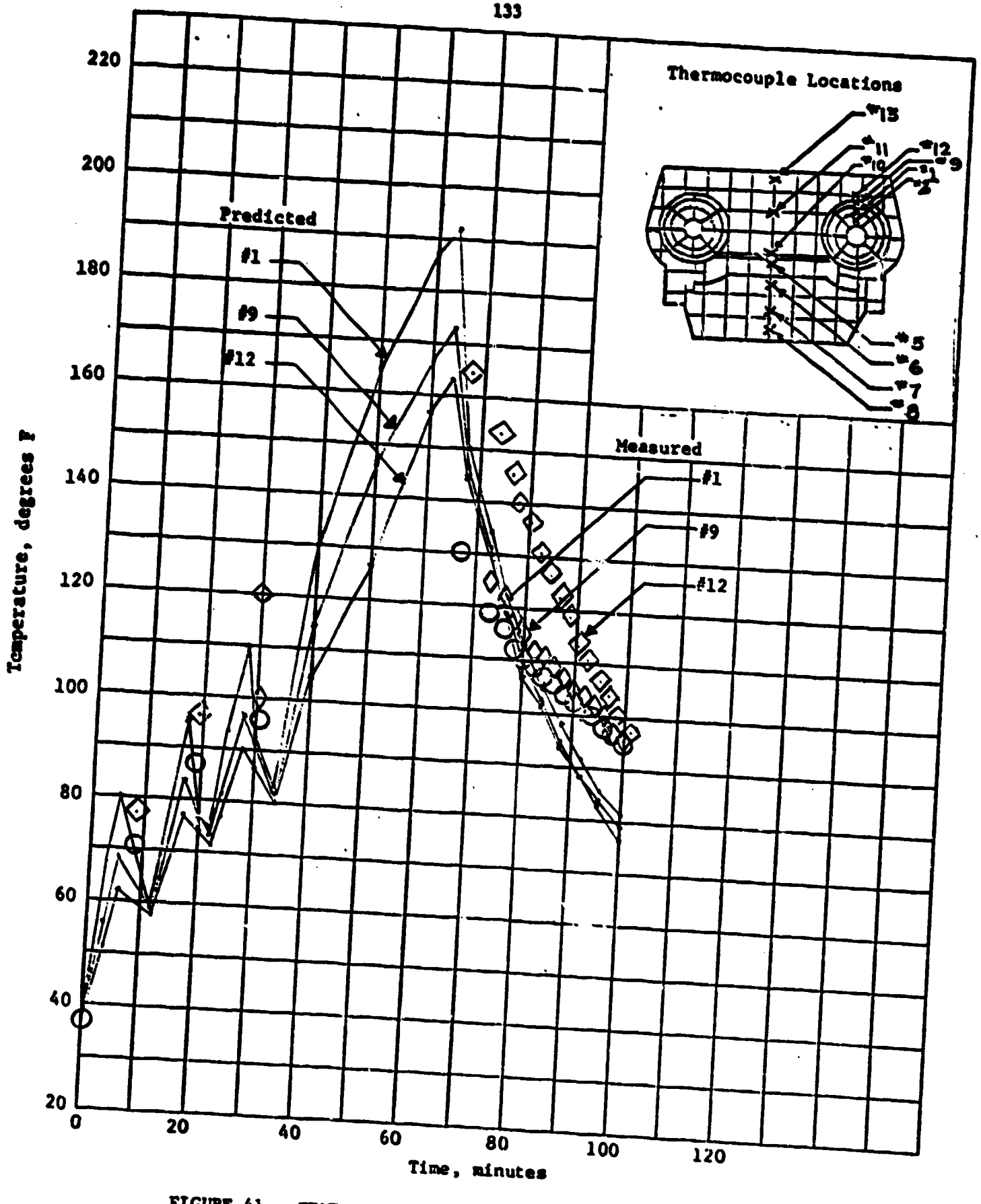

FIGURE 41. TEMPERATURES AT SELECTED LOCATIONS IN T-142 TRACK

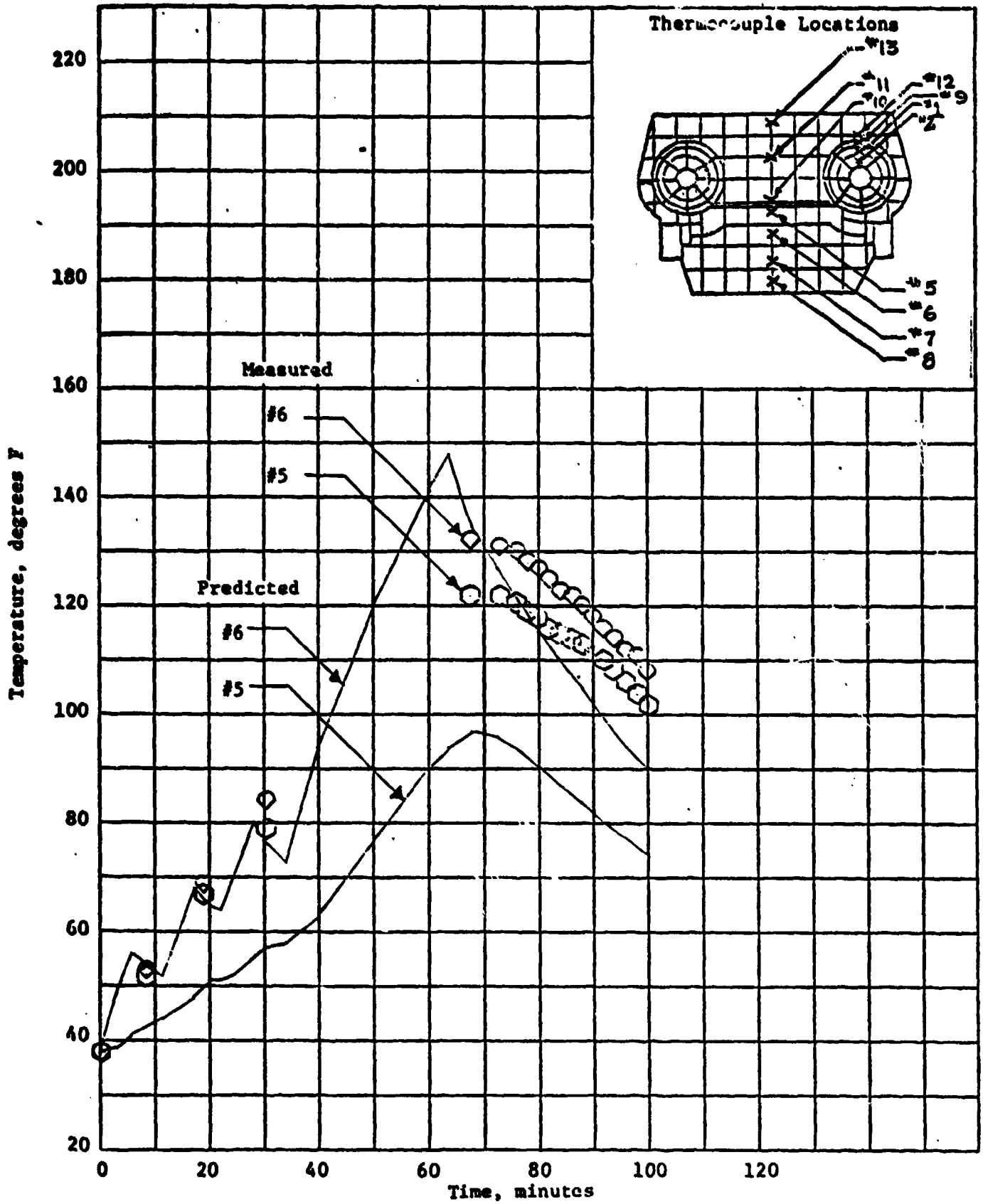

FIGURE 42. TEMPERATURES AT SELECTED LOCATIONS IN T-142 TRACK

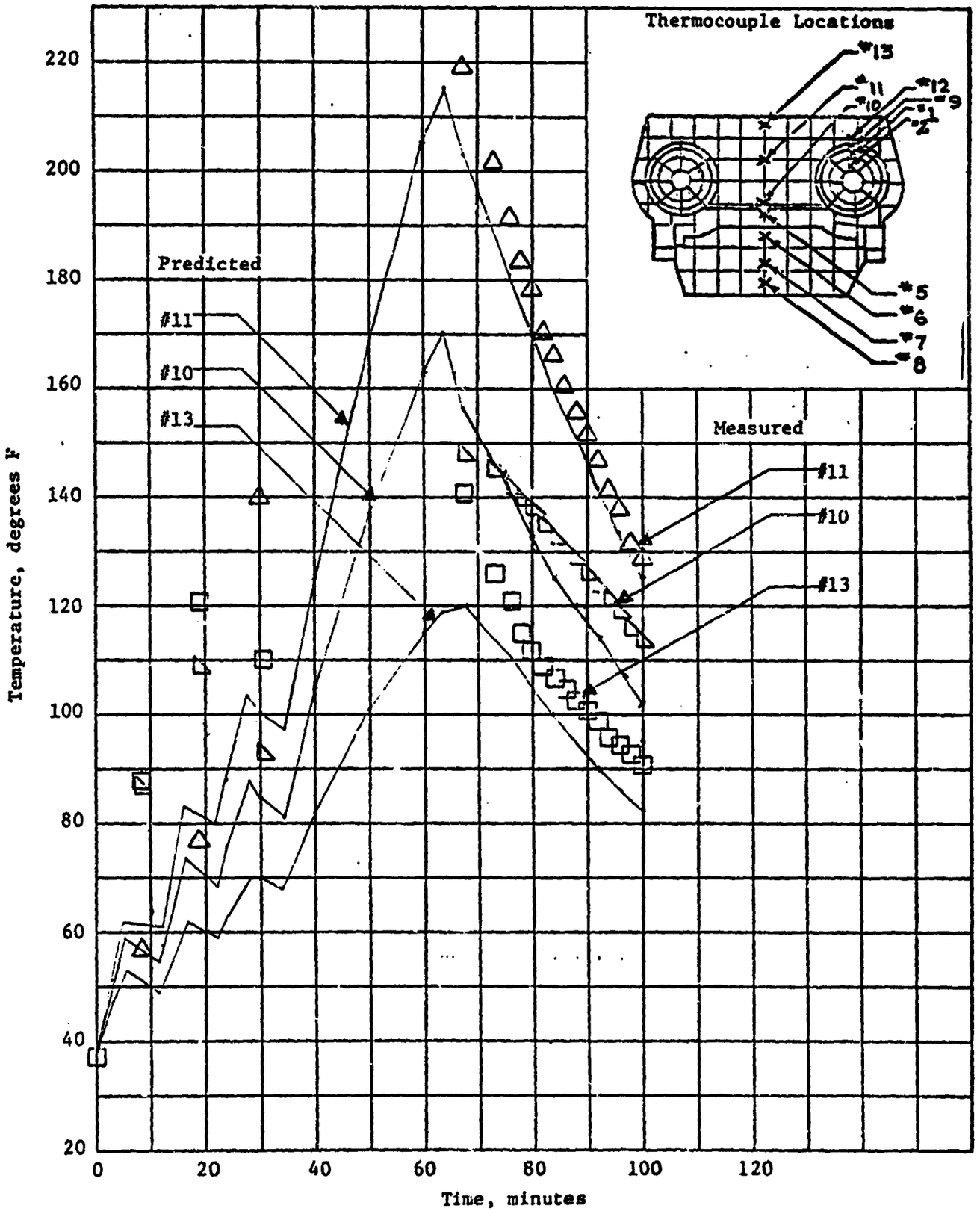

FIGURE 43. TEMPERATURES AT SELECTED LOCATIONS IN T-142 TRACK

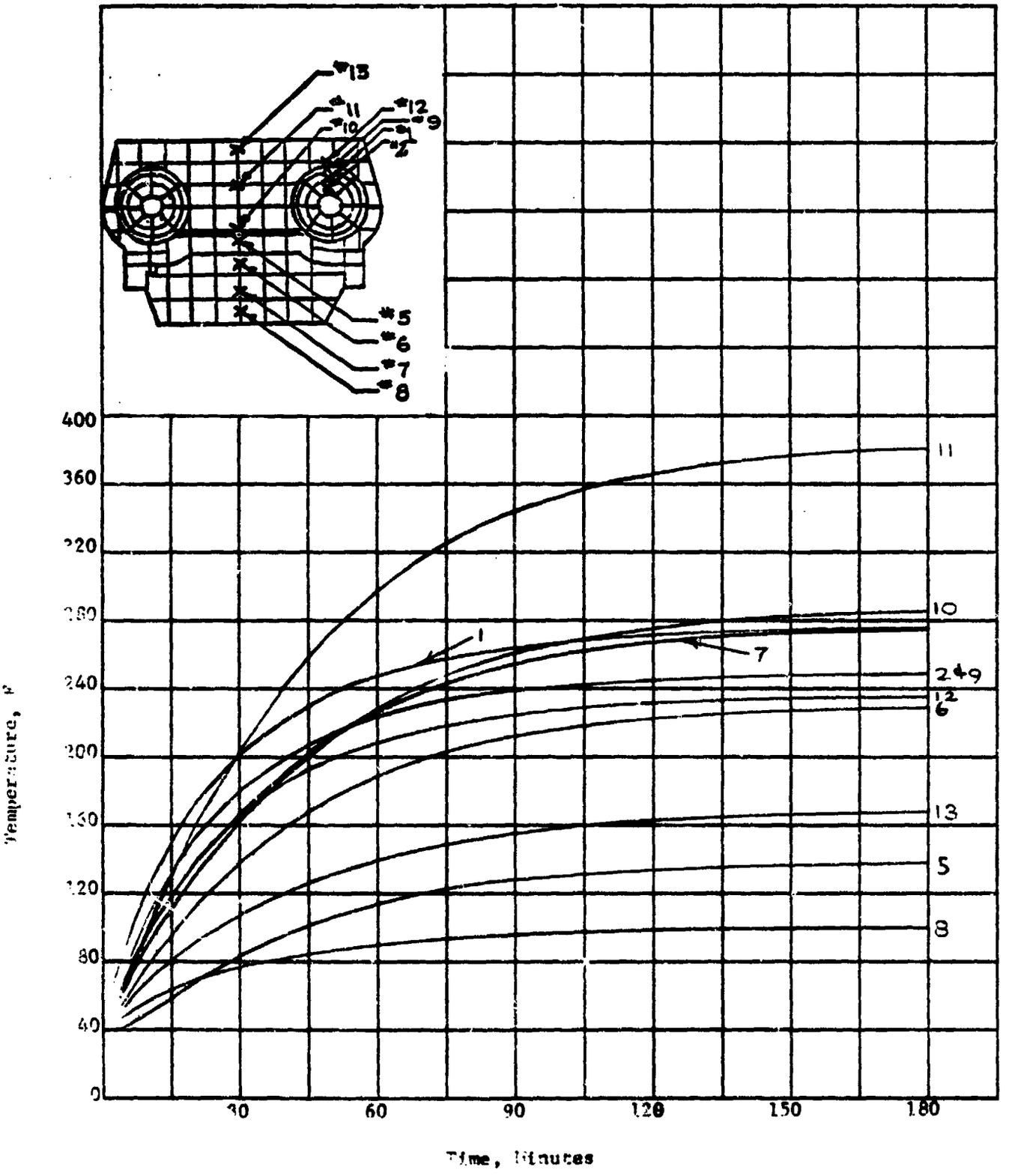

FIGURE 44. PREDICTED TEMPERATURES IN T-142 TRACK-CONTINUOUS OPERATION AT 30 MPH

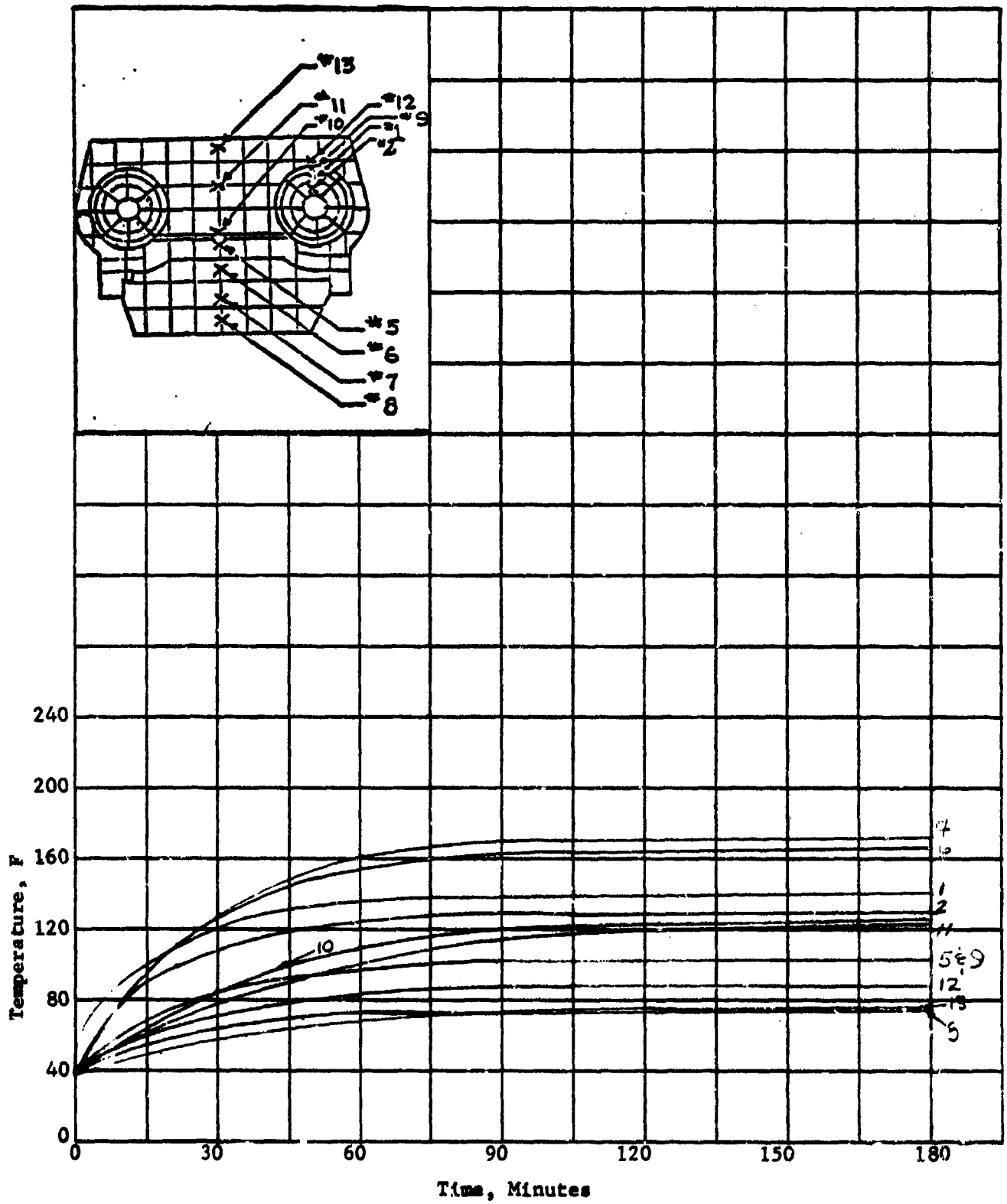

FIGURE 45. PREDICTED TEMPERATURES IN XM-1 TRACK-CONTINUOUS OPERATION AT 30 MPH

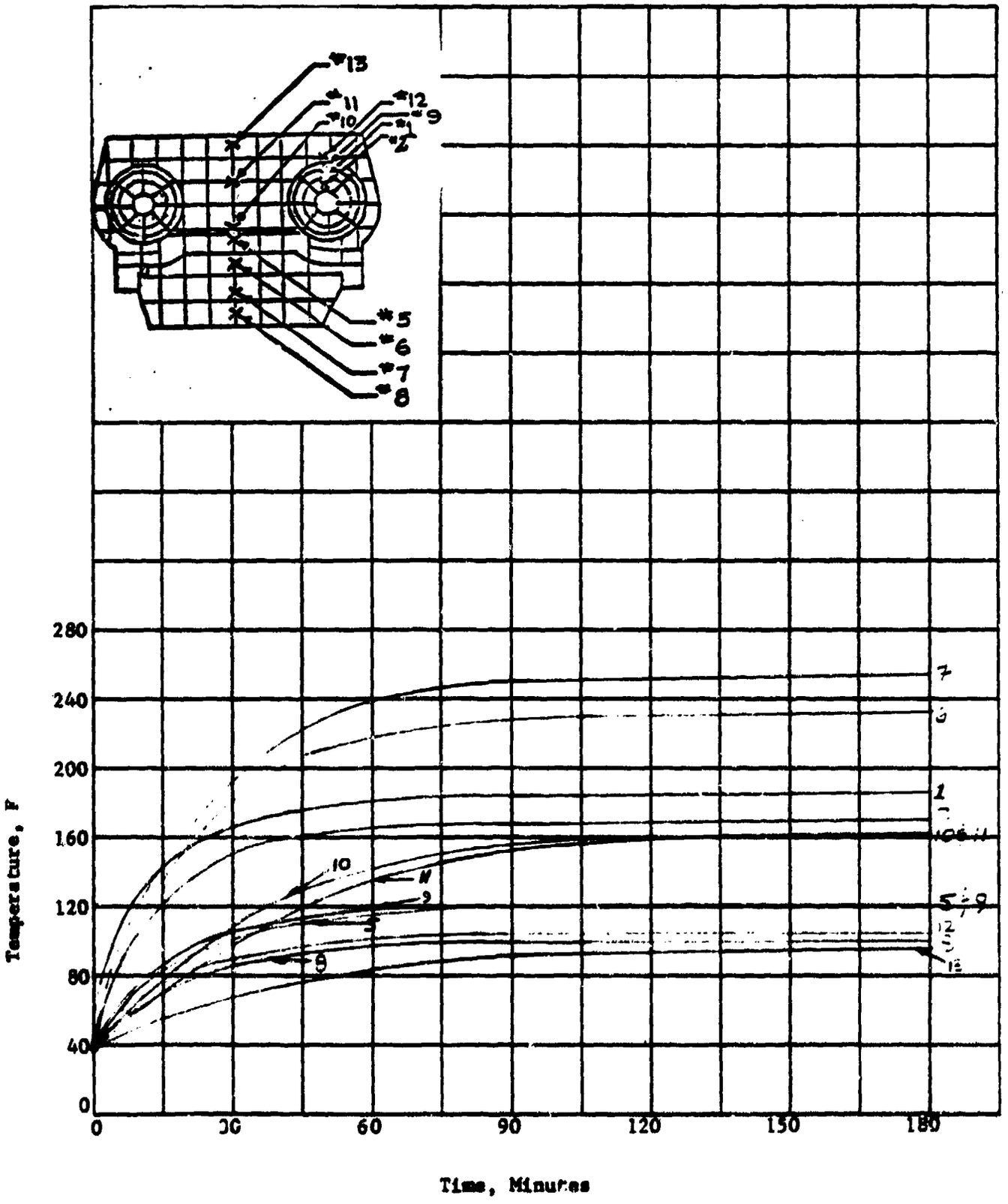

FIGURE 46. PREDICTED TEMPERATURES IN XM-1 TRACK-CONTINUOUS OPERATION AT 50 MPH

Track Bushing Research

One of the key elements of track is the rubber bushing which occupies the volume between the pins and the tubular portion of the shoe. Bushings do have some problems, particularly in single-pin track where their torsional displacements are higher. It was noted that the bushings must deform grossly when the track is assembled. Therefore, it was decided to study bushing assembly stresses and other aspects of the bushings to determine ways in which bushing life could be improved.

In a track assembly, the bushing is mounted on the track pin to provide an adequate seating in the tube which links the track shoes. In the unassembled state, the rubber bushings are in the form of a series of "donuts" separated by a thin rubber layer. The manufacturer is required to size the donut such that the oversize between the bushing and the tube is just sufficient to cause the bushing to deform into the shape of a homogeneous cylinder.

It is believed that this specification is approximately met by the manufacturer by merely equating the volume of the oversize to the volume of the space between the donuts, assuming that rubber is incompressible and that there is no deformation in the rubber at the end of the bushing. This latter assumption is very approximate, but there is no indication of a more formal analysis being undertaken, based on elasticity theory, to prove that the specification is satisfied. The necessity of a more sophisticated analysis arises due to the two-dimensional, large-deformation behavior of the rubber bushing when the pin bushing assembly is inserted into the track tube. The final shape in the initially straight sides of the donuts will become curved in the deformed state. Also, the points at the base of two adjacent donuts cannot be expected to coalesce after deformation to avoid infinite axial strains in the rubber membrane layer which is bonded to the pin. Thus, it appears a priori that the bushing offers discontinuous support for the pin and also that high stress concentration is likely to occur in the bushings due to deformation of the bushings during assembly.

Analysis of Assembly Stresses

The finite element method of structural analysis was employed to analyse the pin/bushing assembly stresses. The installation of the bushing in the "binocular" tube was simulated by applying a radial interference to a single rubber bushing finite element model. To confirm that a convergent solution was obtained, both a coarse and fine model were employed in the analysis. The coarse model is shown in Figure 47. The finite elements representing the rubber bushing utilize the Mooney-Rivlin formulation which requires that two material parameters be known. Unfortunately, the form of these parameters bears little resemblance to the reported engineering properties of rubber.

In order to define these parameters in their proper form, a computer program was written that would calculate the Mooney-Rivlin parameters for a given stress-strain relationship. Information supplied to Battelle indicated that the bushing material is similar to the U.S. Rubber Company's Number 6270 rubber, for which a stress elongation curve was available. It can be seen from Figure 48 that the Mooney-Rivlin parameters estimate the response of Number 6270 rubber quite well up to an elongation of 150 percent.

The results of the analysis indicated that while the installation of the bushing in the "binocular" tube does not produce significant stress in the pin, extremely high strains were produced in the rubber bushing. These strains were particularly large at the corner where the bushing and pin meet (near Node 34 in Figure 47). In reality there is a small fillet that could not be modeled at this corner that might slightly reduce these deformations. Nevertheless, the location of high strain in the model is precisely where many bushing failures occur. Figure 49 shows the displaced geometry of the finer model superimposed upon the unloaded geometry for a radial interference of 0.06 inch, which is 55 percent of the total applied interference.

In the past, these failures have been attributed to abrasion of the highly deformed rubber bushing by the pin. This abrasion occurs because the rubber bushing is in contact with, but unbonded to, the pin. This analysis indicates that the failure may actually be initiated by the installation of the bushing tube. It is still likely that abrasion contributes to the failure even if this is the case.

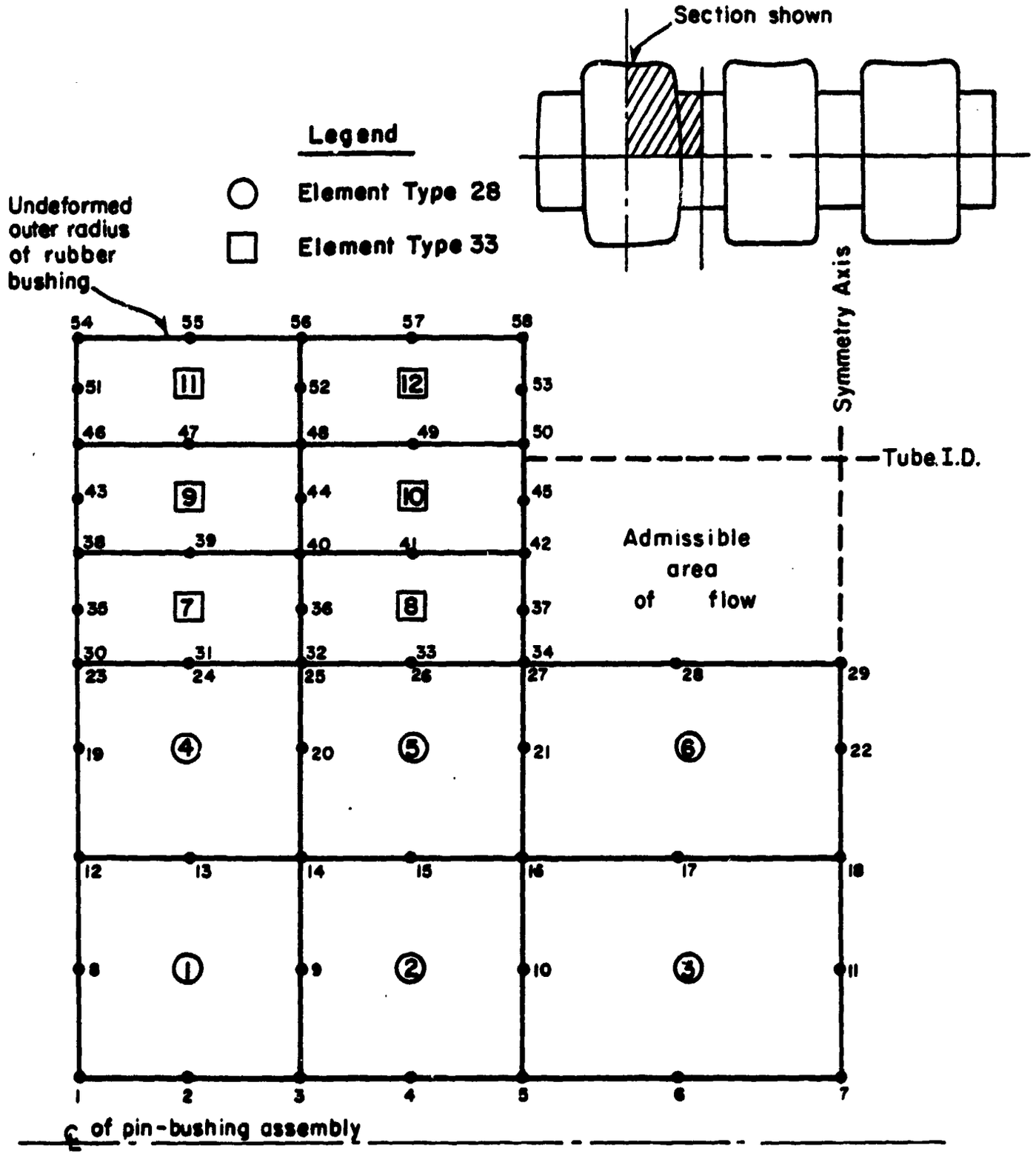

FIGURE 47. COARSE FINITE-ELEMENT MODEL OF PIN--BUSHING

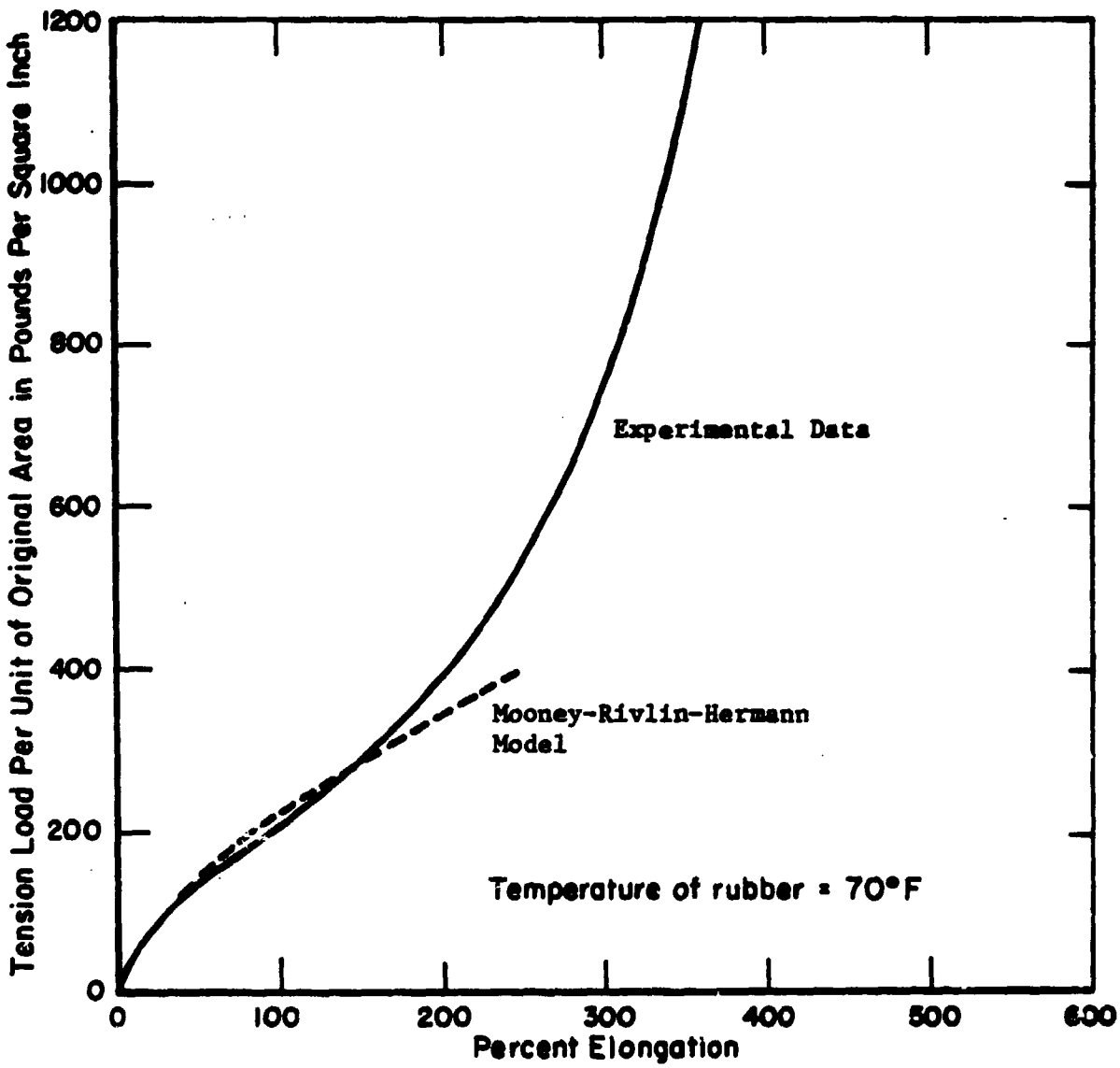

FIGURE 48, ANALYTICAL MATERIAL MODEL FOR #6270 RUBBER

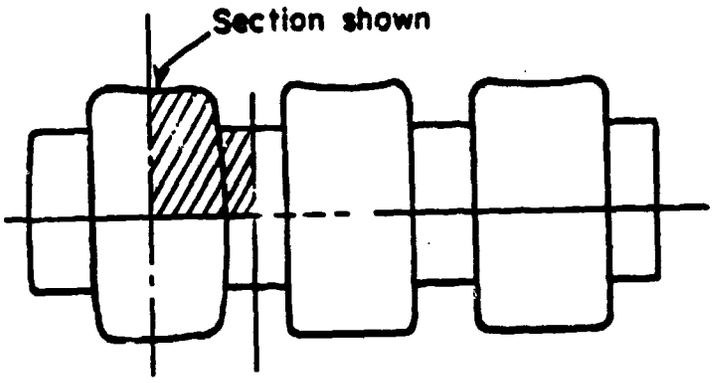

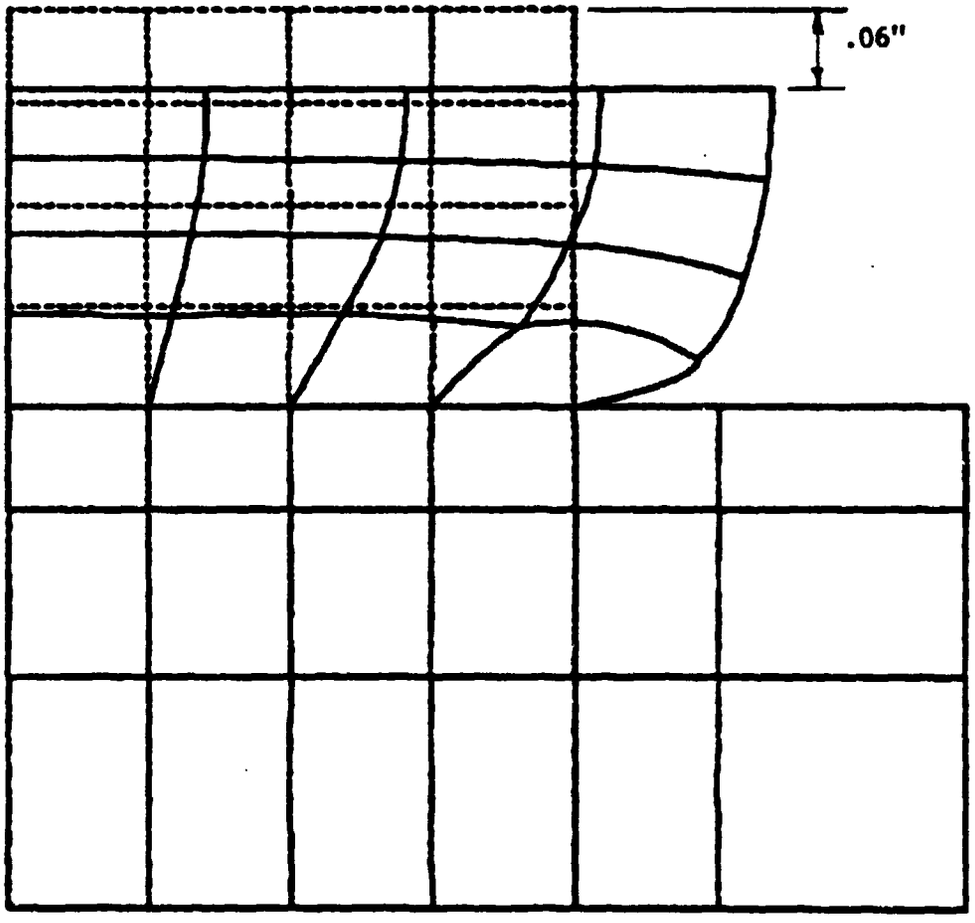

FIGURE 49. DISPLACED GEOMETRY OF THE REFINED RUBBER BUSHING MODEL SUPERIMPOSED ON THE ORIGINAL GEOMETRY FOR A RADIAL INTERFERENCE OF 0.06 INCH

Bushing Insertion Tests

The computer results indicated the areas in which high stresses occur, and it was decided to perform some laboratory insertion tests to see if the results correlated with the analysis. Therefore, insertion ("shooting") experiments were performed for nine T-130 bushings. The objectives of the experiments were to determine:

- Donut deformation shape during insertion
- Repose of the donuts after insertion and before and after recentering
- If and where strain damage occurs in the rubber.

All nine of the bushings were measured beforehand to assure that they conformed to the dimensional requirements of MIL-T-11891B. Three of the nine bushings were "shot" into a Lucite® tube that is used to check bushing "fill" and repose of the donuts. The tube had a long lead-in "funnel" at one end to ease the insertion by funneling the donuts into its ID. The first of the three was shot dry (unlubricated) and even though the ID of the tube was the largest allowable by MIL-T-11891B (1.194-inch diameter), an area that appeared to contain trapped air bubbles was visible through the tube on the deformed OD of the inserted donuts. After extraction, this area turned out to be surface damage (apparently due to friction) that was initiated at the leading edge of the donuts that first contacted the wall of the tube during insertion. (See Figure 50.) Strain damage was noted also around the circumference of two of the donuts in the unlubricated specimen. This damage, which

® is registered trademark.

appeared at the points indicated in Figure 9, looks like a "split" caused by fold-over of the corners. The damage nearly circumscribed the two donuts; however, it was the greatest where the surface damage due to friction was greatest.

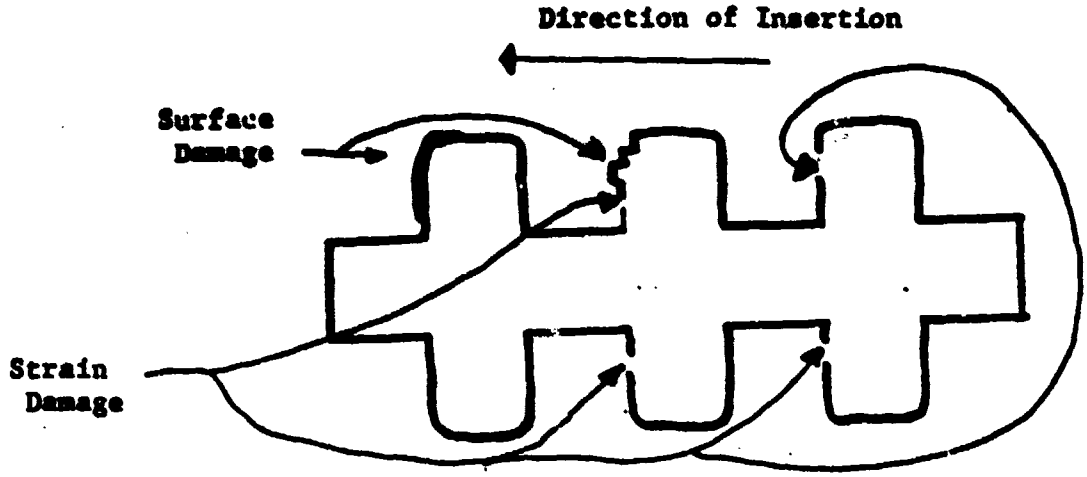

FIGURE 50. DAMAGE OF T-130 BUSHING DURING INSERTION

For the dry shot in the Lucite® tube, 5400 lb maximum force was required. As indicated in Figure 50 surface damage resulted in a serious loss of material, particularly for the second donut. Unfortunately, there appeared to be no correlation of damage with the dimensions of the donuts. After re-centering, the parting lines between the three donuts were distinct even though the donuts had been forced into solid contact in both directions. The parting lines were not parallel, however. Apparently, nonuniform friction caused some portions of the donuts to drag more than others.

The other two bushings that were shot into the Lucite® tube were lubricated*, and no serious surface damage or material loss occurred. However, the direction of insertion can be verified by a slight scuffing (removal of gloss) over a small area of the circumference at the leading edges of all three donuts in the same regions as are shown in Figure 50. The insertion force was about 2000 lb. maximum and the parting lines were rather indistinct and parallel.

* The lubricant was described as a "vegetable oil or a paraffin-base oil as is used in production". Lubrication consisted of hand wiping a generous quantity of lubricant on the donuts.

® is registered trademark.

Six of the nine bushings were inserted into a metal split collet that is used as the fixture for fatigue tests. In contrast with the larger ID of the Lucite® tube (still within the specification), the test collet represents the low end of the acceptable OD prescribed by MIL-T-118913 (1.187 in. diameter). All bushings shot into the test collet were lubricated. In contrast with the Lucite® tube, the test collet had only a slight chamfer on the insertion end; therefore, a funnel (a block with a hole that necks down to the collet diameter) is required to ease insertion (as in production assembly) by "funneling" the donuts into the tube. The following comments summarize the results of the insertions into the split collet:

(1) Each bushing showed varying degrees of lead-edge damage due to insertion. Most damage appeared to have been initiated when the donuts were forced through the conjunction of the funnel and the tube, as evidenced by the rubber shavings produced there.

(2) Small axial slits showed up in most bushings on opposite sides of the donuts. These slits corresponded to the split collet's parting plane. Because the slits showed up nearer and sometimes "around the corner" of the lead edge of the donuts, they probably occurred during insertion, rather than during removal from the collet, as has been suggested.

(3) The six specimens required maximum forces of 3,500, 4,400, 4,800, 4,400, 4,700 and 4,100 lbs to shoot the bushings.

(4) One bushing was marked at the trailing-edge corner of the third donut. The mark was visible after insertion as shown in Figure 51.

It appeared that even for undamaged donuts, the friction/deformation during shooting caused leading-edge rollback or foldover.

One of the bushings that had remained relatively undamaged following insertion into a Lucite® tube was again shot (lubricated) into a Lucite® tube, this time using AA USP Castor Oil as the lubricant. The use of castor oil reduced the bushing insertion force by a factor of 4 (495 lb versus 2,000 lb) when compared with shooting the bushing into the tube using the conventional lubricant! The bushing has now been residing in the Lucite® tube for more

® is registered trademark.

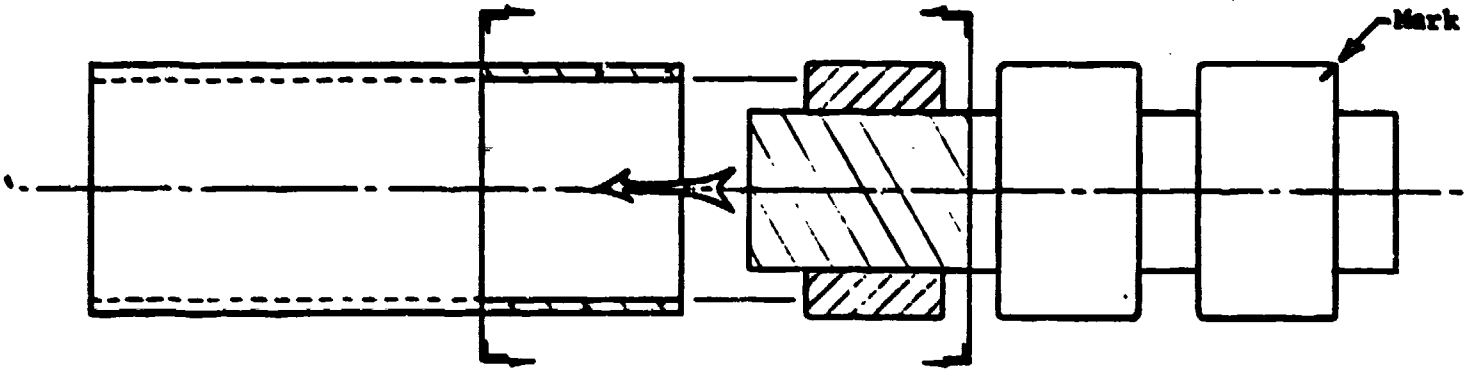

a. Before Assembly

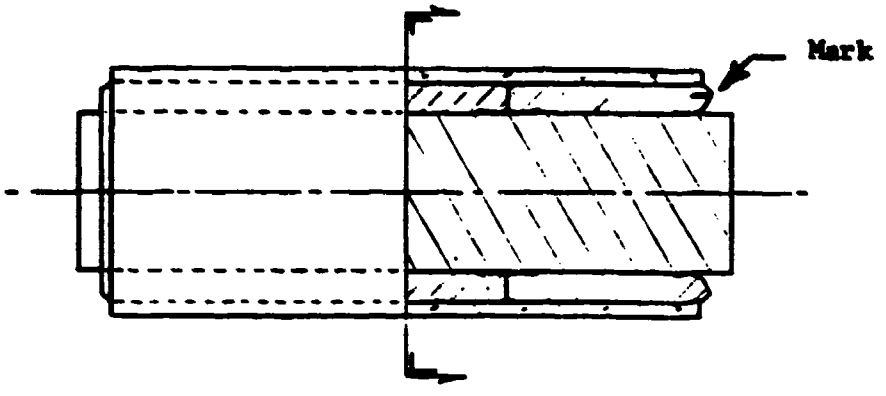

b. After Assembly

FIGURE 51. SKETCH ILLUSTRATING LARGE BUSHING DEFORMATIONS OCCURRING DURING ASSEMBLY OF RUBBER BUSHED PIN IN SHOE

than four weeks, and it is significant that a portion of the lubricant remains trapped between the deformed donuts at their parting lines.

It can be concluded that (at least for Lucite® tubes where the surfaces are much smoother than are those of a binocular tube) the use of a viscous lubricant having good boundary lubrication properties represents a very effective way of reducing insertion forces--and, concomittantly, surface damage--by dramatically lowering the friction. However, if one desires a bushing that does not slide relative to the tube when torqued during service, the lubricant must find its way out of the interface, or if it remains, it must not be too effective in lowering friction. The ideal, of course, would be to employ a lubricant which is very effective during shooting in precluding surface damage and foldover of donut corners and yet one which can migrate out of the tube, evaporate, or congeal--to produce a relatively high friction contact between the deformed donuts of the bushing and the ID of the tube. There appears to be a fine line between selecting precompression values that preclude bushing slippage during torsion in service and their interaction with lubrication during shooting. If on the other hand, lubrication is too persistent and/or precompression is too low, the bushing will slip in the tube when torqued in service and probably fail by wear. The selection of improved lubricants for the shooting operation and optimization of the interaction between lubrication, precompression and shooting techniques offer a fertile area for research that might improve bushing life.

Design of Bushing Research Machine

Based on information obtained during the first 60 days of the program, it was concluded that three distinct types of laboratory setups should be considered for providing data for track dynamics and design criteria for new track concepts. One of these setups was a laboratory machine for track pin-bushing research.

Because of the significant investment in costs and time required to build and fixture such a machine, the next step was to verify its appropriateness and refine its design features. Therefore, an investigation was undertaken

---

® is a registered trademark.

of past and current experience in the development and testing of the track pins and bushings. It was found that the history of these developments as disclosed by the literature and by tradition was imposing in size and breadth. In addition to the plethora of well-documented studies in this area, it appeared that there exists a design/testing rationale which has either been largely undocumented or is difficult to piece together because of the difficulty of finding the literature, or of deciphering the sequence of events for that which is "documented".

Review of Previous Bushing Research. To assess what had been done in the past on this subject, the report literature of TARADCOM-supported and -conducted work was studied, and the track contractor community and TARADCOM personnel were interviewed. Immediately, it became apparent that the report literature--which was responsible for relating the development of (1) the design of currently-used bushings and (2) the design and hardware for the currently-used bushing test machines--was quite old (1948 and earlier).

In addition, it appeared that no company in the track community is entirely satisfied with the designs and capabilities of its own bushing machines. Because most of them cannot reproduce the data for the 1946-developed Armour Research Foundation (ARF) bushing machine (which now resides at TARCOM and is performing QPL tests), TARADCOM personnel believe only in the data from the ARF machine. Because of the current "channel black crisis", each of the track contractors needs in-house a more reliable bushing test machine, and at least one of them has a new machine currently under construction by an outside organization.

The channel black crisis has produced even another perturbation in bushing machine genesis; because the ARF machine is too slow in producing data required to qualify channel-black-substitute materials (and for other lesser reasons), TARADCOM is also in the process of designing and building a new "R&D" bushing tester. This machine is expected to reproduce the data of the ARF machine so that the baseline fatigue criteria are not lost and, in addition, the machine will probably be duplicated for use by contractors and by TARADCOM to yield statistically significant and valid data for new bushing materials and designs--including shapes and sizes other than the T-130 designs to which the ARF machine and all of the others have been limited. As a result, it became obvious that bushing test machine development which had been almost static and out of mind for 30 years suddenly is active and in a state of flux.

Armour Reports. As indicated above, ARF was responsible for the development of the current TARCOM QPL bushing tester. Consequently, it was

important to review their reports, even though the program on which the machine was used to investigate the fatigue life of rubber donut bushings was carried out over the period 1946 to 1948. Analysis of these early reports (22 of them) provided an important background on the bushing machine as well as on the design, fatigue life, and properties of the bushings themselves. Even though some of this series of reports could not be located at TARADCOM, (and even some existing copies appear to be missing important details of the work) this compendium still represents the most in-depth study of bushing design parameters, and the test machines described in the program represent the best method of simulating bushing stresses available thus far. Each of the reports was synopsized, and a short summary of the entire program was developed as described below.

A bushing test machine was constructed that applied radial and torsional stresses to bushings as follows:

Radial Load, psi (pin area)	0 to 3000
Radial Load Cycle, cpm	64
Torsional Strain (Flex Angle, °)	± 7-1/2 or ± 15 (± 22.5 for later experiments)
Torsional Load Cycle, cpm	255 (400 and 500 for some experiments)
Precompression of Bushings, %	20, 27.7, 33.8, 36.6, 40, and 50

For some experiments, bushings were water-cooled by circulating water through hollow pins. However, most experiments were run in air without cooling. With this machine and other pieces of apparatus, including an experimental strain analysis that was used to conclude how the bushing deformed in the tube, experiments were made which resulted in the following conclusions:

(1) To prevent abrasion/wear at the bushing ends, bushings should at least completely fill the sleeve, or preferably extend only a small amount beyond it. (See Figure 51.)

(2) Fatigue life is a linear function of the testing (radial compressive) load when referred to semilogarithmic coordinates (See Figure 52.)

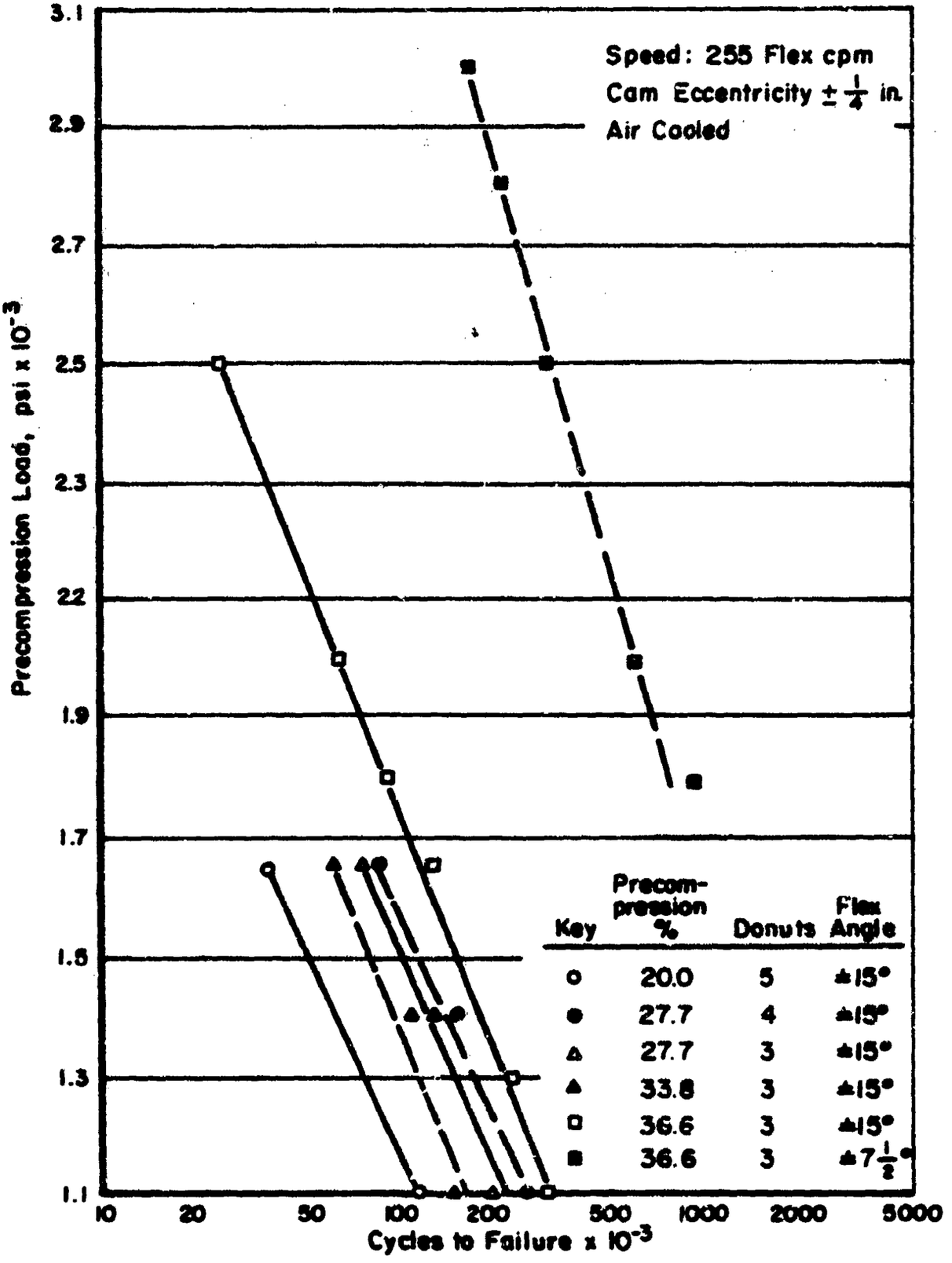

FIGURE 52. FATIGUE LIFE CURVE FOR RUBBER BUSHINGS

(3) Design calculations can be based upon average unit load measured in pounds per square inch of projected area of the pin

(4) Restraining caps on the ends of the bushings improve fatigue life

(5) All bushings should be bonded to the pins

(6) Failure is initiated by abrasion of the donuts against the pin

(7) A small decrease in flex angle results in a large increase in fatigue life

(8) Bushing donuts should be designed to have

(a) Large fillets at the base, particularly on the outboard end

(b) Radii at the upper corners

(c) A slight taper toward the center of the donut (see Figure 53b).

For conventional rectangular-shape bushings (as are characteristic of T-130 and T-142 bushings in use today), the fatigue-life curves shown in Figure 52 were developed.

Because of the dramatic improvement in fatigue life that results from decreasing the flex angle (see Figure 52 and Conclusion 7, above) and the conclusion that failure is initiated by abrasion of the donuts against the pins (see Conclusion 6), a new bushing shape was developed. Experimental strain measurements on flat specimens showed that the conventional donut (which is bonded to the pin and is rectangular in cross-section) deformed under radial compression loads typical of the precompression loads used in bushing assembly in such a manner that a significant area of the unbonded rubber contacts the pin and rubs against it when the torsional stress is applied, as shown in Figure 53a . Even a greater area of rubber contacts the pin as the radial compression loads found in service are superimposed on the precompression load. Therefore, the same kind of experimental strain measurements were made for shapes contoured to provide strain relief so that during deformation no unbonded rubber would contact the pin. One of

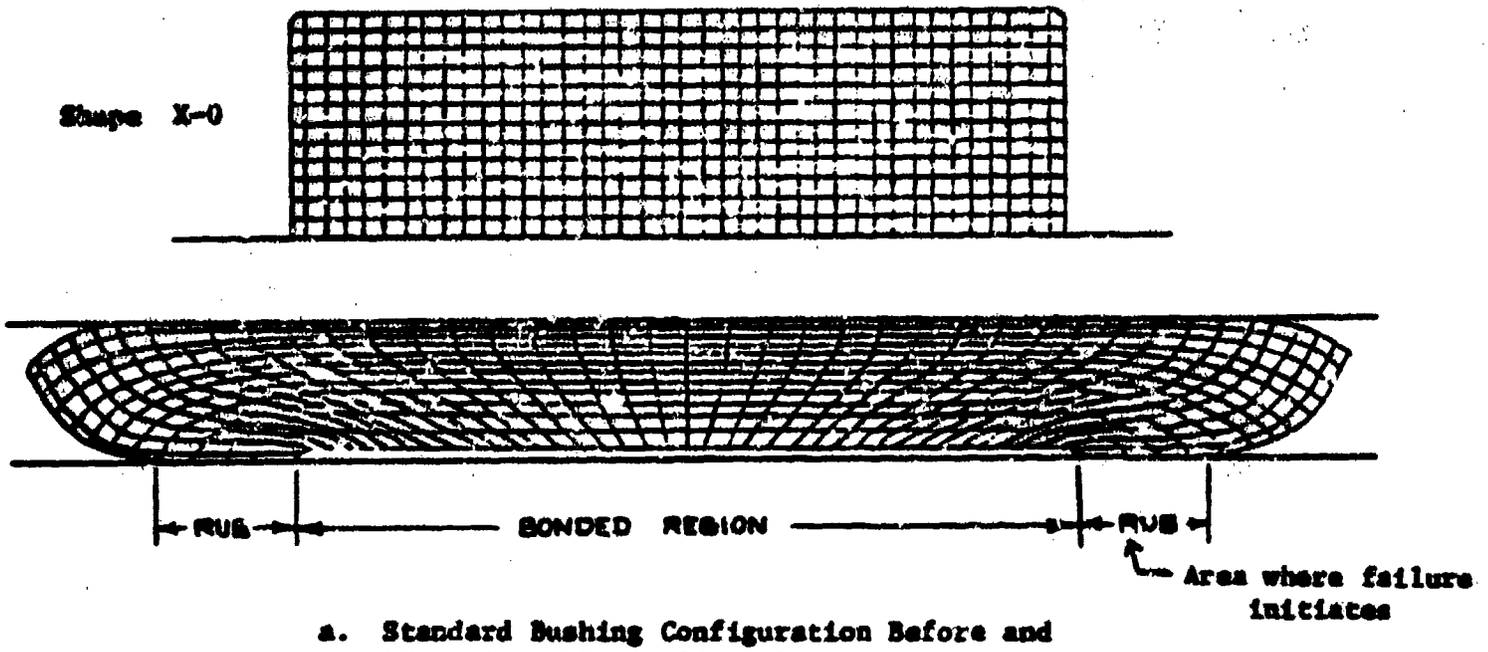

a. Standard Bushing Configuration Before and After Assembly in Binocular Tube

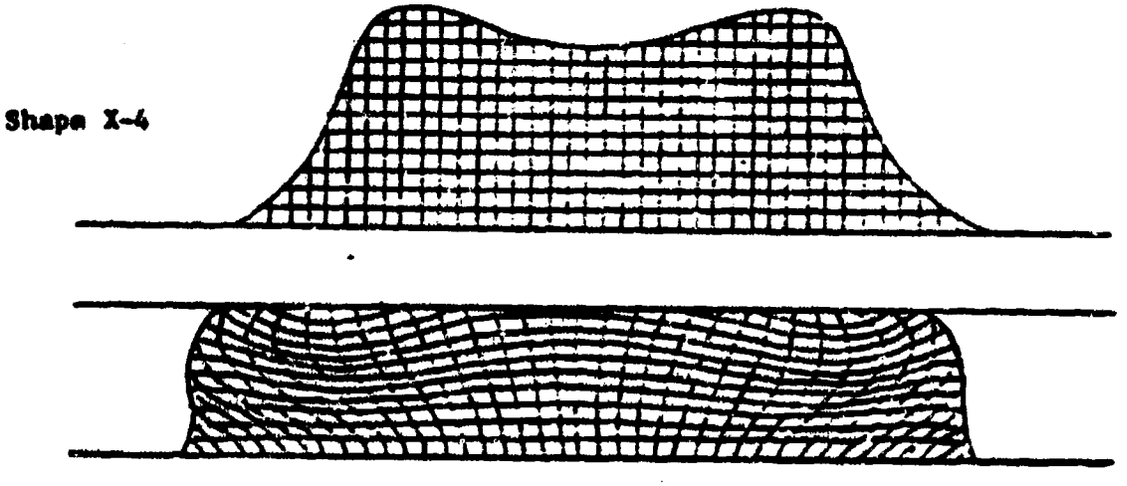

b. Experimental Bushing Configuration Before and After Assembly in Binocular Tube

FIGURE 53. BUSHING CROSS-SECTIONS SHOWING DEFLECTIONS CAUSED BY ASSEMBLY IN SHOE

the best of the new bushing shapes resulting from these studies is shown in Figure 53a. Figure 53a represents strain deflection pattern of the conventional rectangular bushing, while Shape X-4 in Figure 53b illustrates the strain pattern developed with the contoured bushing shape. Note the difference between areas of contact of unbonded rubber with the pin, as well as the differences between the bond shear angles of the area of rubber bonded to the pin. It was concluded, of course, that the deformation pattern of Shape X-4 would preclude contact of unbonded rubber with the pin as well as help preserve the integrity of the bond of rubber to the pin by preserving a low shear angle at the bond.

This new bushing shape, which is also described in Conclusion 8, above, was developed at the end of the ARF program. As a consequence, it was never tested in that program, even though a mold was made and some bushings were ordered from a rubber company. Moreover, TARADCOM personnel have recently concurred that the experimental shapes were probably never tested by anyone. This kind of bushing design work should be resumed and it should become part of any fatigue studies that might be done with the new bushing tester.

1963 Studies by Rose. The 1963 work of Carol Rose at TARADCOM which dealt with fatigue life of rectangular donut bushings was also studied. Rose used the same bushing test machine (the current TARCOM QPL machine) that was used in the ARF work, but he added some statistical credence to some of the findings of the ARF studies. In addition, he defined the magnitude of the interaction between the stresses--radial-compressive and torsional--as well as the cyclic-rate effects on the conventional rectangular (T-130 type) donut bushing. A summary of Rose's data appears in Table 13.

As shown by the data, Rose's conclusions were that:

(1) Compressive load and torsional flex angle each have a major effect of fatigue life

(2) Cyclic rate has a relatively small effect (even though fatigue life increased more than 50 percent (from 403.2 x 10^3 cycles to 611.8 x 10^3 cycles) when cyclic rate was decreased from 255 to 85 cpm at loads of 1,500 psi and flex angles of $\pm$ 15 degrees).

TABLE 13. SUMMARY OF BUSHING FATIGUE-LIFE DATA FROM ROSE'S REPORT(*)

Compressive Load, psi	Torsional Flex Angle, ± degrees	Cyclic Rate, cpm	Fatigue Life, torsional cycles X10^{-3}
750	15	255	3,000
2,250	15	255	76
1,500	7.5	255	> 3,000
1,500	22.5	255	44.5
1,500	15	255	403
1,500	15	85	612

(*) Rose, C. D., "Laboratory Investigation on Fatigue Life of Rubber-Bushing Track Pin Assemblies", Report No. 7908, Ordnance Tank Automotive Command, Detroit Arsenal, July 16, 1963.

Rose's work represents a well-planned and executed study that scientifically sorted out and statistically confirmed the ARF work. In addition, it was useful in establishing a basis for a number of types of studies that might facilitate reaching the objectives of improved bushings for track pins. Among these are included:

- A finding that a simple torque measurement on the track-pin specimen assembled for bushing testing correlated well with fatigue life. Such a finding should be studied in more detail in all bushing tests conducted by TARCOM, the track community of contractors, and in any work dealing with bushing tests that might become active. In addition, field tests on track ought to include taking torque data during assembly of the track to be tested. If the correlation holds, a simple torque measurement might be able to predict fatigue life of a bushing assembly.

- Wear data showed that greater than 50 percent of bushing wear takes place during the last 10 percent of the fatigue life. This suggests that a fatigue-life criterion could be set up on the basis of wear. During experimental programs where bushing testing is being carried out, wear debris should be collected. If the wear rate could be determined early during the process, one would have a failure-prediction criterion that could be used to predict the fatigue life of bushings being tested in laboratory bushing machines, as well as the possibility of generating a retirement/replacement criterion for field use (provided one could correlate wear in the bushing machine with wear in the field).
- The data were taken under conditions that were purposely accelerated in the area of torsional stress (high flex angles) to produce fatigue failure in a reasonable amount of time, and yet certain of the stress levels were selected to be consistent with what is now a comparatively slow-moving lightweight tank*. It is recognized that flex angles in a track operating over all but extremely large protuberances are in the order of only $\pm$ 7 to $\pm$ 9 degrees. The data show an extreme sensitivity to flex angle, confirming that finding in the ARF work that decreasing the flex angle from $\pm$ 15 degrees to $\pm$ 7-1/2 degrees results in about a 1000 percent improvement in fatigue life. A bushing R&D machine that is expected to recognize the promise of bushing materials and designs formulated to withstand the higher compressive

* M-47 tank track parameters were used to specify test conditions:
At 10 mph (level ground) 150 psi load, 7-1/2° at 85 cpm
At 20 mph (level ground) 150 psi load, 7-1/2° at 170 cpm
At 30 mph (level ground) 150 psi load, 7-1/2° at 255 cpm
At any speed (maximum grade) = 1,500 psi load.

> loads and the higher cyclic rates of today's heavier and faster tanks should have a more refined capability to impose more realistic torsional stresses. For this reason, it would be appropriate that the bushing testers being currently designed for assessing the merits of new bushing materials and designs, be capable of varying the flex angle from 7 degrees to angles representative of running over protuberances and back bending--but, in the order and magnitude of the way the torsional stress is incurred in service. This suggests a programmable, hydraulically actuated torsional input that would reproduce the flex angles for various types of terrains in the magnitude, the order and the time frame in which they are incurred. Data could be taken from a real operating track, and taped inputs could be made to the bushing machine. Thus, a rubber or bushing design formulated to withstand high loads and high cyclic rates would not be discriminated against, declared a failure, and lost in a bushing test.

This review led to the final conclusion that there is a need by the Army for an R&D bushing machine that has capabilities that reside in no other existing or planned bushing machine (except possibly a machine being built by one of the track prime contractors). Bushing problems existing currently in single-pin track, problems anticipated in bushings for the XM-1 track and the need for new bushing materials/designs as a result of the world shortage of EP channel black — all represent incentives for this course of action. Accordingly, a bushing tester design effort was initiated, leading to a final design of a laboratory machine for pin-bushing research. This design phase is discussed below.

Detailed Machine Design. The goal of the design effort on the track-pin bushing laboratory research machine was to develop a bushing fatigue-testing apparatus that is well instrumented, able to test a variety of bushing sizes, and able to administer any realistic load-deflection test cycle. Inputs to the test machine could range from tapes of recorded field data to standard test cycles such as the TARCOM QPL bushing test cycle. Output will be not only the number of cycles sustained before failure, but also a short strip-chart plot that records how any or all of the instrumented variables (radial deflection, radial load, angular deflection, applied torque, temperature) change throughout the life of the test, or during any period of interest.

The performance criteria to which this machine was designed were determined by considering the variety of capabilities that would be important in a research tool for track-pin bushing design. The machine design criteria considered the loads and deflections that would be imposed on a bushing in a T-97 track operating over the M-60 geometry at a tank speed equivalent to 50 mph, and these conditions were used to define angular velocities, frequencies, and loading criteria. Study of previous bushing tests and projections of the requirements of possible new bushing designs provided additional input to the performance specifications. It was determined that the machine should:

- Accommodate any bushing pin size up to 2 inches in pin diameter (sized to accommodate projected experimental bushing and pin designs). Axial dimensions of the bushing specimens between 3 and 4 inches can be handled.
- Impose controlled angular deflections of the bushing up to ± 22-1/2° at maximum rates of 72 rad/sec. (This rate corresponds to the angular velocity imposed on a track pitch riding on the sprocket of an M-60 at 50 mph.)
- Control the radial loading cycle up to a maximum load of ± 25,000 lb. (This corresponds to a maximum of 5,000 psi load on a 4-inch length of a T-97 bushing.)

- Use a collet (into which the bushing is compressed for the test) that is temperature controlled (to simulate any reasonable temperature environment), and one that can be disassembled along an axial bushing plane to allow removal of the bushing specimen from the collet for inspection without incurring further damage to the bushing as a result of removal.
- Operate 24 hours a day, generally unattended, and monitor variables of interest.

A comparison of the "standard" QPL test cycle with angular deflections experienced by the bushings in an M-60 T-142 track is shown in Figure 54a, and a comparison of radial loads is shown in Figure 54b. The differences between the test and actual cycles in both cases is striking, and the objective of the bushing research machine design effort was to design a machine which could more realistically duplicate the actual cycle.

These requirements define a machine with three independent control systems: a radial load actuator that will follow a force level command; a torsional actuator that will cause bushing angular deflection to follow a displacement command; and a temperature controller that will track a temperature set-point.

A mechanically actuated machine would be very efficient, but would not have the ability to reproduce the actual mix of the load-deflection cycles that might be seen in service. Pneumatic systems, for these loads and frequencies, would be ungainly. Thus, an electrohydraulic, servocontrolled approach was chosen.

The configuration of the machine which evolved is shown in Figure 55 and is one in which the track-pin is free to rotate, as it is mounted in bearings on each side of the collet. Radial loads are applied through the collet, which undergoes no angular displacement. Torsional loads are applied to the pin, causing rotation of the pin with respect to the collet. Machines which fix the pin completely (allowing no pin rotation) and apply both torque and radial deflections through the collet eliminate the need for the bearing support of the pin and the associated wear and deflection problems.

"Actual" Cycle versus Standard Test

-- Actual cycle defined by M-60 track geometry only

-- Standard test practice defined by Armour Research Foundation developed machine that is currently running QPL tests

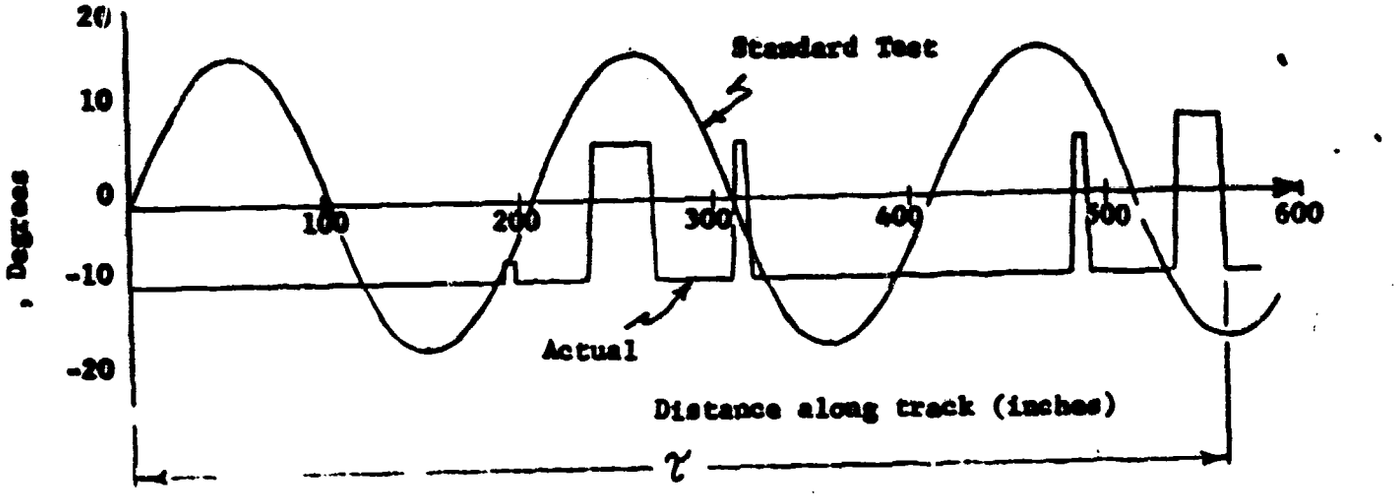

a. Tank Track Bushing Angular Deflection

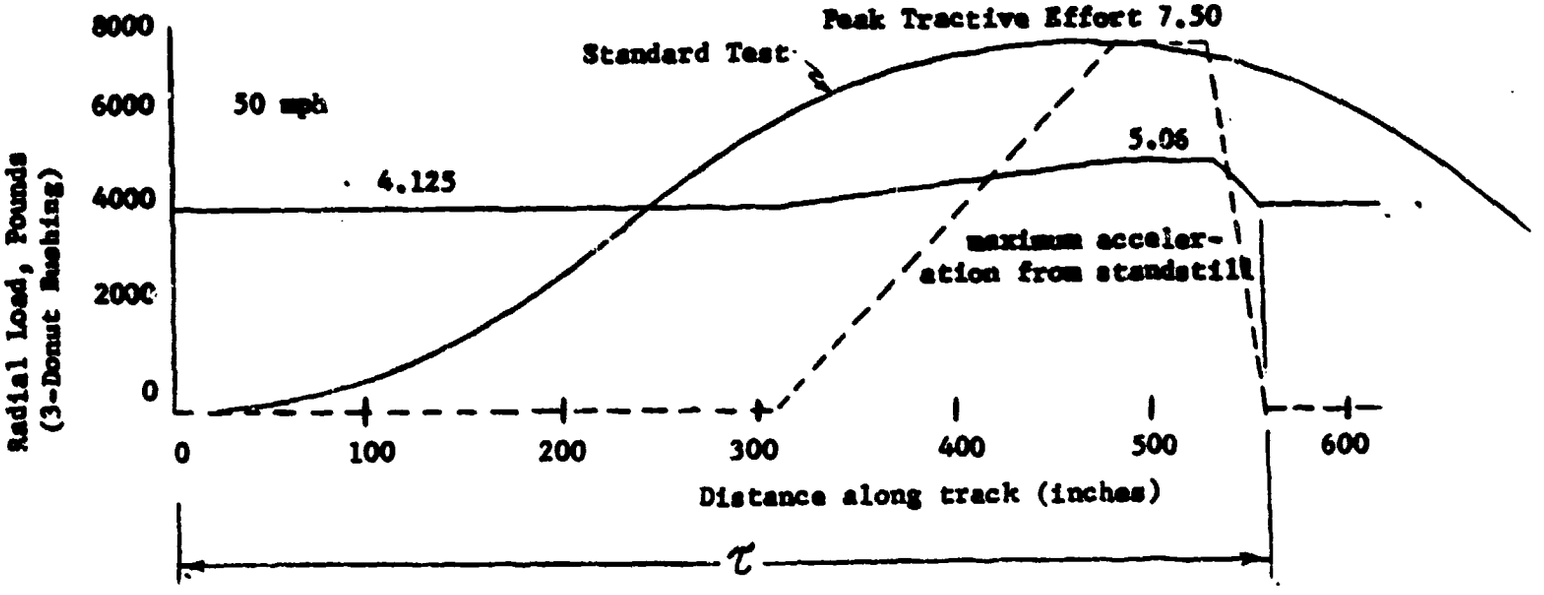

b. Tank Track Bushing Radial Load

FIGURE 54. COMPARISON OF QPL TEST CYCLE WITH ACTUAL BUSHING LOADS AND DEFLECTIONS

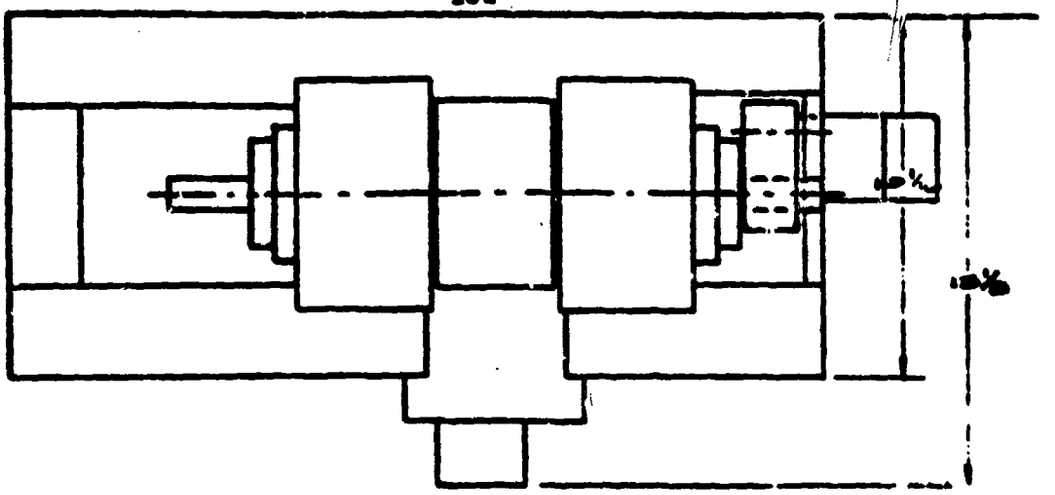

TOP VIEW

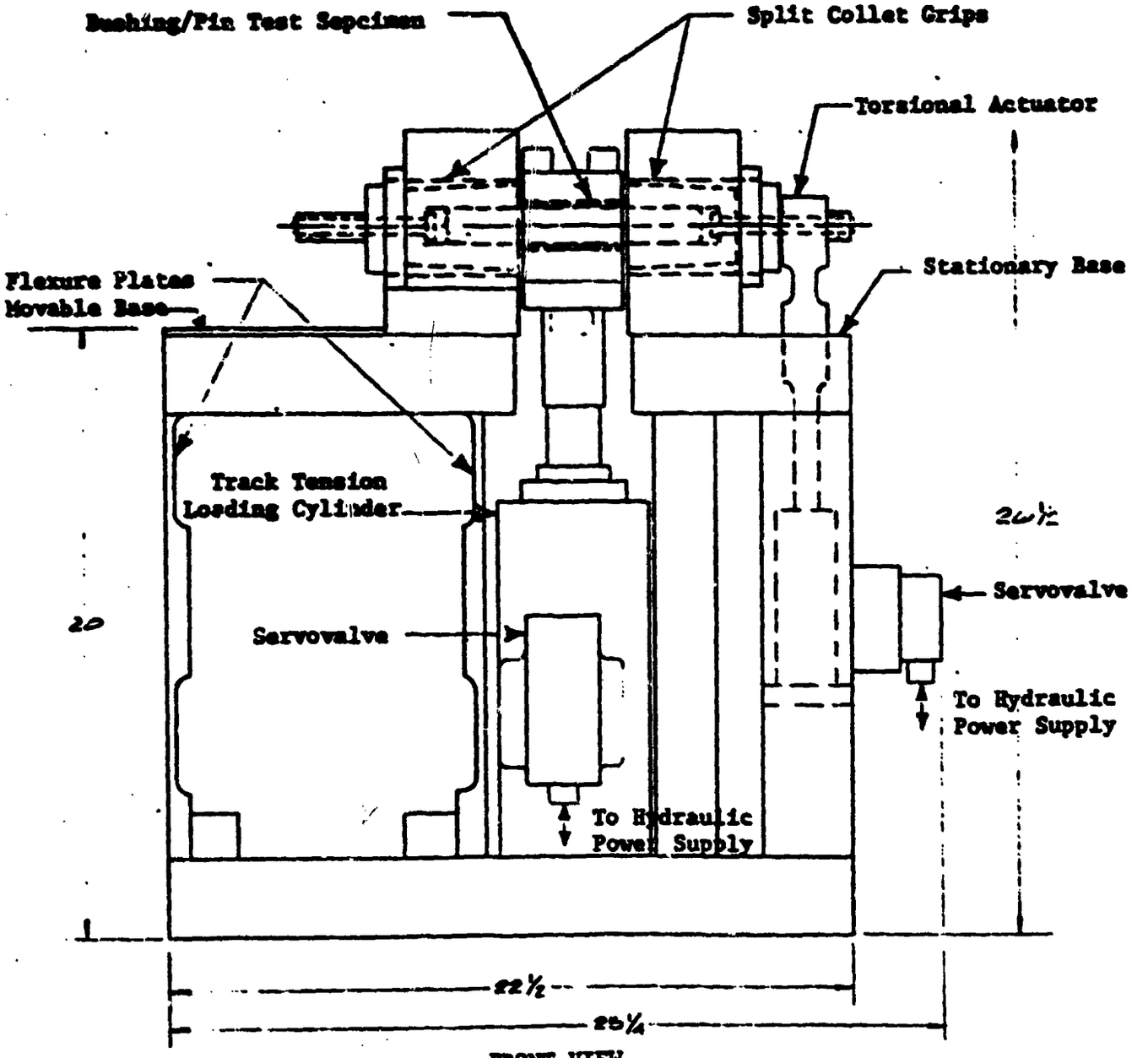

FRONT VIEW

FIGURE 55. BUSHING RESEARCH MACHINE

However, this approach was not used, for in applying torque to the collet in this manner, one would be forced by geometry to use a greater lever arm than is desirable dynamically, difficulty in applying reversing radial loads would be encountered, and torsional and radial loading would not be controllable independently.

Because pin breakage has been a problem in previous test machines, and because pin bending would cause non-uniform bushing compression, pin deflection was minimized by the use of a set of preloaded tapered roller bearings on each end of the pin to fix the pin horizontally as rigidly as possible. This reduces pin deflection to about 1/5 of that occurring in the case of a simply supported end. The bearings selected have a fatigue life (90 percent probability) of 123 x 10^6 cycles at maximum load, or one year of continuous (24 hour-per-day) operation at the standard load cycle rates. At the load used in QPL tests, the bearing life would be increased by a factor of 50.

Tests that may be run at bushing temperatures to 300 F will cause the pin to grow axially about 0.010 inch. This growth must be accommodated to prevent higher stresses from overloading the pin-support bearings. Thus, the left bearing block was supported by flexure plates. These are rigid in the direction required to resist a possible 25,000-lb. radial load, and yet flexible enough axially to deflect axially to permit thermal pin growth.

The pin clamping device must have a positive grip to transmit the required torques, allowing for easy pin insertion and removal, and be easily adaptable to the various diameters of pins to be tested. A tapered collet chucking device was designed for this purpose that is housed within the 2.95-inch I.D. of the pin-support bearings. The pin is to be loaded into the two bearing blocks by sliding one block aside, inserting one end of the pin into the stationary block, then returning the block to its original location over the other end of the pin. The collet draw screws are then tightened to secure the pin.

Because of the high angular velocities required to reproduce bushing torsion cycle rates that might be imposed in service, special attention was given to minimizing the moment of inertia and selecting the hydraulic servovalve. There is a combination of piston area and crank level arm length that will give the best

speed of response to the system, balancing the effect of dissipating energy in high flow through the servovalve (as will occur with a large cylinder area) against the effect of the lower accelerations available with a smaller cylinder area. A 1-1/8-inch-diameter hydraulic cylinder activated through two Moog 76-233 servovalves operating on a 1.16-inch crank arm will supply the torsion requirements. Radial loads will be provided by a 4-inch-diameter cylinder actuated through a Mood 72-101 servovalve.

Instrumentation will include strain gages on the crank arm to measure torque input, a rotary DCDT to measure angular displacement, a strain-gage-type load cell to measure radial load, a DCDT to measure radial deflection, and thermocouples for measurement of the bushing collet temperature. Because the machine is to operate unattended for long periods, several safety monitors, to automatically shut the test down if necessary, must be employed. Pin breakage, extreme hydraulic oil temperatures, loss of control signal, the pin slipping in the collet, or other unsafe or abort conditions will be monitored to terminate the test.

A split-collet block has been designed to house the bushing for its test. Temperature control fluid that flows through passages around the bushing is introduced into each block half through double shut-off, quick-disconnect couplers. This block is attached to the radial load cylinder through a mounting plate.

More detailed information on the bushing laboratory research machine is included in Appendix E, including data on the control system and instrumentation. Due to limited funding and an establishment of priorities for tasks remaining in last phases of the Track Dynamics Program, the bushing research machine did not progress beyond the drawing board.

Advanced Track Concepts

Early in the program it was decided to focus a modest portion of the effort on attempts to conceive and develop new track concepts. At the outset both revolutionary (long-term) and evolutionary (short-term) ideas were considered. However, the revolutionary concepts were not carried forward and the attention was primarily given to evolutionary ideas. The prime target for the conceptual efforts was linked track for heavy armored vehicles as opposed to linked track for lighter vehicles or unusual track such as the band track.

An understanding of the problems of current track was gained early in this program by a series of visits with the major elements of the track community. This understanding was enhanced and revised during the program. Figure 56 is a tabular display of the latest version of this understanding of track problems. The conceptual efforts were guided by this understanding as it developed during the program.

The conceptual design was iterated a number of times as the design constraints and problem understanding varied. Figure 57 illustrates the major design iterations and interactions with the track community during this process. The four versions of the concept will be discussed separately. An investigation of end connectors will be treated separately also, since it is germane to all of the versions (as well as to current XM-1 and M-60 designs). A brief discussion of revolutionary (longer term) concepts is also included.

First Version

This version was an integral pad design with no aggressive grouser other than that provided by the pad itself. It was intended for the XM-1 but required a sprocket change because of a greater end connector pitch. It could have been designed for the M-60 as well.

Various pitch lengths were studied, and the design was based on an 8.38-inch overall pitch. The pitch of the pins in the shoe was the same as the current XM-1 tracks, 4.94 inch. The pitch of the pins in the end

PROBLEM	DOUBLE PIN				SINGLE PIN
	XM-1				
	MOD. T-97	MOD. T-142	T-97	T-142	
PIN BREAKAGE			1	3	
SHOE STRUCTURAL FAILURES					2
END CONNECTORS	?	?	1	1	
SPROCKET AND DRIVE SURFACE WEAR	1	1	1	1	1
ROAD PAD WEAR	?	2	1	2	1
THERMAL PROBLEMS AT HIGH SPEED	3	2	1	1	1
ROAD PAD CHUNKING	?	2		2	
BUSHING LIFE					2
TRACK GUIDANCE AND THROWING	1	1	1	1	1

Legend

1 – MINOR 2 – MODERATE 3 – SEVERE

FIGURE 56. TRACK PROBLEM AREAS

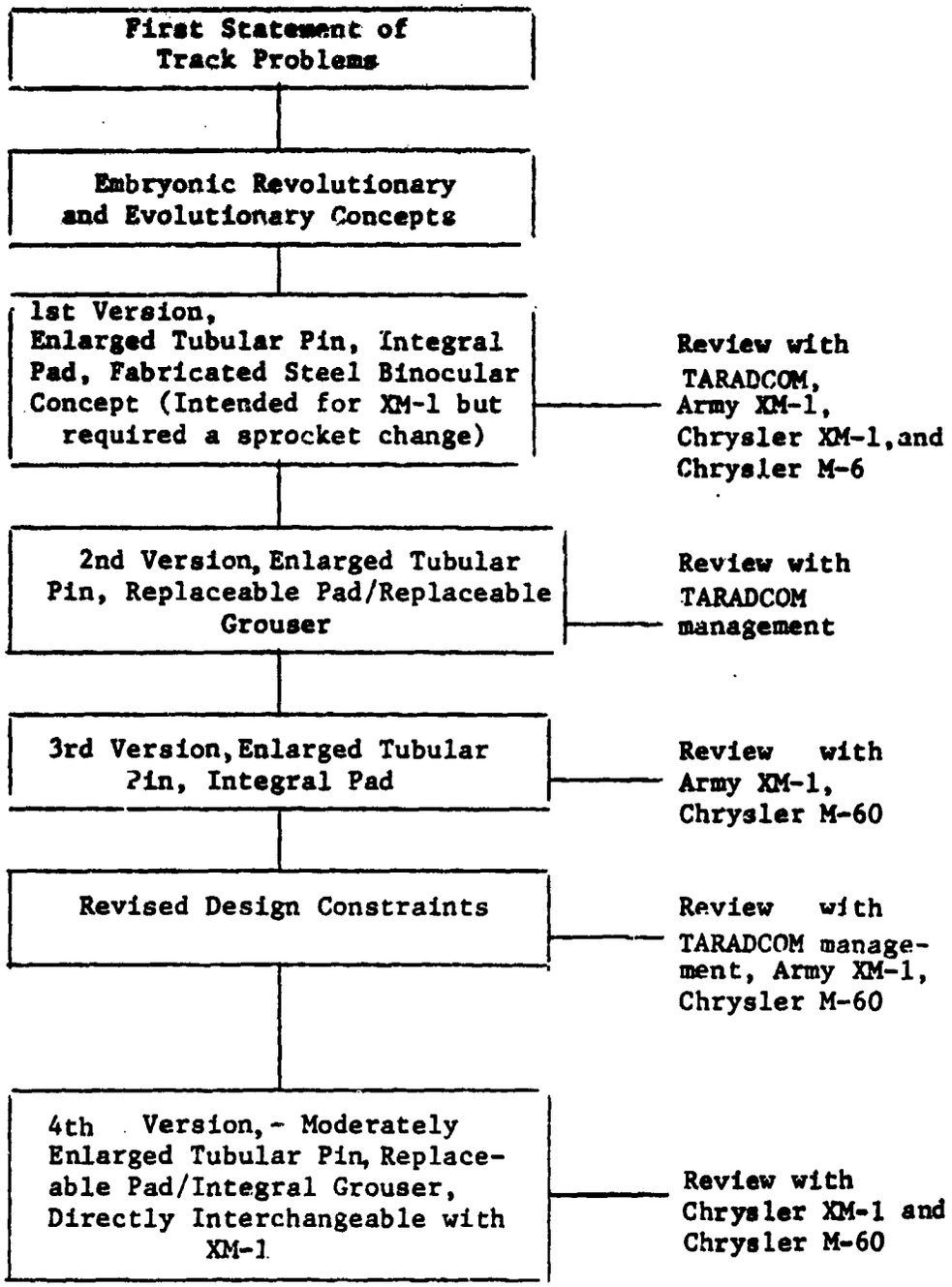

FIGURE 57. EVOLUTION OF TRACK DESIGN CONCEPTS

connector was 3.44 inch, which was, of course, greater than the XM-1 The opinion was that the dynamic characteristics of the XM-1 track would not be adversely affected by increasing the length of the shorter pitch (the end connector pitch). The overall pitch of 8.38 inch would allow a 10-tooth sprocket to be used in place of the current 11-tooth XM-1 sprocket without changing the sprocket diameter. This same design approach could have been applied to the M-60 track. In that case, the overall pitch would have been increased to 7.63 inches and the shorter (or end connector) pitch would have been 3.19 inches.

This version is illustrated by Figures 58 and 59. It employed larger diameter pins (1-3/4 in.) than current designs. The pins were steel and were tubular. The bushings were larger in diameter, but retained the same ratio of inner to outer diameter. The binocular was a fabricated steel structure with larger diameter tubes and multiple closely spaced connecting flanges. The end connector design departed quite radically from the traditional wedges. The center guide was somewhat traditional, but was a partial fabrication to save weight. The overall track structure was stiffer axially and laterally because of stiffer pins and stiffer binocular structure. The bushings were torsionally much stiffer but radially were of similar stiffness to current bushings. The roadwheel path was contoured to reduce forcing vibrations into the roadwheels. The road pad contained the same amount of rubber as the current XM-1 integral pad design, but the shape and thickness were altered to reduce hysteresis and pad rocking.

In addition to reducing pin bending stresses the larger diameter pins (and larger diameter binocular tubes) resulted in a more uniform loading of the bushings along their length. Table 5, Page 81, compares the pin bending stresses and bushing effectiveness of this concept to other designs in current use or development.

This version primarily showed promise for reduced weight, reduced pin breakage, improved bushing life, reduced thermal problems, and reduced end connector maintenance. Referring to the earlier table of track problems and areas for improvement, this concept specifically attacked them as follows:

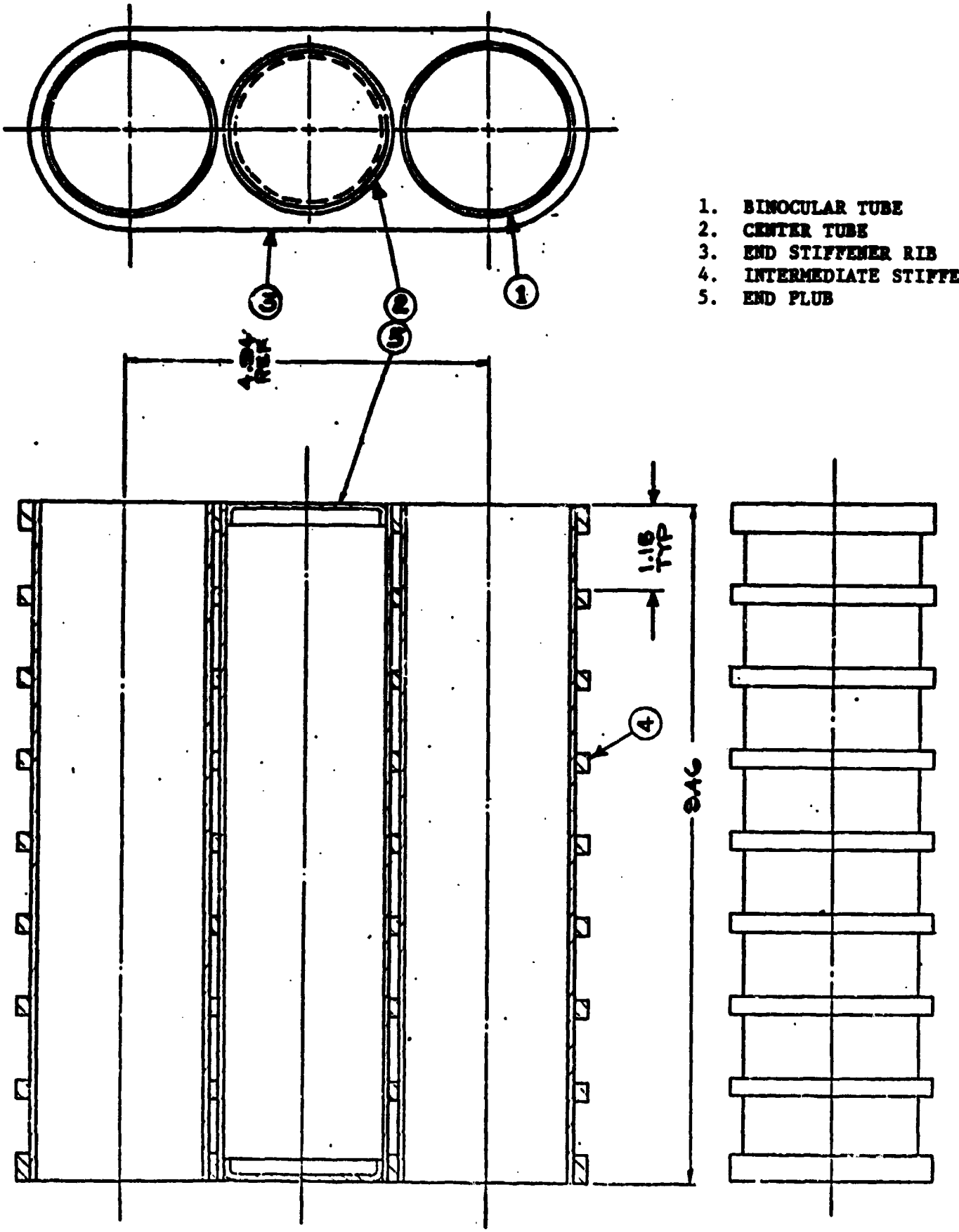

FIGURE 58. CONCEPT FOR LIGHTWEIGHT FABRICATED STEEL TRACK BINOCULAR

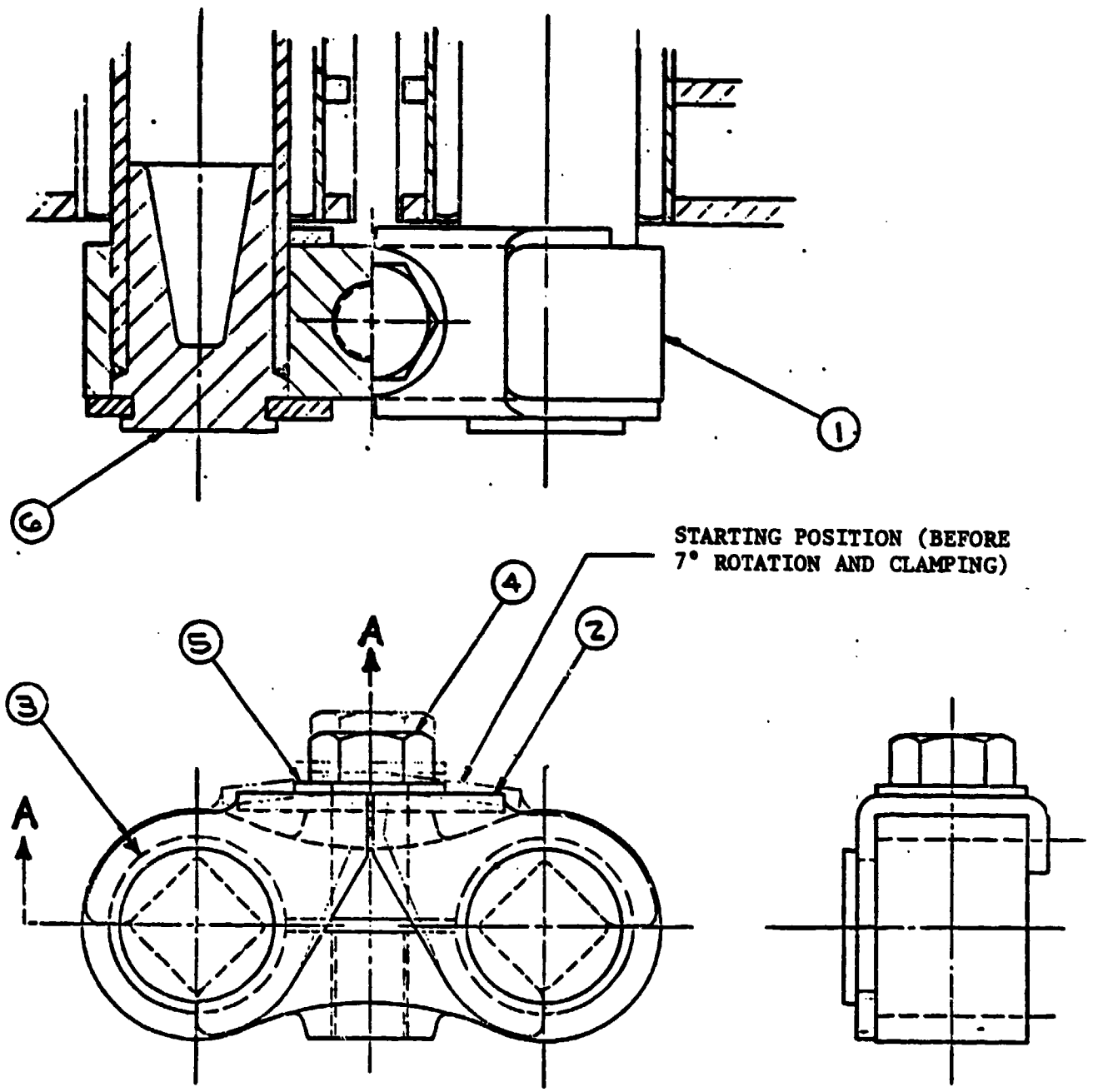

1. END CONNECTOR
2. SADDLE
3. TRACK PIN
4. TIGHTENING BOLT
5. WASHER
6. PIN END PLUG

FIGURE 59. CONCEPT FOR IMPROVED END CONNECTOR ASSEMBLY

(1) Weight - This concept weighed 79 lb/ft versus 91 for the current XM-1 integral pad, steel binocular, modified T-97 design. The modified T-142 aluminum replaceable pad design for the XM-1 weighs 95 lb. The savings per vehicle for this concept would have been approximately 1200 lb and 1600 lb, respectively.

(2) Life-Cycle Costs - Improvement in life-cycle costs may have resulted from long bushing and pin life, improved resistance to road pad and roadwheel path thermal problems, and improved integrity of the end connectors.

(3) Track Throwing - Improved resistance to track throwing may have resulted due to increased lateral stiffness.

(4) Pin Breakage - The pins were designed to be 1.33 times stronger and 1.7 times stiffer than the current 1.375-inch-diameter XM-1 pins, and 1.62 times stronger and 2.29 times stiffer from the current 1.250-inch-diameter T-142 pins.

(5) Pad and Path Thermal Blowout - The stiffness of the pad and path were substantially increased, particularly in the crucial zones in the center. In addition, the length of the conduction paths within the rubber itself were appreciably shortened.

(6) Bushing Life - The larger diameter bushing would have substantially reduced projected area loads. The torsional unit strains would have been the same as current bushings. In addition, the stiffer pins and binocular structure would reduce the concentration of end bushing loads which have been calculated and observed to exist in current designs. If, as expected, the bushing hysteretic heating was small compared to other heating effects, the bushing life should have been much improved.

(7) Maintainability and End Connector Problems - The saddle lock end connector was designed with the goal of eliminating loosening during running, the need for repeated cycles of tightening, and easier removal. However, later design efforts determined that stress levels in this saddle lock end connector were probably not reasonable.

(8) Aggressive Grousers - This concept did not attack the widely debated question of need for aggressive grousers.

(9) Dynamic Problems - The chordal action forces in present heavy vehicle double-pin track have been calculated to be small, so this track's greater axial stiffness should not have been particularly objectionable. The increased length of the end connector pitch was believed to be insignificant from a dynamic standpoint. Parametric comparisons showed the greatest relative dynamic effects were to be expected on lighter, high-speed vehicles with the single-pin, long-pitch track.

Investigations in support of this 1st version included a bushing hysteresis estimate, parametric scaling of bushing characteristics versus size and proportions, and materials and materials processing reviews.

Materials Investigation. A brief materials investigation was conducted with the primary purpose of qualifying aluminum for use in the track shoe binocular. The hope was that some form of aluminum, cheaper than forgings, would be found. If so, aluminum might then be used with a modest weight savings and not too great a cost penalty. This did not prove to be the case.

An aluminum extrusion would locate the material in the correct places. However, the zones of weakness in the extrusion (the zones where the aluminum rewelds after passing around the bridges which support the mandrels which form the holes) would be in critical locations. In addition, the alloys which reweld the best are not the stronger alloys. The cost of aluminum extrusions was estimated to be at least in the $1.25 per pound range. On the basis of these considerations, aluminum extrusions were rejected.

Aluminum die castings were also investigated. Recent high-strength alloys and modern technology die casting techniques have been considered. No alloy was found which combined both high strength and good ductility. In addition, the cost of aluminum die castings was estimated to be at least in the $1.50 per lb range. Therefore, aluminum die castings were rejected.

Aluminum forgings were probably acceptable from a performance standpoint. However, no available commercial capability was found for forging aluminum in two directions simultaneously. Such a capability would have allowed the holes which receive the pin/bushing to be forged rather than wastefully machined. The cost of aluminum forgings was estimated to be in the $2.00 per lb range.

A fabricated steel binocular was then conceived, as shown earlier in Figure 38. This steel binocular would utilize welded thin-wall tubing and multiple load-carrying flanges. The flanges would have been forgings, stampings, or powdered metal. If powdered metal, they would have been hot forged or hot coined after sintering. Whichever method of fabrication for the flanges was chosen, they would have been heat treated and have comparable mechanical properties to the forgings currently used on brazed steel binoculars. The conclusion was reached that a fabricated steel binocular could be designed which would have equal or better strength and stiffness than the current XM-1 modified T-97 steel binocular and perhaps be slightly lower in weight. It would have superior performance in reducing hysteretic heating of the road pad and roadwheel path rubber. Assuming a fabrication tooling investment was made it would probably be cheaper in first cost than a forged aluminum binocular.

A sample of a steel fabricated binocular was made and is pictured in Figure 60. A substantial knowledge was gained during the fabrication on questions of tolerances, assembly techniques, brazing techniques, etc. The general conclusions reached from the fabrication experiment were

- Somewhat greater attention to detail and precision would be required for this fabrication compared to current brazed steel binoculars.
- Proven commercial brazing techniques and materials are satisfactory.
- No long-term or expensive development of fabrication techniques is anticipated to be necessary.
- The assembly appeared to be stiff and structurally sound.
- The center tube may not be necessary, and its inclusion in the design should be carefully evaluated.
- The weight estimate for the assembly was confirmed.

FIGURE 60. PHOTOGRAPH OF BRAZED STEEL BINOCULAR ASSEMBLY FOR TRACK SHOE

Bushing Considerations. Preliminary analysis was conducted on certain aspects of bushing performance in order to determine the acceptability of employing larger diameter bushings around the larger diameter tubular pins. Earlier work on bushings by TARADCOM indicated a desirable improvement in bushing life if either the radial unit load or torsional angle of deflection were reduced. The torsional angles of deflection are fixed by the track geometry and are independent of bushing diameter. The unit strains in the rubber are also independent of diameter as long as similar transverse proportions are used for the bushings. A larger bushing would, however, reduce the radial unit loads. This first version concept would have reduced them by a ratio of 1.25/1.75 or to a value of 71 percent of the loads of the current T-142 bushing. However, consideration had to be given to potentially damaging increases in hysteretic heating of the larger bushings. Parametric estimates were made. Table 14 shows the expected relationships between spring rates, hysteretic heating and thermal gradients versus mean diameter of the bushing for bushings of varying diameter but similar transverse proportions. Of note on Table 14 is the fact that both the amount of hysteretic heat and the thermal gradient in the bushing due to angular deflections can be expected to vary as the diameter squared. Whether or not this is an area of concern depends on the relative values of the bushing's own internally produced hysteresis compared to the hysteresis produced in the surrounding rubber of the road pad and roadwheel path. Table 15 shows an estimate of these relative values. This table is based on experimental determinations of hysteresis which were made on T-142 parts at Battelle during this program. The bushing was estimated to produce only about 11 percent of the total hysteretic heating. With the larger bushing of this first version of the enlarged tubular pin concept the bushing is expected to produce about 18 percent of the total heat.

It is not possible to analytically quantify the gain in bushing life from reduced radial unit loads or the loss in bushing life from possible increases in operating temperatures within the bushing. It was concluded that the potential overall advantages of the larger diameter tubular pins (and the resulting larger bushings) were sufficient to justify their consideration. Laboratory tests would be needed to determine the amount of increase in bushing internal temperatures and the effects on bushing life.

TABLE 14. BUSHING CHARACTERISTICS VERSUS MEAN DIAMETER (D)*

Angular spring rate	Proportional to D^2
Radial spring rate	Constant
Hysteresis heat produced by angular deflection	Proportional to D^2
At in rubber from angular deflection hysteresis heat	Proportional to D^2

* For bushings of dimensionally similar transverse proportions

TABLE 15. HYSTERESIS COMPARISON OF BUSHING, ROAD PAD, AND ROAD WHEEL PATH

	*Value, ft-lb	Percent of total
Bushing	78	11
Road pad	448	66
Road wheel path	157	23
Total -	683	100

*For a T-142 per one full pitch per track revolution

1st Version Summary. This version appeared to be a weight effective alternative to the integral pad modified T-97 version being pursued for the XM-1 with the expectation of less pin breakage, better bushing life and better road pad and road wheel path thermal performance. It remains the best concept of this program for an integral pad design.

However, the review of this concept raised serious questions about the overall life cycle cost effectiveness of any integral pad approach. In addition, concern was expressed over the lack of a wartime aggressive grouser capability. These questions led the conceptual effort toward the 2nd version.

Second Version

The second version utilized a replaceable pad and a replaceable steel grouser plate. It retained the 1-3/4-inch-diameter tubular steel pin. It was intended for the XM-1 but required a sprocket change since it retained the longer end connector pitch (3.44 in.) of the 1st Version. It differed from the 1st Version in that 5 load carrying links were chosen as a compromise rather than 9. Figure 61 illustrates the approach. The features of this concept were

(1) Essentially all the rubber in the replaceable pad was placed so as to be available for wear. This minimized weight and reduced hysteretic heating.

(2) The steel grousers were designed to be storable in the same amount of space as the replaceable pads. (It was expected that a 20 percent complement of grousers would be sufficient.)

(3) Based on providing the above 20 percent complement of grousers, it was estimated that the weight per foot of track would be 89 lb or about 10 lb greater than the integral pad version. This was still less than any other concept with comparable features currently being considered.

(4) A unique attachment scheme was evolved which allows quick removal of pads or grousers with only a hammer and bar.

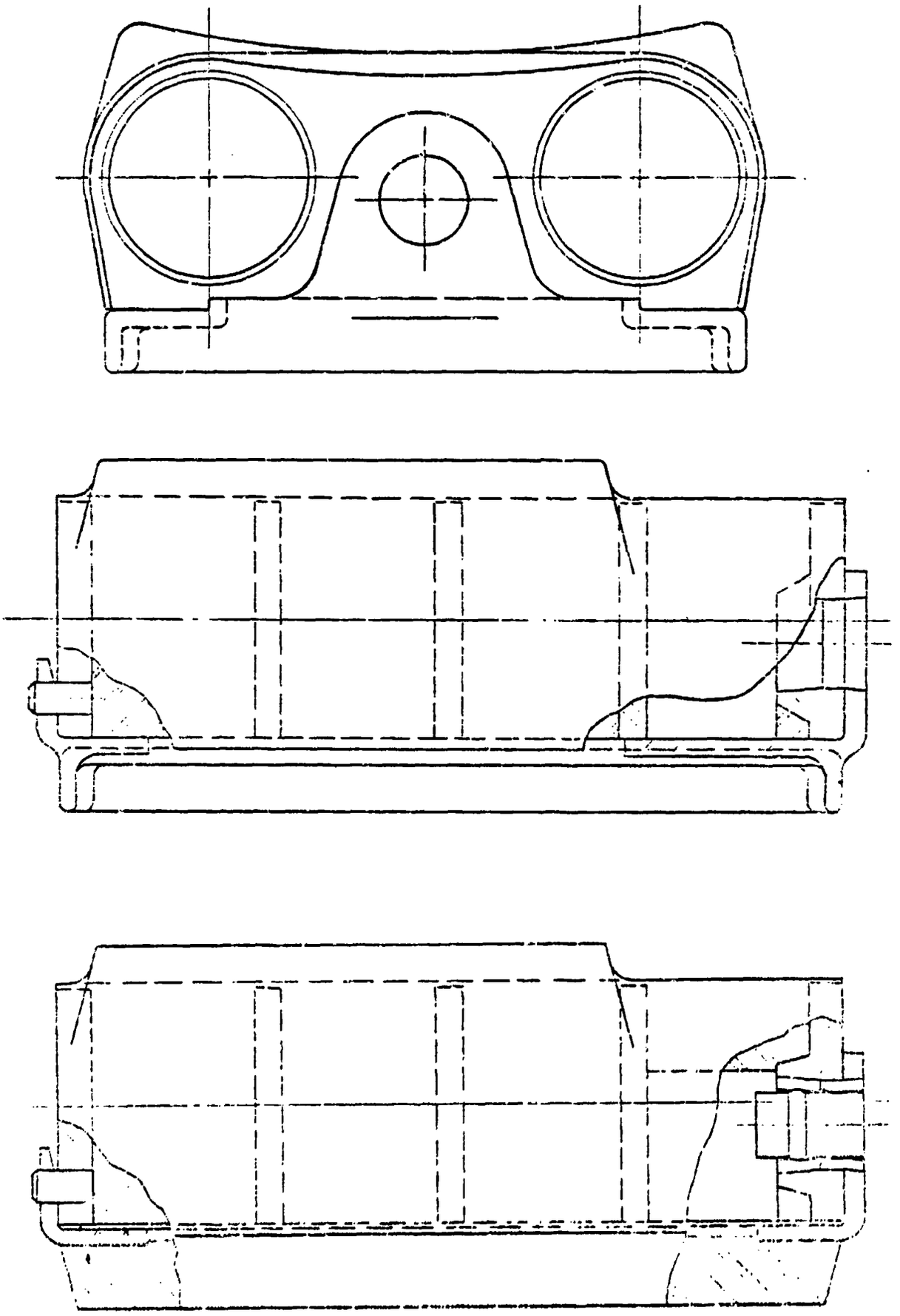

FIGURE 61. 2ND VERSION TRACK SHOE HAVING REPLACEABLE PAD AND GROUSER

The review of this concept by TARADCOM management revealed concern over the pad and grouser attachment means and over the basic idea of carrying along replaceable grousers. Because of the difficulty in achieving an acceptable replaceable pad/replaceable grouser version, attention was redirected concurrently toward a revised integral pad approach (3rd Version) and a replaceable pad/integral grouser approach (4th Version).

Third Version

This version was the final attempt to configure an integral pad, enlarged tubular pin concept during this program. It is shown in Figure 62. While it retained most of the features shown on earlier versions, it differs in two regards. Four ribs were chosen as a compromise between the number on current track (2) and the large number (9) shown on the 1st Version. In this concept the center tube was not fitted tightly (and not brazed) to the center two ribs. This compromise considerably simplified the fabrication of the brazed steel binocular assembly.

This version retained the weight advantages of the 1st Version, weighing 79 lb/ft of track. It required a sprocket change to the XM-1 because of the longer end connector pitch. It surrendered some of the thermal advantages of the large number of ribs.

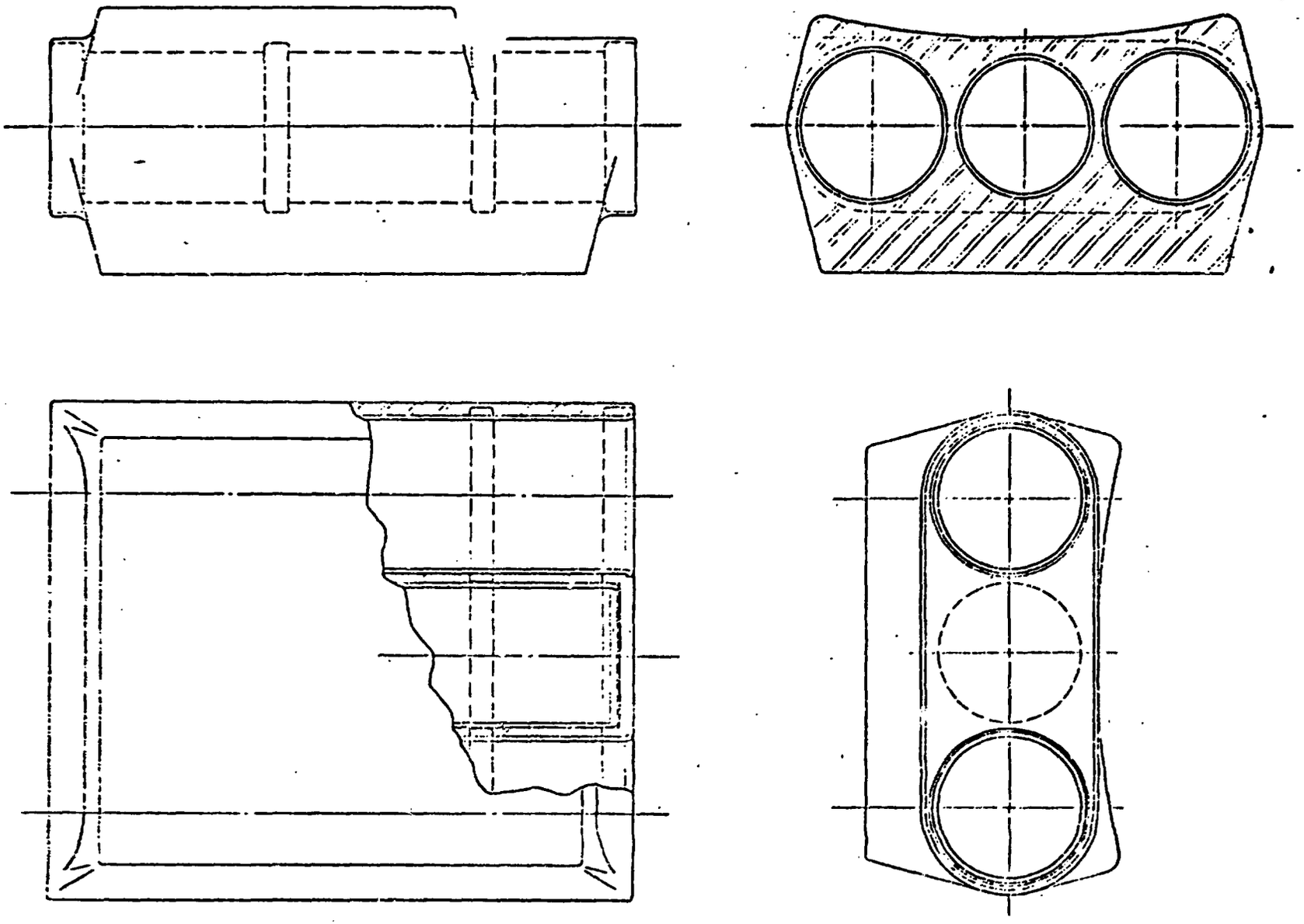

FIGURE 62. CONCEPT FOR A LIGHTWEIGHT FABRICATED STEEL INTEGRAL PAD BINOCULAR

Fourth Version

Design Constraints. A set of design constraints was evolved late in the program to guide the final conceptual effort. The philosophy behind these constraints was basically to move even more toward an evolutionary rather than revolutionary approach in order to maximize the chances of a short-term hardware tryout. The constraints were

- Both the shoe and end connector must use the same pitch as the current XM-1.
- The track must be interchangeable with the Leopard without drive sprocket changes or suspension changes.
- The shoe must have a replaceable pad.
- When the pad is removed the shoe must present at least a short aggressive grouser to the ground.
- The track should be designed to minimize the changes required on the M-60 to allow its later utilization thereon.
- Wedge-type end connectors will be used with the wedge action turned over to improve tightening and improve maintainability.
- Simple, straightforward pad attachment schemes will be used with emphasis on protection against thread corrosion.

4th Version Concept. The effort in response to these constraints included a cast steel approach and a steel forging and tube approach. Brief consideration was also given to a welded fabrication of HSLA steel but time did not allow a thorough investigation. (Future track efforts should include an investigation of the use of welded HSLA steel in more detail.) The steel forging and tube approach was chosen as the most likely to merit additional development and consideration for the XM-1.

A design was carried forward in which the shoe structure consisted of a brazed assembly which employed one steel forging and three steel tubes. It was difficult to control the weight of a replaceable pad, grousered design when a single forging was used. The weight/ft of track which resulted was 105 lb rather than the goal of 95 lb (a 95 lb/ft design would be competitive with the modified T 142 replaceable pad, aluminum forging XM-1 version).

The approach was then modified to utilize a welded assembly of several forgings instead of a single forging. Three forged longitudinal links were welded to a bottom grouser/plate forging. Steel tubes were then brazed into this forged assembly similar to current practice. This change plus some other minor modifications to the design allowed the 95 lb/ft goal to be met.

Appendix F includes a set of five drawings which illustrate this final design concept. Some features of it are:

- It is directly interchangeable with the XM-1 both as track sets or as individual pitches.
- It contains a replaceable pad with ground contact area equal to the current XM-1, modified T-142, replaceable pad version.
- It utilizes wedges with turned over action for greater effectiveness. (Discussion in the following section.)
- It contains a hardened steel forged 1/2-inch integral grouser.
- It includes a scheme for preventing corrosion of the threads on the simple pad-attaching stud.
- It contains a tubular pin which is 10 percent stronger and 30 percent stiffer (in bending) than the current XM-1 pin. Its OD is 1-5/8 inch. This pin does not require reinforcement in the zone under the center guide.
- It has a large center tube in the road wheel path area which reduces the rubber hysteretic heating in that zone.
- It has a stiffer and stronger center guide with greater wear contact area with the roadwheels.

This approach is recommended for tryout as individual pitches in an existing XM-1 track. It can be thought of as a replaceable pad track with a competent steel grouser which is competitive in weight and potentially cheaper than the current XM-1 modified T-142, replaceable pad, aluminum forging version.

End Connector Investigation

A new approach to end connectors was evolved in this program (See earlier Figure 59) and was termed the saddle lock end connector. An attempt to configure the saddle lock end connector for potential use on the T-142 track resulted in the version shown as Item B in Figure 63. It became clear during the design of this version that it would be difficult to handle the stresses under the severe requirement which had been set. This requirement was that one end connector should be capable of twisting two pins into the correct mean bushing angle position when the end connector was disposed on a straight portion of the track. Under this condition the one end connector must develop a maximum total torque (on two pins) of approximately 7500 in-lb. While admittedly a severe requirement, if it could be achieved, it would provide the maximum level of maintainability for the track. The washer lock and wishbone lock shown as Items A and C on Figure 63 were concepts which evolved in an attempt to reduce the stresses dictated by this severe requirement.

Analysis. Figure 64 summarizes the results of an analysis which was made to compare the tightening performance of the washer lock, saddle lock and wishbone lock with the current wedge design. The end connector bolt force required to develop a single bushing torque of 3750 in-lb is plotted against coefficient of friction of the end connector parts. Two curves are shown for the current wedge. The unfavorable orientation is the condition in which the wedge is compelled to rotate the pin in a direction such that the tangential movement of the pin is opposite to the direction of movement of the wedge. This condition occurs when the track is straight or any time the track is bent less than the amount corresponding to the mean bushing position. The favorable orientation occurs any time the track is bent beyond the mean bushing position, such as when the track is fully on the drive sprocket or idler wheel.

Several important observations can be made about Figure 64.

- For the unfavorable orientation of the current wedge, the bolt force becomes asymptotic at the coefficient of friction of about 0.3. For friction coefficients higher than this, the wedge will not tighten, even though the required torque on the bushing is modest.

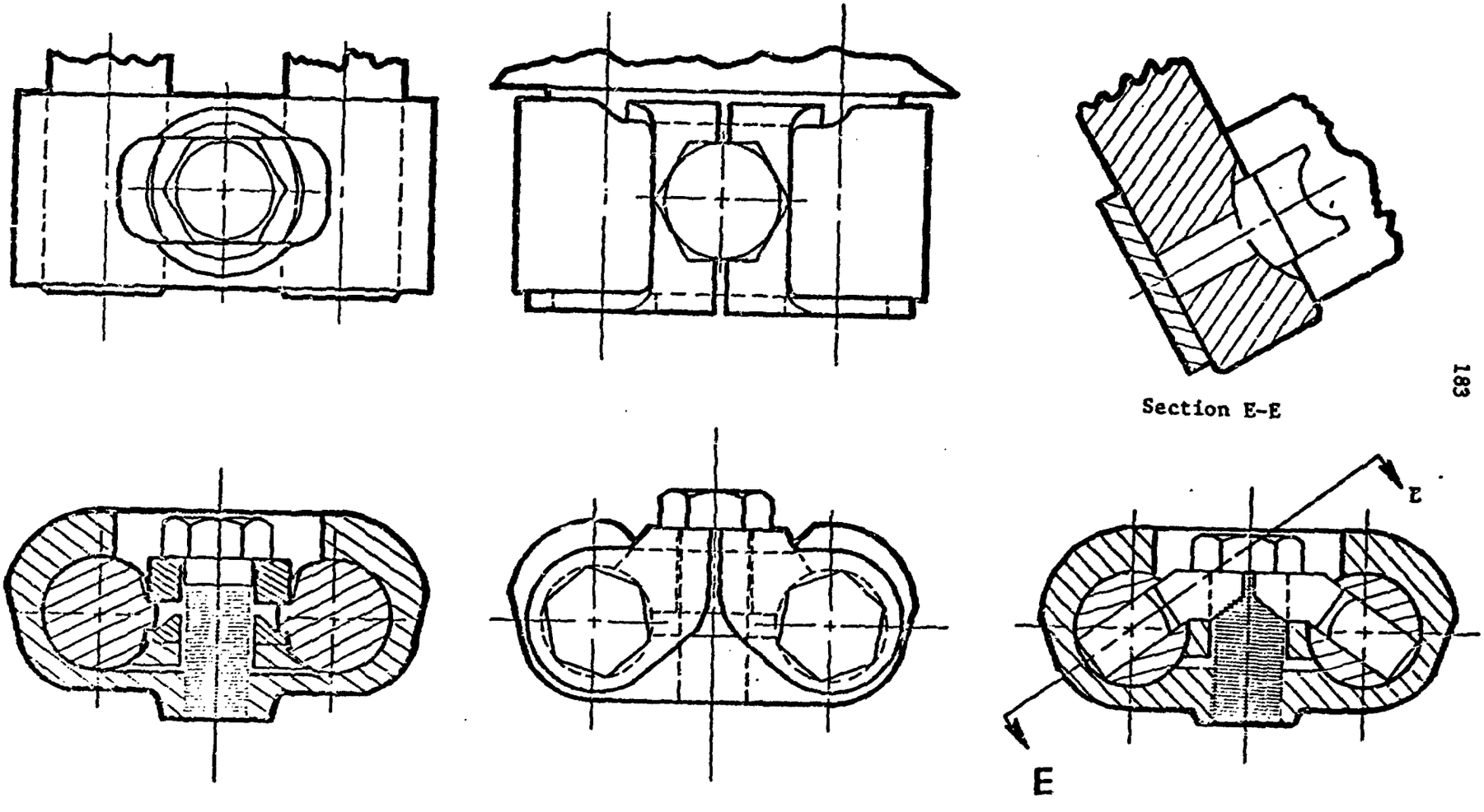

A. Washer Lock

B. Saddle Lock

C. Wishbone Lock

FIGURE 63. CONCEPTS FOR END CONNECTORS

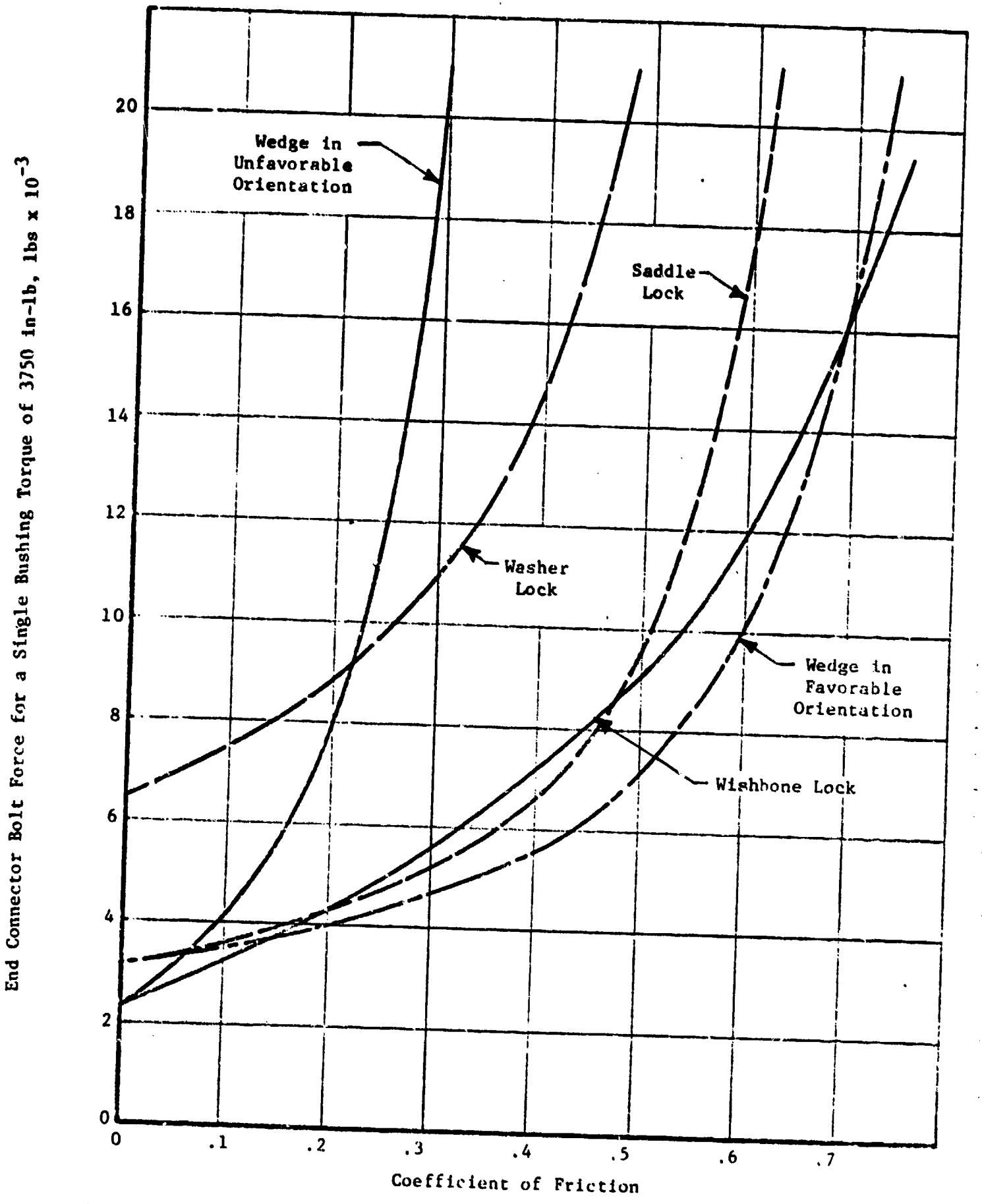

FIGURE 64. TIGHTENING PERFORMANCE OF VARIOUS END CONNECTORS

- Both the saddle lock and the wishbone lock would be superior in tightening to the current wedge when it is unfavorably oriented. The stresses would, however, be difficult to handle during the severe requirement of tightening on a straight portion of the track.
- The current wedge performs well in tightening when in the favorable orientation.

Based on the above, a double wedge design was conceived, with the hope that it would tighten well with the track bent to either more or less than the mean bushing position. However, it proved to work poorly in both conditions, and was not carried further. Figure 65 shows the effects of varying the wedge angle on the tightening performance of the current wedge design connector. The effects are not large.

It was stated earlier in this discussion that an end connector which could fully rotate the pins into the mean bushing position on a straight portion of the track would be the optimum from a maintainability standpoint. Such an end connector would allow the tightening to be done along the full length of the top run of the track with fewer and less precise moves of the tank required to position all of the end connectors for tightening. This simplification would promote keeping the end connectors tight in service by simplifying the job of checking and tightening, and would increase the probability of getting all end connectors correctly tightened initially.

Figure 66 shows an end connector in which the wedge action is reversed. (The bolt still is oriented toward the inside of the track away from the ground.) This reversed design places the wedge action in the favorable orientation when the track is straight and would provide the desired high maintainability.

End Connector Tests. A limited laboratory experiment was conducted to investigate the trends indicated by the above end-connector analysis. The experiment confirmed the great difference between end-connector tightening in the "favorable" and "unfavorable" wedge conditions. The results suggest that if

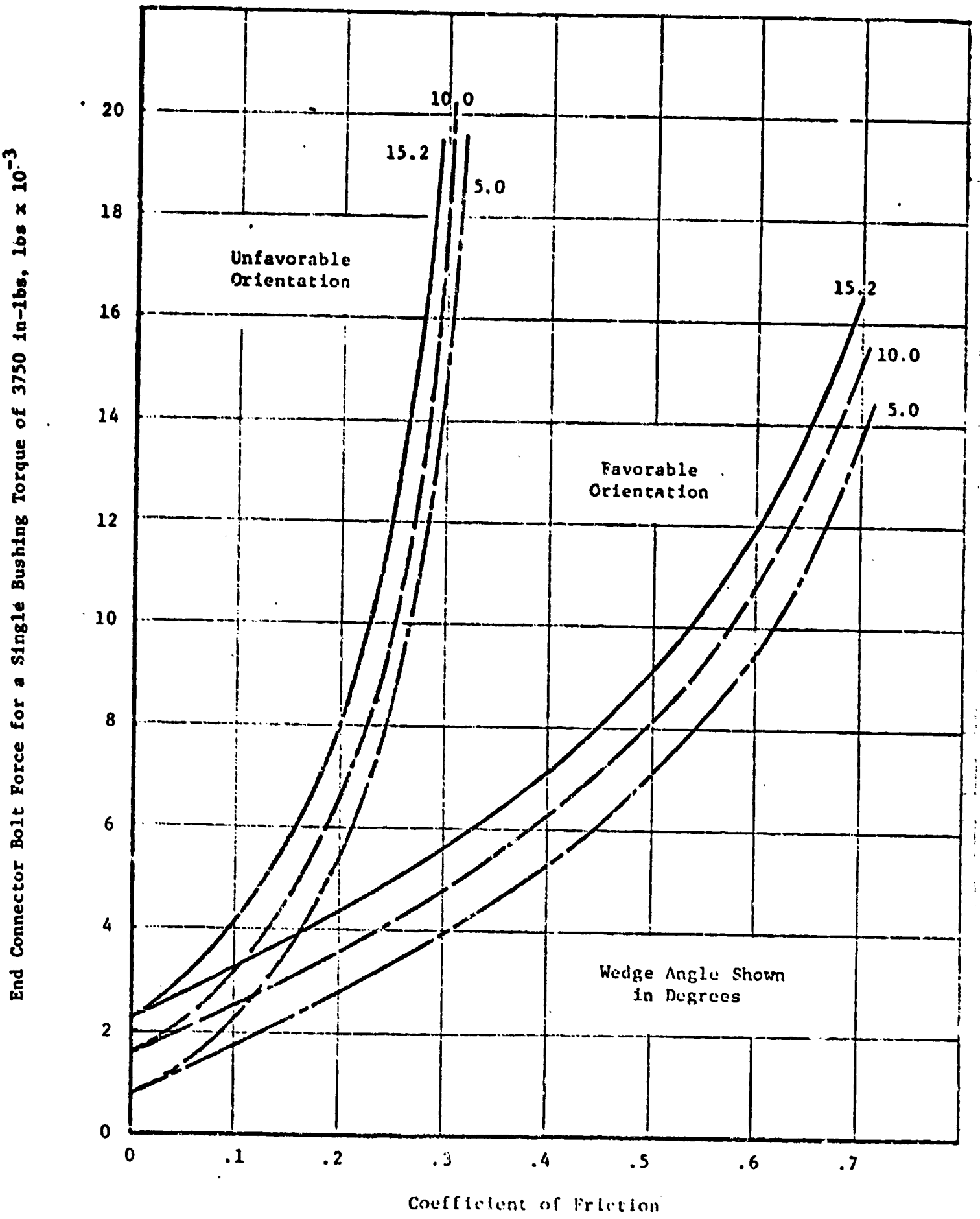

FIGURE 65. WEDGE ANGLE EFFECTS ON CURRENT WEDGE DESIGN

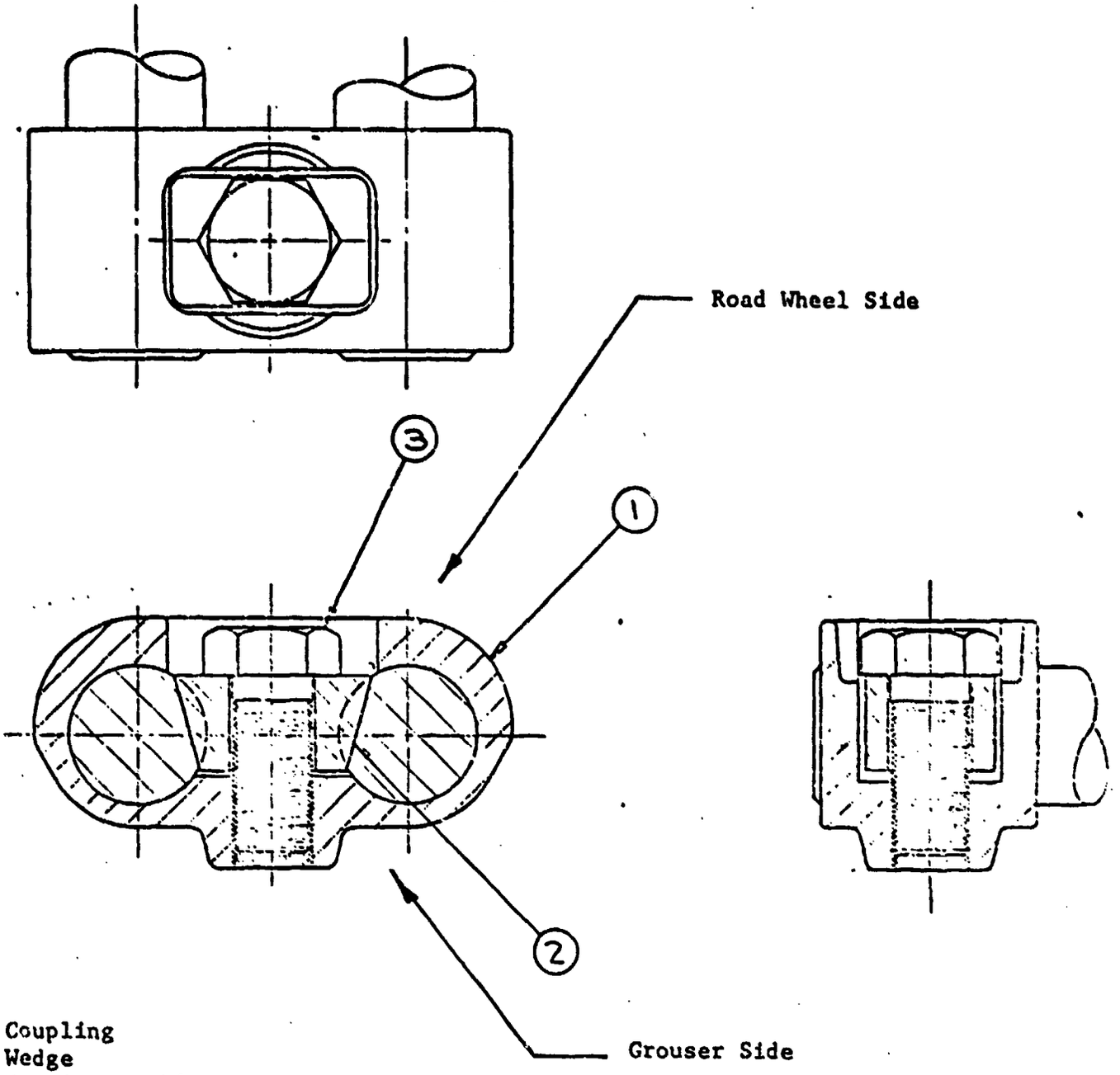

1. Coupling
2. Wedge
3. Cap Screw, 3/4-16

FIGURE 66. REVERSE WEDGE END CONNECTOR

end connectors are tightened when in the favorable wedge condition, the incidence of loose end connectors should be significantly reduced. This conclusion applies both for maintenance on existing track, or for new reversed-wedge-action end connectors that would be designed so that all end-connector bolts could be checked for proper torque with fewer and simpler tank moves.

A view of the end connector experimental setup is shown in Figure 67. The objective of the laboratory evaluation was to determine if actual parts would demonstrate the characteristic trend predicted by analysis. The experiment was conducted using one set of new parts, including a pin, wedge, bolt, and end connector. The pin, which had been shot peened but did not have rubber bushings, was cut in half so its two flats could be utilized. Two long bars were welded to the pins and adjustable scale weights provided to simulate moments up to the maximum bushing torque that can be encountered when tightening end connectors. Relative rotation of the pins was measured at the end connector using a dial indicator, and bolt looseness was noted by observing angular position of the bolt head.

Favorable and unfavorable conditions were simulated by turning the holding fixture over. Two lubrication conditions were evaluated; dry (parts cleaned with acetone) and lubricated (friction surfaces coated with grease). In all cases the bolt was lubricated with grease. Each condition was evaluated by loosening the bolt, applying simulated bushing torque, and then tightening the bolt and observing bolt rotation and relative pin rotation. The experimental results, which are summarized in Table 16, confirmed the great difference between the favorable and unfavorable conditions. These results strongly suggest that the maintenance procedures for current track be changed to insure that tightening occurs in the favorable orientation. They also suggest that consideration be given to a reversed end connector design.

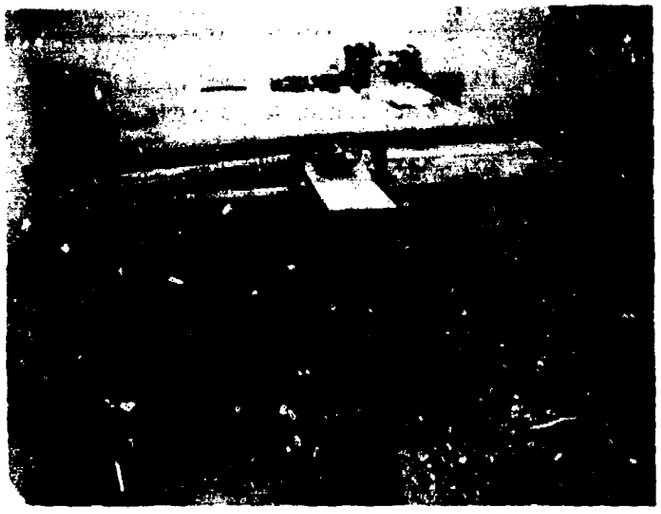

FIGURE 67. LABORATORY SET UP TO [illegible]SURE END CONNECTOR EFFECTIVENESS

TABLE 16. RESULTS OF END CONNECTOR EVALUATION

Symbol	Meaning
R	Pins rotated to, or nearly to, the tighten position
N	Pins did not rotate

Bushing Torque Percent	Favorable		Unfavorable	
	Lubricated	Dry	Lubricated	Dry
5	R	R	N	N
52	R	R	N	
100	R	R		

Longer Term Concepts

A limited number of more radical, longer term concepts evolved during this program. These were not carried forward to any appreciable degree because of cost and time constraints. Some of them are, however, enumerated herein with a brief explanation in the hope that they might provide a conceptual stimulus to future track investigators.

Spring-Loaded Grouser. This concept involves a spring-loaded aggressive steel grouser which would exert sufficient ground contact loading to achieve the required off-road mobility. This spring-loaded grouser would utilize an elastomer as the spring member. It would retract to a position flush with the bottom of the road pad when the tank was operated on hard roads. The unit loads of these spring-loaded steel grousers on the paved hard roads would be many times lower than the loads of the steel grousers of current track types when they operate without pads on hard roads.

The advantage of such an approach over a replaceable pad design such as the T-142 is that off-road mobility could be achieved without manually removing the road pads. The advantage of this approach over an integral pad design with no steel grouser such as the T-97 is that the road pad could be designed to be larger in area and therefore, have better wear life.

The problems with this approach are that it increases track weight and cost, and that it is very difficult to achieve a spring-loaded grouser design which is mechanically rugged enough to tolerate the wide range of severe operating conditions.

Rolling Pivot Bushings. This concept replaces the bushings with a rolling element pivot action similar to that employed in modern high performance silent chain. Rubber is used as the rolling contact surface rather than lubricated hardened steel.

The advantage of such an approach might be that the substantial strains due to rotation in current bushings could be reduced. In addition, the structural requirements on the pins might be lower and result in lighter pin constructions.

Road Pad Studs. This concept involves the use of a multiplicity of hardened studs in the road pad for the purpose of improving traction on ice. A secondary purpose would be to improve heat transfer away from hot internal zones in the road pad rubber.

Double Bonded/External Sleeve Bushings. This concept involves the use of a bushing which is double bonded between the pin and a thin annular outer sleeve. The outer sleeve would be slotted longitudinally to allow sufficient flexibility for pressing into the binocular bore. The assembly would be designed to not slip in the bore under normal loadings but slip under back bending. The presumption is that such a bushing might have better life because of the elimination of slipping between the bushing rubber and the bore. A problem with this concept would be the prevention of corrosion between the outer sleeve and the bore.

Bushing with Rigid Sleeve at its Radial Midpoint. This concept involves the use of a bushing which has a circumferentially rigid thin metallic annular sleeve so arranged to be at about the radial midpoint of the bushing after insertion in the shoe. Such a bushing would be constructed by having the space between the sleeve and pin filled with rubber which was double-bonded to both members. The space between the sleeve and the binocular bore would be essentially filled (after insertion) by rubber donuts which are bonded only to the sleeve. The purpose of this approach is to achieve high radial stiffness without increasing torsional stiffness. Such a bushing might have longer life and a track employing them might be resistant to track throwing.

Monopin/Monoblock Shoe. This concept involves the use of one large tubular pin per shoe and a shoe which extends the full width of the track. The shoe structure is essentially a large diameter thin walled tube. The bushing lies between the pin and tube of the shoe and runs along the full width of the shoe. The advantages of this approach might be in the reduction of center connector problems, pin breakage at or near the center, and lighter weight.

Field Test Program

Field tests were considered to be an important part of the track dynamics program.

During the first quarter of the program, an assessment was made of field tests which would be most valuable to the study of track dynamics. It was concluded that two basic types of field tests would be valuable as follows:

- o Static or low speed tests on smooth terrain; data from the vehicle with an umbilical cord or other hardwired system. These tests were referred to as "preliminary tests".
- o Rough terrain tests or higher speed or high manueverability tests, in which a telemetry-type system is needed to record data. These tests were referred to as rough-terrain tests.

The primary objective of the field test program was to support the Track Dynamics Program by planning and conducting field tests of tank track and suspension systems as required. The requirements for data were principally related to the analytical studies and, for the most part, the data were used to validate the mathematical models of the track, suspension, and shoe thermal models. The following subtasks made up the field test program:

1. Define the field data requirements for validating the mathematical models developed in the Track Dynamics Program
2. Define the functional, environmental and physical requirements for data acquisition systems
3. Establish the feasibility of employing state-of-the-art components for wireless telemetry of data from the track components during full scale rough terrain tests
4. Design, plan, and conduct preliminary tests to satisfy interim data requirements
5. Design, plan, and conduct full scale rough terrain tests, using wireless telemetry in the data acquisition system .

The goals of all but one of these subtasks was accomplished. Subtask 5 was completed except for final scheduling and conducting rough terrain tests. This portion of the program was deferred because of the delays which were initiated when the funding was temporarily curtailed. Details of the field test program are given below.

Preliminary Field Tests

Data Requirements. Information obtained from the staff of the analytical task showed that the following data would be required to validate the analytic models:

1. Shoe-component temperature rise during vehicle operation
2. Resonant, or wheel-hop, frequency of roadwheels
3. Track-tension values during specific low-speed and static maneuvers
4. Track-pad vibration during specific low-speed maneuvers .

Pin bending stress and shoe forging stress were also considered as cadidates for the study, however, these were assigned a lower priority because of the existence of data from prior studies.* It was also determined that some preliminary information on the track shoe environment would be helpful in designing the telemetry system. Accordingly the following tests were planned for a preliminary test program.

1. Response of track tension to obstacles
2. Temperature time history for rubber components of shoes
3. Track vibration amplitude and frequency
4. Road wheel hop frequency
5. Durability of a commercial S-band transmitting antenna for the track-mounted telemetry system.

Working with Goodyear's St. Mary's, Ohio, plant, Battelle completed fabrication of instrumented shoe assemblies for the temperature and tension measurements. It was also necessary to install modified shoe end connectors to carry electrical connections for the transducers.

A vehicle and test site were requested from TARADCOM through the Technical Support Division, and arrangements were negotiated through the Director for engineering support. The test program, including final preparations, was carried out at Warren, Michigan, during the months of January and February, 1978, using a tank furnished by Chrysler.

---

*Wilson, Nuttall, Raimond, "Stress and Load Studies of the T-142 Track", Final Report under Contract No. DA 20-113-AMC-10559(W), and other WNR Reports.

Track Tension Tests. A track shoe was instrumented for measurement of track tension by installing electrical resistance strain gages on the outside surfaces of both pins to measure shearing strain at the transition points where the pins enter and leave the binocular tubes. The gages, four at each of the eight locations, were placed and wired in the bridge circuits in such a way as to respond only to shear produced by tension in the track. Other force components, i.e., those produced by bending, torsion, lateral force and nominal load, are electrically cancelled by the gage arrangement and wiring. Each of the eight strain gage sets was connected, by wires inside the pins, to electrical connectors installed in an extension of the shoe end connector.

Following calibration of the instrumented track shoe in a tensile testing machine, the shoe assembly was installed in T-142 track on an M-60, A-1 vehicle. The voltage analogue signal from the eight strain gage bridges on the two instrumented pins was read out with a digital voltmeter for static values, and recorded on magnetic tape for analysis of dynamic effects, of track traversing obstacles of various heights.

It was necessary to carry out most of the tension test indoors because of severe weather conditions. As a result it was necessary to limit the tests to avoid complications arising from the engine exhaust in the building; however, a substantial amount of useful data was obtained.

Track Shoe Temperature. One shoe assembly was fitted with thermocouples at the locations shown in Figure 68. The forging and pin temperature thermocouples were attached physically to the metal parts. The thermocouples in the rubber components were bonded to small copper bullets which were pressed into tight fitting holes bored in the rubber. The wires leading from the thermocouples were brought out to a 24 pin connector located in the shoe pocket. The thermocouples were read with a digital thermocouple monitor before and after test runs in which the tank was driven at a controlled speed on dry pavement. Temperature changes occurring as equilibrium was approached between runs were accounted for by adhering to a rigid schedule of reading both temperature and time of reading for each thermocouple.

Some temperature data which appeared to be anomalous at the time was subsequently explained when the instrument shoe was disassembled. Glass fiber insulation on the thermocouple lead wires had chafed resulting in short circuits which produced erroneous readings.

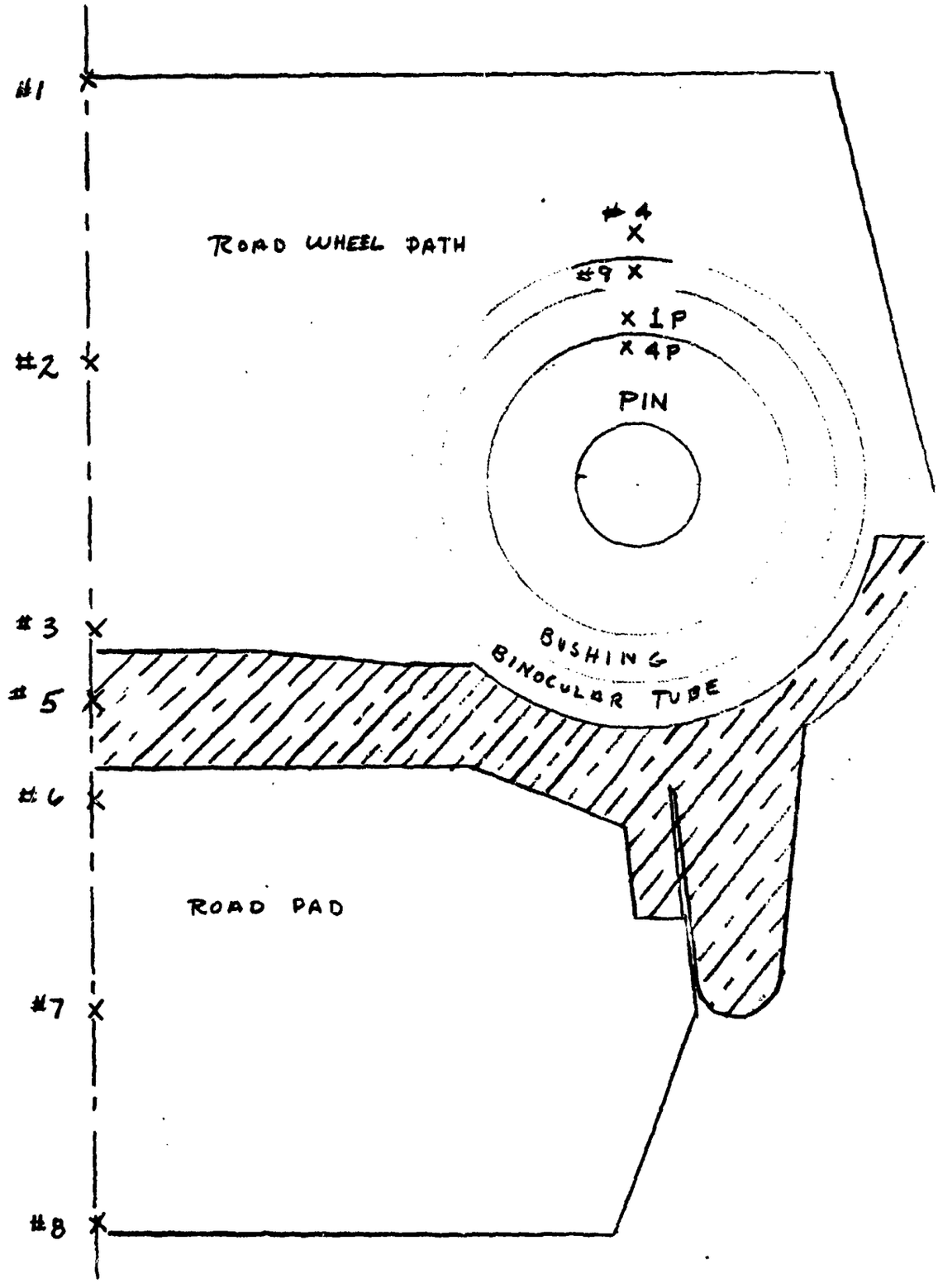

FIGURE 68. Location of Thermocouples In T-142 Shoe

Track Pad Vibration. One of the aspects of dynamic behavior of the track is the interaction between the track and the drive sprocket as the track enters and leaves the sprocket. Direct observation of the track and sprocket reveals a disturbance when the track enters the top of the sprocket in maneuvers which require reverse motion of the track. This disturbance is not readily apparent at the bottom of the sprocket regardless of the direction of track motion.

In an attempt to obtain an understanding of this behavior, miniature accelerometers were installed on a block of steel held in the track pocket by the road pad anchor bolt. Electrical signals from the accelerometers were recorded on an off-board tape recorder while low-speed maneuvers were carried out. The vehicle speed and the movement of the tank were limited by the signal cables; however, some powered turns were executed for the test. In the powered turns the instrumented shoe moved through the sprocket in both directions while the track on the opposite side was braked.

Results of Preliminary Field Tests

The results of the track tension-tests and the shoe temperature tests are discussed in the analytical task section of this report. The wheel hop frequency study showed a resonance at 38 Hz, corresponding to a vehicle speed of 15 mph.

Analysis of the shoe acceleration data shows relatively small acceleration amplitudes (less than 2 g zero-to-peak) occurring in both the line of travel and normal to the line of travel (perpendicular to the road wheel path). The fact that the in-line vibration amplitude is the higher of the two amplitudes, and the two signals are reasonably well correlated, tends to confirm the presence of stick-slip between the shoe end connector and the sprocket as the connector moves through the sprocket. (An audible indication of stick-slip is observed as the track moves backward through the sprocket during low speed neutral turns and similar maneuvers.

No vibration corresponding to chordal action was observed in the data. This is to be expected since it has been calculated that the chordal action at low speed would produce very small acceleration levels, i.e., well below the random vibration level observed at the shoe.

As mentioned earlier, the transmitting antenna held up well during the short running time involved.

Rough Terrain Tests

Feasibility of Wireless Telemetry. The track measurements described above were of a type which could be done either with the tank standing still (static temperature), or with limited motion of the tank (track tension response to obstacles). However, dynamic response to obstacles and rough terrain could not be obtained without some form of wireless link between the track and a receiver mounted either on the tank, or at a separate location.

A literature search was conducted to determine the current state of the art in wireless telemetry, and to determine the identity of the practitioners in the art. The literature search led to work at Sandia and Aberdeen Provery Ground. Direct contacts further narrowed the search to studies of artillery projectiles--using on-board radio telemetry to relay ballistics data to a ground station.

Interviews with investigators at Aberdeen helped establish contact with two firms involved in the manufacture of miniature telemetry components with claimed adequate resistance to shock and vibration. Subsequent discussions with representatives of these companies were helpful in choosing a vendor to supply components for the field test program.

The data acquisition system requirements were defined in terms of functional demands and environmental constraints. Functionally, the system was required to transmit data from the track of an operating vehicle to a data recording system located at some point not on the track. This requirement was dictated by the unavailability of any multiple channel dynamic recorder which was both small enough and rugged enough to install on the track. At a minimum it was decided the system should transmit a minimum of three channels of data in the frequency range of 0-1000 Hz.

Environmental constraints on the system were found to be those associated with the track, i.e., limited space, severe vibration, flying rocks, high temperatures, and contaminants such as dust and water.

It was also determined that a goal of 10 minutes minimum operation of the system on a set of batteries would be reasonable.

After determining that a telemetry system meeting these requirements was feasible, the design of this system proceeded. The telemetry system consisted of three distinct subsystems, namely:

1. The track mounted signal processing components and radio transmitter
2. The hull-mounted receiver and retransmitter
3. The van-mounted receiver, demodulator, and tape recorder .

The components and functions of these subsystems are described briefly in the following paragraphs.

Track Mounted Subsystems. The track-mounted components of the telemetry system were determined to be as follows:

- o Transducers (strain gages, accelerometers, temperature sensor)
- o Signal Conditioners (provide power to transducers and provide amplification, zero suppression, etc.)
- o Subcarrier oscillators (generate a frequency analog of data)
- o Mixer (combines subcarriers to form a frequency domain multiplex)
- o FM Transmitter, S-Band (generates a frequency modulated rf carrier)
- o Antenna, S-band, Transmitting (radiates the FM rf carrier as electromagnetic energy)
- o Battery Pack(s) (provides electrical power for the track-mounted components listed above) .

Figure 69 shows a block diagram of this portion of the system, together with the specific components which were chosen.

Hull-Mounted Subsystems. The hull-mounted components of the telemetry system were determined to be as follows:

- o Receiving Antenna, S-Band (receives rf signal from the S-Band transmitting antenna and converts it to an rf voltage signal)
- o S-Band Receiver--consists of several subsystems including:
  - (a) Tuner (selects frequency band containing the rf signal from the track mounted transmitter)
  - (b) IF Amplifier and Filter (amplifies and further separates the desired rf signal from undesired signals and noise)
- o FM Demodulator (recovers the subcarrier multiplex signal from the intermediate frequency signal)
- o Demultiplexor and Demodulator (on-board). In this case, all steps necessary to recover the data signal are carried out on board the vehicle, and no van is required as it would be for the

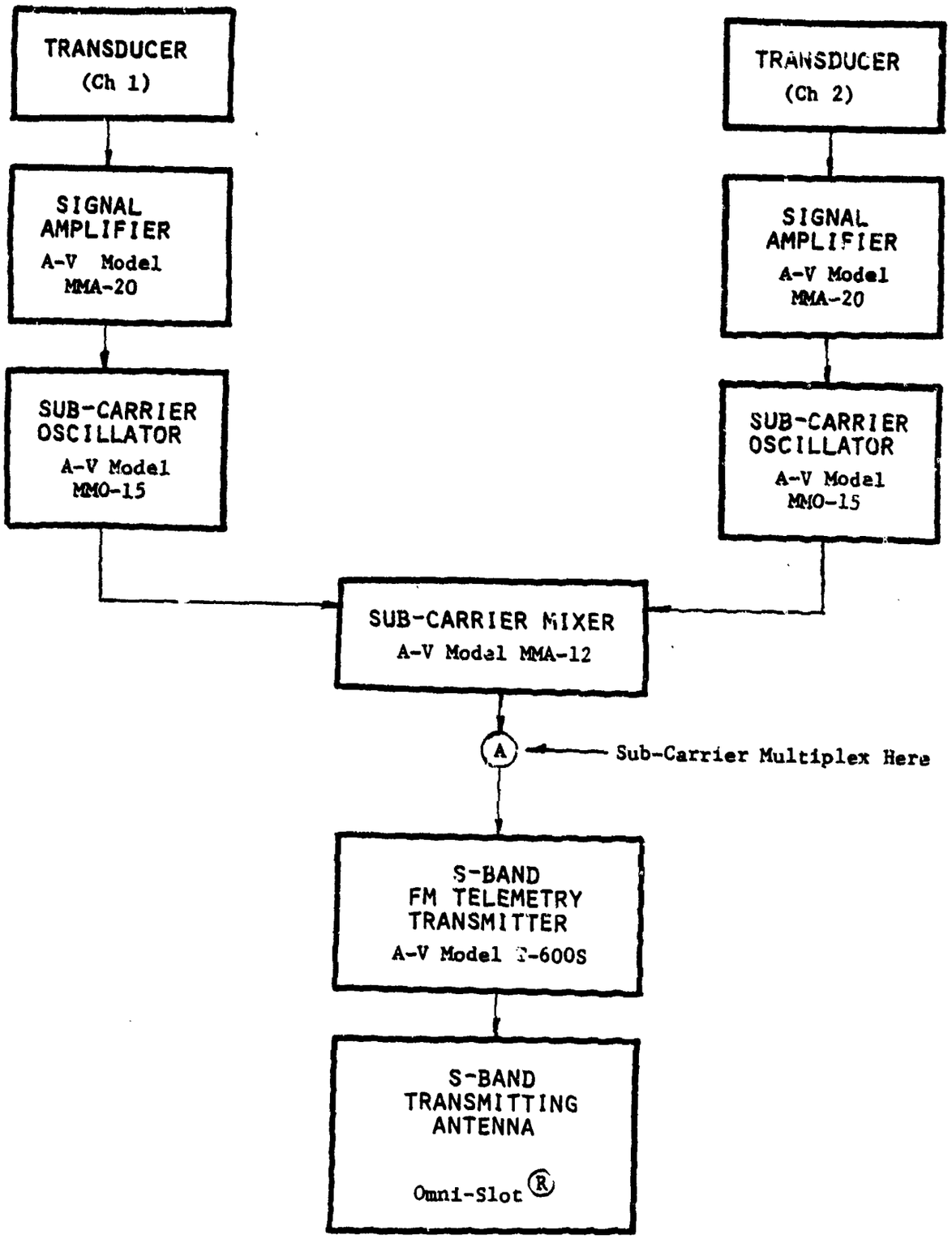

FIGURE 69. TRACK MOUNTED SUBSYSTEM FOR TELEMETERING TRACK DATA

retransmission of the subcarrier multiplex, as described next. The data would be available directly and would be tape recorded on a multichannel FM magnetic tape recorder carried on board the vehicle. (This is Option 1.)

- Retransmission of Subcarrier Multiples. In this option, the subcarrier multiplex, as provided by the demodulator section of the S-Band Receiver, would be retransmitted from the vehicle, using TARADCOM's L-Band telemetry transmitter. (This is Option 2.)

Figure 70 shows a block diagram of this portion of the system, together with the specific components chosen.

Van-Mounted Subsystem. A block diagram of this subsystem is shown in Figure 71. The subcarrier multiplex, from the FM demodulator, obtained either directly or indirectly through the medium of tape or retransmission, is first passed through a bank of band-pass filters to separate out the frequency bands containing the subcarriers. Each subcarrier is then passed through the appropriate demodulator and filter to recover the original analog data. The data can be either tape recorded or written on an oscilloscope or strip chart recorder, or any combination of these, for study and analysis.

Preparation for Full-Scale Tests. To implement this design, some of the telemetry system components were available at Battelle or at TARADCOM. However, all of the telemetry components on the track shoe, the S-Band Receiver, and the S-Band Antenna had to be purchased. An S-Band frequency assignment at 2222.5 MHz was requested, and the request was still being processed at the Electromagnetic Compatibility Assurance Group (ECAG) in Annapolis, Maryland, at the time this report was written.

The shoe-mounted telemetry system was assembled and installed on a group of shoes which included the shoe instrumented for measurement of track tension in previous tests. Mounting plates were designed and built for securing the telemetry components and batteries to the shoes. Interconnection of components was accomplished by means of an intershoe connection system which employs short loops of ribbon connector and quick disconnect plugs and receptacles. Provision was made for using the tension shoe in either a wireless telemetry mode or in a cable connection mode. Figures 72 and 73 show the track-mounted portion of this system and Appendix G contains more detailed information on its design.

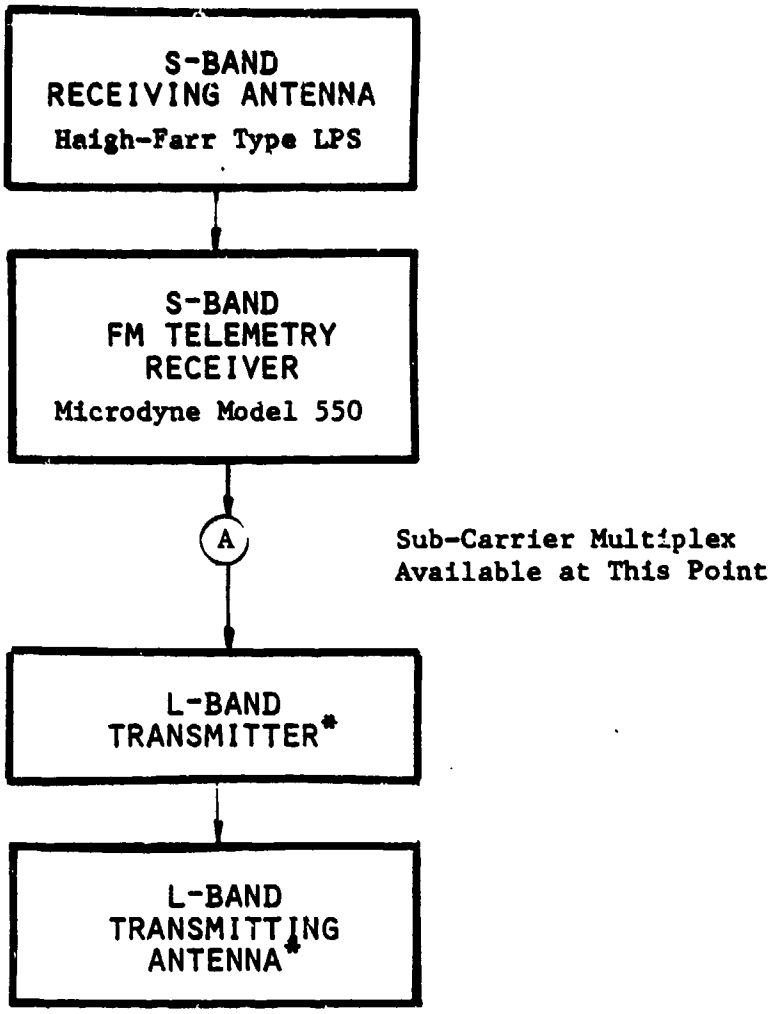

FIGURE 70. HULL MOUNTED SUBSYSTEM FOR TELEMETERING TRACK DATA

The Filter/Demodulator Subsystem Shown in Figure 71 Could be Connected Directly to Point A and Data Tape Recorded on Board the Vehicle.

*To be furnished by TARADCOM.

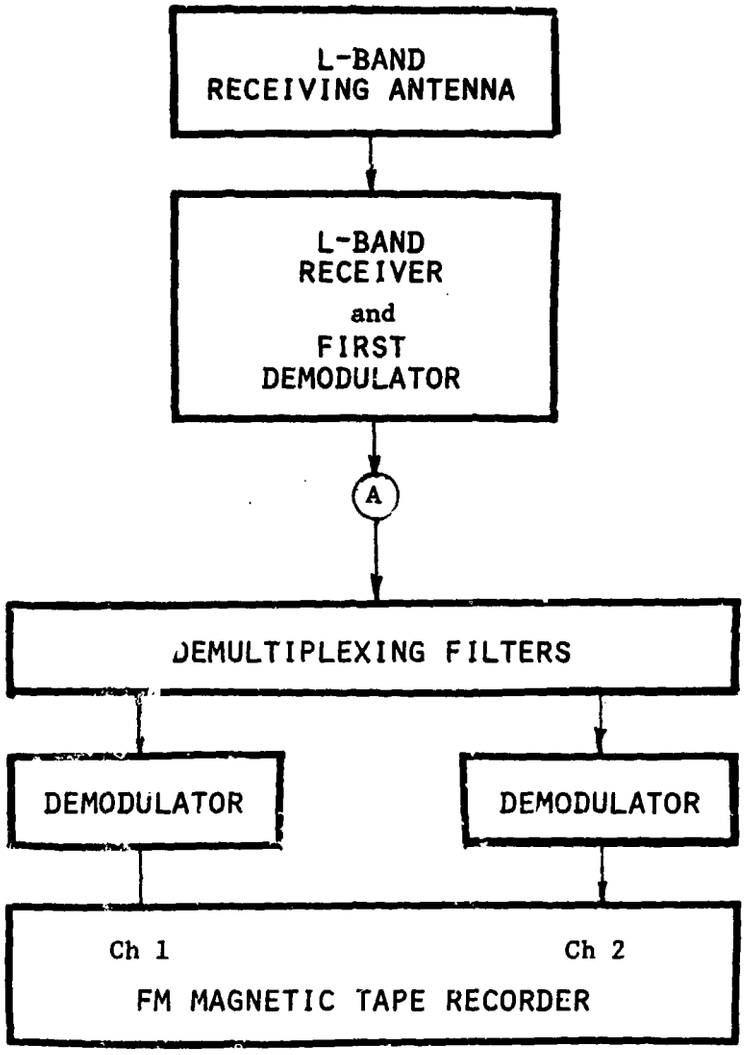

FIGURE 71. VAN MOUNTED SUBSYSTEM FOR TELEMETERING TRACK DATA

If This Subsystem Were to be Used on Board the Tank, the Output of the S-Band Receiver Would be Connected at Point (A) and the L-Band Equipment Shown in This Figure and Figure 70 Would not be Needed.

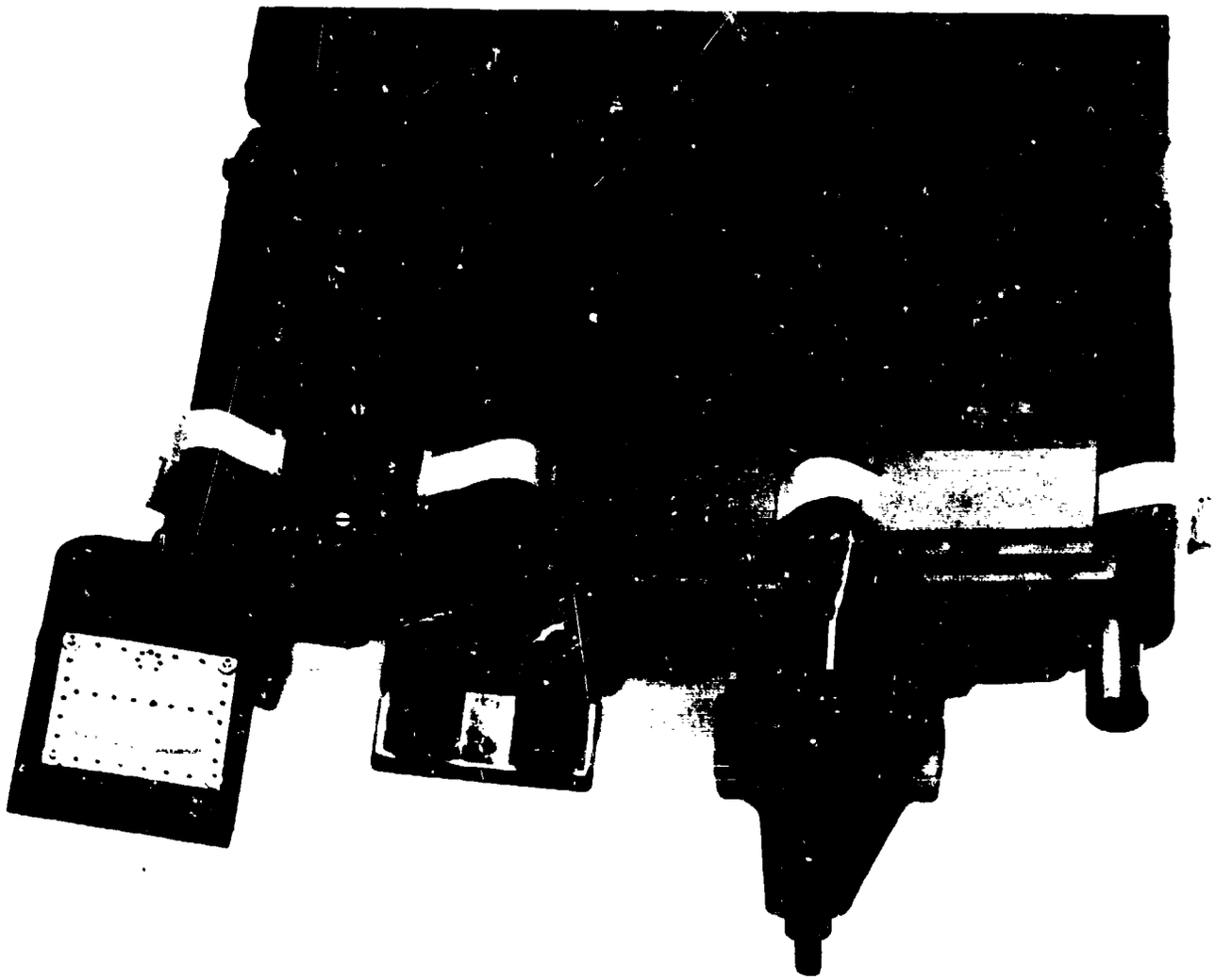

FIGURE 72. OVERALL ASSEMBLY OF TRACK-MOUNTED PORTIONS OF TELEMETRY-TYPE INSTRUMENTATION SYSTEM

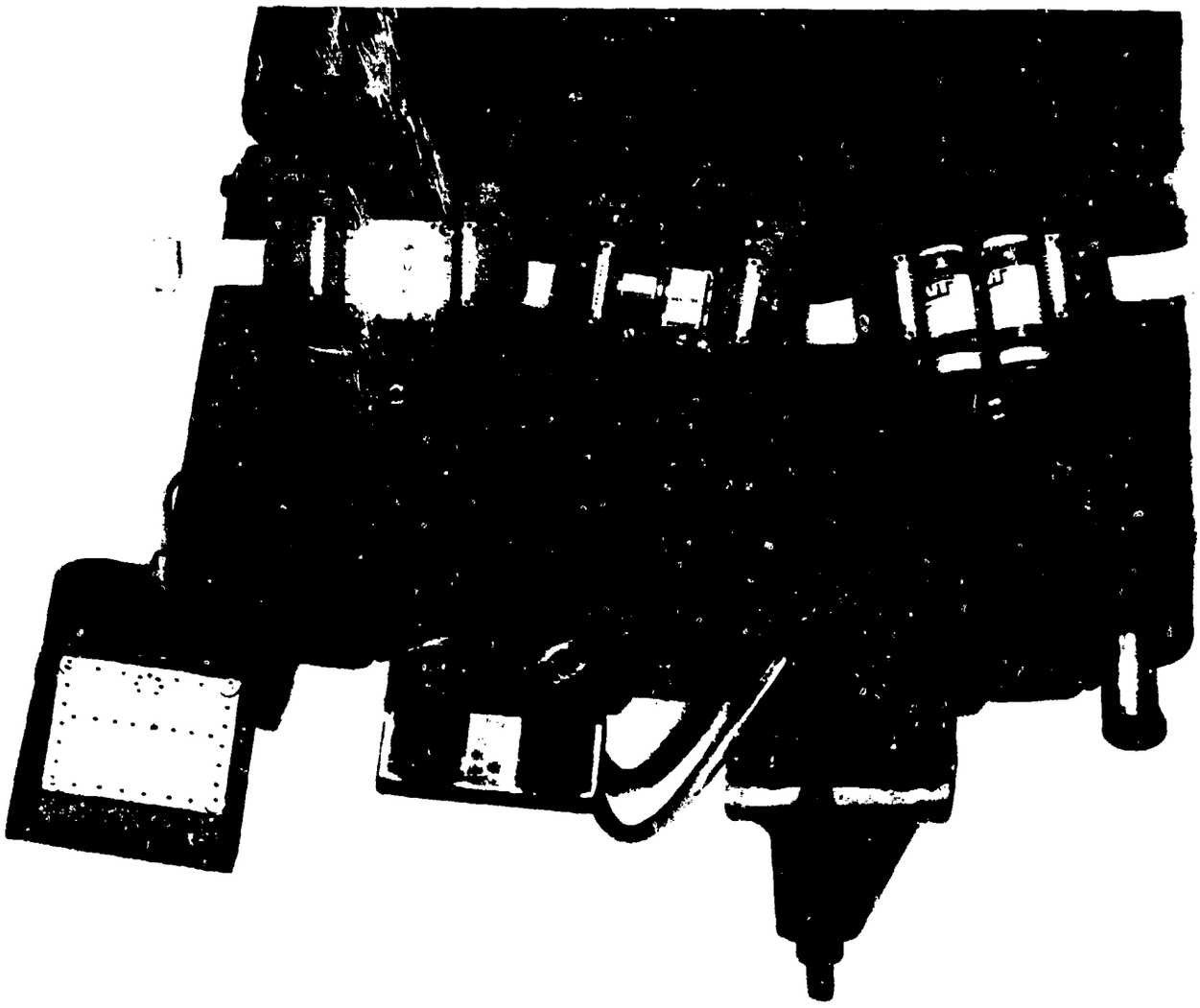

FIGURE 73. VIEW SHOWING COMPONENTS IN TRACK-MOUNTED PORTIONS OF TELEMETRY-TYPE INSTRUMENTATION SYSTEM

RECOMMENDATIONS FOR FUTURE WORK

The Track Dynamics Program has established a foundation for the analysis of track dynamics and other aspects of track which has not existed before. The thrust of the program has been the development of analytical techniques and tools to analyze and evaluate track with the laboratory and field analysis in supportive roles. Now that these tools have been developed or are well under development, more application is needed. This includes not only further parameter studies on the heavy double-linked track analyzed in this program, but extension to heavy single-pin track, all types of lighter track, and various new track concepts. In addition to the analytical work, laboratory studies are needed to provide input data (such as heat generation values) to the analyses, and on their own merit to evaluate track components -- particularly rubber components such as bushings. Field studies are needed to utilize the instrumentation developed during this program and provide data to (1) validate analytically predicted values, and (2) provide data for the many conditions which are too complex to be economically treated by analytical techniques (complex maneuvers over rough terrain, for example).

While these are general areas of future work, more specific areas are listed below.

TRACKDYNE. The development of the TRACKDYNE II program, representing a portion of the track loop, is considered to be one of the most significant accomplishments of the program, as it "automatically" includes the vibration modes, chordal action effects, and other dynamic phenomena. This program should be expanded to include an entire track loop, and then the effects of various parameters -- weight, bushing stiffness and damping, etc. -- examined for various vehicles and types of track to optimize the track design. Although considered to be outside the scope of the present program, the whole area of track-generated noise and vibration can be handled with TRACKDYNE, since it outputs the amplitude and magnitude of forces transmitted to the hull.

Thermal Analyses. The SHOETEMP III model should be exercised to give additional guidance on ways of reducing track temperature buildup. Additional small-scale laboratory studies are needed to provide better input on the thermal properties of track metal and rubber components. Additional work on the

T-142 and T-97 versions of track for the M-60 and XM-1 tanks appears particularly timely.

Bushing Research. Analyses of stresses in bushings with different cross sections should be continued, and this work should be complemented with research studies on a laboratory machine such as the machine designed during this program. Additional studies to determine the relative significance of assembly stresses, tension-induced stresses, and torsion-induced stresses should be conducted.

PINSTRESS II. Many of the track parts are highly stressed by the sprocket tooth loads, which are concentrated at the edge of the track. A three-dimensional analysis of structural distortions in the entire length of track affected is needed to determine the loads on individual teeth and track parts. PINSTRESS II provides a powerful technique for handling the pin, bushing, and tube assemblies as part of the structure, and the other track elements are relatively easy to model. These models of individual parts should be combined into a simultaneous solution that would determine pin and shoe stresses on the sprocket. The effect of various parameters (such as pin bending stiffness or support of the center of the track by the sprocket) should be determined to guide future track development.

End Connector Design. Development of the reversed end connector design developed during this project should be pursued to the point where several pitches of track equipped with the new-type end connectors are inserted into conventional T-142 type track, and tested in the field and/or the laboratory.

Field Tests. The track-mounted telemetry system designed and built during this program should be incorporated into a test program to establish its feasibility and determine the inevitable modifications needed. It should then be used, if possible, to obtain data on track tension, acceleration, and temperature at higher speeds and/or over rough terrain.

Analytical Techniques. To date, the various analytical techniques are based on conditions existing when the tank is going straight ahead--that is, not turning. Attention now needs to be turned to the case where side loads are present due to turns, side slopes, or other factors. Of particular interest is the analysis of track misguiding and/or throwing, which has not yet been attempted. Lateral loads may be equal or greater in importance to the longitudinal tension-type loads analyzed to date.

Design Procedure. Effort needs to be continued on the development of a means for combining the loads and stresses calculated for the various conditions into a meaningful estimate of track/track component life. Only when this is done can the effect of design changes be evaluated in terms of life. The various analytical techniques developed during this program provide the foundation for this procedure, since they enable loads to be calculated for several conditions. Near the end of the program, effort was started on a method of calculating the number of cycles of each type of load (for example, increased tension while negotiating an obstacle), and then converting the load cycle into an equivalent stress cycle and subsequently into life, based on given material properties. However, the nature of the loading cycle and the distribution of load in the track are sufficiently complex that additional work on this type of design procedure is needed. Eventually, it should be possible to "screen" track designs rather thoroughly before they are built by application of a design procedure incorporating the fundamental "building blocks" developed in the Track Dynamics Program.

APPENDIX A

ORIENTATION PHASE CONTACTS

TABLE A-1. ORIENTATION PHASE CONTACTS

ARMY	
TARADCOM	Asokiis, Barnes, Carter, Comito, Decker, Fix, Getz, Gorton, Gow, Grant, Hoffman, Kozowck, Kvet, Lassila, Lee, Majkowski, Newcomb, Otto, Palmer, Parks, Petrick, Puuri, Rose, Wollam
XM-1 Program Office	Appleyard, Harju, Smith
M-60 Program Office	Getz
M-113 Program Office	Burcz
MICV Program Office	Turkiewicz
Aberdeen Proving Grounds	Kotras, Sobczyk, McKay, Gross, Mermagan, Garinther
AMMRC	Shea, Adachi, Fupiano, Parsons, Weiss*
DARCOM	Soukup, Kline
MERADCOM	Comminge
Vicksburg	Nuttal*
Ft. Hood	Meisell, Fuller, Rawles
INDUSTRY	
ALCOA	Johnson, Long
Chrys. XM-1	Hirych, Hartwig, Wells
Chrys. M-60	Wolken, Briggs
Detroit Diesel Allison	Brindle, Leet, Schaefer
FMC	Gibson, Casey, Hare
Firestone	Brandenberg, Millikan, Raines, Ritz, Robinson, Welvaert
Goodyear	Cooper, Fetter
Standard Products	Nichols
Bolt, Beranek & Newman	Galaitsis
ACADEMIA	
San Jose ST	Blythe
University of Michigan	Chace, Felbeck
Wayne State	King

*Telephone contact

APPENDIX B

TRACK RELATED LITERATURE

BIBLIOGRAPHY

1. Alexander, Graham, ACL Comprehensive Plan, C.4 Suspension, 1976.

2. American Ordnance Association, Weapons Technology, 1962.

3. Ames, W. F. and Vicard, A. A., "Longitudinal Wave Propagation on a Traveling Threadline I", Department of Mechanics and Hydraulics, University of Iowa, November, 1968.

4. Amsden, R. T., "Design Study and Test of an Elastomer Backed Lubricated Bearing Supported Pin Track", Technical Report No. 11214, To TACOM MSL by LTV, February, 1971.

5. Amsden, Richard T., "Sprocket Engagement Support Wheel for an Endless Track", Patent 3,567,292, Patented March 2, 1971.

6. Antonescu, N. N., and Dix, R. C., "Stresses in Roller Chain Link Plates", Rev. Roum. Sci. Techn. - Mec. Appl., Tome 20, No. 2, p. 311-322, Bucarest, 1975.

7. Asnis, A. Ye., Gutman, L. M., "Rebuilding Track Blocks on Tracked Vehicles", Academy of Science, Kiev, USSR, 1964.

8. Austin, D., "Factors Contributing to Tendency of Roadwheels to Climb Track Guides, MICV SM723 Test Report", Technical Report 2832, Contract DAAE07-73-C-0100, FMC Corporation, February 19, 1975.

9. Bates, C. L., and Sparks, C. R., "Development of Measurement Techniques for the Analysis of Tracked Vehicle Vibration and Noise", Final Tech. Rpt., Contract No. DA-23-072-AMC-144(T), Southwest Research Institute, October 30, 1964.

10. Beck, R. S., "Idler and Sprocket Rigidity, MICV XM723 Test Report", Technical Report 2796, Contract DAAE07-74-C-0100, FMC Corporation, October 28, 1974.

11. Beck, R., "Rigidity of a Roadarm-Roadwheel Assembly Under Static Vertical Loading, MICV XM723 Test Report", Tech. Rept. 2795, Contract DAAE07-74-C-0100, FMC Corporation, October 28, 1974.

12. Becker, D. G., "Deflection and Durability Study of Roadwheel, P/N 11672634, MICV XM 723 Test Report", Tech. Rept. 2744, Contract DAAE07-73-C-0100, FMC Corporation, September 16, 1974.

13. Bekker, M. G., "Introduction to Terrain-Vehicle Systems", University of Michigan Press, 1969.

14. Bekker, M. G., "Off-the-Road Locomotion: Research and Development in Terra Mechanics", University of Michigan Press, 1960.

15. Bekker, M. G., "Tracked Vehicles for the Arctic", Maching Design, May 30, 1974.

16. Bergstrom, E. W., and Cerny, S. R., "Development of Rubber Pads for Tracked Vehicles", RE TR 70-121, February, 1970.

17. Bergstrom, E. W., "Development of Wear Resistant Elastomers for Track Pads", SWERR-TR-72-74, October, 1972.

18. Bergstrom, E. W., "Material Development for Improved Rubber Track Pads", Rept. No. R-TR-74-021, April, 1974.

19. Bergstrom, E. W., "Prediction of Wear Resistance of Rubber Tank-Pads by Standard Laboratory Tests", RE-TR-71-43, July, 1971.

20. Bergstrom, E. W., Cerny, J. R., "Rubber Pads for Tank Track, RE-TR 71-13, July, 1971.

21. Bergstrom, E. W., "Wear Resistant Rubber Tank Track Pads", Report No. R-TR-76-028, Rock Island Arsenal, October, 1975.

22. Bernshtein, M. L., Gavrielov, R. M., "Heat Treatment and Operating Tests of 55PP Track Shoe Bushings of the ChTZ Caterpillar Tractor", Tadzhik Soviet Socialist Republic, Translated from Metallovedenie I Termicheskaya Obrabotka Metallov, No. 12, pp. 49-51, December, 1972.

23. Binder, R. C., Mechanics of the Roller Chain Drive, Prentice-Hall, 1956.

24. Binowitsch, J. E. (editor) "Tank Theory" (Russian translation) from ATAC, December, 1967.

25. Birley, S. M., "Hitpro Tests and Analyses" Final Report R-TR-76-031, Rock Island Arsenal, September, 1976.

26. Bjerk, Roger O., "Oxygen - An Extreme Pressure Agent", ASLE Transactions, Vol. 16, ?, pp. 97-106, October, 1972.

27. Blythe, W., "Laboratory Evaluation of the T-142 Trackshoe", presented at AOA Track and Suspension Section Meeting, Detroit, Michigan, November 8, 1967.

28. Blythe, Wm., Zsutty, T., San Jose College, "Rational Design and Analysis of Vehicle Suspension System Components: Part 1 - Summary, Part 2 - Experimental Stress Analysis of Prototype Suspension System Components, Static Tests, Part 3 -- Part 4 - The Spectral Density Method of Random Response, 1966.

29. Blythe, W., "Rational Design and Analysis of Vehicle Suspension System Components, Part 5: Experimental Stress Components: Determination of Loading Criteria", San Jose State College, February 15, 1968.

30. Bonkosky, B. B., "Vibration and Damping Ratio Characteristics of T97E2 and T127 Tracks", Rept. No. 9530, Vehicular Components and Materials Lab, March 31, 1967.

31. Brotzman, P. H., Drewes, E. H, Wulff, N., "Application Techniques and Methods for Applying Fused Carbides on Nonlubricated Wear Surfaces for High Volume Production", Technical Report No. 11850, by Firestone to TACOM, June, 1974.

32. Burrows, D. J., "Soviet Track Shoe and Pin Metallurgical Evaluation", Report No. 11831, October 25, 1973.

33. Carlson, R. B., "Design, Fabrication and Testing of a Pitchless Band Track", Final Technical Report No. 11345, Chrysler Defense Div., Contract No. DAAE07-67-C-4181, May 6, 1971.

34. Carter, Barry, "Stress Analysis of T-142 Track Pins".

35. Chace, M. A. Angell, J. C., Report to Chrysler Defense Division on Phase One of "The Simulation of M60 Suspension Dynamics", University of Michigan, September 12, 1974.

36. Chace, M. A. Angell, J. C., Report to Chrysler Defense Division on Phase Two of "The Simulation of the M60 Suspension Dynamics", University of Michigan, February, 1975.

37. Cleare, G. V., "Some Factors Which Influence the Choice and Design of High-Speed Track Layers", Journal of Terramechanics, 1971, Vol. 8, No. 2.

38. Cline, H. T., "Road Shock and Vibration Environment for a Series of Wheeled and Track-Laying Vehicles", Report No. DPS-999, Aberdeen Proving Ground, June, 1963.

39. Collins, Marshall, "Track Drawing Numbers".

40. "Comparison of U. S., U.S.S.R., and West German Tanks" Army Foreign Science and Technology Center, February, 1972.

41. Conrad, H. M., "Distribution of Tension and Frictional Forces Along a Model Band Track", Stevens Institute of Technology, March, 1974.

42. Cummings, A. L., "Military Potential Test of Diehl Foreign Track (types 213B, 828G, and 208B), Report No. TECOM Proj. No. 1-VC-087-000-001, August, 1974.

43. Cummings, A. L., "Product Improvement Test of Hard-Coated Aluminum T-142 Track for M-60 Series Tanks", Final Letter Report, APG, July, 1975.

44. Cushman, P. G., "Hitpro, Volume II, User's Manual", Final Report, Contract DAAF-03-69-C-0085, Ordnance Systems, G-E Company, November 15, 1971.

45. Cushman, P. G., "Hitpro II, Volume II (User's Manual", Volume III", Technical Report, Contract DAAF-03-69-C-0085, Ordnance Systems, G-E Company, April 1, 1972.

46. Cushman, P. G., "Study of Gunner Aids for Automatic Cannon Type Weapons", Final Report, Contract DAAF-03-73-C-0107, Ordnance Systems, General Electric Company, December, 1973.

47. Dadds, F. S., Johnson, H. R., and Shrier, W. C., "A Concept Feasibility Study of a Single Pin Sealed and Lubricated Track for the M48 and M60A1 Vehicle", prepared by Caterpillar Tractor Company, Contract DA-20-113-

48. Dailey, Wayne, "Product Improvement Test of Polyurethane Track Pads" YPG Report 0039, June, 1970.

49. Dobbins, J. E., "Evaluation of 3 Tracks Manufactured for the Armored Personnel Carrier M113A1", TACOM Mobility Systems Lab, August, 1974.

50. Dubbeldam, J. W., dePater, A. D., Van Rijssen, R. H., "The Vibrations of a Homogeneous Chain, Composed of Material Points and Springs, Brought about by Longitudinal Forces", 1976.

51. Durelli, A. J. and Buitrago, J., "State of Stress and Strain in a Rectangular Belt Pulled Over a Cylindrical Pulley", Strain, July, 1973.

52. "Effect of Design Changes on Vehicle Performance; a Limited Study of the M35A2 (modified) and the M113A1", Misc. Paper M-72-2, Army Engineer, WES, April, 1972.

53. Elmaraghy, R., Tabarrok, B., "On the Dynamic Stability of an Axially Oscillating Beam", Journal of the Franklin Institute, Vol. 300, No. 1, July, 1975.

54. Engineering Properties of Rubber, U. S. Rubber Company, Engineered Rubber Products, Fort Wayne, Indiana, 1941.

55. Eppinger, R. H., King, A. I., and Lee, R. A., "Experimental and Mathematical Simulation of a Multi-Wheeled Vehicle With and Without an Elastic Track", Proceedings of the Second International Conference on Vehicle Mechanics, Paris University, Paris, France, September 6-9, 1971.

56. Evans, D. L., "Military Potential Test of Diehl 208B Track", USAYPG Reports 198 and 199, July, 1974.

57. Evans, D. L., "Product Improvement Test of Track Pad Rubber Compounds for T142 Track Shoe", TECOM Project No. 1-VC-087-142-009, June, 1974.

58. Felbeck, D. K., "SEM Study of Track Pin Fractures", Chrysler Def. Div., USATACOM T-142 Track Task Force Report, September 11, 1974.

59. Fix, S. O. and Peck, T. G., "Track Design Study (Task No. 26) XM179, S. P., 155 mm", Technical Report 10613, TACOM Mobility Systems Lab., August, 1969.

60. Freitab, D. R., "Tracks Versus Wheels in Soft Soil and Snow", Miscellaneous Paper No. 4-651, U. S. Army Engineer WES, May, 1964.

61. FRG (DIEHL) versus U. S. Track Design (Looks like a series of viewgraphs used in a presentation.)

62. FVRDE Specification 1277, Rubber Bushes and Pads for Track Links", War Department, England, March 4, 1966.

63. Gerbert, B. G., "Tensile Stress Distribution in the Cord of V-Belts", Transactions of the ASME, February, 1975.

64. Goldsmith, Werner, Impact, Edward Arnold (Publishers) Ltd., 1960.

65. Goto, Kaname, "On the Estimation of Traction of Tracked Vehicles", FSTC-HT-23-0311-73, November, 1973.

66. Gow, Ed J., "Radial Pin Shift Investigation", TACOM, Task No. 2-7, September 26, 1974.

67. Gow, Ed, Track Data Book, 1971 Edition, TACOM.

68. Haddock, K. R., "Comparison of Track Disengagement Tendencies with Two Different Idler Wheel Configuration, MICV XM723 Test Report", Technical Report 3021, Contract DAAE07-73-C-0100, FMC Corporation, June 11, 1976.

69. Haddock, K. R., "Durability of M109 Type Roadwheels at the Idler Positions, MICV XM723 Test Report", Tech. Report 3010, Contract DAAE07-73-C-0100, FMC Corporation, April 26, 1976.

70. Haddock, K. R., "Durability of Track Assembly, XM723 MICV Test Report", Tech. Report 2674, Contract DAAE07-73-C-0100, FMC Corporation, April 19, 1974.

71. Hanomoto, Ben, "Cobra: Positive Pitch Controlled Articulated Testbed", U. S. Army Cold Regions Research and Engineering Laboratory, Hanover, New Hampshire, May, 1974.

72. Hanamoto, B., "Effect of Snow Cover on Obstacle-Crossing Performance of Vehicles", Technical Report 239, D A Project IT062112A130, U. S. Army Cold Regions Research and Engineering Laboratory, November, 1972.

73. Hausenblas, H., "Problems Caused by the Track Adjuster in Tracked Vehicles with Front-Wheel Drive", Wehrtechnik, March, 1972.

74. Howard, B. L., Chace, M. A., "Track-A Program to Compute the Damped Multi-Freedom Response of a Tank Track", University of Michigan, 1971.

75. "Investigation of Physical Properties of Rubber and the Characteristics of Rubber Donut Bushings Used in Army Tank Track Treads", Armour Research Foundation, Chicago, Illinois, Contract No. W-11-022-ORD-10694, Reports 1 through 17, 20, and Final Design Manual, February 25, 1946 to October 28, 1948.

76. Johnsen, John L., "The Effect of Drawbar-Pull in Sand of the Lateral Spacing of Cleats", Davidson Laboratory, Stevens Institute of Technology, Report SIT-DL-71-1533, June, 1971.

77. Jurkat, M. P. Nuttall, C. J., and Haley, P. W., "The AMC '74 Mobility Model", Stevens Institute of Technology, May, 1975.

78. Kasprik, J. E., "Physical Properties of Two Goodyear Track Bushing Compounds, SM1652 and SM1010, MICV XM723 Test Report", Technical Report 3049, Contract DAAE07-73-C-0100, FMC Corporation, September 17, 1976.

79. Kasprik, J. E. "Roadwheel Deflection Compared with M113, AIFV, and LVTP7 Wheels, MICV XM723 Test Report", Technical Report 2774, Contract DAAE07-73-C-0100, FMC Corporation, October 2, 1974.

80. Kaufman, L., Kulin, S. A., and Neshe, P. P., "Noise Abatement and Internal Vibrational Absorption in Potential Structural Materials", Manlabs, Inc., Contract No. DAAG46-74-C-0048, December 31, 1976.

81. Kilgore, Ullmann, "Hydrodynamic Aspects of Tracked Amphibians", Naval Engineers Journal, December, 1969.

82. Kotras, E. C., "Product Improvement Test of Road Test of RRAD Production T97 Track and Roadwheels", Report No. APG-MT-4717, September, 1975.

83. Kulesia, J., "Cast-in-Place Track Shoe Backing Inserts", Contract No. DAAE07-74-C-0059, Technical Report No. 12112, November, 1975.

84. Lambert, R. A., "Research Study of Dynamic Characteristics of Tracked Vehicles, Suspension Geometry Signature", September, 1964.

85. Lassila, J. I., "Load Distribution in the Track Pin-Subhing-Tube System", letter from TARADCOM, March, 1977.

86. Lane, W. J., and Staursky, M. V., "Concepts for Design of Lightweight Track for the U. S. Marine Landing Vehicle Assault (LVA), Prepared by Alcoa, Prepared for NSRDC, Contract N00167-76-C-0004, February 20, 1976.

87. Lanyon, John T., "Conservation of M29C Weasel Tracks", U. S. Army Cold Regions Research and Engineering Laboratory, Hanover, New Hampshire, September, 1962.

88. Lee, R. A., Wollam/Comito (TACOM) "Computer Analysis of T-142 Track Pads and Pins", Technical Report No. (TACOM-AVSL), January, 1976.

89. Lee, R., and Yollick, S., "Track Tension", Technical Report No. 12209 (TACOM-MSL), October, 1976.

90. Lee, Sung M., "The Study of Vibrations Generated by the Tracks of Tracked Vehicles", Keweenaw Research Center and Department of Physics, Michigan Technical University, July, 1976.

91. Lessem, A. S., and Murphy, N. R., "Studies of the Dynamics of Tracked Vehicles", Technical Report M-72-1, U. S. Army Engineer WES, June, 1972.

92. Luttrell, D. A., "Static Loading of Aluminum Model Track Shoe, XM723 MICV", Technical Report 2513, Contract DAAE07-73-C-0100, FMC Corporation, January 31, 1973.

93. Macksey, K., and Batchelor, J. H., Tank: A History of the Armoured Fighting Vehicle, Ballantine Books, 1973.

94. Mac Rostie, J. J., "Shock, Vibration, Ride Dynamics and Suspension are Main Factors in Ground Missile-Carrier Design", SAE Journal, p. 56, July, 1967.

95. McConnell, B. C., "Rubber Compound Variation to Improve T-142 Tank Pad Life", Standard Products, September, 1975.

96. McGarvey, J. W., Veroeven, W. M., "The Development of Elastomeric Vulcanizates for Track Pad Applications", Rock Island Arsenal, Report No. 64-2678, September 10, 1964.

97. Mclean, R. G., and Jent, J. P., "Product Improvement Test of Sheridan Weapon System, M551 (Arctic/Universal Track and Wide Sprocket Wheel), USATECOM Project No. 1-UC-087-551-002, December 1, 1970.

98. Melzer, K. J., and Swanson, G. D., "Performance Evaluation of a Second-Generation Elastic Loop Mobility System", Technical Report M-74-7, U. S. Army Engineer WES, June, 1974.

99. Melzer, R. J., and Green, A. J., "Performance Evaluation of a First-Generation Elastic Loop Mobility System", Technical Report M-71-1, U. S. Army Engineer WES, May, 1971.

100. MIL-T-1189B (ORD), "Military Specification, Track Shoe Assemblies, Track Shoe Pads, and Track Shoe Sets, Vehicular: Rubberized", June 24, 1960, Amendment 3, April 24, 1972.

101. Mobility Systems Laboratory (TACOM), Annual Posture Report, FY 1973.

102. Mobility Systems Laboratory (TACOM), Annual Posture Report, FY 1974.

103. Morris, D. F., "Product Improvement Test of Sheridan Weapon System, M551, Arctic/Universal Track and Wide Sprocket Wheel" APG, Md., Report No. APG-MT-3799, March, 1971.

104. Morris, Eric, "Modern Military Series, Tanks, Tank Weaponry and Warfare", Octopus Books Limited, London, 1975.

105. Mote, C. D., and Thurman, A. L., "Oscillation Modes of an Axially Moving Material", Journal of Applied Mechanics, March, 1971.

106. Muller, R., "Modern Designs in Tank Tracks", Kampftruppen, January, 1973.

107. Murphy, N. R., and Ahlvin, R. B., "AMC-74 Vehicle Dynamics Module", Tech. Report M-76-1, U. S. Army Engineer WES, January, 1976.

108. Muth, N. J., "Development of Compounding and Bonding Agent for Improved T-142 Track Pad", Technical Report No. 11445, Contract No. DAAE07-67-C-5141, To: TACOM VC&ML, by GT&R, July, 1971.

109. Nagaj, R. F., "T-142 Lateral Pin Shift Investigation", Chrysler Defense Div.,/ USATHCOM, October 18, 1974.

110. Neargarder, R. F., and Reynolds, R. K., "25-Inch Lubricated-Pin Track", Tech. Report No. 10995, to: TACOM MSL by FMC, July, 1970.

111. Norris, T. R., "Tracked Vehicles: Noise and Vibration Study Using a Reduced Scale Model", Technical Report No. 12099 (TACOM-MSL), Bolt, Beranek, and Newman, Inc., August, 1975.

112. Northon, F. E., "Product Improvement Test of Track Rubber Compounds for T-142 Track Shoes", USAYPG Report 244, November, 1975.

113. Nuttall, C. J., "Ground-Crawling: 1966, The State of the Art of Designing Off-Road Vehicles", Contract Report No. 3-162, by Wilson, Nuttall, Raimond Engineers, Inc., May, 1967.

114. Otto, R. J., ATAC "Briefing for Army Material Command on Comparison of U. S. and Italian Produced T-130 Track for M-113 Vehicle Family", April 18, 1969.

115. Otto, R., et al, "Endless Track Pin Assembly", Patent 3,680,924, patented August 1, 1972, filed March 6, 1970.

116. Payne, J. A., "Track Maintenance Tool", Patent 3,150,859, patented September 29, 1964, filed August 27, 1963.

117. "Pneumatic Track Pads - Concept Feasibility Study", prepared by Chrysler, Defense Operations Division, Contract DA-20-113-AMC-11911(T), May 6, 1969.

118. Renus, Otto, "Investigation of a Laser Illuminator-Thermal Imaging System for the Detection of Voids and Disbonds", Technical Report No. 11169 (TACOM-PSL), January, 1971.

119. Replogle, D. S., "Design, Laboratory Test, and Manufacture of a Double-Pin, Rubber-Bushed Track", Technical Report No. 10958, Contract DAA307-67-C-5446, to: TACOM MSL, by Chrysler, February 16, 1970.

120. Rhodes, J. E., Jr., "Parametric Self-Excitation of a Belt into Transverse Vibration", Journal of Applied Mechanics, Decmeber, 1970.

121. Roach, C. D., "On-Road, Off-Road Track Carrying Vehicle", Patent 3,182,741, patented May 11, 1965, filed February 26, 1964.

122. Root, J. R., "Grouser and Pad Wear of Track Shoe, on the ED Vehicles, MICV XM723 Test Report", Tech. Report 2962, Contract DAAE07-73-C-0100, FMC Corporation, January 30, 1976.

123. Root, J. R., "Wear Ring/Track Guide Interface Investigation, MICV XM723 Test Report", Tech. Report 2792, Contract DAAE07-73-C-0100, FMC Corporation, October 21, 1974.

124. Rose, C. D., "Laboratory Investigation on Fatigue Life of Rubber-Bushing Track Pin Assemblies", Report No. 7908, Detroit Arsenal, July 16, 1963.

125. Rosenbluth, Murray, "Telemetry Instrumentation for Acceleration Track Test System", Picatinny Arsenal, Dover, New Jersey, April, 1976.

126. Rothstein, S., and Kimball, R., "Ausforging Grouser Sections for Track Shoes", Report No. 9973, U. S. Army Tank Automotive Center, March, 1968.

127. Salathe, E. P., "An Analysis of the Deformation and Stresses in an Endless Belt Passing Over Cylindrical Rollers", Transactions of the ASME, March, 1975.

128. Sattinger, I. J., Therkelsen, E. B. (U. of Michigan), "Simulation of Military Vehicle Suspension Systems", National Simulation Conference Proceedings, January 19-21, 1956, Dallas, Texas.

129. Schmidtchen, H., "Tracks with Rubberized Metal Joints", Militaertechnik, East Germany, 11/74, pp. 495, October 24, 1975.

130. Schmidtchen, H., "Tracks with Rubberized Metal Links", Militaertechnik, East Germany, 11/74, pp 495-497, August 21, 1975.

131. Schuring, D., and Belsdorf, M. R., "Analysis and Simulation of Dynamical Vehicle-Terrain Interaction", Tech. Memo CAL No. VJ-2330-G-56, Cornell Aeronautical Lab, May, 1969.

132. Shigley, J. E., "The Mechanics of Walking Vehicles" TACOM (LLL) Report No. LL-71, September, 1960.

133. Shimizu, H. and Sueoka, A., "Nonlinear Forced Vibration of Roller Chain", Bulletin of the JSME, Vol. 18, No. 124, October, 1975.

134. Shimizu, H. and Sueoka, A., "Nonlinear Free Vibration of Roller Chain Stretched Vertically", Bulletin of the JSME, Vol. 19, No. 127, January, 1976.

135. Siddall, J. N. and Southwell, P. H., "Proceedings of the Second International Conference of the International Society for Terrain-Vehicle Systems" University of Toronto Press, September, 1966.

136. Siorek, R., "U. S. Army/FRG Army Mobility Symposium Proceedings", Tech. Report, No. 12101 (TACOM-MSL), November, 1975.

137. Smalley, A. J. and Tessarzik, J. M., "Development of Procedures for Calculating Stiffness and Damping Properties of Elastomers in Engineering Applications - Part III. The Effects of Temperature, Dissipation Level and Geometry", NASA CR-13439, MTI 76TRJ, November, 1975.

138. Sofiyan, A. P. and Maximenko, Ye. I., "The Distribution of Pressure Under a Tracklaying Vehicle", Journal of Terramechanics, 1965, Vol. 2, No. 3.

139. Soft-Soil Vehicle Mobility, U. S. Army Test and Evaluation Command, Common Engineering Test Procedure, Material Test Proceedings, 2-2-619, APG, May 21, 1970.

140. Speidal, L. and Gow, Ed, "Aggressive Dual Pin Track", Patent 3,140,127, patented July 7, 1964, filed April 25, 1961.

141. Strause, P. W., "Suspension System Lateral Rigidity MICV XM723 Test Report", Technical Report 2733, Contract DAAE07-73-C-0100, FMC Corporation, September 5, 1974.

142. Stroebel, H. H., "Design Development of Forged Aluminum Track Shoe for M60/M48 Medium Tanks", Aluminum Company of America, July 15, 197C.

143. Sturgeon, R. C., "Produce Improvement Test of Cast-in-Place Track Shoe Backing Inserts", TACOM Project No. 1-VC-087-130-001, November 22, 1976.

144. T-142 Aluminum Lateral Pin Shift Investigation (DRAFT) from TARADCOM.

145. T-142 Track Pin Push Test (DRAFT), Hq. U.S. Army Tank Automotive Command, Armour and Components Division.

146. Taylor, J. H. and Burt, E. C., "Track and Tire Performance in Agricultural Soils", Transactions of the ASAE, 1975.

147. The AMC '71 Mobility Model - Vol. I, Report. No. 11739, U. S. Army Tank-Automotive Command, TACOM and WES, June, 1973.

148. The AMC '71 Mobility Model - Vol. II, Appendices A, B, and C. Technical Report No. 11789 (LL 143), Army Engineer WES, June, 1973.

149. The (Diesel) M113 Multipurpose Vehicle Family, FMC Ordnance Division, June, 1974.

150. Thomas, I. A., "Northern Off-Road Transportation in the 70's", Journal of the Construction Division, September, 1975.

151. Thurman, A. L. and Mote, C. D., "Free, Periodic, Nonlinear Oscillation of an Axially Moving Strip", Journal of Applied Mechanics, March, 1969.

152. Toboni, J. C., "XM723 Suspension System Lateral Rigidity Compared with M113A1 and LVTP7", Technical Report 2701, Contract DAAE-07-73-C-0100, FMC Corporation, June 17, 1974.

153. Tracked Vehicles, an Annotated Bibliography up to 1967, TDCK Report No. 49993, The Hague, 1968.

154. "Tracks", U. S. Army Test and Evaluation Command, Common Engineering Test Procedure, Material Test Proceedings 2-2-705, Aberdeen Proving Ground, July 1, 1970.

155. Turnage, G. W., "Performance of Soils Under Track Loads, Report 1 - Model Track and Test Program", Technical Report M-71-5, U. S. Army Engineer WES, July, 1971.

156. Turnage, G. W., "Performance of Soils Under Track Loads, Report 2 - Prediction of Track Pull Performance in a Desert Sand", Technical Report M-71-5, U. S. Army Engineer WES, November, 1971.

157. Turnage, G. W., "Performance of Soils Under Track Loads, Report 3 - Track Mobility Number for Coarse-Grained Soils", Technical Report M-71-5, U. S. Army Engineer WES, May, 1976.

158. Turnage, G. W., "Using Dimensionless Prediction Terms to Describe In-Soil Tracked Performance", Transactions of the ASAE, 1973.

159. Turnbull, S. R. and Fawcett, J. N., "Dynamic Behavior of Roller Chain Drives", The Institution of Mechanical Engineers, Mechanisms 1972 Conference, September 6, 1972.

160. Uffelmann, F. L. and Evans, I. "The Performance of Heavy Tracked Vehicles on Soft Cohesive Soil", Journal of Terramechanics, 1965, Vol. 2, No. 2.

161. U. S. Army Test and Evaluation Command Test Operation Procedure, "Vehicle Test Course Severity", U. S. Army APG, AMCR 310-6, April 12, 1976.

162. Ustic, Dan, "Feasibility Analysis of Track Pulse Equalizing Mechanism", about 1970.

163. Van Cauwenberg, P. H. (1st author), "New Developments in Track and Suspension Systems", American Ordnance Association, Technical Division Reports, March, 1962.

164. Van Deusen, B. D., "A Study of the Vehicle Ride Dynamics Aspect of Ground Mobility - Volume III - Theoretical Dynamic Aspects of Vehicle Systems", U. S. Army Engineer WES, Report No. 3-114, April, 1965.

165. Van Wyk, T. B., "Noise Reduction From Sprocket and Idler Modifications, MICV XM723 Test Report", Technical Report 2977, Contract DAAE07-73-C-0100, FMC Corporation, February 24, 1976.

166. Veroeven, W. M. and McGarvey, J. W., "Polyurethane Vulcanizates for Track Pad Application", Rock Island Arsenal Laboratory, Report No. 64-3579, December 21, 1964.

167. Vodyanik, I. I., "The Motion of a Tracked Vehicle on Deformable Ground", Journal of Terramechanics, 1966, Volume 3, No. 1.

168. Weihs, H., "Experience in the Utilization of Tracks with Closed Links", Militaertechnik, No. 1, 1975, January, 1975.

169. Weihs, H., "Experience with Double-Pin Tank Tracks", Militaertechnik, January, 1975.

170. Whitlock, K. H., "Mechanical Performance of Polyester Elastomers", Plastica, 26 (1973) 10.

171. Wilson, Nuttall and Raimond, "Stress Studies of the T-142 and T-97 Tracks", March, 1966.

172. Wilson, Nuttall and Raimond, "Stress and Load Studies of the T-142 Track", June, 1967.

173. Wilson, Nuttall and Raimond, "Studies of Stresses in and Loads on the T-142 Track While in Operation (Part 2), September, 1970.

174. Wollam, Joe, "Omega Correlation", Technical Report No. 11429, TACOM MSL, September, 1971.

175. Zastera, R. J., Engineering Design Handbook, Automotive Series, Automotive Bodies and Hulls, AMC Pamphlet 706-357, April, 1970.

176. Zastera, R. J., Engineering Design Handbook, Automotive Series, Automotive Suspensions, AMC Pamphlet 706-356, April, 1967.

APPENDIX C

TRACKDYNE PROGRAM

APPENDIX C. TRACKDYNE PROGRAM

Structure of Run

In response to each control card, the simulation will be run at the requested speed and tension for an integral number of pitch-passage cycles that may be varied from one to any requested number. If this run is a continuation of a previous run, initial conditions may be read from a data deck and the cycle numbers will begin where the previous run left off, the data produced being the same as if there had been no interruption. Otherwise, initial conditions will be calculated to begin cycle number one. Each cycle is divided into 100 equal time increments called stations. Each station interval is divided into a requested number of equal time increments over which the integrations are performed. For efficient operation, the number of integration steps per station should be varied with track velocity to keep the integration interval an approximately constant time period. For instance, 10 steps per station have been found adequate for satisfactory accuracy at 35 mph, and 5 steps per station gives comparable accuracy at 70 mph.

During the last cycle requested, data describing the state of the system is available at each station interval. Data can be printed at every other station. Calcomp plots can be made if requested. At the end of the last cycle, the state of the system can be punched into a deck of cards if requested. This deck serves as an initial condition deck if it is desired to continue the run at some later time. If the run is to be continued immediately by another control card, an initial condition deck is not required. The energy balance is also based only on the last cycle. Only a limited amount of data is printed at the end of the earlier cycles.

A typical set up might be to run for ten cycles and plot so that the degree to which transients have settled may be observed, then to continue to the fifteenth cycle and plot again, this time punching an initial condition deck so that the run can be further continued if the plots indicate it is still unsettled.

Any number of control cards may be submitted. The integration interval may be changed when a run is continued. If any dimensions or other specifications of the system are to be changed, the entire system data deck must be read in again.

Speed and Tension Control

Since the 23-link system is removed from the rest of the track circuit, artificial means must be used to cause the simulation to operate at the requested speed and apparent tension at the inlet point, which is in mid span. Speed is determined at the inlet point by causing Connector 1 to move in a straight line at the desired velocity. The path of Connector 1 is offset from the straight-line tangent at speeds below the transition point by an amount calculated by the initial condition section of the program.

Tension is determined by a constant force and moment applied to the 23rd shoe, which is on the road wheel. When setting these forces, the initial condition program must estimate the centrifugal tension, the difference between tension on the wheels and on the straights, and the energy losses in the system. The results are necessarily approximate, since much of this information is to be determined by the run. Consequently, the desired apparent tension at the inlet is not exactly achieved. The program averages inlet tension during the last cycle and prints out the value actually occurring.

Shoe-to-Wheel Contact Model

Four elements are taken to be in parallel: a linear spring of rate SW1, a spring whose force varies as the square of deflection times SW2, a viscous damper having coefficient CD2, and a modified dry damper producing force FDD. In series with the dry damper is also a stiff viscous damper having coefficient CD1. The dry damper is modified in that, for deflections less than a threshold value in the neighborhood of .080 inch, its force is made proportional to deflection. In other words, the dry damper force is the minimum of FDD or CDD times deflection.

The characteristics of the real system are reproduced primarily by the square rate spring and the dry damper. Since the contact situation is either a round wheel impinging on a flat shoe or a pointed shoe corner impinging on a relatively flat wheel, the area of contact increases with deflection and the spring force is more nearly a square function than linear. Damping characteristics are based on hysteresis tests made at Battelle using a cylindrical steel die representing the wheel in contact with a real track shoe. The energy absorbed per cycle was found to vary only a little with frequency, so that it is

represented by the dry damper with some variation with frequency provided by the viscous damper CD2. The shape of the experimental hysteresis curves suggested the modifications to the dry damper. It is also convenient in programming to have a system that will return itself to zero deflection when external force is removed. This is insured by the linear spring SW1, which should have a rate greater than CDD. The damper CD1 is also included as a programming convenience to avoid large step changes in force as the rate of change of deflection changes sign. Its coefficient is made high enough that it rarely influences the system. The numerical values used for normal contact between a wheel or idler and the center of the flat of the shoe are:

SW1 = 10,000 lb/in
SW2 = 95,000 lb/in^2
FDD = 1,300 lb
CDD = 8,125 lb/in
CD1 = 800 lb sec/in
CD2 = 20 lb sec/in .

The same model is used for tangential deflections, though the numerical parameters may be separately specified. In the absence of experimental data, all values were simply cut in half. While normal deflection can be calculated from the relative positions of the shoe and wheel, tangential deflection is an integrated variable that depends on the history of relative motion between the shoe and the wheel, and also upon any sliding that may occur. The coefficient of friction between shoe and wheel is specified on the control card, and has been taken to be .80 in all runs. When sliding occurs or when the shoe is out of contact with the wheel, the rate of change of tangential deflection is controlled by the dampers.

System parameters are taken to be independent of the location of the center of contact on the shoe so long as it is no farther from the center of the flat than DS1, taken to be 1.0 inch. As the center of contact moves from DS1 to the edge of the flat, parameters vary linearly to another set of values that are specified for contact at the edge. In the absence of experimental data, all values were reduced to 0.4 times those given above. As the attitude of the shoe continued to vary, the parameters vary linearly to a third set of values that are specified for contact of the point of the shoe with the wheel. This condition is considered to be reached when the perpendicular

to the flat of the shoe through the center of the wheel passes farther from the center of the flat than DS3, taken to be 4.0 inches. (The flat has a half-width PSW of 3.02 inches.) In the absence of experimental data, parameters for point contact were taken to be 0.2 times the values given above.

Bushing Model

The tensile spring rate of the track is represented in the program as radial deflection of the bushings. Based on experiments at TARADCOM, the value used was 740,000 lb/in for the bushings associated with one pin across the width of the track. The torsional spring rate was determined for a used track shoe under laboratory conditions at Battelle as 24,350 in lb/radian.

In the absence of experimental data, damping was assumed to be viscous and values were set to give coefficients of restitution on the order of 80% for representative conditions of energy input. In torsion, the rate of flexing was taken to be the angular velocity of a wheel at 50 mph. In tension, energy was considered to be stored by stretching the track to 40,000 lb tension during pitch passage interval at 50 mph. This yielded damping values of 3.6 inch lb sec/rad and 290 lb sec/in. Early experience with the simulation suggested that the system was not sufficiently damped, so these values were arbitrarily increased to 7.2 in lb sec/rad and 500 lb sec/in. Data from a properly-instrumented bushing texting machine would be very helpful in setting these parameters.

Data Deck

The structure of the data deck is as follows:

(1) Control card for first run
(2) System data deck for first run
(3) Initial condition deck for first run (if required)
(4) Control card for 2nd run
(5) System data deck for 2nd run (if different from first)
(6) Initial condition deck for 2nd run (if required)
(7) Control card for 3rd run, etc.

The control card is punched in the format (3F10.3, 6I4) with the following information:

(1) Speed of vehicle, mph

(2) Apparent tension at mid span approaching idler, lb

(3) Coefficient of friction between track shoes and idler or road wheel

(4) Number of integration intervals per station

(5) Number of last cycle to be run. (Cycle numbering starts at the cycle for which initial conditions were computed, not necessarily at the beginning of this run.)

(6) Control integer for data input, using the following code:

0 = Read in system, compute initial conditions

1 = Read in system, read in initial conditions

2 = Use system of run just completed, compute initial conditions

3 = Use system of run just completed, read in initial conditions

4 = Continue previous run .

(7) Control integer for card punch:

1 = Punch final conditions for use as an initial condition deck

2 = Do not punch

(8) Control integer for plotter:

1 = Plot last cycle

0 = Do not plot

(9) Control integer for continuing to additional runs:

0 = Stop after this run

1 = Continue to an additional control card, but shut off plotter

2 = Continue as is .

The system data deck contains 12 cards punched as follows, with numerical data given for T-142/M-60 system:

Card 1. Modification factors for computing initial conditions. Format (5F10.3)

(1) Modification factor applied to moment of inertia of links for use in continuous band equations, 0.65

(2) Modification factor applied to bushing torsional spring rate for use in continuous band equations, 1.25

3,4,5) Estimates of energy loss at entrance and exit of idler and at entrance of road wheel, respectively, 100 in lb/link each place.

Card 2. Track geometry. Format (8F10.6)

(1) Pitch length of shoe, 4.442 inch

(2) Pitch length of connector, 2.500 inch

(3) Mass of shoe, 0.1316 lb sec^2/in.

(4) Mass of connector, .0648 lb sec^2/in.

(5) Moment of inertia of shoe, 0.526 in lb sec^2/rad

(6) Moment of inertia of connector, 0.1095 in lb sec^2/rad

(7) Distance from plane of pin centerlines to center of mass of shoe, 0.7 inch

(8) Distance from plane of pin centerlines to wheel-contact flat, 1.69 inches .

Card 3. Track geometry continued. Format (3F10.6)

(1) Distance from center of flat to point where wheel contact parameters begin to change (DS1 described above), 1.00 inch

(2) Half-width of flat, 3.02 inch

(3) DS3 (described above), 4.00 inch .

Card 4. Track circuit geometry. Format (8F10.4)

(1) Radius of idler, 13.00 inch

(2) Moment of inertia of idler, 45.0 in lb sec^2/rad

(3) X coordinate of idler center, 0.0 inch

(4) Y coordinate of idler center, 0.0 inch

(5) Radius of front road wheel, 13.00 inch

(6) Moment of inertia of front road wheel, 45.0 in lb sec^2/rad

(7) X coordinate of front road wheel, -30.732 inch

(8) Y coordinate of front road wheel, -24.010 inch

Card 5. Track circuit geometry continued. Format (6I4,F8.2)

(1) Number of first shoe to be checked for contact with idler, 7

(2) Number of last shoe to be checked for contact with idler, 14

(3) Number of first shoe to be checked for contact with front road wheel, 17

(4) Number of last link, 23

(5) Number of link to be monitored for offset of Span 1, 6

(6) Number of link to be monitored for offset of Span 2, 15

(7) X coordinate of dummy wheel for establishing entrance span to idler in initial condition calculations, -96.6 inch .

Card 6. Rubber bushing parameters. Format (2F10.I,3F10.5)

(1) Radial spring rate of one pin and bushing assembly, 740,000 lb/in

(2) Torsional spring rate of one pin and bushing assembly, 24,350 in lb/rad

(3) Angle of articulation between shoe and connector when bushing is at zero torque, 0.143 rad

(4) Coefficient of viscous damping in radial direction, 500 lb sec/in

(5) Torsional damping coefficient, 7.2 in lb sec/rad .

Card 7. Shoe-to-wheel contact parameters at center of flat. Format (8F10.2).

(1) SW1 in normal direction, 10,000 lb/in

(2) SW1 in tangential direction, 5,000 lb/in

(3) SW2 in normal direction, 95,000 lb/in^2

(4) SW2 in tangential direction, 47,500 lb/in^2

(5) FDD in normal direction, 1300 lb

(6) FDD in tangential direction, 650 lb

(7) CDD in normal direction, 8125 lb/in

(8) CDD in tangential direction, 4062 lb/in .

Card 8. Shoe-to-wheel contact parameters at center of flat, continued. Format (4F10.5).

(1) CD1 in normal direction, 800 lb sec/in

(2) CD1 in tangential direction, 400 lb sec/in

(3) CD2 in normal direction, 20.0 lb sec/in

(4) CD2 in tangential direction, 10.0 lb sec/in .

Cards 9 and 10. Shoe-to-wheel contact parameters at edge of flat. Format same as Cards 7 and 8. Values reduced by factor of 0.4.

Cards 11 and 12. Shoe-to-wheel contact parameters for point contact. Format same as Cards 7 and 8. Values reduced by factor of 0.2.

The initial condition deck is a 96-card set punched by the program, and does not require manipulation by the operator. The number of the last cycle run may be read from Columns 4 and 5 of the first card.

APPENDIX D

PINSTRESS II

APPENDIX D. PINSTRESS II

Objectives

The system considered by the PINSTRESS analysis is the pin, bushing, and tube assembly associated with one end of one pin. There are four such systems per track link, related to one another by the continuity of the pins through the center of the track, by the movements and deflections of the shoes, end connectors, and centerguides, and by the forces transmitted through these parts. Structural analysis of a number of links considered simultaneously is, in general, required to define the forces and stresses at any point in the track. The objectives of the PINSTRESS analysis are to define the PINSTRESS system so that it may be treated as a single element in the structural analysis, and to provide a method for calculating pin stresses and bushing loads, once the forces or deflections imposed on the system are known.

As noted in the text, there are a few symmetrical loading situations where the structural analysis becomes trivial. The PINSTRESS analysis alone is then adequate for calculating pin stresses and bushing loads.

Definition of System

Consider the pin, bushing, and tube assembly for one side of the track as shown in Figure D-1. The pin is taken to be free to bend over a span u between effective anchor points where the end forces and moments are applied. The tube and the rubber bushing are taken to extend over a span r which is less than u and centered within it. The X axis is taken tangent to the pin at its effective anchor point in the centerguide, with positive direction toward the end connector. The y axis is taken at the center of the span, with positive direction toward the shoe.

The resultant of all forces applied to the tube by the shoe is taken to be a force F_s acting along the y axis and a moment M_s as shown. (The shoe can also apply a force in the X direction which causes shearing deflection of the bushing, but this is independent of the bending analysis and may be handled as part of the structural analysis.) The end connector applied a force F_e in the negative y direction at $X = u/2$, and a moment M_e as shown. (There is also a force in the X direction that causes axial compression of the pin; this too can be handled separately.) Assuming the shoe body to be defined by the tube

ends, the system responds with a displacement of the shoe relative to the centerguide that corresponds to track stretching, a rotation $_s$ of the shoe body that is a component of structural warpage, a displacement of the end connector relative to the centerguide that is another component of structural warpage, and a rotation $_e$ of the pin end that is related to, but not equal to, end connector rotation.

The analysis can also be applied in the plane perpendicular to the track, with suitable interpretation of the deflections.

Assumptions

(1) The rubber bushing acts as a linear spring having the same rate per unit length everywhere within span r.

(2) The effective anchor points of the pin ends are 0.5 inches inside the bodies of the end connector and the centerguide.

(3) Deflections are small compared to the dimensions of the system.

(4) The bending deflection of the tube is of the form

$$y_T = y_{OT}\left(1 - \frac{4x^2}{r^2}\right)$$

where the deflection at the center of the tube is given by

$$y_{oT} = \frac{\partial y_{oT}}{\partial \delta}\delta + \frac{\partial y_{oT}}{\partial \theta_e}\theta_e + \frac{\partial y_{oT}}{\partial \Delta}\Delta$$

and the stiffness of the tube and its end constraint by the binocular plates is defined by

$$\frac{1}{K_T} = \left.\frac{\partial y_{oT}}{\partial F_s}\right|_{\theta_e = 0,\ \Delta = 0}$$

(5) Deflections of the system are energy conservative, so that

$$\frac{\partial F_e}{\partial \delta} = -\frac{\partial F_s}{\partial \Delta}$$

$$\frac{\partial M_e}{\partial \delta} = \frac{\partial F_s}{\partial \theta_e}$$

$$\frac{\partial F_e}{\partial \theta_s} = -\frac{\partial M_s}{\partial \Delta}$$

Numerical Definitions

The system, then, can be specified by the following parameters, with numerical values given as used for the T-97 track:

Pin span u, 11.95 in

Rubber span r, 10.94 in

Pin moment of inertia I, 0.1139 in^4

Pin modulus of elasticity E, 30×10^6 psi

Rubber spring rate K_R, 56,400 lb/in^2

Tube spring rate K_T, 1.647×10^6 lb/in .

Summary of Results

Define the simplifying constant

$$a = \sqrt[4]{\frac{K_R}{4EI}}$$

Then the deflection of the pin at any point within the span r is of the form

$$y = A \sinh ax \sin ax + B \sinh ax \cos ax + C \cosh ax \sin ax + D \cosh ax \cos ax + \zeta + \theta_s X - y_{OT}\left(1 - \frac{4x^2}{r^2}\right) \quad \text{(D-1)}$$

where A, B, C, D, and y_{OT} are constants to be calculated below. The bending moment in the pin at any point within the span r is given by

$$M = 2EIa^2 \left\{ A \cosh ax \cos ax - B \cosh ax \sin ax + C \sinh ax \cos ax - D \sinh ax \sin ax + \frac{4\, y_{OT}}{a^2 r^2} \right\} \quad \text{(D-2)}$$

and the bushing load at any point within the span r is

$$f = K_R \left\{ A \sinh ax \sin ax + B \sinh ax \cos ax + C \cosh ax \sin ax + D \cosh ax \cos ax \right\}$$

Define simplifying nondimensional constants as follows: (numerical values for T-97)

$$\psi_1 = \sinh\frac{a\lambda_1}{2}\sin\frac{a\lambda_1}{2} - \cosh\frac{a\lambda_1}{2}\cos\frac{a\lambda_1}{2} \quad (2.2931)$$

$$\psi_2 = \sinh\frac{a\lambda_2}{2}\sin\frac{a\lambda_2}{2} - \cosh\frac{a\lambda_2}{2}\cos\frac{a\lambda_2}{2} \quad (1.4536)$$

$$\psi_3 = \sinh\frac{a\lambda_2}{2}\cos\frac{a\lambda_2}{2} + \cosh\frac{a\lambda_2}{2}\sin\frac{a\lambda_2}{2} \quad (2.4330)$$

$$\psi_4 = \sinh\frac{a\lambda_1}{2}\cos\frac{a\lambda_1}{2} - \cosh\frac{a\lambda_1}{2}\sin\frac{a\lambda_1}{2} \quad (-1.7452)$$

$$\beta_1 = \psi_2 + \frac{a}{2}(u-\lambda_1)(\psi_3-\psi_4) - \frac{a^2}{4}(u-\lambda_1)^2\psi_1 \quad (2.0250)$$

$$\beta_2 = \psi_1 + \frac{a}{2}(u-\lambda_1)(\psi_3+\psi_4) - \frac{a^2}{4}(u-\lambda_1)^2\psi_2 \quad (2.2975)$$

$$\beta_3 = \psi_4 - \frac{a}{2}(u-\lambda_1)(\psi_1-\psi_2) - \frac{a^2}{4}(u-\lambda_1)^2\psi_3 \quad (-2.2569)$$

$$\beta_4 = \psi_3 + \frac{a}{2}(u-\lambda_1)(\psi_1-\psi_2) - \frac{a^2}{4}(u-\lambda_1)^2\psi_4 \quad (2.5042)$$

$$\beta_5 = \psi_3 - \psi_4 - \frac{a^2}{4}(u-\lambda_1)^2(\psi_3-\psi_4) - \frac{a^3}{6}(u-\lambda_1)^3\psi_1 \quad (0.7625)$$

$$\beta_6 = \psi_3 - \psi_4 - \frac{a^2}{4}(u-\lambda_1)^2(\psi_3+\psi_4) - \frac{a^3}{6}(u-\lambda_1)^3\psi_2 \quad (4.1710)$$

$$\beta_7 = \psi_1 - \psi_2 + \frac{a^2}{4}(u-\lambda_1)^2(\psi_1+\psi_2) + \frac{a^3}{6}(u-\lambda_1)^3\psi_3 \quad (0.8467)$$

$$\beta_8 = \psi_1 + \psi_2 - \frac{a^2}{4}(u-\lambda_1)^2(\psi_1-\psi_2) - \frac{a^3}{6}(u-\lambda_1)^3\psi_4 \quad (3.6798)$$

$$\gamma_2 = \frac{\psi_4\beta_7 + \psi_3\beta_8}{\psi_4\beta_2 + \psi_3\beta_4} \quad (0.7449)$$

$$\gamma_3 = \frac{(\psi_1-\psi_2)\beta_7 - (\psi_1+\psi_2)\beta_8}{\psi_4\beta_3 - \psi_3\beta_4} \quad (1.4178)$$

$$\gamma_4 = \frac{\beta_4\beta_7 - \beta_3\beta_8}{\psi_4\beta_3 + \psi_3\beta_4} \qquad (1.0390)$$

$$\gamma_{12} = \frac{\psi_1\beta_6 - \psi_2\beta_5}{\psi_1\beta_2 + \psi_2\beta_1} \qquad (1.0164)$$

$$\gamma_{13} = \frac{(\psi_3 - \psi_4)\beta_2 + (\psi_3 + \psi_4)\beta_5}{\psi_1\beta_2 + \psi_2\beta_1} \qquad (2.2235)$$

$$\gamma_{14} = \frac{\beta_1\beta_6 + \beta_2\beta_5}{\psi_1\beta_2 + \psi_2\beta_1} \qquad (1.2631)$$

then

$$\beta_\Delta = -\frac{1}{\gamma_4 a \frac{K_T}{K_K} + \frac{4}{a^2\lambda^2}\left[a\mu\gamma_2 + \frac{a^2}{2}(\mu-\lambda)^2\right]} \qquad (-0.1128^2) \qquad (D\text{-}4)$$

$$\beta_e = \frac{\beta_\Delta}{2}\left\{\frac{2\gamma_4 - a\mu\left[\gamma_3 - a(\mu-\lambda)\gamma_2\right] - \frac{a^2}{2}(\mu-\lambda)^2\left[\gamma_2 + a(\mu-\lambda)\right]}{a\mu\gamma_2 + \frac{a^2}{2}(\mu-\lambda)^2}\right\}$$

$$(.06454)$$

$$\chi_e = \frac{\left\{\begin{array}{l}\gamma_2^2 - \gamma_3 - \frac{8\beta_8}{a^2\lambda^2}\left[a\mu(\gamma_2^2 - \gamma_3) + 2\gamma_4\right] \\ \quad - \frac{4\beta_4}{a^2\lambda^2}\left[2\gamma_4(\gamma_2 + a(\mu-\lambda)) + \frac{a^2}{2}(\mu^2-\lambda^2)(\gamma_2^2 - \gamma_3)\right]\end{array}\right\}}{a\mu\gamma_2 - \frac{a^2}{2}(\mu-\lambda)^2}$$

and

$$\nu_{OT} = -\beta_\Delta(2\zeta - \Delta) - \frac{\beta_e}{\chi_e}\zeta_2$$

$$A = \frac{\left\{ \begin{array}{l} \frac{\theta_2}{2a}\left[\beta_7\left(1 - \frac{8\mu}{a\lambda^2}\beta_8\right) - \beta_3\left(a(u-\lambda) - 4\beta_8\left(\frac{u-\lambda}{\lambda}\right)^2\right)\right] \\ +(26-\Delta)\left[\beta_3\left(1 + 2\beta_\Delta\left(\frac{u-\lambda}{\lambda}\right)^2\right) - \beta_7\frac{4\mu}{a\lambda^2}\beta_\Delta\right] \end{array} \right\}}{\beta_4\beta_7 - \beta_3\beta_8} \quad \text{(D-5)}$$

$$B = \frac{\frac{1}{a}\left(\theta_3 - \frac{\theta_2}{2}\right)\left[\beta_6 - a\lambda\beta_2\right] + \left(\Delta - \frac{\mu}{2}\theta_2\right)\beta_2}{\beta_2\beta_5 + \beta_1\beta_6} \quad \text{(D-6)}$$

$$C = \frac{-\frac{1}{a}\left(\theta_3 - \frac{\theta_2}{2}\right)\left[\beta_5 - a\lambda\beta_1\right] + \left(\Delta - \frac{\mu}{2}\theta_2\right)\beta_1}{\beta_2\beta_5 + \beta_1\beta_6} \quad \text{(D-7)}$$

$$D = -\frac{\left\{ \begin{array}{l} \frac{\theta_2}{2a}\left[\beta_8\left(1 - \frac{8\mu}{a\lambda^2}\beta_8\right) + \beta_4\left(a(u-\lambda) - 4\beta_8\left(\frac{u-\lambda}{\lambda}\right)^2\right)\right] \\ +(26-\Delta)\left[\beta_4\left(1 + 2\beta_\Delta\left(\frac{u-\lambda}{\lambda}\right)^2\right) + \beta_8\frac{4\mu}{a\lambda^2}\beta_\Delta\right] \end{array} \right\}}{\beta_4\beta_7 - \beta_3\beta_8} \quad \text{(D-8)}$$

The forces returned to the track structure in response to imposed displacements are as follows:

$$F_3 = \frac{4EIa^3}{\gamma_4}\left\{ \frac{\theta_2}{2a}\left[\gamma_2 - a(u-\lambda) - \frac{8\beta_8}{a\lambda^2}\left(au\gamma_2 + \frac{a^2}{2}(u-\lambda)^2\right)\right] \right. \quad \text{(D-9)}$$

$$\left. +(26-\Delta)\left[1 + \frac{4\beta_\Delta}{a^2\lambda^2}\left(au\gamma_2 + \frac{a^2}{2}(u-\lambda)^2\right)\right]\right\}$$

$$F_2 - \frac{F_3}{2} = \frac{2EIa^3}{\gamma_{14}}\left\{\frac{1}{a}\left(\theta_3 - \frac{\theta_2}{2}\right)\left(a\lambda - \gamma_{12}\right) - \left(\Delta - \frac{\mu}{2}\theta_2\right)\right. \quad \text{(D-10)}$$

$$M_3 = \frac{2EIa^2}{\gamma_{14}}\left\{\frac{1}{a}\left(\theta_3 - \frac{\theta_2}{2}\right)\left(\gamma_{13} - 2a\lambda\gamma_{12} - a^2\lambda^2\right)\right. \quad \text{(D-11)}$$

$$\left. -\left(\Delta - \frac{\mu}{2}\theta_2\right)\left(\gamma_{12} - a\lambda\right)\right\}$$

$$2M_e + M_s - u\left(F_e - \frac{F_s}{2}\right) - \frac{u-r}{2} F_s = M_e - M_c$$

$$= \frac{2EIa^2}{\gamma_4}\left\{\frac{\delta_e}{2a}\left[\gamma_3 - \gamma_2 a(u-r) + \frac{9\beta_2}{a^2 r^2}\left(2\gamma_4 - au\gamma_3 - \frac{a^2}{2}(u-r)^2\gamma_2\right)\right]\right.$$

$$\left. - (2\delta - \Delta)\left[\gamma_2 - \frac{4\beta_\Delta}{a^2 r^2}\left(2\gamma_4 - au\gamma_3 - \frac{a^2}{2}(u-r)^2\gamma_2\right)\right]\right\} \qquad \text{(D-12)}$$

The displacements of the system in response to forces applied by the track structure are as follows:

$$\delta_e = \frac{\gamma_4}{2EIa^2 x_e}\left\{F_s\left[\frac{\gamma_2 + a(u-r)}{au\gamma_2 + \frac{a^2}{2}(u-r)^2} - \frac{8\beta_2}{a^2 r^2}\right]\right.$$

$$\left. - 2a(M_e + M_c)\left[\frac{1}{au\gamma_2 + \frac{a^2}{2}(u-r)^2} + \frac{4\beta_\Delta}{a^2 r^2}\right]\right\} \qquad \text{(D-13)}$$

$$\delta_s - \frac{\theta_e}{2} = \frac{\gamma_{14}}{2EIa^2}\left\{\frac{-M_s a + (F_e - \frac{F_s}{2})(ar - \gamma_{12})}{\gamma_{12}^2 - \gamma_{13}}\right\} \qquad \text{(D-14)}$$

$$\Delta - \frac{u}{2}\theta_e = \frac{\gamma_{14}}{2EIa^3}\left\{\frac{-M_s a(ar - \gamma_{12}) + (F_e - \frac{F_s}{2})(\gamma_{13} - 2ar\gamma_{12} - a^2 r^2)}{\gamma_{12}^2 - \gamma_{13}}\right\} \qquad \text{(D-15)}$$

$$2\delta - \Delta = \frac{\gamma_4}{4EIa^3 x_e}\left\{-F_s\left[\frac{\gamma_3 + 2a(u-r)\gamma_2 + a^2(u-r)^2}{au\gamma_2 + \frac{a^2}{2}(u-r)^2} + \frac{16\beta_2^2}{a^2 r^2 \beta_\Delta}\right]\right. \qquad \text{(D-16)}$$

$$\left. + 2a(M_e + M_c)\left[\frac{\gamma_2 + a(u-r)}{au\gamma_2 + \frac{a^2}{2}(u-r)^2} - \frac{8\beta_c}{a^2 r^2}\right]\right\}$$

Outline of Derivation

By reference to Figure D-1, it can be seen from simple geometry and Assumption 4 that the force per unit length applied to the pin at any point X within the span r is given in terms of the pin deflection g(x) and the rubber spring rate K_R

$$f(X) = K_R\left[\delta + \theta_s X - y_{OT}\left(1 - \frac{4X^2}{r^2}\right) - y\right]$$

where the tube deflection y_{OT} is taken to be positive when the tube deflects in the negative y direction (toward the pin). Outside the span r, the applied force is zero. Consequently, the moment in the pin anywhere within span r is

$$M = M_e - F_e\left(\frac{d}{2} - X\right) + \int_X^{\frac{r}{2}} f(X')(X'-X)\,dX'$$

Putting this into the well-known beam

$$EI\frac{d^2y}{dX^2} = M$$

and differentiating twice, we have

$$EI\frac{d^4y}{dX^4} = f(X) \qquad \text{(D-17)}$$

$$\frac{d^4y}{dX^4} + \frac{K_R}{EI}y = \frac{K_R}{EI}\left[\delta - \theta_s X - y_{OT}\left(1 - \frac{4X^2}{r^2}\right)\right]$$

The solution is given by Equation D-1, which is valid within the span r and contains the five unknown constants A, B, C, D, and y_{OT}. These may be determined from boundary conditions at the ends and from Assumptions 4 and 5.

The slope of the deflection curve, the moment, and the shear force in the pin at any point in the span r may be found by successive differentiations of Equation D-17. At the left end of the span, in particular, X = r/2 and

$$y = \frac{1}{2}\left[A(\psi_1+\psi_2) - B(\psi_3+\psi_4) + C(\psi_3-\psi_4)\right.$$
$$\left. - D(\psi_1-\psi_2)\right] + \delta + \theta_s \frac{r}{2}$$
$$\frac{du}{dx} = \alpha\left[A\psi_3 - B\psi_2 + C\psi_1 - D\psi_4\right] + \theta_s - \frac{\Delta u_{pT}}{r}$$
$$M = EI\alpha^2\left[A(\psi_1-\psi_2) - B(\psi_3-\psi_4) - C(\psi_3+\psi_4)\right.$$
$$\left. - D(\psi_1+\psi_2)\right] + 8EI\frac{u_{pT}}{r^2}$$
$$F = 2EI\alpha^3\left[A\psi_4 - B\psi_1 - C\psi_2 - D\psi_3\right]$$

Considering now the beam span from r/2 to u/2, the only loads are at the ends, and for X = r/2 we have

$$y = \Delta - \theta_e\left(\frac{u-r}{2}\right) + \frac{M}{2EI}\left(\frac{u-r}{2}\right)^2 - \frac{F}{3EI}\left(\frac{u-r}{2}\right)^3$$

$$\frac{du}{dx} = \theta_e - \frac{M}{EI}\left(\frac{u-r}{2}\right) - \frac{F}{2EI}\left(\frac{u-r}{2}\right)^2$$

where the moment and force are given above. For continuity of the pin, deflection and slope at X = r/2 must be the same for both beam segments. Equating the above expressions yields two boundary equations on the four constants:

$$\beta_3 A + \beta_5 B + \beta_6 C + \beta_7 D = 2\Delta - 2\delta - \theta_e r - (u-r)\theta_e + 2\left(\frac{u-r}{r}\right)^2 \frac{r}{2} y_{pT}$$

$$\beta_4 A - \beta_1 B - \beta_2 C + \beta_3 D = \frac{1}{\alpha}(\theta_e - \theta_s) - \frac{\Delta u}{r^2} y_{pT}$$

Similarly at the other end of the central span, the beam segment from -u/2 to -r/2 must yield consistent deflection and slope at X = -r/2. The resulting boundary equations are

$$\beta_3 A - \beta_5 B - \beta_6 C - \beta_7 D = -2\delta + \theta_s \frac{}{} + 2\left(\frac{u-r}{r}\right)^2 y_{0T}$$

$$\beta_4 A + \beta_1 B - \beta_2 C - \beta_3 D = \frac{1}{a}\theta_s - \frac{4u}{ar^2} y_{0T}$$

Simultaneous solution of these four boundary equations yields the asymmetrical components of the solution, B and C, in terms only of the externally applied displacements, as given by Equations D-6 and D-7. A and D, however, still contain the unknown y_{0T}:

$$A = \frac{\left\{\frac{\theta_e}{2a}\left[\beta_1 + a(u-r)\beta_3\right] - \frac{4u y_{0T}}{a^2 r^2}\left[2u\beta_7 - \frac{a^2}{2}(u-r)^2\beta_3\right] + (2\delta - \Delta)\beta_3\right\}}{\beta_4\beta_7 - \beta_3\beta_5} \qquad \text{(D-18)}$$

$$D = \frac{\left\{-\frac{\theta_e}{2a}\left[\beta_3 + a(u-r)\beta_4\right] + \frac{4u y_{0T}}{a^2 r^2}\left[2u\beta_8 + \frac{a^2}{2}(u-r)^2\beta_4\right] - (2\delta - \Delta)\beta_4\right\}}{\beta_4\beta_7 - \beta_3\beta_5} \qquad \text{(D-19)}$$

The tube deflection will now be determined. By equilibrium, the shoe force is given in terms of pin shear force as

$$F_s = F\Big|_{\frac{r}{2}} - F\Big|_{-\frac{r}{2}} = 4EIr^3(\beta_4 A - \beta_2 C)$$

Substituting from Equations D-18 and D-19,

$$F_e = \frac{8EIa^3}{\gamma_4}\left\{\delta - \frac{\Delta}{2} - \frac{\theta_e}{4a}\left[\gamma_2 - a(u-r)\right] - \frac{2\nu_{ot}}{a^2\gamma_2^2}\left[a\sin\gamma_2 + \frac{a^2}{2}(u-r)^2\right]\right\} \tag{D-20}$$

$$\frac{\partial F_e}{\partial \delta} = \frac{8EIa^3}{\gamma_4}\left\{1 - \frac{2}{a^2\gamma_2^2}\left[a\sin\gamma_2 + \frac{a^2}{2}(u-r)^2\right]\frac{\partial \nu_{ot}}{\partial F_e}\bigg|_{a,\theta_e}\frac{\partial F_e}{\partial \delta}\right\}$$

$$= \frac{2K_R}{a\gamma_4}\left\{1 - \frac{2}{a^2\gamma_2^2}\left[a\sin\gamma_2 - \frac{a^2}{2}(u-r)^2\right]\frac{1}{K_T}\frac{\partial F_e}{\partial \delta}\right\}$$

$$= \frac{1}{\frac{a\gamma_4}{2K_R} + \frac{2}{a^2\gamma_2^2K_T}\left[a\sin\gamma_2 + \frac{a^2}{2}(u-r)^2\right]}$$

$$= -2\beta_\Delta K_T$$

$$\frac{\partial \nu_{ot}}{\partial \Delta} = \frac{\partial \nu_{ot}}{\partial \theta}\bigg|_{\theta_e,\Delta}\frac{\partial \theta_e}{\partial \Delta} \tag{D-21}$$

$$\frac{\partial \nu_{ot}}{\partial \theta} = -2\beta_\Delta$$

By equilibrium of the span from r/2 to u/2, the end connector force F_e is equal to the shear in the pin at r/2:

$$F_e = 2EIa^3\left[\psi_4 A - \psi_1 B - \psi_2 C - \psi_3 D\right] \qquad \text{(D-22)}$$

$$F_e = 2EIa^3\left\{\frac{\theta_e}{2a}\left[\frac{\gamma_2 + a(u-2)}{\gamma_4} + \frac{\gamma_{12} - a(u-2)}{\gamma_{14}}\right]\right.$$
$$- \frac{\theta_3}{a}\left[\frac{\gamma_{12} - a2}{\gamma_{14}}\right] - \frac{4u_{3T}}{a^2\lambda^2\gamma_4}\left[au\gamma_2 + \frac{a^2}{2}(u-2)^2\right]$$
$$\left. - \varepsilon\frac{2}{\gamma_4} - \Delta\left(\frac{1}{\gamma_4} - \frac{1}{\gamma_{14}}\right)\right\}$$

$$\frac{\partial F_e}{\partial \delta} = \frac{4EIa^3}{\gamma_4}\left\{1 - \frac{2}{a^2\lambda^2}\left[au\gamma_2 - \frac{a^2}{2}(u-2)^2\right]\frac{\partial u_{3T}}{\partial \delta}\right\}$$

Also, from Equation D-20,

$$\frac{\partial F_e}{\partial \Delta} = -\frac{4EIa^3}{\gamma_4}\left\{1 + \frac{4}{a^2\lambda^2}\left[au\gamma_2 - \frac{a^2}{2}(u-2)^2\right]\frac{\partial u_{3T}}{\partial \Delta}\right\}$$

By Assumption 5, these expressions are equal except for sign. Consequently,

$$\frac{\partial u_{3T}}{\partial \Delta} = -\frac{1}{2}\frac{\partial u_{3T}}{\partial \delta} = \phi_3 \Delta \qquad \text{(D-23)}$$

Similarly, the end connector moment M_e may be found from equilibrium of the span from r/2 to u/2 and the moment in the pin at r/2:

$$M_e = EIa^2\left[A(\psi_1-\psi_2) - B(\psi_3-\psi_2) + C(\psi_3+\psi_4)\right. \tag{D-24}$$
$$\left. - D(\psi_1+\psi_2)\right] + \frac{8EI}{r^2}\frac{\partial y_{OT}}{\partial\theta} + F_e\frac{u-r}{2}$$

$$\frac{\partial M_e}{\partial\theta} = EIa^2\left[(\psi_1-\psi_2)\frac{\partial A}{\partial\theta} - (\psi_3-\psi_4)\frac{\partial B}{\partial\theta} + (\psi_3+\psi_4)\frac{\partial C}{\partial\theta}\right.$$
$$\left. - (\psi_1+\psi_2)\frac{\partial D}{\partial\theta}\right] + \frac{8EI}{r^2}\frac{\partial y_{OT}}{\partial\theta} + \frac{u-r}{2}\frac{\partial F_e}{\partial\theta}$$
$$= \frac{2EIa^2}{\gamma_4}\left\{\gamma_2 + a(u-r) - \frac{4B}{a^2r^2}\left[2\gamma_4 - au\left(\gamma_3 + a(u-r)\gamma_2\right)\right.\right.$$
$$\left.\left. - \frac{a^2}{2}(u-r)^2\left(\gamma_2 + a(u-r)\right)\right]\right\}$$

Again using Equation D-20,

$$\frac{\partial F_s}{\partial\theta_e} = \frac{2EIa^2}{\gamma_4}\left\{\gamma_2 + a(u-r) - \frac{a}{a^2r^2}\frac{\partial y_{OT}}{\partial\theta_e}\right.$$
$$\left.\left[au\gamma_2 - \frac{a^2}{2}(u-r)^2\right]\right\}$$

By Assumption 5, these expressions are equal. Consequently,

$$\frac{\partial y_{OT}}{\partial\theta_e} = \frac{1}{2}\frac{\partial F_e}{\partial\theta_e} \tag{D-25}$$

Equation D-4 for y_{OT} is obtained by substituting Equations D-21, D-23, and D-25 into the expression for y_{OT} found in Assumption 4. This expression for y_{OT} is then substituted into Equations D-18 and D-19 to obtain A and D as given by Equations D-5 and D-8. Substituted in Equation D-20, it yields Equation D-9 for F_s.

Equation D-10 may be obtained easily by noting that

$$F_e - \frac{F_3}{2} = -2EIa^2(\phi_1 \Xi - \nu_2 C)$$

Equation D-11 for M_s is obtained from the equilibrium equation

$$M_s = \frac{d}{2}(F_e - F_c) - (M_e - M_c)$$

The remaining manipulations are straightforward.

APPENDIX E

DESIGN OF LABORATORY MACHINE FOR BUSHING RESEARCH

APPENDIX E

DESIGN OF LABORATORY MACHINE FOR BUSHING RESEARCH

Track-Pin Bushing Laboratory Research Machine

The material in this appendix relating to the design of the laboratory research machine is organized as follows:

(1) Design Goals

(2) Analysis of Angular Position Servocontrol Circuit

(3) Analysis of Radial Force and Position Servocontrol Circuit

(4) General Requirements for Controllers

(5) Instrumentation and Signal Processing

(6) Detail Drawings of Laboratory Research Machine

Design Goals

- Angular Deflections: Variable, Servocontolled Cycles up to $\pm 22\frac{1}{2}$ degrees, rates up to 86 rad/s.
- Radial Loading: Variable, Servocontrolled Cycles between $\pm 25{,}000$ lbf maximum
- Temperature Regulated, Split Collet to House Bushing Specimen
- Fixturing to Accept a Range of Bushing Sizes up to 2-in. Pin Diameter
- Instrumented to Continuously Monitor
  - Bushing Torque
  - Angular Deflection
  - Radial Deflection
  - Collet Temperature
  - Various Operational Safety Checks

  and Record the Variation of These Quantities Throughout The Life of a Test
- Continuous, Unattended Operation.

Analysis of Angular Position Servocontrol Circuit

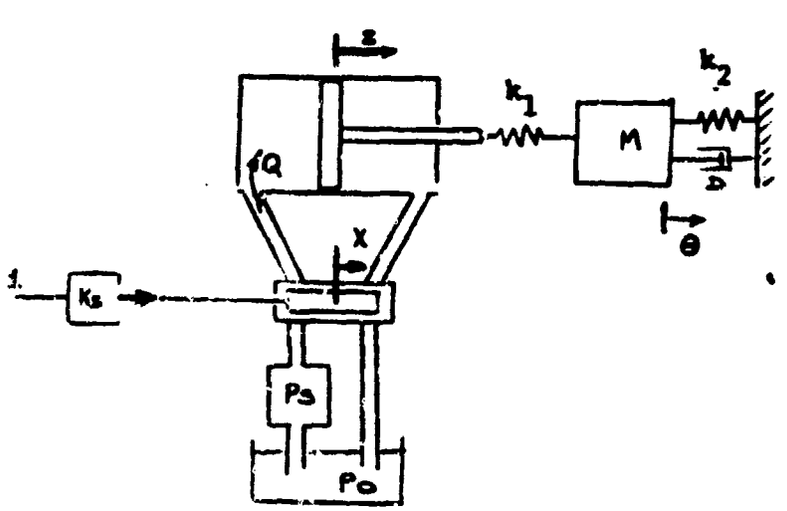

FIGURE E-1. SIMULATION MODEL REPRESENTING BUSHING MACHINE

Equations of State:

$$\frac{d^2\theta}{dt^2} = \frac{1}{J}\left(F_{k_1} - F_{k_2} - D\dot{\theta}\right)$$

$$\frac{dF_{k_2}}{dt} = k_2\dot{\theta}$$

$$\frac{d\dot{x}}{dt} = 2c\omega_n\dot{x} - \omega_n^2 x + k_s i$$

$$\frac{dF_{k_1}}{dt} = k_1\left(-\dot{\theta} - x\frac{Q_m}{A}\sqrt{\frac{P_s - P_d - F_{k_1}/A}{P_s}}\right)$$

$$\frac{dx}{dt} = \dot{x}$$

i = current to servovalve
x = valve spool position (-1 to +1)
k_s = scaling factor
P_s = supply pressure
P_d = drain pressure
Q = oil flow, Q_m = max rated valve flow
z = piston position
$\dot{x}$ = servovalve spool position
c = equivalent valve spool damping
k_1 = equivalent rotational oil compressibility spring constant
k_2 = bushing spring constant
D = bushing damping
θ = bushing position
J = equivalent linear inertia
A = piston area

Angular Position Control

Summary

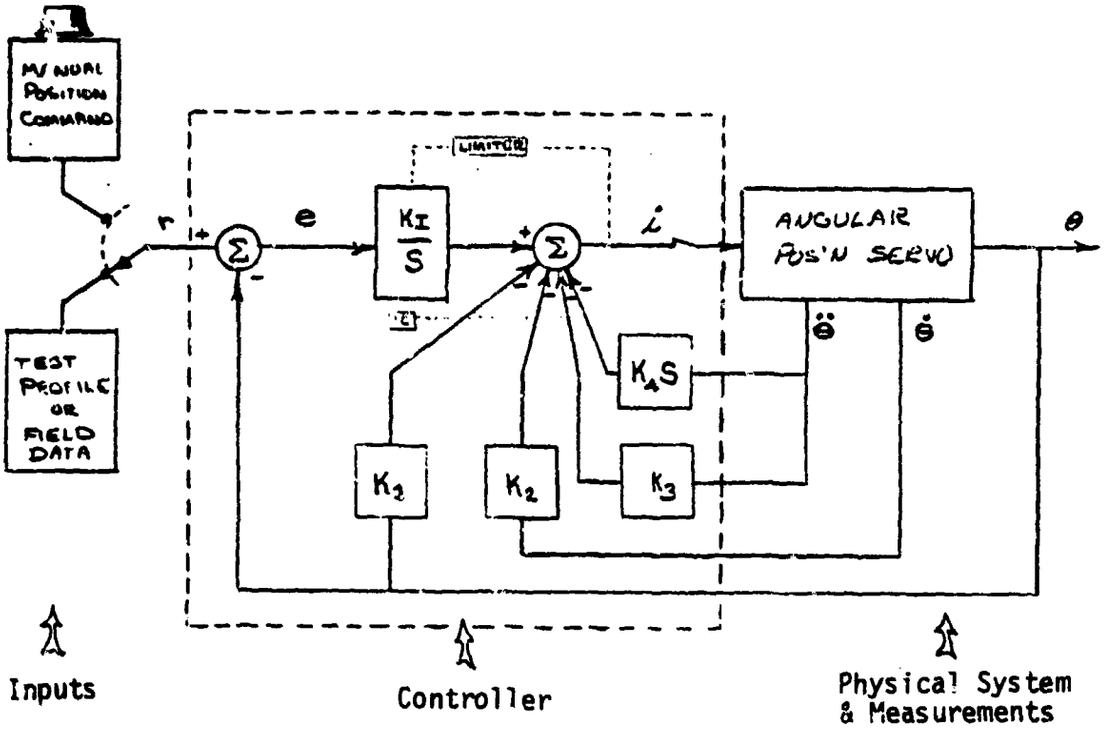

FIGURE E-2. SIMULATION MODEL REPRESENTING ANGULAR POSITION CONTROLLER

Symbols

r = reference input signal

θ = bushing angular pos'n

$\dot{\theta}$ = bushing angular velocity

$\ddot{\theta}$ = bushing angular acceleration

e = error signal ($r - \theta$)

i = current input to servovalve

s = d/dt

for: r, e, θ in degrees

$\dot{\theta}$ deg/sec

$\ddot{\theta}$ deg/sec^2

i dimensionless, $i = i_v/i_m$, where i_v = current into valve in ma

i_m = maximum rated current, ma

then KI = 350 $k_1 = 2.10$ $k_2 = 0.0050$

$k_3 = 4 \times 10^{-6}$ $k_4 = 3 \times 10^{-9}$

Response: 0 to 90 percent rise time: approximately 10 ms

max overshoot: approximately .01 percent

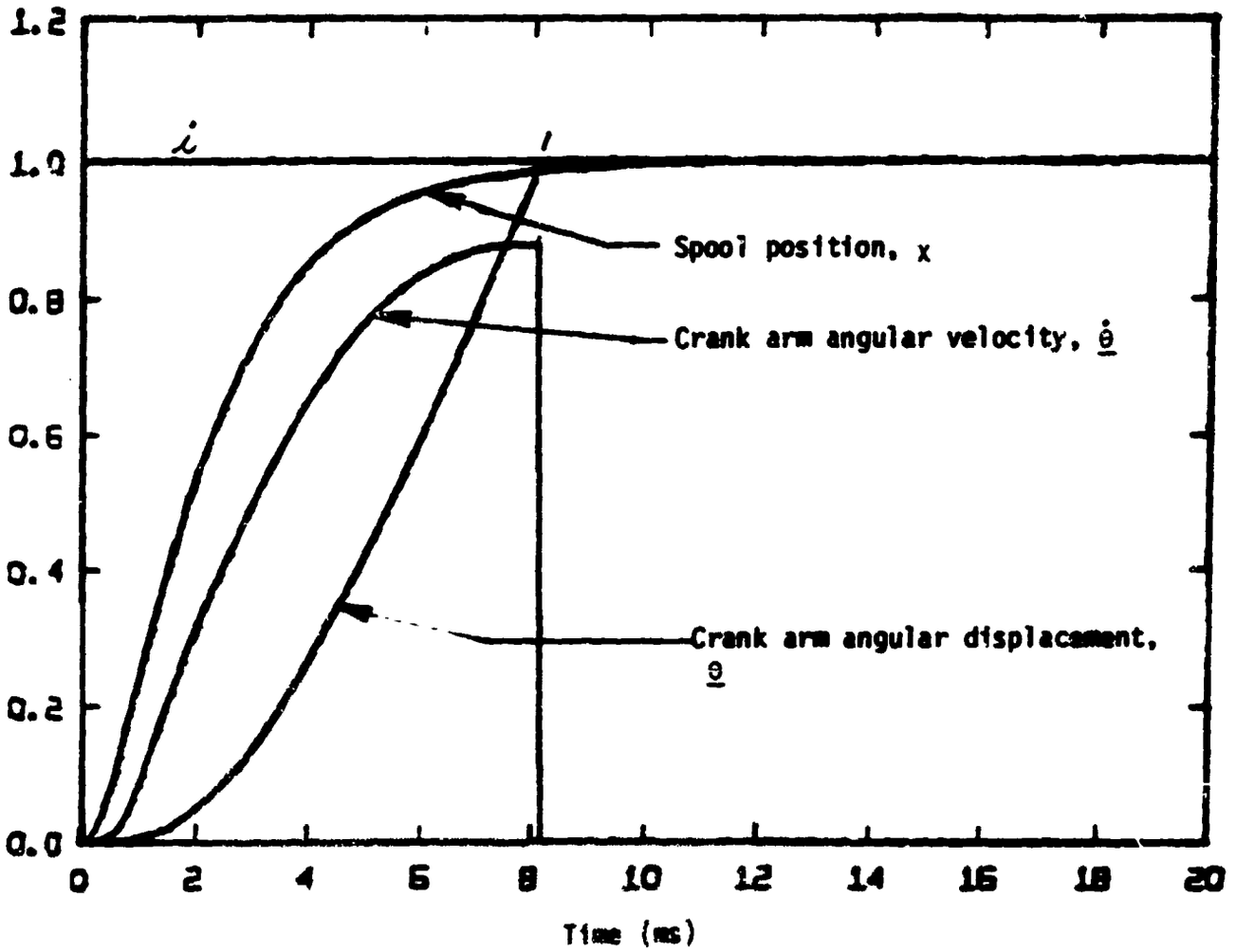

$\underline{\theta} = \theta/22.5^{\circ}$

$\underline{\dot{\theta}} = \dot{\theta}/5000^{\circ}/sec$

FIGURE E-3. OPEN LOOP STEP RESPONSE

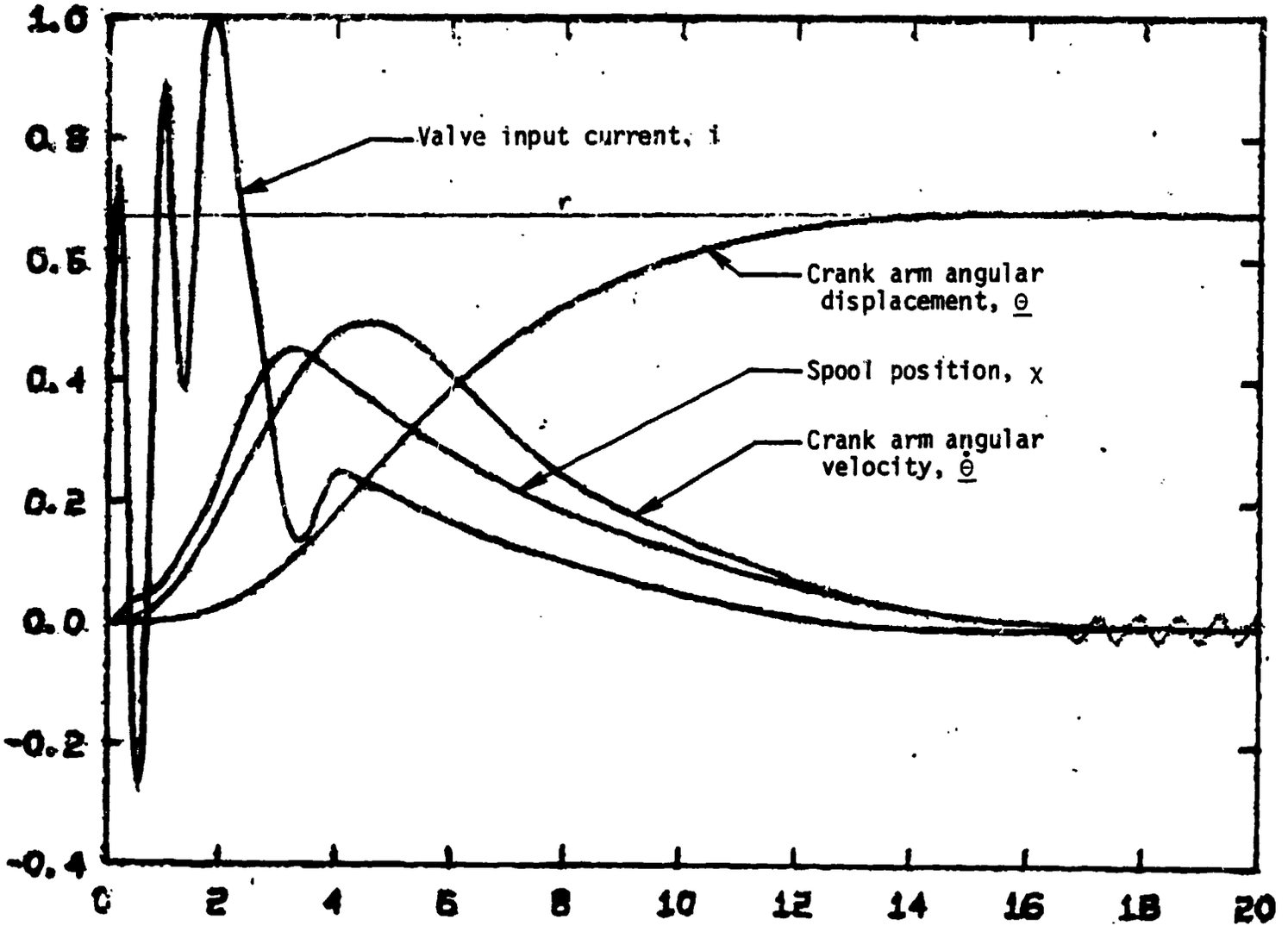

FIGURE E-4. CLOSED LOOP RESPONSE TO 15-DEGREE STEP

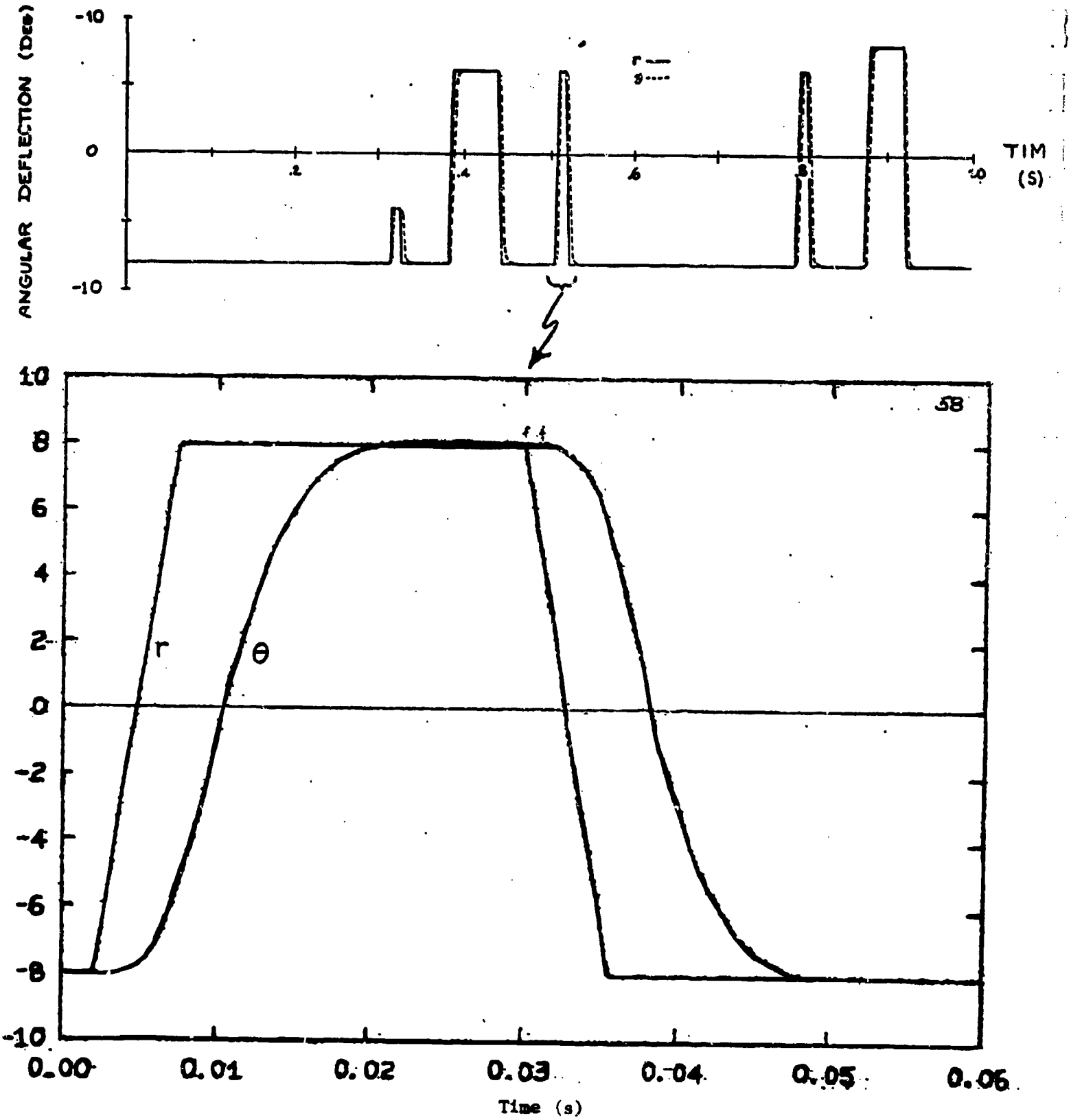

FIGURE E-5. RESPONSE OF BUSHING RESEARCH MACHINE COMPARED TO ACTUAL BUSHING ANGULAR DEFLECTION IN T-142 TRACK (M-60 Tank at 35 mph)

-- Real cycle defined by M-60 track geometry only

-- Standard test practice defined by Armour Research Foundation developed machine that is currently running QPL tests

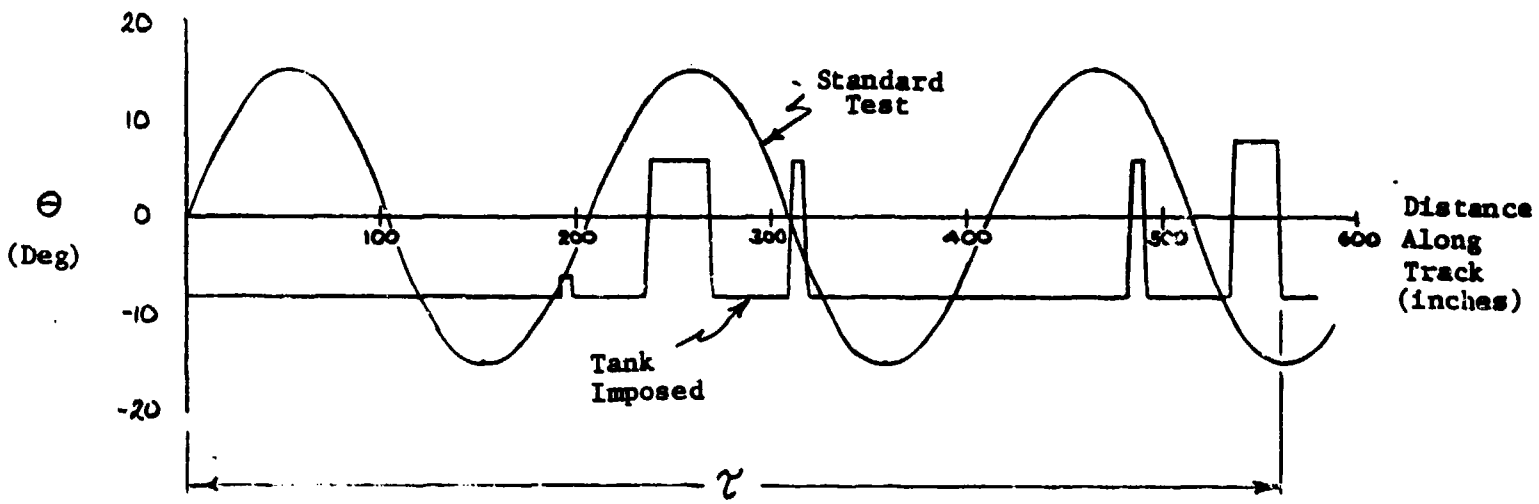

	Tank Imposed Defl'ns (50 mph)	Standard Testing Practice
Input Waveform	See above, τ = .64 sec	255 cpm (4.25 cps) SINE
Max. Defl'n, θ_{max}	±8°/S	±15°/S
Max. Defl'n Rate, $\dot{\theta}_{max}$	±4125°/S	±401°/S
Number of $\dot{\theta}_{max}$ Regions/Sec	12.5/s	8.5/s
Peak Power Req'd, P_{max}	7.0 hp	0.63 hp
"Avg." Power $\left(\frac{1}{2\tau}\int_0^{\tau} K\theta/\dot{\theta}/dt\right)$	0.075 hp	0.214 hp
Approx. Hysteresis Loss (torsion only)	10 watts (0.01 hp)	30 watts (0.04 hp)
Peak Torque	640 in-lb	1200 in-lb

FIGURE E-6. PRESENT "QPL" MACHINE TEST CYCLE COMPARED TO ACTUAL BUSHING ANGULAR DEFLECTION IN T-142 TRACK (M60 Tank at 35 mph)

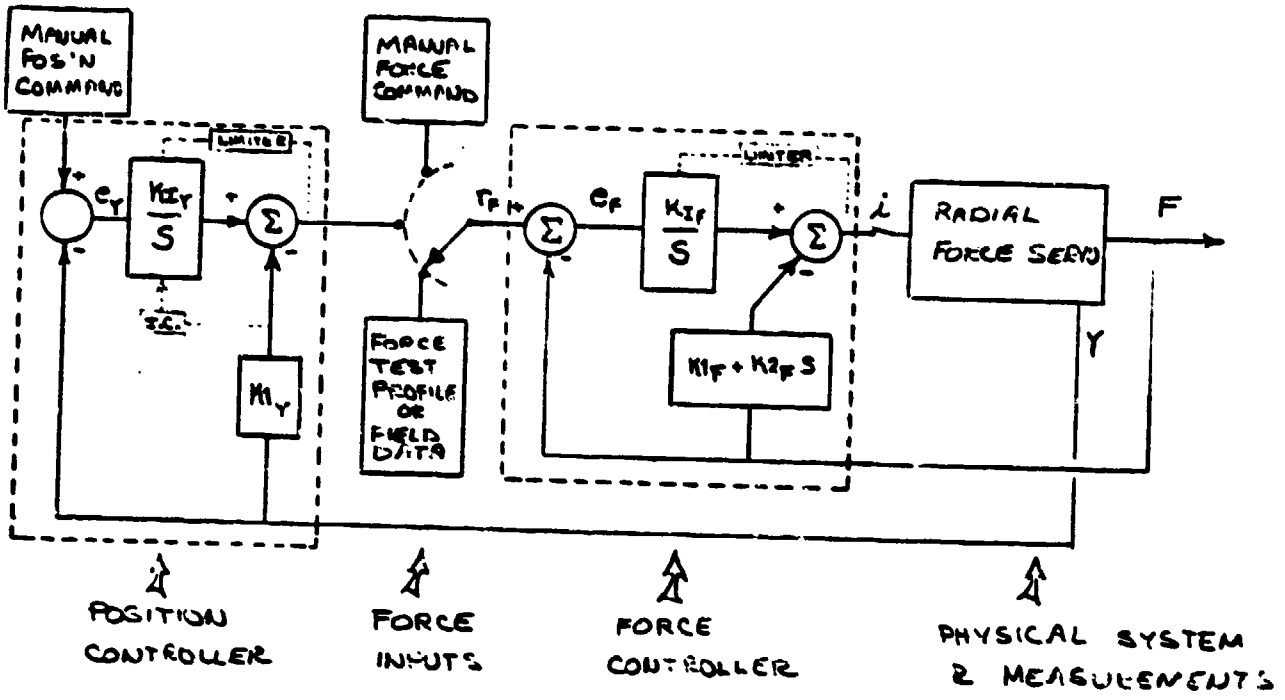

Symbols

r_Y = Position reference input
r_F = Force reference input
e_Y = Position error
e_f = Force error
Y = Radial position
F = Radial force
i = Current input to servovalve
s = d/dt

FIGURE E-7. SIMULATION MODEL REPRESENTING RADIAL FORCE/POSITION CONTROLLER

TANK TRACK BUSHING RADIAL LOAD:

"Real" Cycle versus Standard Test

-- Real cycle from JPW 3-18-77 memorandum

-- Standard test practice from Armour Machine

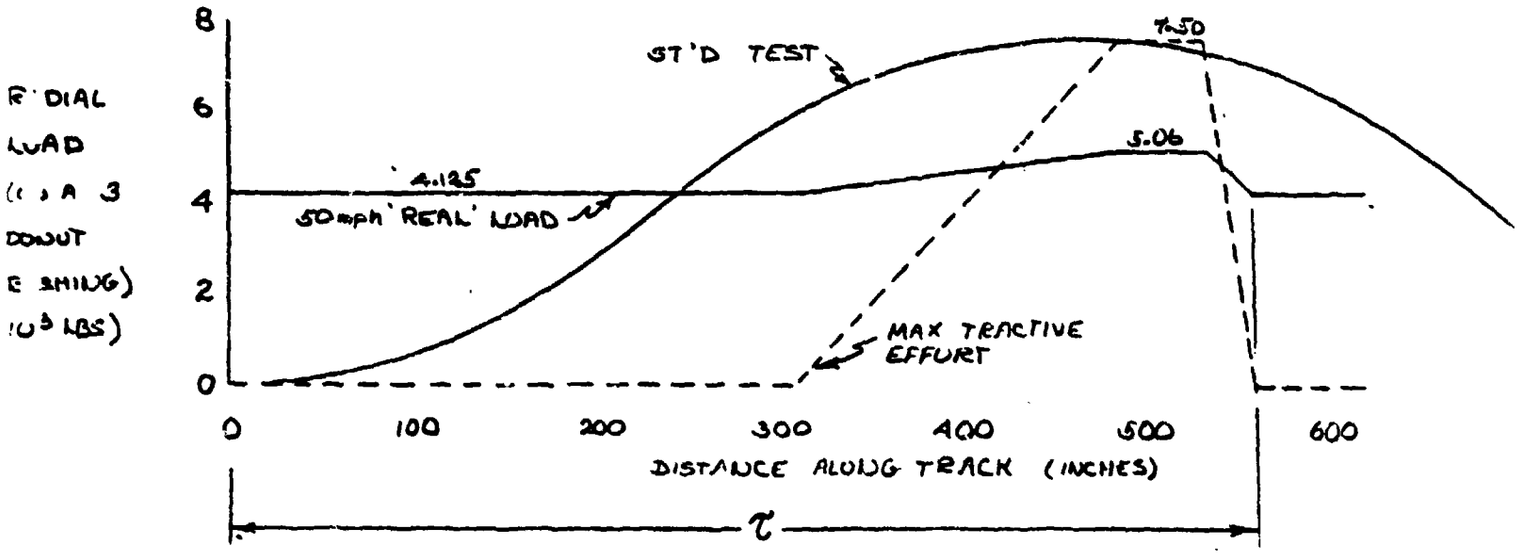

	Tank Imposed Loads (50 mph)	Standard Test Practice
Input Waveform	See above, τ = .64 s	64 cpm (1.1 cps) SINE
Max. Load, P_{max} (lb)	5060	7500
Min. Load, P_{min} (lb)	4125	0
Max. Slope, $\frac{dF}{dt}$ $\frac{lb}{sec}$	+5000, -29,000	±25,000
Peak Power Req'd (hp)	.025	.051
Max. Defl'n (in)	.042	.060

FIGURE E-8. PRESENT "QPL" MACHINE TEST CYCLE COMPARED TO ACTUAL BUSHING RADIAL LOAD IN T-142 TRACK (M-60 TANK AT 35 mph)

General Requirements for Controllers

-- Machine start up: sequence must be such that no transient inputs are introduced: all inputs at 0 as hydraulic pressure comes up. All integrator initial conditions set.

-- Position and force measurements: Must have means of zeroing measurement signal to correspond with physical zero which may vary with specimens.

-- Integrators: Must be output limited to prevent windup and/or instability.

-- Manual to automatic switching: Must provide for proper initial conditions on integrators for smooth switching between modes of operation.

-- Cylinder bypass: physical valve to short circuit hydraulic cylinder may be desirable to allow physical motion of cylinder when system is off.

-- Controller tuning: Controller gains should be adjustable to provide ability to tune system once at installation. Data available to show general effect of each control gain.

Instrumentation and Signal Processing

Basic Measurement	Device
Radial:	
Deflection	DCDT
Force	Strain gage load cell*
Angular:	
Position	DCDT
Velocity	LVSYN
Acceleration	Accelerometer
Torque	Strain gaged torque arm
Temperature:	Thermocouple
No. of Cycles:	Mechanical and/or electrical counter

— all measurements will be used in the feedback control system

— all measurements will have output jacks on instrumentation panel to provide for direct access to signal before processing

Processing

A signal corresponding to that torque required to twist the bushing will be generated by rolling out that part of the torque signal due to equipment inertia (using the acceleration measurement).

The above torque signal and the radial deflection signal will each be sampled at their peak valve every cycle to generate a signal of maximum torque and maximum deflection versus time.

The accelerometer signal will be low-pass filtered and differentiated to provide a $d^3\theta/dt^3$ signal to stabilize the angular control system (Note: It may be possible to use torque and torque rate signals in the control system, rather than acceleration and acceleration rate).

The radial force signal will be low-pass filtered and differentiated to provide a force rate signal for the radial load control system.

Bushing radial and angular displacements and/or velocities will be monitored to indicate pin breakage, collet slippage, or other adverse conditions, and initiate system shutdown.

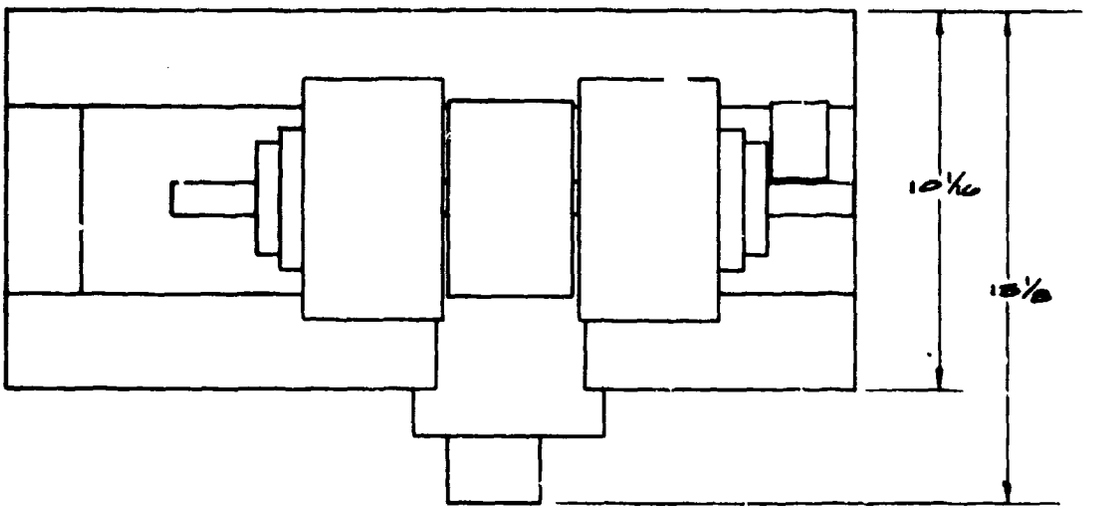
10 1/16
15 1/8

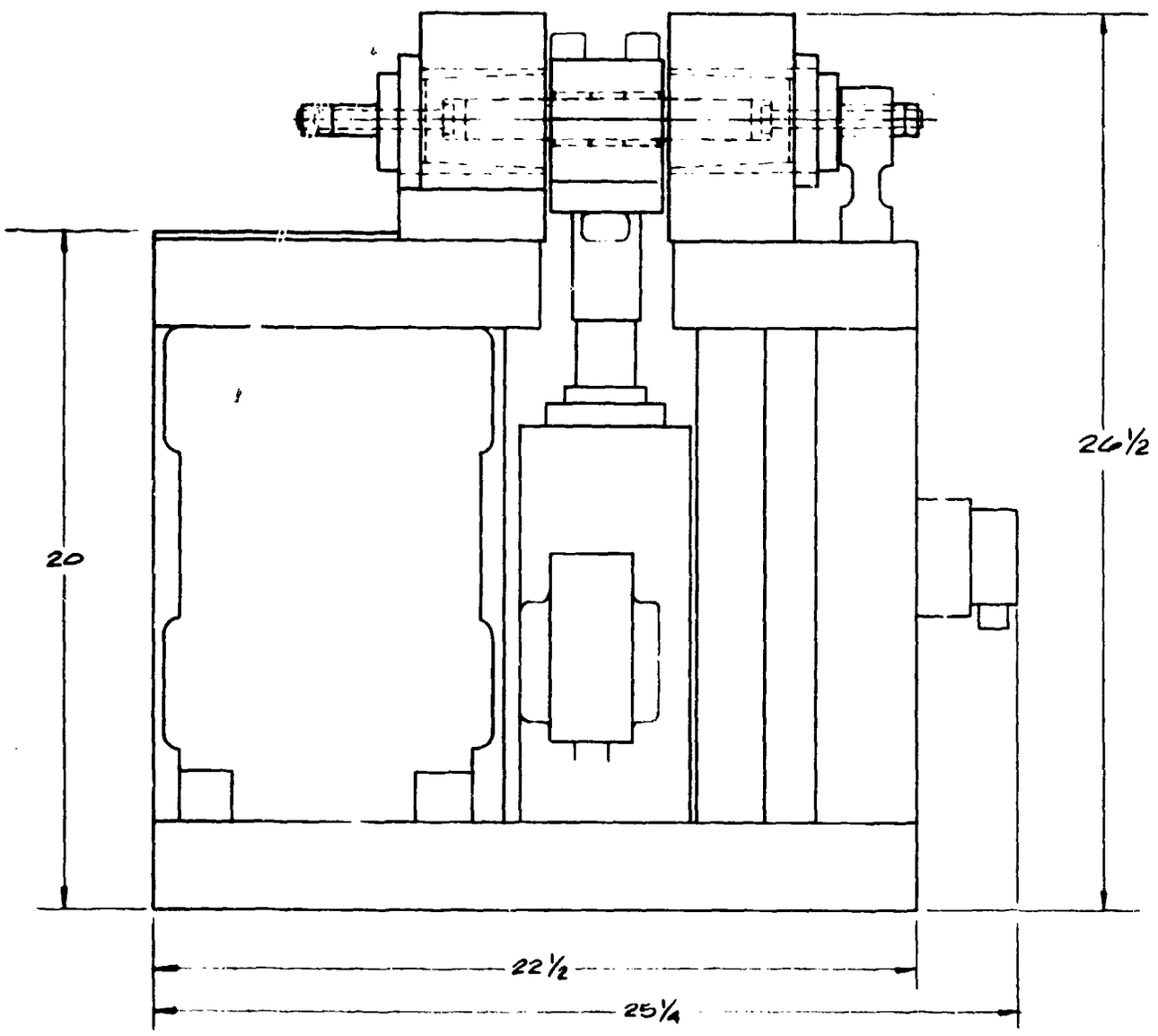
20
26 1/2
22 1/2
25 1/4

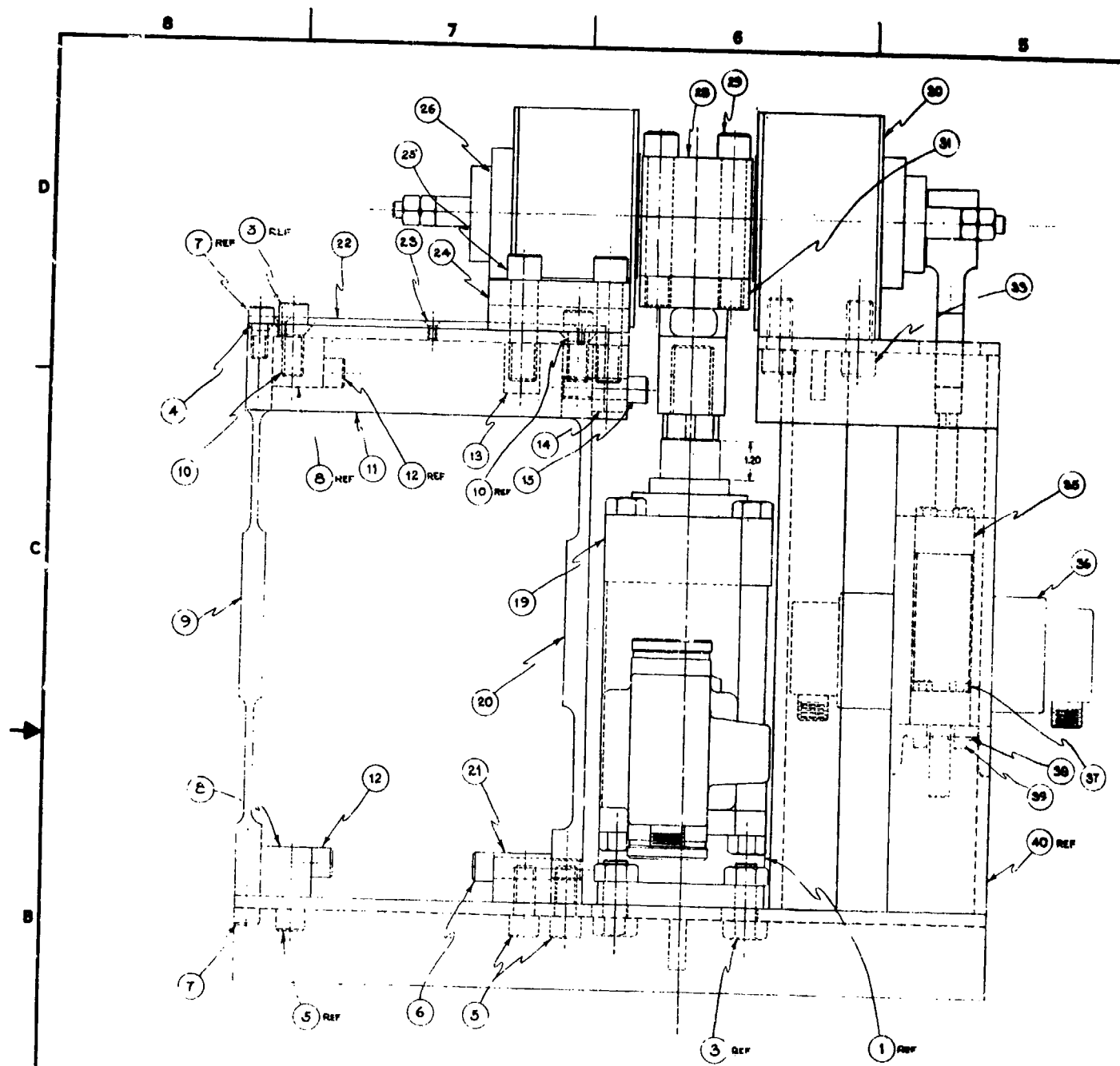

NOTE C: ASSEMBLE WITH ANAEROBIC NUT-LOCK SEALANT ON PISTON ROD THREAD (STA-LOK #400 OR EQUIV.)

NOTE B: ASSEMBLE WITH EXTERNAL-TOOTH LOCK WASHER.

NOTE A: ASSEMBLE WITH ANAEROBIC STUD-LOCK SEALANT (STA-LOK #800 OR EQUIV.)

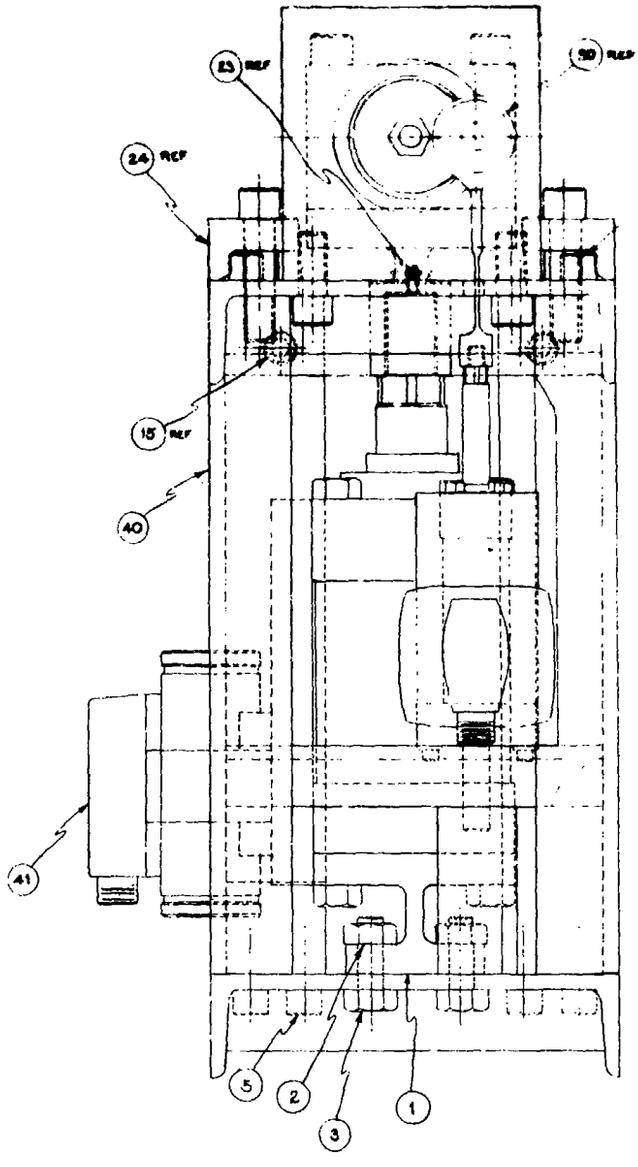

FIND NO.	QTY.	PART NO. OR IDENTIFYING NO.	DWG. SIZE	DESCRIPTION	SPECIFICATION	NOTE NO.
41	1	—		MOOG 72-101 SERVO-VALVE & MANIFOLD		
40	1			FRAME WELDMENT		
39	4	—		¼-20 × 2 SKT HD SCR.		
38	4	—		¼ FLAT WASHER (HARD)		
37	4	—		¼-20 HEX NUT		
36	2	—		MOOG A076-233 SERVO-VALVE & MANIFOLD		
35	1	—		1⅜" CYLINDER (SHEFFER 1⅜ HH RHF2 D)		
34				—		
33	4	—		¾-16 × 1½ SKT HD SCR.		B
32				—		
31	1	SK 3		LOAD-SENSING HOUSING MOUNT		C
30	1	C-100	C	BEARING & CRANK ARM ASS'Y		C
29	4	—		¾-16 × 4½ SKT. HD. SCR.		
28	1	SK 13		SPLIT BUSHING BLOCK ASS'Y		
27				—		
26	1	SK-200		LEFT BEARING BLOCK		
25	4	—		¾-16 × 3 SKT. HD SCR.		
24	2	SK 2		CLAMP BLOCK		
23	3	—		¼-20 × ⅜ FLAT HD SCR.		
22	1	SK 12		DOVETAIL STRIP		
21	2	SK 11		FRONT FLEXURE MOUNTING BLOCK		
20	2	SK 7		FRONT FLEXURE		
19	1	—		4" CYLINDER (SHEFFER 4 HH RH 3 CC)		
18						
17						
16						
15	2	—		⅝-18 × 2" SKT. HD. SCR.		A
14	1	SK 9		FRONT CLAMP BAR		
13	1	SK 1		CLAMP BAR		
12	4	—		⅜-16 × 2¼ SKT. HD. SCR		A
11	1	SK 8		BEARING BLOCK SLIDE		A
10	2	—		⅜-16 × 1½ FLAT HD. SCR		A
9	2	SK 6		REAR FLEXURE		
8	4	SK 5		FLEXURE MOUNTING BLOCK (REAR)		
7	6	—		½-20 × 1¼ SKT. HD. SCR.		A
6	2	—		⅝-18 × 3 SKT. HD SCR		A
5	16	—		⅝-18 × 1½ SKT. HD. SCR.		A
4	2	—		½-20 × 1¼ FLAT HD. SCR.		A
3	4	—		¾-16 × 2¼ HEX HD. SCR.		
2	4	—		¾-16 NUT		B
1	1	SK 10		RADIAL LOAD FLEXURE		

PARTS LIST

APPLICATION	DO NOT SCALE DRAWING	SIGNATURE	DIV.	DATE
THIS ITEM IS USED ON SUBASSEMBLIES	UNLESS OTHERWISE SPECIFIED DIMENSIONS ARE IN INCHES. TOLERANCES ARE: .XX = ± .XXX = ± .XXX = ± ANGLES = ±	DRAWN BY DUM	634	9/30/77
DRAWING NO. / PER ASSY / NO. OF ASSY'S / TOTAL	MATERIAL AND TREATMENT	CHECKED APPR.		
		ENGR APPR.		
		APPR.		
		APPR.		
		PROJECT APPR.		
		SPECIAL APPR.		
TO MAKE FINAL ASSEMBLY / ORDER QUANTITY				

Battelle Columbus Laboratories
505 King Avenue, Columbus, Ohio 43201, Telephone (614) 299-3151

TITLE: BUSHING FATIGUE TEST MACHINE - MAIN STRUCTURE ASS'Y

SIZE	CAGE IDENTIF. NO.	DIV. NO.	DWG. NO.	REV.
D	79986		-	-

SCALE 1/2 | ASST. | SHEET

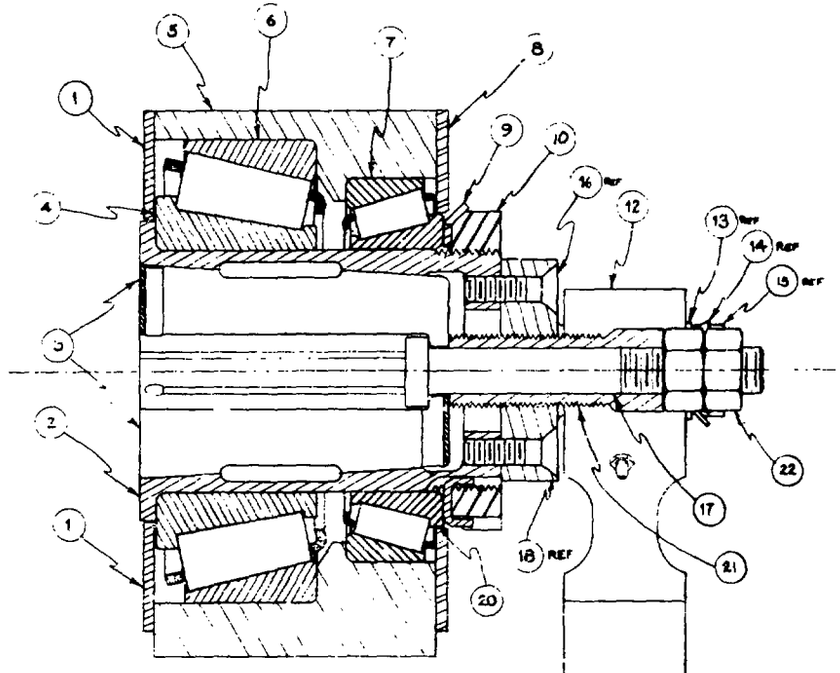

SEC 'AA'

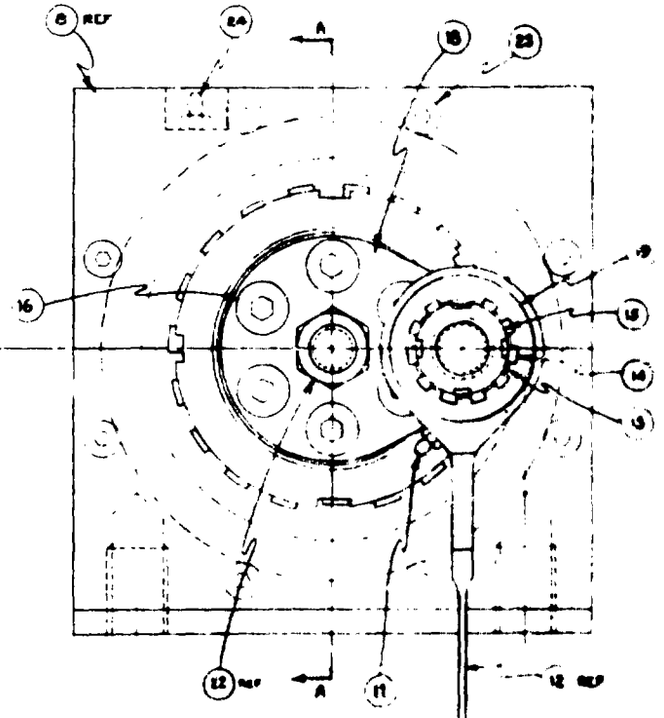

DET NO.	QTY	DESCRIPTION	DWG NO	NOTE
24	1	GREASE FITTING (TO SUIT)	—	
23	16	12-24 × ½ FLAT HEAD SCR	—	
22	2	COLLET DRAW SCREW NUTS (⅝-18)	—	
21	4	COLLET PUSH-OUT SLEEVE	SK 106	
20	1	REAR BEARING CONE (TIMKEN JM714249)	—	
19	1	TWO OPPOSED LM11910-49 BEARINGS & SEALS	—	
18	1	CRANK ARM	SK 102	
17	1	COLLET DRAW SCREW	SK 105	
16	6	⅝-24 × 1⅛ FLAT HD. SCR.	—	B
15	1	LOCKNUT AFBMA Nº TW03	—	
14	1	LOCKWASHER AFBMA Nº TW104	—	
13	1	KEYED WASHER (TIMKEN K91303)	—	
12	1	CRANK ARM FLEXURE	SK 104	
11	1	GREASE FITTING (TO SUIT)	—	
10	1	LOCKNUT AFBMA Nº TAN15	—	
9	1	LOCKWASHER AFBMA Nº TW15	—	
8	2	REAR GREASE BAFFLE	SK 107	
7	1	REAR BEARING CUP (TIMKEN JM714210)	—	
6	1	FRONT BEARING CUP (TIMKEN JH415610)	—	
5	1	MAIN BEARING BLOCK	SK 101	
4	1	FRONT BEARING CONE (TIMKEN JH415647)	—	C
3	1	TAPERED CHUCK COLLET	SK 103	A
2	1	TAPERED CHUCK CUP	SK 101	
1	2	FRONT GREASE BAFFLE	SK 108	

NOTE B: ASSEMBLE WITH ANAEROBIC NUT-LOCK SEALANT

NOTE A: TAPERED CHUCK COLLET (DET 3) IS VARIED WITH SPINDLE PIN DIA. SHOWN IS COLLET FOR .94 PIN DIA.

NOTE C: ASSEMBLE WITH ANAEROBIC SEALANT

REVISIONS

ZONE	LTR	DESCRIPTION	DATE	APPROVED

PARTS LIST

PART NO.	QTY.	PART NO. OR IDENTIFYING NO.	SIZE	DESCRIPTION	SPECIFICATION	MATL

APPLICATION

THIS ITEM IS USED ON NEXT ASSEMBLY

DRAWING NO.	NEXT ASSY	QTY REQ'D

DO NOT SCALE DRAWING

UNLESS OTHERWISE SPECIFIED DIMENSIONS ARE IN DECIMAL TOLERANCES ARE:

.XX± .XXX±

.XXX± ANGLE±

MATERIAL AND TREATMENT

SIGNATURES		DATE
DRAWN	JOHN	4/19/1977
ENGINEER		
CHECKED		
MFG.		
QUAL.		
PURCHASING		
MANAGER		

Caterpillar

TITLE: BEARING & CRANK ARM ASS'Y

SIZE	CAGE CODE	DWG NO.	REV. NO.	SHEET NO.
C	79986	624	C-100-	

SCALE: FULL WEIGHT: SHEET 1

APPENDIX F

CONCEPT FOR ADVANCED XM-1/M-60 TRACK SHOE (REPLACEABLE-PAD VERSION)

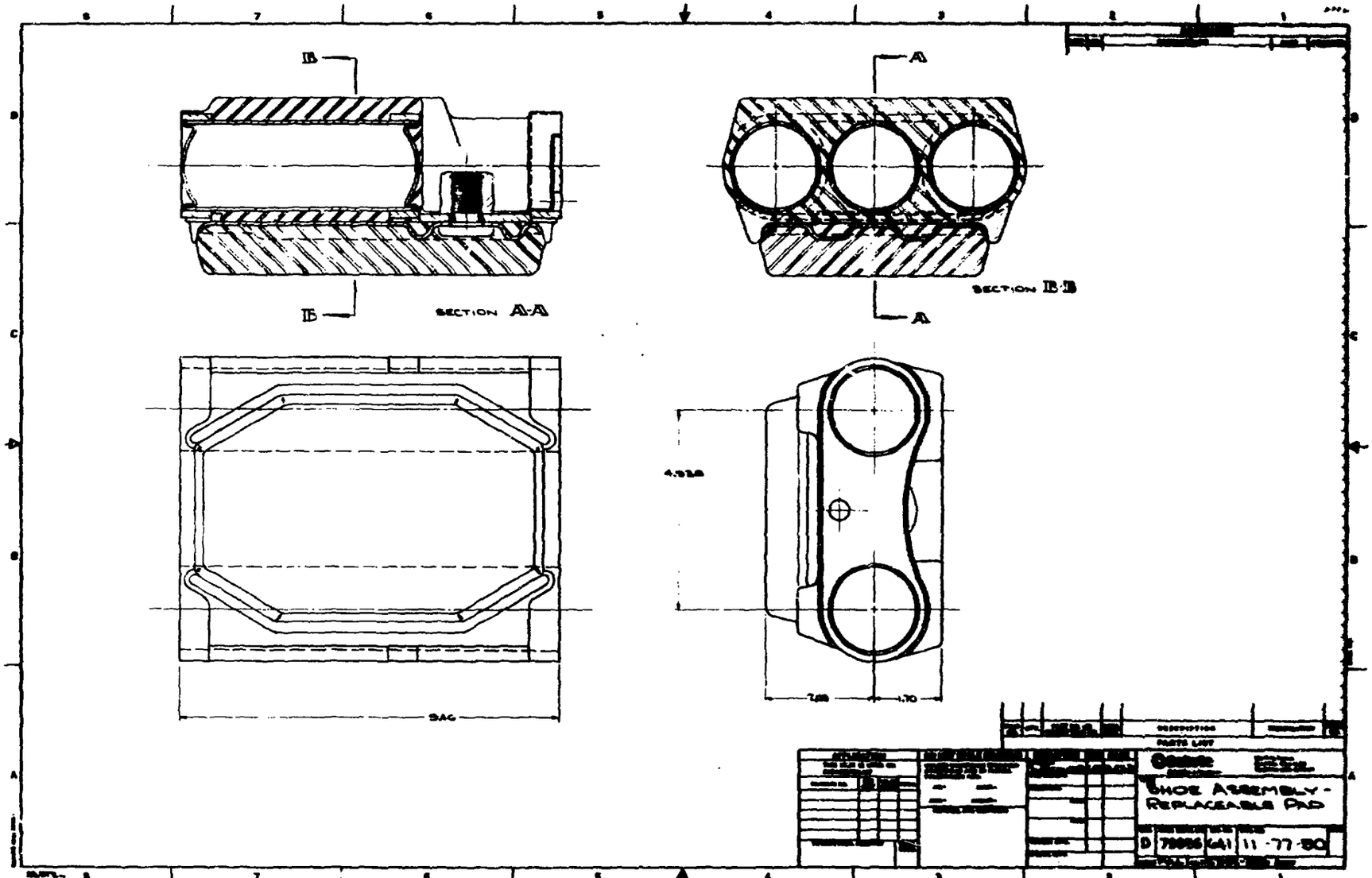
B
B
SECTION A-A
A
A
SECTION B-B
4.938
7.88
1.70
9.46
SHOE ASSEMBLY - REPLACEABLE PAD
D 78086 641 11-77-80

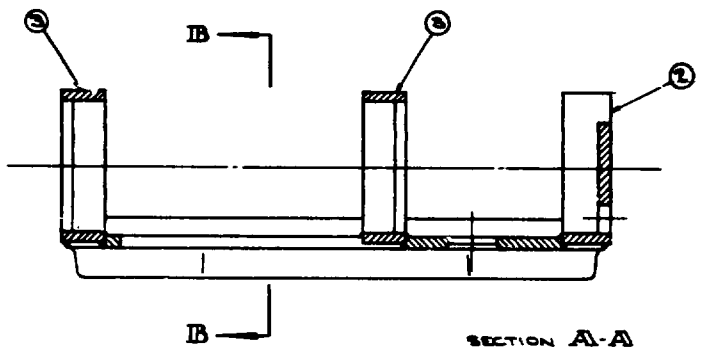
B
B
SECTION A-A

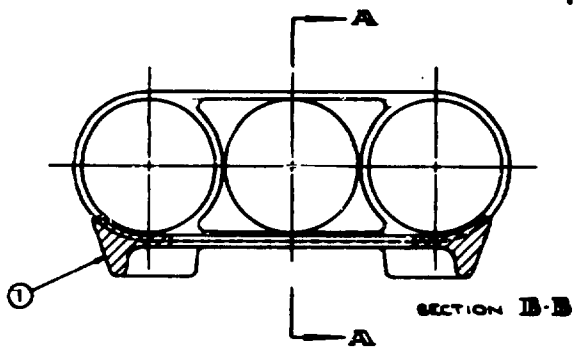
A
A
SECTION B-B

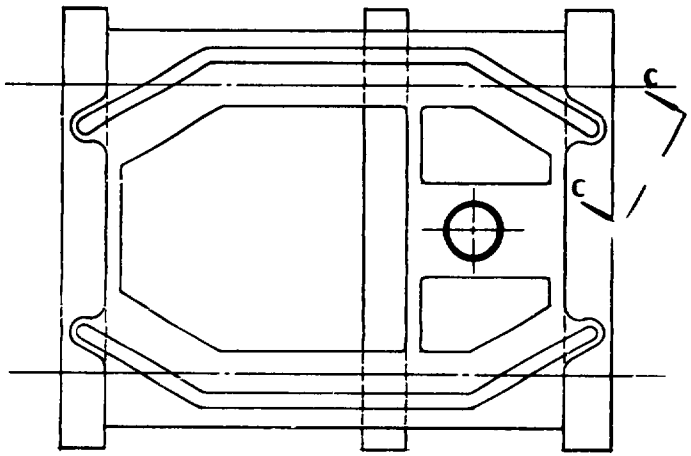
C
C


VIEW C-C

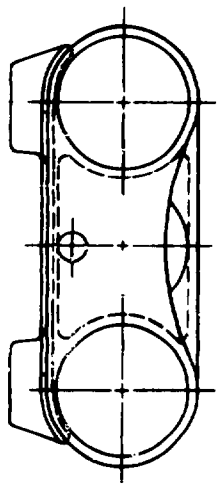

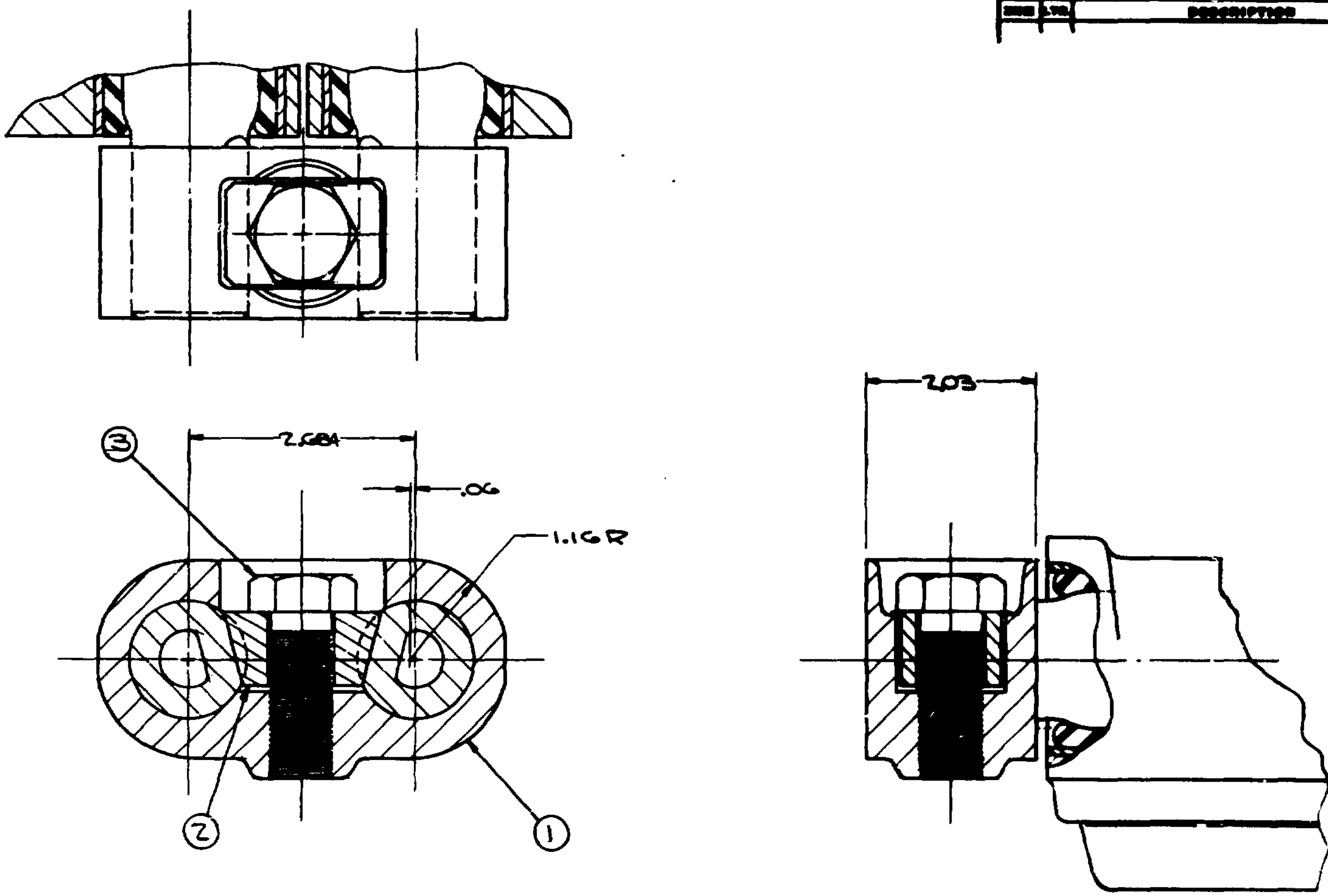

NOTES-
1- DIMENSIONS & SPROCKET MATING SURFACES SAME AS EXISTING XM1 END CONNECTOR.

FIND NO.	QTY.	PART NO. OR IDENTIFYING NO.		DESCRIPTION	SPECIFICATION	NOTE NO.
3	1			SCREW-HEX 3/8-16 SAE GRADE 8		
2	1			WEDGE		
1	1			COUPLING		

PARTS LIST

APPLICATION

THIS ITEM IS USED ON SUBASSEMBLIES

DO NOT SCALE DRAWING

UNLESS OTHERWISE SPECIFIED DIMENSIONS ARE IN INCHES. TOLERANCES ARE:

MATERIAL AND TREATMENT

SIGNATURE | DIV | DATE

Battelle
Columbus Laboratories

END CONNECTOR ASSEMBLY
(REVERSED ACTION WEDGE)

C 79986 641 11-77-44

REVISIONS

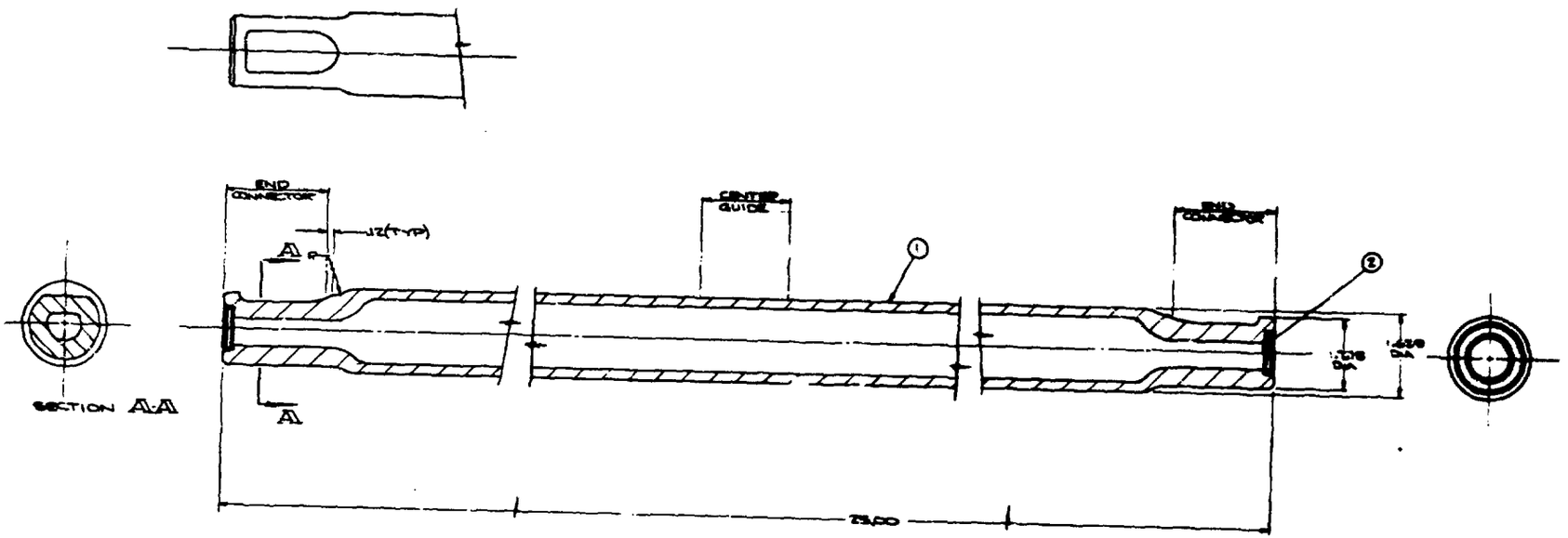

NOTES:-
1- MATERIAL - SAE 4130 TUBING 1.750 OD x 1.25 ID
2- ENDS TO BE HEATED & SWAGED/FORGED TO PROVIDE THE DIAMETER & A FLAT, LEAVING STOCK FOR CLEANUP.
3 - HEAT TREATMENT - QUENCH & TEMPER TO
4 - THE EXTERNAL CONFIGURATION OF THE END IS IDENTICAL TO EXISTING [illegible] IN THE END CONNECTOR AREA.

PARTS LIST

Pin Assembly

D 79000

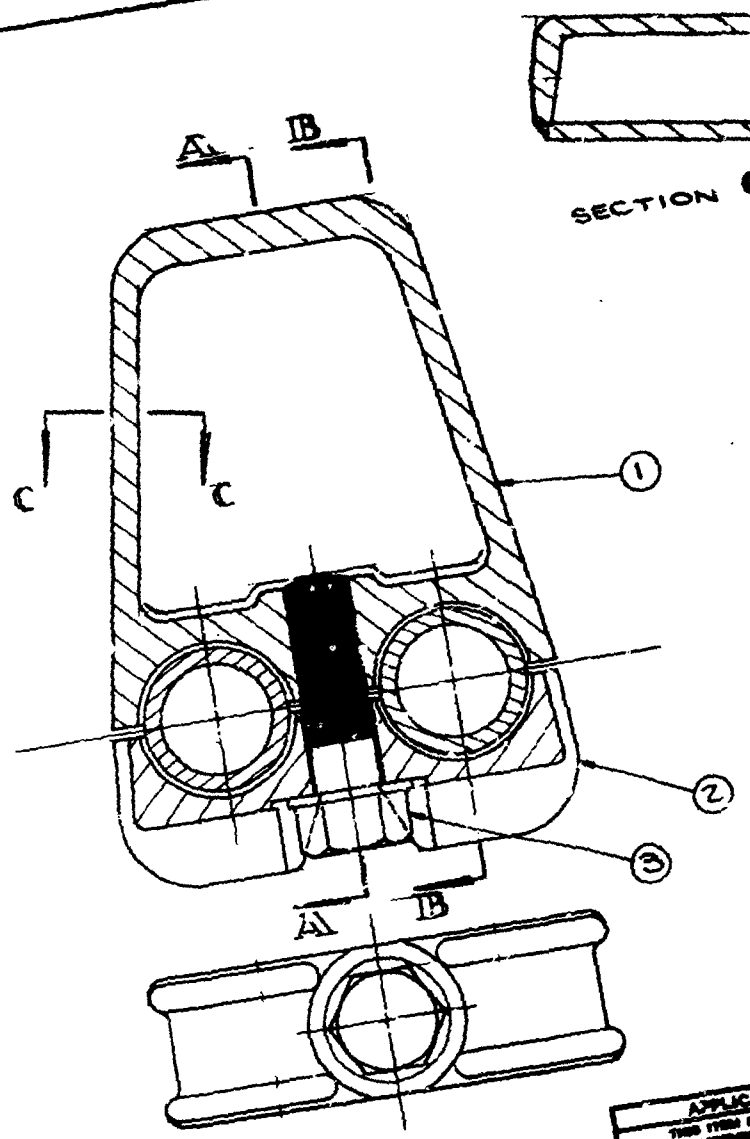

SECTION C-C

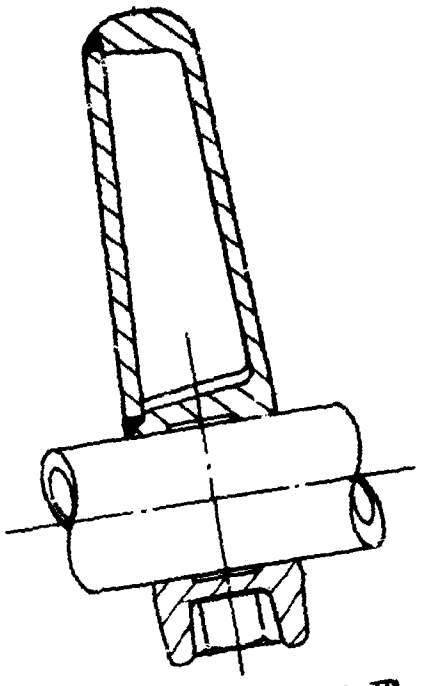

SECTION B-B

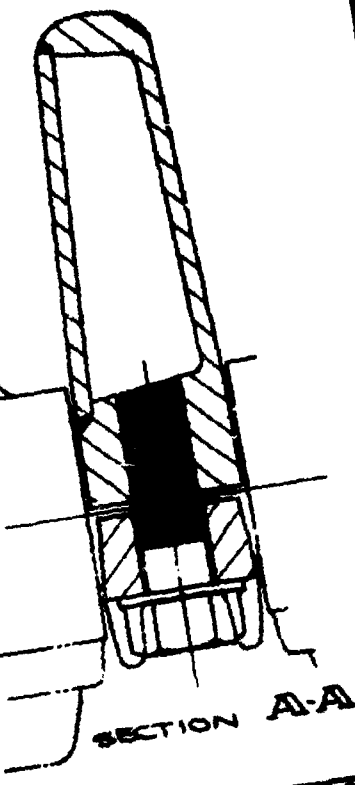

SECTION A-A

ITEM NO.	QTY.	PART NO. OR IDENTIFYING NO.	MATERIAL	DESCRIPTION
3	1			SCREW-HEXHD 5/16-18x2.75
2	1			CAP
1	1			GUIDE

PARTS LIST

APPLICATION	DO NOT SCALE DRAWING	ORIGINATOR	DATE
THIS ITEM IS USED ON THE FOLLOWING	UNLESS OTHERWISE SPECIFIED DIMENSIONS ARE IN INCHES. TOLERANCES ARE:		

Ottotic

CENTER GUIDE ASSEMBLY

C 79986 CAI 11-17-43

APPENDIX G

TRACK-MOUNTED INSTRUMENTATION SYSTEM

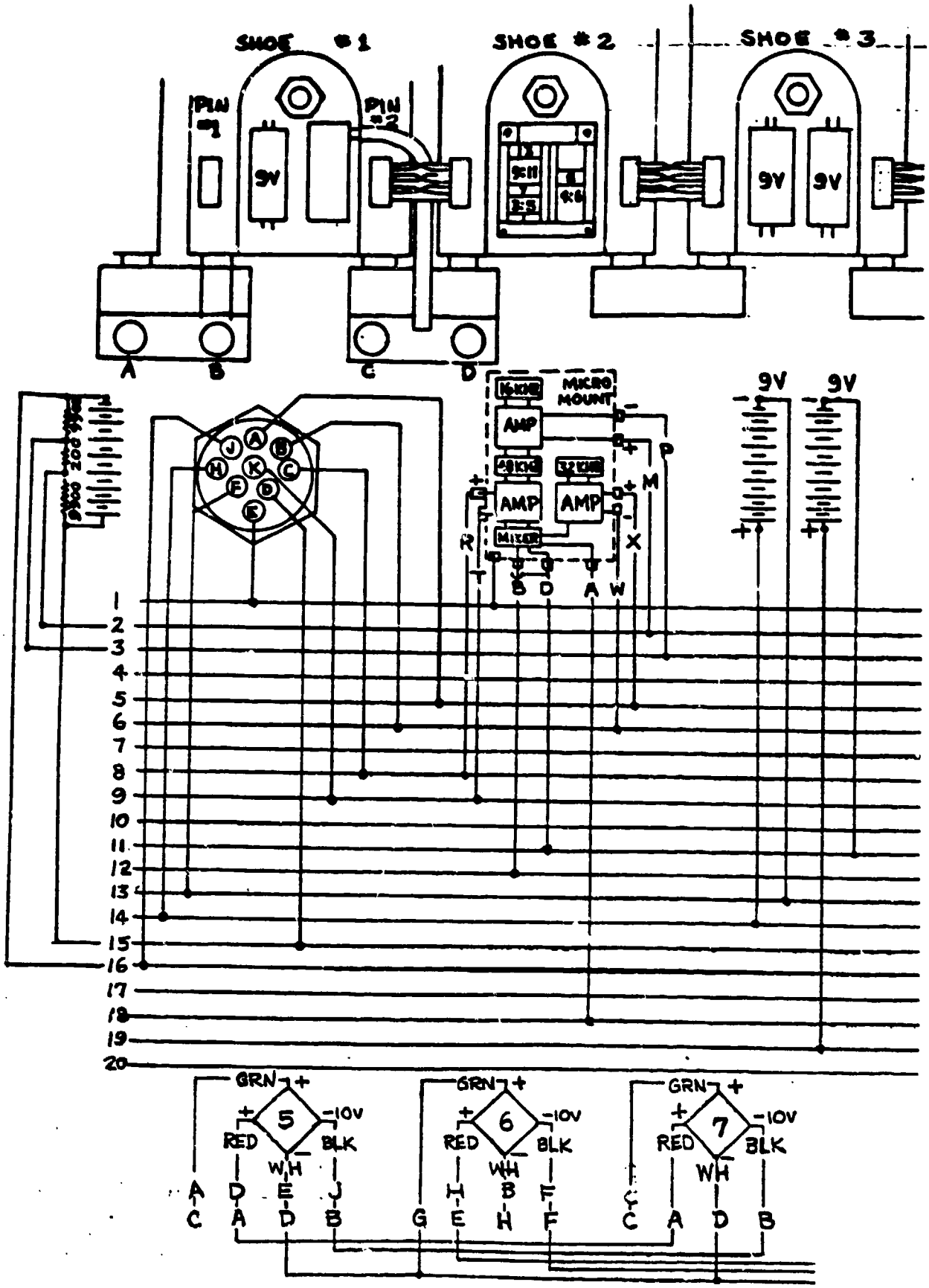

FIGURE G-1. SCHEMATIC DIAGRAM OF TRACK-MOUNTED INSTRUMENTATION CIRCUIT

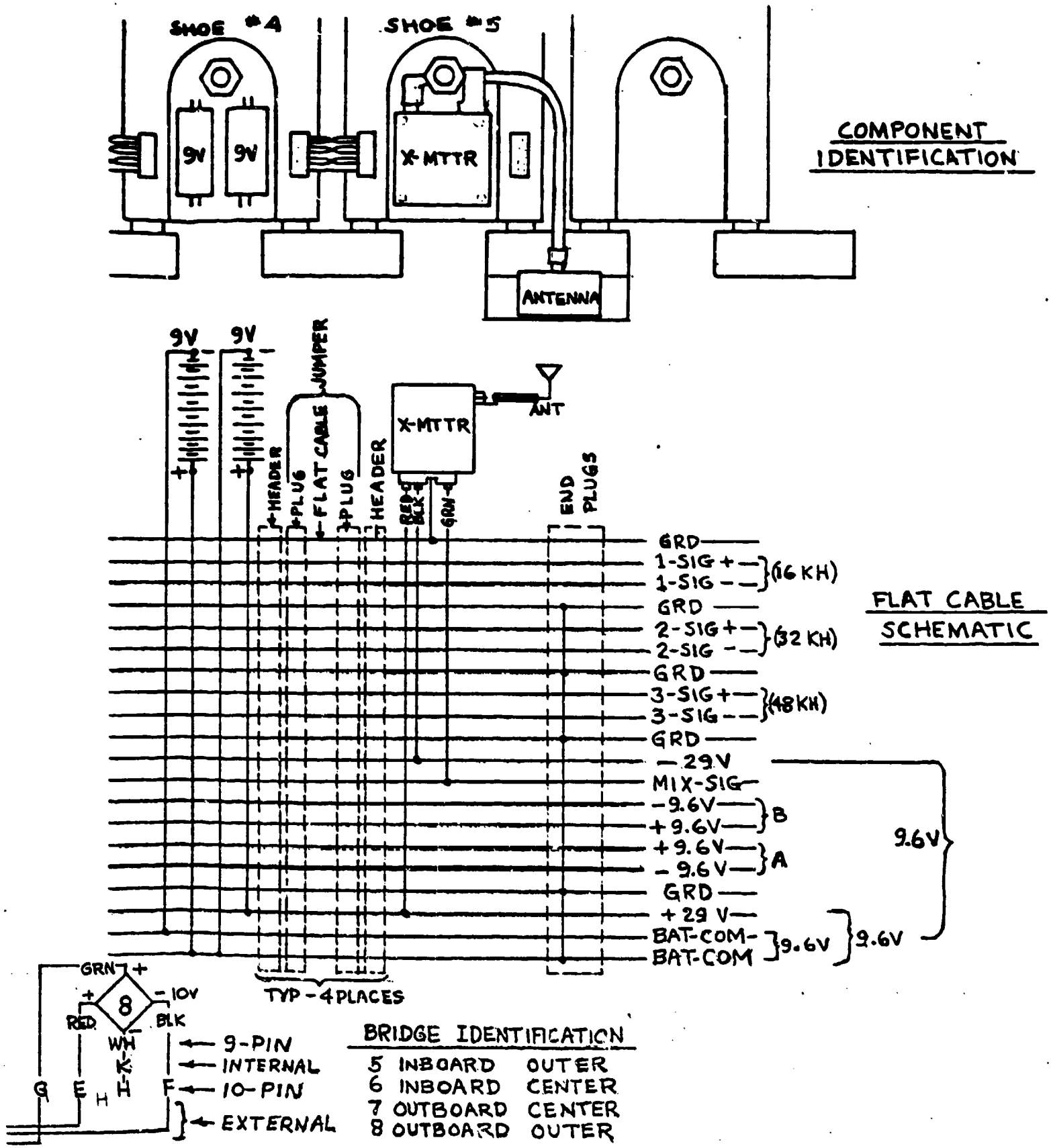

FIGURE G-1. SCHEMATIC DIAGRAM OF TRACK-MOUNTED INSTRUMENTATION CIRCUIT (Continued)

SIGNAL CONDITIONING AMPLIFIER
Model MMA-20

actual size

- Differential Input
- Ground Isolation
- Space Qualified

The Vector Model MMA-20 is a high gain, stabilized dc amplifier which is used to amplify outputs from thermocouples, strain gages, or other millivolt transducers. The characteristics of this unit are specified for any 5-volt output range from –5 volts to +5 volts dc. This is sufficient to drive any Vector subcarrier oscillator. The output is single-ended.

The unit has been designed for use in airborne applications, and has been qualified to the most severe aerospace environments. The microminiature design offers the user small size, high accuracy, low power consumption, and high reliability. The unit is fully compatible with standard low level transducers. Variations in gain setting are available on special order.

BASIC UNIT VECTOR MODEL MMA-20

ELECTRICAL SPECIFICATIONS
(at 25°C ±5°C, 28 volts dc)

GAIN: 250, ±2%.

FREQUENCY RESPONSE: Flat within ±1.0 dB from dc to 8 kHz.

INPUT IMPEDANCE: 100,000 ohms minimum.

OUTPUT IMPEDANCE: Less than 1000 ohms.

INPUT SIGNAL: ±10 millivolts.

NOMINAL OUTPUT SIGNAL: ±2.5 volts.

OUTPUT OFFSET: ±25 millivolts, with input short-circuited.

LINEARITY: ±0.1% of best straight line over any 5-volt segment between –5 volts dc and +5 volts dc.

COMMON MODE REJECTION: 80 dB from dc to 1000 Hz.

MAXIMUM COMMON MODE VOLTAGE: 12 volts peak-to-peak ac. (±6 V dc.)

STABILITY WITH LINE VOLTAGE: Output changes less than ±25 millivolts for 28 volts dc ±10% at any output voltage within specified range.

POWER REQUIREMENTS: 10 milliamperes nominal at +28 volts dc.

ENVIRONMENTAL SPECIFICATIONS

TEMPERATURE: Operating range from –55°C to +100°C. Gain stable within ±1% of full scale output from –20°C to +80°C.

ZERO DRIFT: Output changes less than ±50 millivolts from –20°C to +80°C with input shorted.

VIBRATION: Capable of withstanding 30 g in each major axis from 55 to 2000 Hz.

SHOCK: Capable of withstanding at least 200 g.

ACCELERATION: Capable of withstanding at least 100 g in the direction of each major axis.

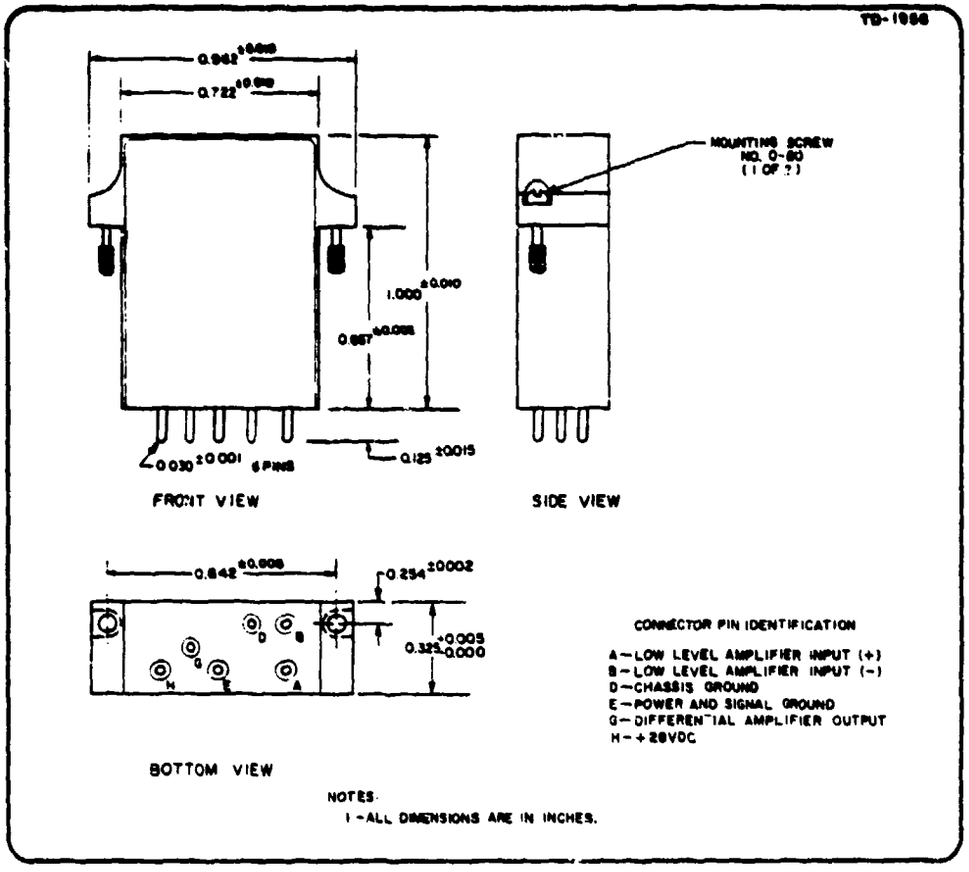

MECHANICAL SPECIFICATIONS

SIZE: See outline drawing.

WEIGHT: 5 grams (0.176 oz.) nominal.

MOUNTING: Vector MMM Series mounts.

CONNECTION: Two pins each for input, and for ground. One pin each for output, and for power.

CONTROLS: No controls are supplied. (Gain is set at factory.)

DESIGN VARIATION VECTOR MODEL MMA-20-1

The model MMA-20-1 is the same as the basic unit except for the following:

INPUT SIGNAL: 0 to +20 millivolts

NOMINAL OUTPUT SIGNAL: 0 to +5 volts

MARKING: Model designation shown on nameplate as MMA-20-1.

ORDERING INFORMATION

When ordering specify model number and part number as defined in the tabulation. For special applications or additional information, contact the nearest sales representative or Vector.

Model No.	Part No.
MMA-20	15002000
MMA-20-1	15002001

SUBCARRIER OSCILLATOR
MMO-15 Series

actual size

- **Constant Bandwidth**
- **Reliability: MTBF in Excess of 2 x 10^6 Hours**
- **Space Qualified**
- **Off-the-Shelf Delivery**

The Vector Model MMO-15 microminiature voltage-controlled constant bandwidth subcarrier oscillator is used to convert high-level dc voltages into frequency modulated subcarrier signals. It is specifically designed for telemetry applications where space, weight, and reliability considerations are critical.

The unique microminiature design provides extremely small size, high accuracy, low power consumption, and high reliability. The unit is fully compatible with existing input and output equipment such as transducers, signal conditioners, and transmitters. The unit has been qualified to stringent aerospace environments on numerous NASA and DOD programs.

The major functional sections contained in the MMO-15 are a temperature compensated amplifier, a free-running multivibrator, an output filter, and a voltage regulator. The unit is designed to provide excellent transient response.

BASIC UNIT VECTOR MODEL MMO-15

ELECTRICAL SPECIFICATIONS at 25°C ±3°C unless otherwise noted:

INPUT VOLTAGE:	0 to +5 volts. Positive-going voltage produces an increase in output frequency.
INPUT IMPEDANCE:	500 kilohms ±10% (dc to 5000 Hz)
STANDARD CHANNELS:	All IRIG constant bandwidth channels.
SPECIAL CHANNELS:	Non-IRIG channels with center frequencies between 400 Hz and 250 kHz and with deviations between ±2.5% and ±25% are available on special order.
SOURCE IMPEDANCE SENSITIVITY:	Oscillator output frequency is stable within ±1% of design bandwidth as the source impedance is changed from zero to infinity for output frequencies under 100 kHz. Stability is ±2% for output frequencies above 100 kHz.
REVERSE DC CURRENT:	0.1 microampere maximum measured from signal input to ground through a dc microammeter.
AC FEEDBACK:	75 millivolts peak to peak maximum measured across a 10 kilohm resistor connected between signal input and ground.

LINEARITY:	Less than ±0.5% of design bandwidth from a straight line through the end points. Less than ±0.25% of design bandwidth for best straight line. This linearity is maintained at temperatures from −40°C to +85°C.
AMPLITUDE MODULATION:	5% maximum over the design bandwidth, at any temperature from −40°C to +85°C.
TIME DRIFT:	Stable within ±0.5% of design bandwidth during a period of 15 minutes continuous operation at 25°C ±1°C following a stabilization period of 30 seconds. Oscillators having output frequencies under 100 kHz are stable within ±0.25% of design bandwidth over a period of 8 hours operation at 25°C following a 1 minute stabilization period. Oscillators having center frequencies above 100 kHz are stable within ±0.5% of design bandwidth.
DISTORTION:	1.0% maximum for any frequency within the design bandwidth. Output terminated into 10 kilohms shunted by 40 picofarads.
MODULATION FEEDTHROUGH:	Harmonics of the input intelligence or any other undesired frequency are suppressed 40 dB minimum below the output signal level.
INPUT INTELLIGENCE FREQUENCY RESPONSE:	±0.25 dB of dc response for a modulation index of 5; ±1.0 dB of dc response for a modulation index of 2; ±2.0 dB of dc response for a modulation index of 1.
ACCURACY AT BANDEDGE SETTINGS:	±1.0% of design bandwidth for all frequencies below 100 kHz. ±2.0% of design bandwidth for all frequencies above 100 kHz.
TEMPERATURE STABILITY:	At any information input the output frequency is stable within ±2.0% of design bandwidth (based on best reference) for oscillator output frequencies below 100 kHz over a temperature excursion of −40°C to +85°C. Stable within ±3.0% of design bandwidth (based on best reference) for oscillator center frequencies above 100 kHz.
OUTPUT IMPEDANCE:	47 kilohms ±10% (10 kHz to 200 kHz). 47 kilohms ±20% for oscillator center frequencies below 10 kHz and above 200 kHz.
OUTPUT IMPEDANCE SENSITIVITY:	Oscillator output frequency is stable within ±1% of design bandwidth if the output load is changed by a factor of 10.
OUTPUT VOLTAGE:	0.3 volt rms ±5% at center frequency into a 10 kilohm load shunted by 40 picofarads. Stable within ±10% under all conditions of supply voltage (28 ±4 volts), and temperature −40°C to +85°C.
POWER SUPPLY STABILITY:	For output frequencies below 100 kHz, at any frequency in the design bandwidth, the output frequency is stable within ±0.5% of design bandwidth for a power supply voltage variation of 1 volts, centered at 28 volts. Stable within ±1.5% for output frequencies above 100 kHz. This stability is maintained at temperatures from −40°C to +85°C.
POWER SUPPLY VOLTAGE INTERRUPTION:	Oscillator will return to normal operation within 20 milliseconds after the supply voltage has been reduced to zero volts for a period of 10 milliseconds or greater, then reapplied. This capability applies for any signal voltage in the range of −5 to +5 volts and at any temperature from −40°C to +85°C.
INDUCED LINE RIPPLE:	20 millivolts p-p maximum, measured across a 1.0 ohm source, feedback into the power source.
RIPPLE:	Ripple with a p-p value of 2 volts and a bandwidth of 1 kHz to 200 kHz, superimposed onto the power source, will not deviate the output frequency more than ±0.5% of design bandwidth or cause amplitude modulation that exceeds 10%.

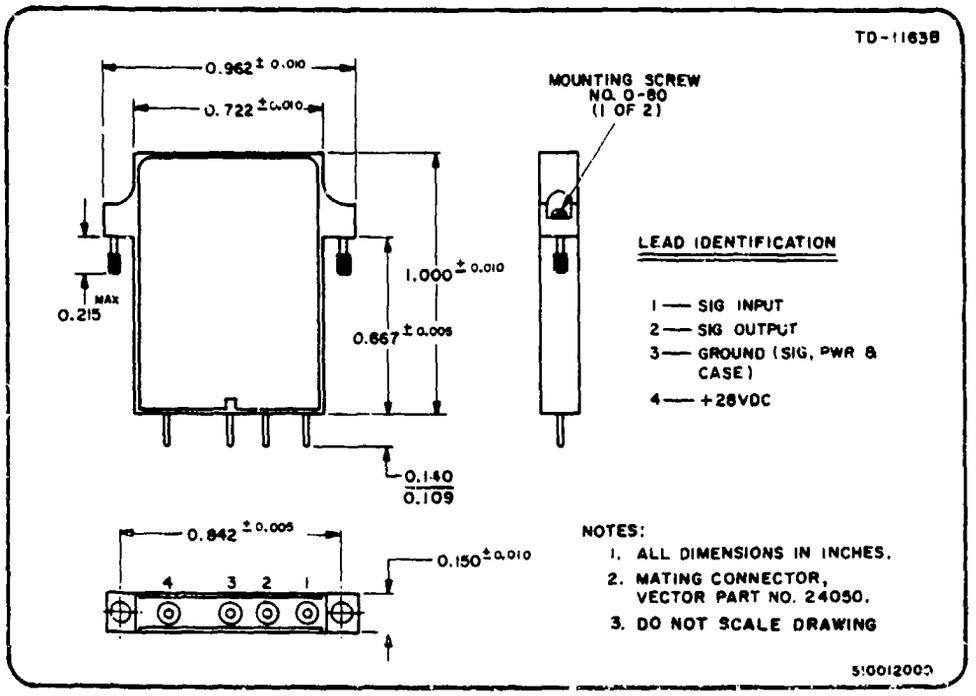

RANDOM NOISE: Random noise on the power supply line with an rms value of 500 mV measured over a bandwidth of 1 kHz to 200 kHz will not deviate the output frequency more than ±0.5% of design bandwidth or cause amplitude modulation that exceeds 10%.

OVERVOLTAGE PROTECTION: The oscillator will not be damaged or subsequently fail to perform as specified after being subjected continuously to a ±40 Vdc at the power input terminal.

POWER REQUIREMENTS: +28 ±4 Vdc, 6.5 mA maximum.

ENVIRONMENTAL SPECIFICATIONS

TEMPERATURE: Operating range from −55°C to +125°C. All electrical specifications maintained from −40°C to +85°C.

HUMIDITY: When exposed to a relative humidity of 95% for 2 hours at +50°C, center frequency is stable within ±1% of design bandwidth.

ALTITUDE: With constant temperature and at any altitude from sea level up, center frequency is stable within ±0.5% of design bandwidth.

VIBRATION: Center frequency is stable within ±0.5% of design bandwidth when subjected to 30g rms sine vibration from 55 to 2000 Hz in each major axis for 15 minutes.

SHOCK: After a half sinewave shock of 200g of 10 millisecond duration in the direction of each major axis, center frequency is stable within ±0.5% of design bandwidth.

ACCELERATION: Under constant acceleration of 200g for 1 minute in the direction of each major axis, center frequency is stable within ±1% of design bandwidth.

MECHANICAL SPECIFICATIONS

SIZE: See outline drawing.

WEIGHT: 3.8 grams (0.134 ounce) nominal, 5.0 grams maximum.

MOUNTING: Vector MMM-652, 655, and 855 Series mounts.

CONNECTION: See outline drawing.

CONTROLS: No controls are required; frequency is preset at factory.

DESIGN VARIATION VECTOR MODEL MMO-15-2

The Vector Model MMO-15-2 Subcarrier Oscillator is the same as the basic Vector Model MMO-15 Subcarrier Oscillator except for the following:

INPUT VOLTAGE: ±2.5 volts dc. Positive-going voltage produces an increase in output frequency.

MARKING: Model designation shown on nameplate as MMO-15-2.

ORDERING INFORMATION

When ordering, specify the desired model number and corresponding part number with a three digit dash number suffix defining IRIG channel and deviation (see tabulation). Example: for a 0 to 5 volt unit operation at 32 ±2 kHz, specify Model MMO-15, part number 10012000-003. For special applications or additional information, contact Vector or the nearest sales representative.

Model No.	Part No.
MMO-15	10012000
MMO-15-2	10012002

IRIG CHANNEL NUMBER	CENTER FREQUENCY (kHz)	ORDERING DASH NUMBER
DEVIATION ±2 kHz		
1A	16	–001
2A	24	–002
3A	32	–003
4A	40	–004
5A	48	–005
6A	56	–006
7A	64	–007
8A	72	–008
9A	80	–009
10A	88	–010
11A	96	–011
12A	104	–012
13A	112	–013
14A	120	–014
15A	128	–015
16A	136	–016
17A	144	–017
18A	152	–018
19A	160	–019
20A	168	–020
21A	176	–021
DEVIATION ±4 kHz		
3B	32	–103
5B	48	–105
7B	64	–107
9B	80	–109
11B	96	–111
13B	112	–113
15B	128	–115
17B	144	–117
19B	160	–119
21B	176	–121
DEVIATION ±8 kHz		
7C	64	–207
11C	96	–211
15C	128	–215
19C	160	–219

MIXER AMPLIFIER
Model MMA-12

actual size

- **Reliability: MTBF in Excess of 3 x 10^6 Hours**
- **Space Qualified**
- **Off-the-Shelf Delivery**
- **Extended Bandwidth to 300 kHz**

The Vector model MMA-12 is a high-gain, feedback type amplifier which is used for summing the outputs of subcarrier oscillators. The overall linearity of the unit is accomplished by utilizing high open loop gain circuits with overall negative feedback.

The unit has been designed for use in airborne equipment such as rockets, missiles, and similar equipment. Employing thick-film circuit design techniques the amplifier offers small size, high accuracy, low power consumption, and high reliability. This amplifier has been fully space qualified on numerous NASA and DOD aerospace programs. The unit provides extended bandwidth capabilities to 300 kHz.

ELECTRICAL SPECIFICATIONS

At 25°C ±3°C with a 10 kilohm 300 pF load unless otherwise noted:

VOLTAGE GAIN: 20.0 ±2.5%.

GAIN STABILITY: ±1% total.

INPUT IMPEDANCE: 10 kilohms ±5%, 20 pF maximum.

HARMONIC DISTORTION: Less than 0.3%.

FREQUENCY RESPONSE: 300 Hz to 300 kHz, within ±0.1 dB.

NOISE: Less than 20 μV referred to input, with input shorted, dc to 500 kHz bandwidth.

OUTPUT VOLTAGE: 0 to 3 V rms minimum with a maximum of 0.3% distortion maximum over the frequency range from 300 Hz to 300 kHz.

OUTPUT IMPEDANCE: 200 ohms.

INDUCED LINE RIPPLE CURRENT: 7 mA p-p max.

POWER REQUIREMENT: 28.0 Vdc 9.0 mA nominal, 12 mA maximum.

OVERVOLTAGE: ±40 Vdc continuous.

SUPPLY INTERRUPTION: Output recovers to 3 V rms in less than 50 ms for a supply interruption greater than 10 μs.

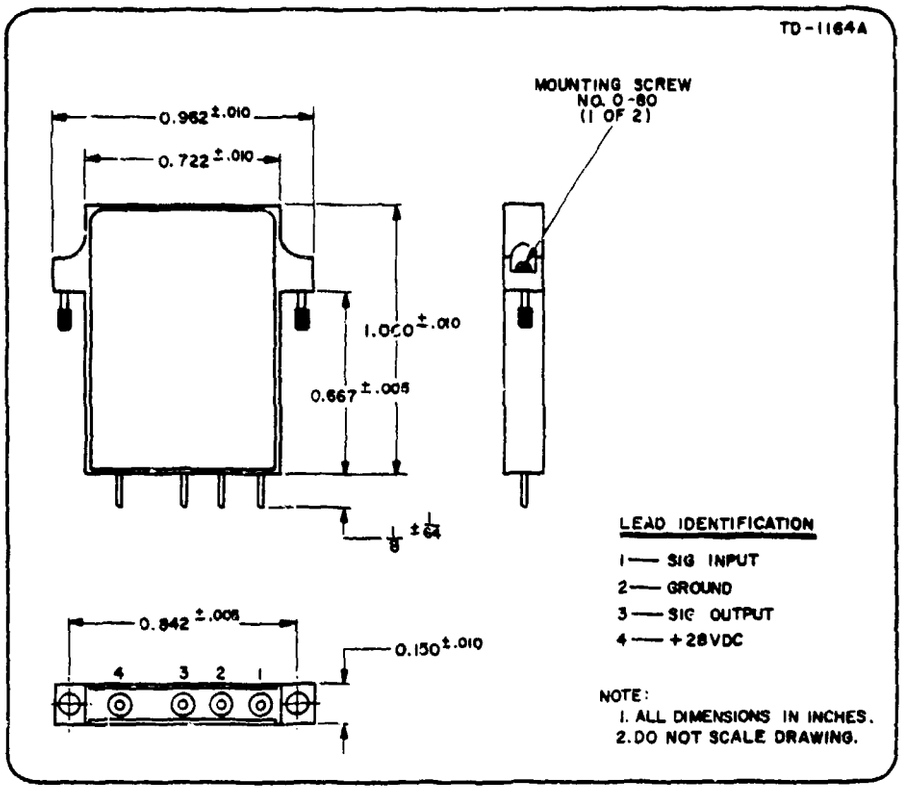

MECHANICAL SPECIFICATIONS

SIZE: See outline drawing.

WEIGHT: 3.5 grams (0.123 ounce) nominal, 4.0 grams maximum.

CONNECTION: Four pins for input, output, power, and ground.

CONTROLS: Due to the small size no controls are supplied (Gain is set at factory.)

ENVIRONMENTAL SPECIFICATIONS

TEMPERATURE: Operating range from –55°C to +125°C. Output stable within ±1.0% maximum from –40°C to +85°C.

HUMIDITY: Meets specifications after exposure to a relative humidity of 95% for 2 hours at +50°C.

ALTITUDE: Output stable within ±0.1 volt from sea level to vacuum.

VIBRATION: Capable of withstanding 30 g in each major axis from 55 to 2000 Hz.

SHOCK: Capable of withstanding at least 200 g.

ACCELERATION: Capable of withstanding at least 200 g.

ORDERING INFORMATION

When ordering, specify the model number and part number. For special applications or additional information, contact Vector or the nearest sales representative.

Model No.	Part No.
MMA-12	10011000

UHF TELEMETRY TRANSMITTER
T-600 S/L Series

- Less Than 5.4 Cubic Inches
- 0.2 or 0.5 Watts Minimum Power
- L- and S-Band Models
- Meets Latest IRIG Specifications for Stability and EMI
- Wideband Response
- Internal Power Line Regulator

The Vector T-600 Series UHF Transmitters are designed for operation in aerospace environments where size, weight and power efficiency are critical.

These transmitters incorporate the most advanced component technologies. Extensive utilization is made of recently developed integrated circuits to enhance overall unit performance. Sophisticated circuit techniques based on many years of experience in RF circuit design are employed providing exceptional performance specifications. The T-600 series transmitters offer superior modulation characteristics: i.e., frequency response from dc to 500 kHz, deviation sensitivity of ±500 kHz/volts rms and low harmonic distortion. The T-600 contains a power line regulator assuring uniform performance over the entire allowable input voltage range and compliance to power line conducted susceptibility and interference requirements.

The standard T-600 transmitter specifications meet the requirements of the majority of telemetry applications. Numerous modifications can be accommodated and additional features incorporated to meet customer requirements.

ELECTRICAL SPECIFICATIONS

T-600 performance specifications are in accordance with the latest requirements of the telemetry ranges as well as all applicable IRIG standards.

OUTPUT CHARACTERISTICS

RF Power Output: T-602-0.2 watts, T-605-0.5 watts minimum into 50 ohm load.

RF Load: Stable operation into 50 ohm load impedance with VSWR up to 1.5 : 1. Operates into open or short circuit load without damage.

Output Frequency: Crystal controlled center frequency for S-band (between 2200-2300 MHz) and for L-band (between 1435-1540 MHz).

Output Frequency Stability: ±0.003% of specified, including setting tolerance and drift due to environment.

Harmonic and Spurious Outputs: In accordance with IRIG-106-73.

MODULATION CHARACTERISTICS

Modulation Type: FM (PM available)

Input Impedance: 20 k ohm minimum.

Deviation Sensitivity: T-600/S ±500 kHz/volt rms. T-600/L ±300 kHz/volt rms.

Frequency Response: Dc to 500 kHz ±1.5 dB (wider response available).

Deviation Capability: T-600/S ±1000 kHz maximum. T-600/L ±600 kHz maximum.

Linearity: 1.0% maximum, best straight line for; T-600/S ±500 kHz deviation; T-600/L ±300 kHz deviation.

Total Harmonic Distortion: 1.0% maximum for, T-600/S ±500 kHz deviation; T-600/L ±300 kHz deviation.

POWER SUPPLY CHARACTERISTICS

Input Voltage: 28 ±4 volts, with reverse polarity protection.

Input Current: 0.2 amp maximum, T-602
0.4 amp maximum, T-605

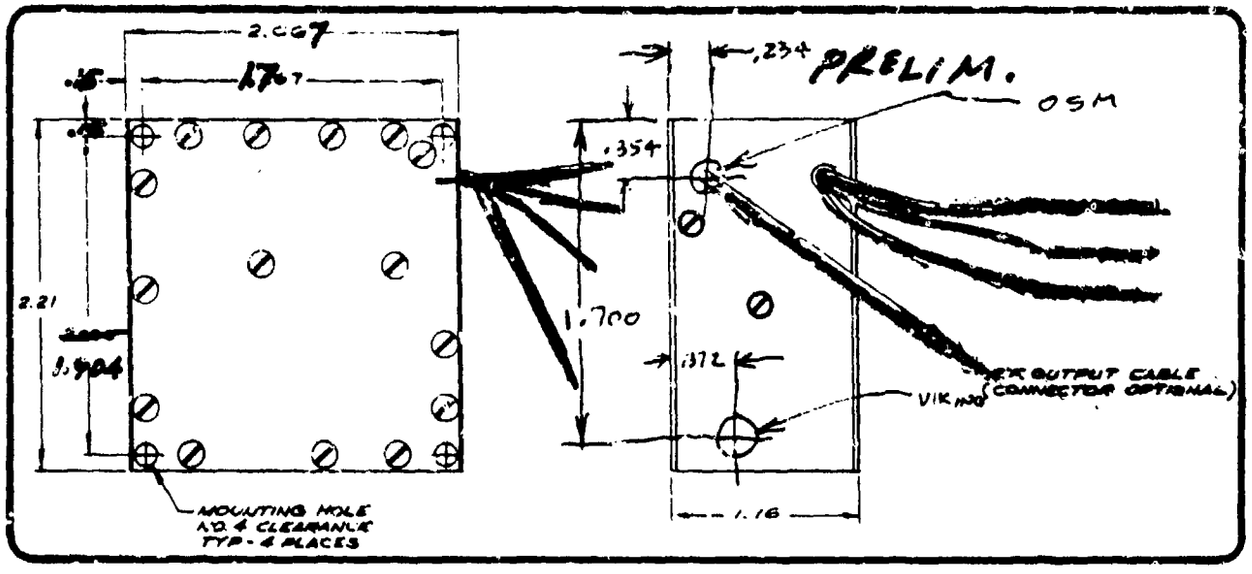

MECHANICAL SPECIFICATIONS

Size: 2.22" x 2.07" x 1.17".

MATES OSM 501-3 RF

VIKING VP5/4CE IS POWER.

Mounting: 4-40 screw on 4 corners, options available.

Weight: 6 ±1 oz.

ENVIRONMENTAL SPECIFICATIONS

All performance specifications will be met under the following conditions:

Baseplate Temperature: -20°C to +71°C.

Vibration: Sinusoidal at 20g from 20 to 2000 cps in each axis.

Shock: ½ sine at 50g for 11 milliseconds in each axis.

Acceleration: 100g, each axis.

Altitude: Unlimited.

Connectors: Modulation and Supply, wire leads; RF output, flexible cable.

QUALITY CONTROL AND PRODUCT ASSURANCE

The Vector T-600 Series transmitter is manufactured under strict Quality Control procedures in accordance with the requirements of MIL-Q-9858A. Additionally, all semiconductors and integrated circuits used in the T-600 are subjected to intensive component preconditioning procedures. Each assembled unit is fully tested to a comprehensive Acceptance Test Procedure which includes full performance testing at the thermal extremes.

Vector has participated in numerous "hi-rel" aerospace programs which have required exhaustive component screening, preconditioning and selection procedures. These "hi-rel" procedures or specific customer generated requirements can be invoked in the manufacture of the T-600 series transmitters if necessary.

ORDERING INFORMATION

When ordering specify model number (T-600/S for S-band T-600/L for L-band, 602 for 200 milliwatts, 605 for 500 milliwatts) and exact operating frequency in megahertz. For special applications or additional information, contact Vector or the nearest sales representative

MICROMINIATURE MOUNT
Model MMM-655

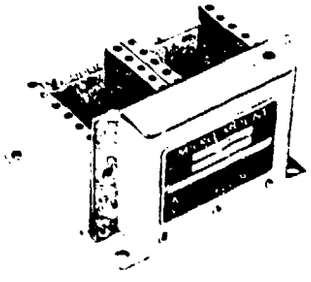

½ actual size

- Space Qualified
- Rugged Design
- Customized Variations Available

Vector Model MMM-655 Micromounts are designed to accommodate up to 19 high-level microminiature subcarrier oscillators and one microminiature amplifier. The mount is constructed of aluminum with a satin chrome plate finish, thus preserving the low weight, small size, and high reliability of Vector telemetry systems. Convenient provisions for pre-emphasis resistors are located within a rear access panel of the mount. These resistors are normally not included in the mount since their value depends on the overall system application; however, they can easily be included as an option (see Ordering Information). Since the plug-in mixer amplifier has no adjustment control, the composite output amplitude is adjusted by an OUT ADJ potentiometer on the mount.

This double row mount is normally provided in increments of two positions ranging from eight to 20 positions. Various combinations of high and low level oscillators can be provided; however, the number of plug-in components is reduced since each low-level oscillator occupies the space of three high-level oscillators. Reasonable variations of the standard design can be supplied.

Other models with provisions for four to 30 positions in single and triple row configurations are available.

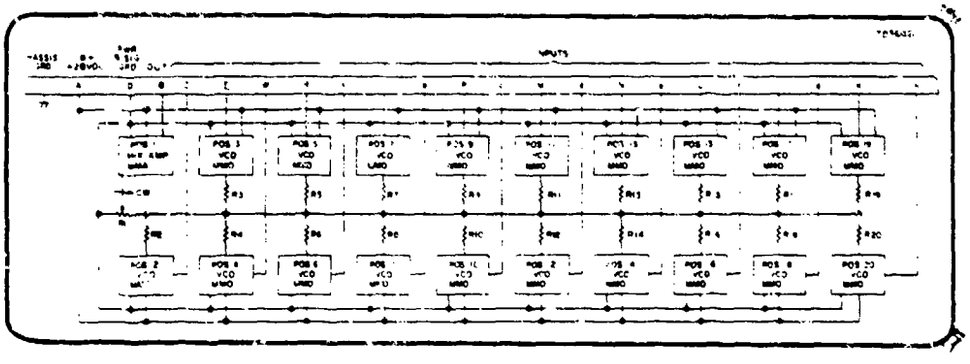

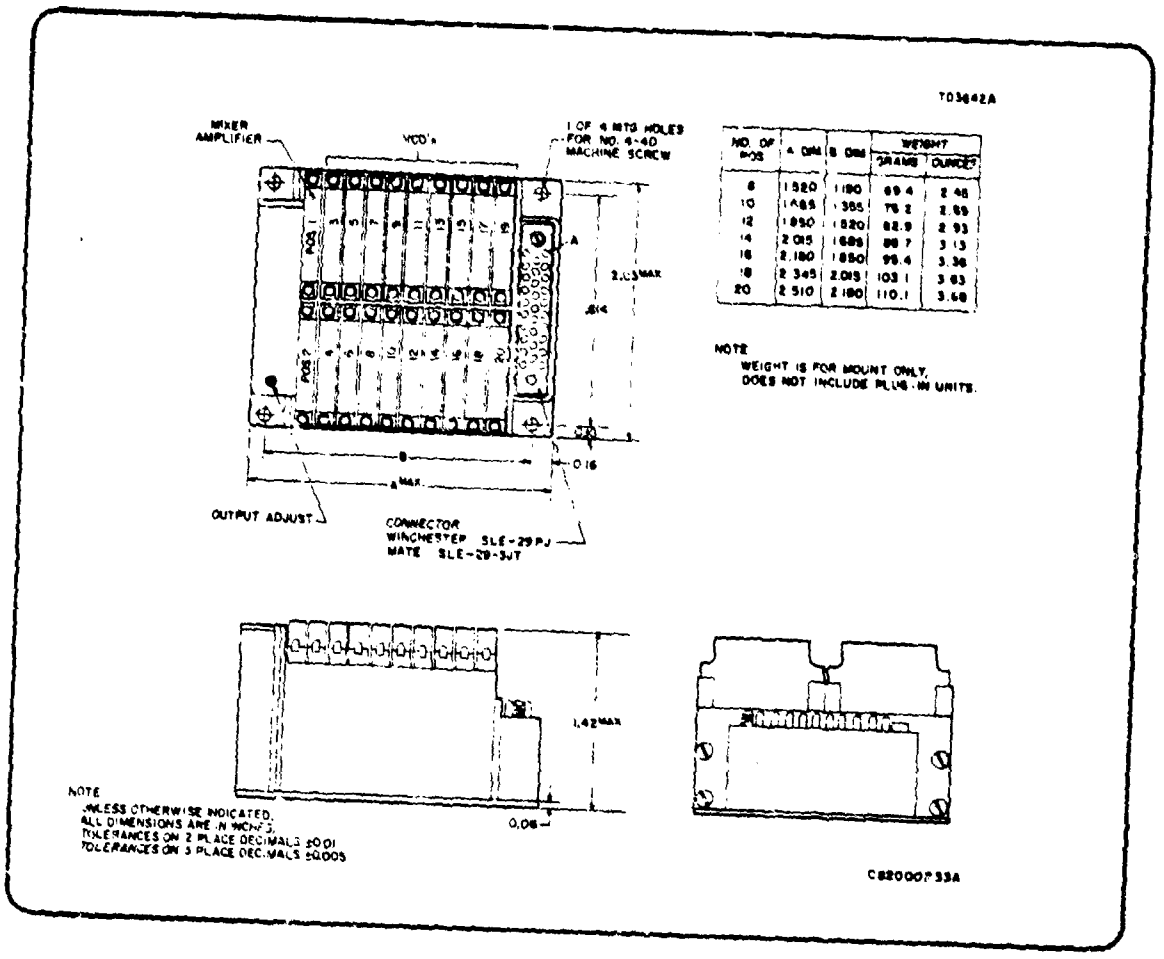

NO. OF POS	A DIM	B DIM	WEIGHT GRAMS	WEIGHT OUNCES
8	1.320	1.190	69.4	2.48
10	1.485	1.355	76.2	2.69
12	1.650	1.520	82.9	2.93
14	2.015	1.685	88.7	3.13
16	2.180	1.850	95.4	3.36
18	2.345	2.015	103.1	3.63
20	2.510	2.180	110.1	3.88

NOTE
WEIGHT IS FOR MOUNT ONLY, DOES NOT INCLUDE PLUG-IN UNITS.

MECHANICAL SPECIFICATIONS

SIZE: See outline drawing.

WEIGHT: See outline drawing.

CONNECTOR: Winchester SLE-29PJ (29 pin connector); mating Connector Winchester SLE-29 SJT.

CONTROL: Output Adjust.

ORDERING INFORMATION

When ordering, specify model number (MMM-655) and part number (see tabulation). For special variations or for mounts with components and/or pre-emphasis resistors installed in accordance with your particular requirements, contact the nearest sales representative or Vector.

Number of Positions	Part Number
8	30010000-008
10	30010000-010
12	30010000-012
14	30010000-014
16	30010000-016
18	30010000-018
20	30010000-020

Bulletin 30010 / 9-69-3M / Printed in USA
S30010000

VHF through X-Band

FLUSH BROAD-BEAM AIRBORNE ANTENNA

Conical, cylindrical geometry. UHF Command, Video, Telemetry, Beacon, Transponder.

The Haigh-Farr Flexislot is a building block, antenna designed for simple mounting and retrofit on cylindrical and conical bodies. Exceptionally thin, 1/16" to 1/8", with uncritical mounting characteristics and ruggedness. They are ideal for drone, missile and aircraft use. Flight proven broad beamwidth Flexislot Antennas in the 300MHz to12GHz range are available for "off-the-shelf" delivery.

Guided missile before impact.

CHARACTERISTICS:

Low Silhouette:	1/16"–1/8" thick for 1 GHz and above
Broad Beam:	190° × 120°
Building Block:	May be arrayed for directive beam
Transmit/Receive:	VHF through X-Band
Rugged:	High-G, hard landing, rough landing
Temperature:	Protection for extreme ranges
Altitude:	Subsurface to space
Simple Mounting:	Uncritical; any surface, cement, bond, strap, screw
Applications:	Ballistic, aircraft, drone, missile, helicopter, Command Control, Video, Telemetry, Beacon, Transponder.

CALL: (617) 944-9145

Request bulletins on other Haigh-Farr antenna series, power dividers and specialized applications.

IMPORTANT

Before investing in antenna R & D, check with Haigh-Farr design group. Antennas for your configuration/performance parameters may already exist. Haigh-Farr experience may provide additional options, making use of computer design and extrapolation from existing models with minimum cost. Haigh-Farr antenna design group has many years of experience in antenna development meeting critical requirements for military and aerospace applications. This backlog of experience is now also available for industrial and specialized end uses.

The FLEXISLOT™ is a broad beam, low silhouette antenna designed for extremely simple mounting on cylindrical or conical bodies, either flush, directly on outer skin, or under heatshield or radomes. The antenna, originally designed for L-Band air-to-ground video link, may be readily adapted for special uses, such as secure air-to-air control.

X-Band E Plane

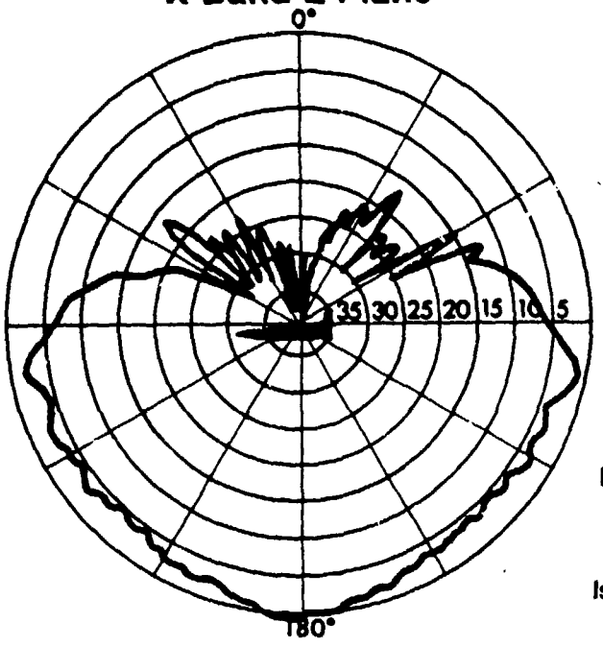

Radiation Patterns in dB

Isotropic is 6dB

X-Band H Plane

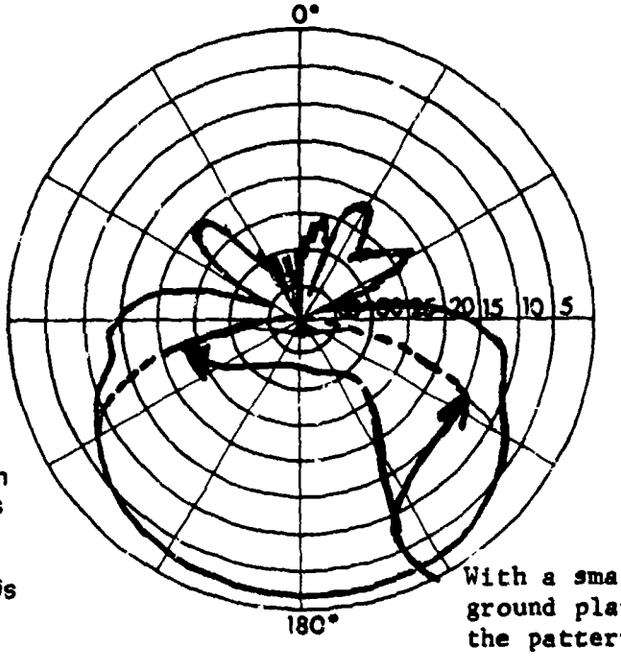

With a small ground plane the pattern will assume the inner form

X-BAND VSWR

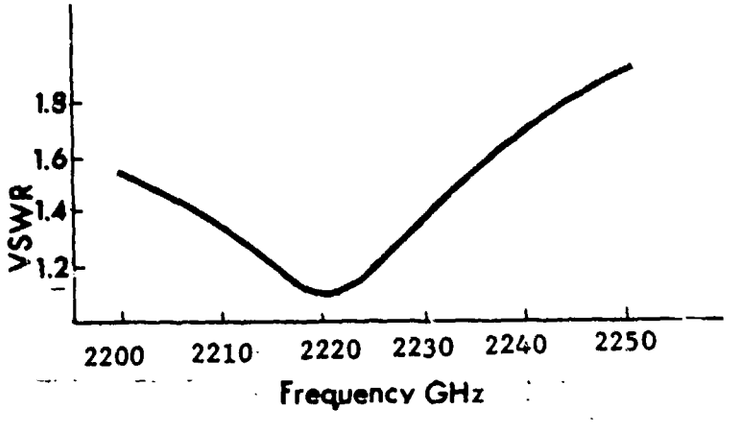

TYPICAL SPECIFICATIONS:

OPERATING BANDS:	VHF through X-Band
INPUT IMPEDANCE:	50 Ohms
BANDWIDTH:	4% to 6%
VSWR, MAX.:	1.5:1 at f_0; 2:1 across bandwidth
POWER:	Design parameter, normally 40W cw, 10Kw peak
RADIATION PATTERN:	Typically 190° × 120°, see above. Directive beams for gain, or secure transmission may be provided.
POLARIZATION:	Linear
DIMENSIONS:	S-Band, 3" × 2-1/2" × 1/16"—typical
WEIGHT:	Less than 2 ounces for S- to X-Band
FORM:	Provided for specified mounting curvatures on cylinder or cone.
MOUNTING:	Uncritical, any surface; adhesive bond, tape, screw
CONNECTOR:	OSM preferred
	Subsurface to space
Γ:	High G, high over-pressure, high temperature.
	Extreme environment is a design parameter.

DISTRIBUTION LIST

COMMANDING GENERAL
U. S. ARMY TANK-AUTOMOTIVE
RESEARCH AND DEVELOPMENT COMMAND
WARREN, MICHIGAN 48090

ATTENTION: LIBRARY SERVICES DIVISION
DRDTA-UL
(3 copies)

Tank-Automotive Concepts Laboratory
(TACL)
DRDTA-Z
(17 copies)

SECURITY CLASSIFICATION OF THIS PAGE (When Data Entered)

REPORT DOCUMENTATION PAGE

READ INSTRUCTIONS BEFORE COMPLETING FORM

1. REPORT NUMBER: 12397	2. GOVT ACCESSION NO.
3. RECIPIENT'S CATALOG NUMBER	
4. TITLE (and Subtitle): TRACK DYNAMICS PROGRAM	5. TYPE OF REPORT & PERIOD COVERED: Final
	6. PERFORMING ORG. REPORT NUMBER
7. AUTHOR(s): Howard C. Meacham, Jr., James C. Swain, John P. Wilcox, George R. Doyle	8. CONTRACT OR GRANT NUMBER(s): DAAE07-76-C-0165
9. PERFORMING ORGANIZATION NAME AND ADDRESS: Battelle-Columbus Laboratories, 505 King Avenue, Columbus, Ohio 43201	10. PROGRAM ELEMENT, PROJECT, TASK AREA & WORK UNIT NUMBERS
11. CONTROLLING OFFICE NAME AND ADDRESS: U. S. Army Tank-Automotive Research and Development Command Warren, Michigan 48090	12. REPORT DATE: October, 1978 13. NUMBER OF PAGES: 290
14. MONITORING AGENCY NAME & ADDRESS(if different from Controlling Office)	15. SECURITY CLASS. (of this report): Unclassified 15a. DECLASSIFICATION/DOWNGRADING SCHEDULE

16. DISTRIBUTION STATEMENT (of this Report)

Approved for public release -- distribution unlimited

17. DISTRIBUTION STATEMENT (of the abstract entered in Block 20, if different from Report)

18. SUPPLEMENTARY NOTES

19. KEY WORDS (Continue on reverse side if necessary and identify by block number)

Advanced track, chordal action, double-pin track bushings, dynamics, end connectors, field tests, laboratory tests, pins, stresses, T-97 track, T-142 track, telemetry, thermal analysis, track, track concepts, track dynamics, track temperature, track tension, tracked vehicles, vibration, XM-1 track.

20. ABSTRACT (Continue on reverse side if necessary and identify by block number)

A comprehensive study of track/track dynamics was undertaken, utilizing analytical, laboratory test, and field test techniques to develop a better understanding of track dynamics and performance. Analytical techniques were developed to predict track vibration modes, chordal action effects, dynamic tension and path, energy dissipation, tension going over obstacles, tension distribution, pin/bushing stresses and deflections, temperature buildup, and end connector tightening effectiveness. Double-pin track for heavy tanks was analyzed with these techniques, and designs for improved track suitable for the XM-1 tank were

DD FORM 1 JAN 73 1473 EDITION OF 1 NOV 65 IS OBSOLETE

Unclassified

SECURITY CLASSIFICATION OF THIS PAGE (When Data Entered)

20. (Continued)

developed. A laboratory bushing research machine was designed, and a track-mounted telemetry system was built.